Alma Mater Studiorum
– Università degli Studi di Bologna –

Dipartimento di Ingegneria Energetica Nucleare
e del Controllo Ambientale

Dottorato di Ricerca in Ingegneria Energetica Nucleare e del Controllo Ambientale

– Ciclo XXII –

Settore Scientifico Disciplinare di afferenza: ING-IND 18

Neutronics Analyses for Fast Spectrum Nuclear Systems and Scenario Studies for Advanced Nuclear Fuel Cycles

Presentata da:

Ing. Giacomo Grasso

Coordinatore Dottorato:

Chiar.mo Prof. Antonio Barletta

Tutor:

Chiar.mo Prof. Marco Sumini

Corelatori:

Ing. Carlo Artioli

Ing. Stefano Monti

Esame finale anno 2010

A Chiara

ABSTRACT

Neutronics Analyses for Fast Spectrum Nuclear Systems and Scenario Studies for Advanced Nuclear Fuel Cycles

The present PhD thesis summarizes the three-years study about the neutronic investigation of a new concept nuclear reactor aiming at the optimization and the sustainable management of nuclear fuel in a futurible European scenario. A new generation nuclear reactor for the nuclear reinassance is indeed auspicated by the actual industrialized world, both for the solution of the energetic question arising from the continuously growing energy demand together with the corresponding reduction of oil availability, and the environment question for a sustainable energy source free from Long Lived Radioisotopes and therefore geological repositories.

Among the Generation IV candidate typologies, the Lead Fast Reactor concept has been pursued, being the one top rated in sustainability.

The European Lead-cooled SYstem (ELSY) has been at first investigated. The neutronic analisys of the ELSY core has been performed via deterministic analysis by means of the ERANOS code, in order to retrieve a stable configuration for the overall design of the reactor. Further analyses have been carried out by means of the Monte Carlo general purpose transport code MCNP, in order to check the former one and to define an exact model of the system.

An innovative system of absorbers has been conceptualized and designed for both the reactivity compensation and regulation of the core due to cycle swing, as well as for safety in order to guarantee the cold shutdown of the system in case of accident.

Aiming at the sustainability of nuclear energy, the steady-state nuclear equilibrium has been investigated and generalized into the definition of the "extended" equilibrium state. According to this, the Adiabatic Reactor Theory has been developed, together with a New Paradigm for Nuclear Power: in order to design a reactor that does not exchange with the environment anything valuable (thus the term "adiabatic"), in the sense of both Plutonium and Minor Actinides, it is required indeed to revert the logical design scheme of nuclear cores, starting from the definition of the equilibrium composition of the fuel and submitting to the latter the whole core design.

The new paradigm has been applied then to the core design of an Adiabatic Lead Fast Reactor complying with the ELSY overall system layout. A complete core characterization has been done in order to asses criticality and power flattening; a preliminary evaluation of the main safety parameters has been also done to verify the viability of the system.

Burn up calculations have been then performed in order to investigate the operating cycle for the Adiabatic Lead Fast Reactor; the fuel performances have been therefore extracted and inserted in a more general analisys for an European scenario. The present nuclear reactors fleet has been modeled and its evolution simulated by means of the COSI code in order to investigate the materials fluxes to be managed in the European region. Different plausible scenarios have been identified to forecast the evolution of the European nuclear energy production, including the one involving the introduction of the Adiabatic Lead Fast Reactor, and compared to better analyze the advantages introduced by the adoption of new concept reactors.

At last, since both ELSY and the ALFR represent new concept systems based upon innovative solutions, the neutronic design of a demonstrator reactor has been carried out: such a system is intended to prove the viability of technology to be implemented in the First-of-a-Kind industrial power plant, with the aim at attesting the general strategy to use, to the largest extent. It was chosen then to base the DEMO design upon a compromise between demonstration of developed technology and testing of emerging technology in order to significantly subserve the purpose of reducing uncertainties about construction and licensing, both validating ELSY/ALFR main features and performances, and to qualify numerical codes and tools.

The Author
Giacomo Grasso

ACKNOWLEDGMENTS

At the end of a fruitfull work, an inevitable gratefulness feeling is due to all people who collaborated, more or less directly, to the completion of the work itself.

At first, the Author is grateful to prof. Sumini and ing. Monti, who provided the Author the possibility of spending his PhD period in ENEA, on such an interesting research field.

Again, thanks to prof. Sumini, who accorded the Author also the honour of teaching at the "Advanced nuclear systems design and management" master course.

The second thanks goes to ing. Rocchi, who continuously encouraged the Author by demonstrating interest and appreciation in his work.

The Author is then aware of the precious connection with ing. Artioli, priceless mentor and incomparable anecdoteteller, fundamental (tour) guide and inexplicable compliment dispenser, affectionate friend.

Thanks to ing. Cinotti, for his professional esteem and fruitful collaboration along these three years, up to the writing of the Handbook chapter.

Thanks to all ENEA colleagues, who made the Author's workplace a pleasant friends' haunt: dr. Sarotto (with Cristina, Tommaso and Iris), who tolerated the Author's oddities as an old friend; dr. Petrovich, who shared part of the Author's frustrations and joys; ing. Polidori (with Barbara and the small Anakin – may the Force be with you!), for his unconditioned friendship from the very first moment; dr. Nava, for having heard (without judging...?!) the Author's confessions; ing. Console Camprini and ing. Bortot, for having patiently stood the collaboration with the Author; the nicely nasty ing. Lombardo, who almost presented the Author with an original Sicilian cloth cap; ing. Giusti, for the wise foolishness of his speeches and the tennis-table matches; dr. Glinatsis, ing. Meloni and ing. Bandini for having been perfect workmates.

Thanks to all friends at the Nuclear Engineering Laboratory of Montecuccolino, who welcomed back the Author after three years with the same affection. And thanks also to prof. Scardovelli and prof. Amadesi for the pleasant chats between a simulation and a lesson.

Thanks to David, Marco, Simone, Martina, Francesco, Amelia and Carlotta, the "Nuclears", for the Nuclear dinners and wines; thanks to Michele and Cinzia, Simone and Silvia, and Francesco and Cecilia, for the sausages and the dancing: all of them helped the Author not to drive crazy during the last three years.

Thanks to the Author's housemates, Federico and Alessio, who relegated the Author in the smallest room to remember him his duties (even if at last they gave in with the Wii). Thanks also to Antonella, Carmen, Leuzzi, Chiara, Laura, Ale-e-Vi and Pietro for beeing so kindly alcoholic friends.

Thanks to Maicolengel, Annapaola (the "Incommensurable"), "the Doc", the bagatelle table and everyone/everything in Kanta: surely the best way to begin a week!

Thanks to Mauro (the Author's best friend), Ciccio (sorry, but he is the third among the Author's best friends! ;), Mario, Vittorio and Kika: more than half of the Author's life has passed because of them.

Thanks to the Author's family, who continuously supported (in both senses) the present work.

And, last but not least, thanks to Chiara: without her nothing of this would have been.

The Author
Giacomo Grasso

CURRICULUM VITAE

Education

June 22, 2006

Alma Mater Studiorum University, Bologna, ITALY. M.S. degree with honours in Nuclear Engineering. Advisor: prof. Marco Sumini. Dissertation: Application of Particle In Cell methods to the modeling of the plasma dynamics in Plasma Focus devices.

1998

'Liceo' specializing in classical and scientific studies "Ariosto-Spallanzani", Reggio Emilia, ITALY. Scientific school-leaving certificate with honours.

Schools

October 19 - 21, 2009

Aix-en-Provence, FRANCE. Participation to the "2nd ERANOS user's workshop".

July 1 - November 19, 2008

ENEA, Bologna, ITALY. V. Peluso, "Introduction to the deterministic neutronics code ERANOS".

May 1 - July 31, 2007

CINECA, Casalecchio di Reno (BO), ITALY. Stage for the study and the application of parallelization techniques for scientific code.

June 18 - 29, 2007

CINECA, Casalecchio di Reno (BO), ITALY. Participation to the "7th Summer School of Scientific Visualization and 3D Interactive Graphics".

October 9 - 13, 2006

CINECA, Casalecchio di Reno (BO), ITALY. Participation to the "2nd Specialized School of Parallel Computing".

September 4 - 15, 2006

CINECA, Casalecchio di Reno (BO), ITALY. Participation to the "15th Summer School of Parallel Computing".

Ph.D courses and seminars, International conferences and meetings

March 15, 2007

CINECA, Casalecchio di Reno (BO), ITALY. C. Gottbrath, "Debugging high performance applications with Totalview".

July 11, 2007

LIN Montecuccolino, Bologna, ITALY. C. Siewert, "Some computational aspects relative to transport theory".

September 15, 2007

LIN Montecuccolino, Bologna, ITALY. C. Artioli, "A-BAQUS: a multi entry graph for core design of ADS".

September 19, 2007

LIN Montecuccolino, Bologna, ITALY. G. Gambarini, "Dosimetria per BNCT".

September 19, 2007

LIN Montecuccolino, Bologna, ITALY. M. Valente, "Imaging di dose con Fricke gel".

October 2, 2007

LIN Montecuccolino, Bologna, ITALY. U. Scherer, "Nuclear applications at Aachen university of applied sciences".

February 4, 2008

ENEA, Bologna, ITALY. "STREP ELSY Work Package 2 meeting".

February 5, 2008

ENEA, Bologna, ITALY. "STREP ELSY PCC meeting".

May 18, 2008

LIN Montecuccolino, Bologna, ITALY. L. Monti, "Neutronics (ERANOS) and thermoidraulics (RELAP) coupling".

September 24 - 25, 2008

Ansaldo Nucleare, Genova, ITALY. "STREP ELSY Work Package 2 meeting".

September 26, 2008

Ansaldo Nucleare, Genova, ITALY. "STREP ELSY PCC meeting".

January 15, 2009

University of Bologna, Bologna, ITALY. "Neutronics calculations with MCNP for the FRJ-2 research reactor and the ITER CXRSPP".

February 17, 2009

SCK-CEN, Brussels, BELGIUM. "STREP ELSY Work Package 2 meeting".

March 13, 2009

University of Bologna, Bologna, ITALY. J. van der Mullen, "Exploring the plasma zoo in search for equilibrium: the myth of LTE".

October 12 - 13, 2009

SCK-CEN, Brussels, BELGIUM. "Central Design Team Work Package 1 meeting".

November 13, 2009

CEA, Cadarache, FRANCE. "2nd COSI users' group meeting".

Publications

2007

M. Frignani, **G. Grasso**, F. Rocchi and M. Sumini. PIC-MCC simulation of the electrical breakdown in a plasma focus device. In *Joint International Topical Meeting on Mathematics & Computation and Supercomputing in Nuclear Applications (M&C + SNA 2007)*, Monterey, California, April 15-19, 2007, on CD-ROM, American Nuclear Society, LaGrange Park, IL (2007).

C. Artioli, G. Glinatsis, S. Monti, M. Sarotto, **G. Grasso**, L. Monti, F. Rocchi, M. Sumini and J. Ghassoun. EFIT fuel cycle analysis by deterministic and Monte Carlo methods. In *First International Conference on Physics and Technology of Reactors and Applications (PHYTRA1)*, Marrakech, Morocco, March 14-16, 2007, on CD-ROM, (2007).

2008

G. Grasso, F. Rocchi and M. Sumini. Development of a Particle In Cell code with Structured Adaptive Mesh Refinement for Plasma Focus devices breakdown simulation. In *Il Calcolo Scientifico nella Fisica Italiana (CSFI2008)*, Rimini and Senigallia, Italy, May 27-31, 2008.

R. Ghazy, E. Padovani, M. E. Ricotti, C. Artioli and **G. Grasso**. A Coolant Void Reactivity Evaluation of ELSY LFR: Optimization of a Mid-Plane Blanket for Void Effect Reduction. In *International Topical Meeting on Safety of Nuclear Installations 2008 (TopSafe 2008)*, Dubrovnik, Croatia, September 30-October 3, 2008.

G. Grasso, C. Artioli, S. Monti, F. Rocchi and M. Sumini. On the Effectiveness of the ELSY Concept with respect to Minor Actinides Transmutation Capabilities. In *Tenth Information Exchange Meeting on Actinide and Fission Product Partitioning and Transmutation (IEMPT10)*, Mito, Japan, October 6-10, 2008.

G. Grasso, M. Sumini, F. Rocchi and A. Tartari. Perspectives for the Application of Plasma Focus Technology to Neutron Capture Therapy. In *13$^{\text{th}}$ International Congress on Neutron Capture Therapy (13$^{\text{th}}$ ICNCT)*, Florence, Italy, November 3-7, 2008.

2009

G. Grasso, F. Rocchi and M. Sumini. Development of a Particle In Cell code with Structured Adaptive Mesh Refinement for Plasma Focus devices breakdown simulation. *Il Nuovo Cimento C* **32C(2)**:147-51, doi:10.1393/ncc/i2009-

10390-y (2009).

C. Artioli, **G. Grasso**, M. Sarotto, J. Krepel and M. Sumini. ELSY Neutronic Analysis by deterministic and Monte Carlo methods: an innovative concept for the control rod systems. In *2009 International Congress on Advances in Nuclear Power Plants (ICAPP '09)*, Tokyo, Japan, May 10-14, 2009.

D. Gugiu, G. Glinatsis, **G. Grasso** and C. Artioli. Radiation damage and activation evaluations for the ELSY reactor. In *2009 Annual International Conference on Sustainable Development through Nuclear Research and Education (Nuclear 2009)*, Pitesti, Romania, May 27-29, 2009.

G. Glinatsis, D. Gugiu, **G. Grasso** and C. Petrovich. Nuclear data impact on the core neutron design. In *2009 Annual International Conference on Sustainable Development through Nuclear Research and Education (Nuclear 2009)*, Pitesti, Romania, May 27-29, 2009.

G. Grasso, M. Frignani, F. Rocchi and M. Sumini. Hierarchical Agglomerative Sub-Clustering technique for variance reduction in PIC simulations. In *Ions Acceleration with high Power Lasers: Physics and Applications (Coulomb '09)*, Senigallia, Italy, June 15-18, 2009.

S. Bortot, C. Artioli, **G. Grasso**, V. Peluso and M. E. Ricotti. Approach to a Preliminary Core Characterization of a Generation IV Lead-cooled Fast Reactor Demonstration Project: Goals and Rationales. In *14$^{\text{th}}$ International Conference on Emerging Nuclear Energy Systems (ICENES 2009)*, Ericeira, Portugal, June 29-July 3, 2009.

S. Bortot, M. E. Ricotti, P. Console Camprini, **G. Grasso**, C. Artioli and V. Peluso. Feedback Coefficients Evaluation for an Advanced LFR Demonstrative Reactor. In *International Conference on Nuclear Energy for New Europe 2009 (NENE '09)*, Bled, Slovenia, September 14-17, 2009.

C. Artioli, **G. Grasso**, M. Sarotto, S. Monti and E. Malambu. European Lead-cooled SYstem core design: an approach towards sustainability. In *International Conference on Fast Reactors and Related Fuel Cycles (FR09)*, Kyoto, Japan, December 7-11, 2009.

L. Barzotti, **G. Grasso**, F. Rocchi, M. Sumini and E. Greenspan. Deterministic analysis of the Encapsulated Nuclear Heat Source by the European transport code ERANOS. In *International Conference on Fast Reactors and Related Fuel Cycles (FR09)*, Kyoto, Japan, December 7-11, 2009.

G. Grasso, C. Oppici, F. Rocchi and M. Sumini. A Neutronics Study of the 1945 Haigerloch B-VIII Nuclear Reactor. *Phys. perspect.* 11:318-335 (2009), doi:10.1007/s00016-008-0396-0.

2010

G. Grasso, M. Frignani, F. Rocchi and M. Sumini. Hierarchical Agglomerative Sub-Clustering technique for variance reduction in PIC simulations. *Nucl. Inst. and Meth. in Phys. Res. A* (2010), doi:10.1016/j.nima.2010.01.060.

S. Bortot, C. Artioli, **G. Grasso**, V. Peluso and M. E. Ricotti. Preliminary Core Characterization of a Generation IV Lead Fast Reactor DEMO: Goals, Design Rationales and Options. *En. Conv. and Management, (IN PRESS).*

S. Bortot, P. Console Camprini, **G. Grasso**, C. Artioli and S. Monti. Core design of a Generation IV LFR demonstration plant. In *International Conference on the Physics of Reactors: Advances in Reactor Physics to Power the Nuclear Renaissance (PHYSOR2010)*, Pittsburgh, Pennsylvania, USA, May 9-14, 2010 *(ACCEPTED).*

C. Petrovich, C. Artioli and **G. Grasso**. Solution of the equilibrium fuel vector in closed fuel cycles and application to a Lead Fast Reactor. In *International Conference on the Physics of Reactors: Advances in Reactor Physics to Power the Nuclear Renaissance (PHYSOR2010)*, Pittsburgh, Pennsylvania, USA, May 9-14, 2010 *(ACCEPTED).*

L. Cinotti, C. F. Smith, C. Artioli, **G. Grasso** and G. Corsini. Lead-cooled Fast Reactor (LFR) Design: Safety, Neutronics, Thermal-Hydraulics, Structural Mechanics, Fuel, Core and Plant Design. In *Handbook of Nuclear Engineering*, Springer, *(IN PRESS).*

C. Artioli, **G. Grasso** and C. Petrovich. A new paradigm aimed at the sustainability of nuclear energy: the solution of the extended equilibrium state. *Ann. of Nucl. En. (ACCEPTED).*

Teaching Experiences

December 1-23, 2009

Contract professor at the University of Bologna for a 20 hours cycle of lessons regarding "Deterministic and Monte Carlo codes applied to neutronics", within the second edition of the master "Design and Management of Advanced Nuclear Systems".

July 1, 2009

Invited speaker at ENEA for the seminary "Neutronic Design of a Lead Fast Reactor: general guidelines, aims and constraints", within the VELLA (Virtual European Lead LAboratory) school, a Euratom FP6 project.

February 10-28, 2009

Contract professor at the University of Bologna for a 20 hours cycle of lessons regarding "Deterministic and Monte Carlo codes applied to neutronics", within the first edition of the master "Design and Management of Advanced Nuclear Systems".

October 9, 2008

CINECA, Casalecchio di Reno (BO), ITALY. Relator for the seminary "A Gentle introduction to SAMRAI" held within the "4^{th} Specialized School of Parallel Computing".

October 8, 2007

CINECA, Casalecchio di Reno (BO), ITALY. Relator for the seminary "A Gentle introduction to SAMRAI" held within the "3^{rd} Specialized School of Parallel Computing".

CONTENTS

Preface **1**

1 Introduction **3**

I The Present European Nuclear Scenario **7**

2 The Nuclear Legacies **9**
2.1 National policies within the western European frame 11
2.2 Spent Fuel stocks inventory 12

3 Present Regional Scenario **15**
3.1 Fuel management strategy 18
3.2 Scenario model 19
3.3 Energy demand forecast 21

4 Scenario Results **25**
4.1 Overall environmental and economical performances 27
4.2 Mass fluxes and inventories evolution 32

5 Introducing Remarks **45**
5.1 Implied horizons 47
5.2 Desirable scenario features 49

II The Nuclear Reactors Generation-IV **51**

6 The Generation-IV Initiative **53**
6.1 The present generation reactors . . . 55
6.2 The Generation-IV philosophy . . . 58
6.2.1 Sustainability . . . 59
6.2.2 Safety and reliability . . . 60
6.2.3 Economics . . . 60
6.2.4 Proliferation resistance and physical protection . . . 61
6.3 The candidates typologies . . . 62
6.3.1 Gas-cooled Fast Reactor . . . 64
6.3.2 Very-High-Temperature Reactor . . . 64
6.3.3 Supercritical-Water-cooled Reactor . . . 65
6.3.4 Sodium-cooled Fast Reactor . . . 66
6.3.5 Lead-cooled Fast Reactor . . . 66
6.3.6 Molten Salt Reactor . . . 67

7 Lead Fast Reactors and the ELSY Project **69**
7.1 General neutronic properties of LFR . . . 71
7.1.1 Lead properties . . . 71
7.1.2 Fuel properties . . . 73
7.2 Lead cooling choice . . . 76
7.3 The ELSY project . . . 79
7.3.1 Expected ELSY features . . . 80

8 Neutronic Design of ELSY: Preliminary Configuration **83**
8.1 Geometric and material description . . . 86
8.2 ELSY computational model . . . 89
8.2.1 ERANOS model . . . 90
8.2.2 MCNP model . . . 90
8.3 Results and final layout . . . 91
8.3.1 Final layout . . . 94
8.3.2 Results . . . 94

9 Neutronic Design of ELSY: Final Configuration **99**
9.1 Geometric and material description . . . 101
9.2 ELSY computational model . . . 105
9.2.1 ERANOS model . . . 106
9.2.2 MCNP model . . . 107
9.3 ELSY design: operative parameters optimization . . . 108
9.4 Results and final layout . . . 110
9.4.1 Final layout . . . 110
9.4.2 Results . . . 112

III A Sustainable Nuclear Scenario Hypothesys 117

10 The Adiabatic Reactor Theory 119
10.1 The Adiabatic core concept . . . 121
10.2 The nuclear equilibrium state . . . 122
10.2.1 Steady-state equilibrium . . . 124
10.2.2 Extended equilibrium state . . . 124
10.3 Numerical formulations for nuclear equilibrium solution . . . 125
10.3.1 Steady-state equilibrium . . . 125
10.3.2 Extended equilibrium state . . . 126

11 A New Paradigm for Core Design 129
11.1 Present design philosophy . . . 131
11.1.1 First step: viability region identification . . . 133
11.1.2 Second step: preliminary estimate of shape factors . . . 134
11.1.3 Third step: iterative core characterization . . . 135
11.1.4 Fourth step: whole core design . . . 139
11.2 The New Paradigm for Nuclear Power . . . 141

12 Neutronic Design of an Adiabatic Lead Fast Reactor 145
12.1 Elementary cell design . . . 148
12.2 Geometric and material description . . . 151
12.3 ALFR computational model . . . 153
12.3.1 ERANOS model . . . 153
12.3.2 MCNP model . . . 155
12.4 Results and final layout . . . 155
12.4.1 Final layout . . . 156
12.4.2 Results . . . 158

13 A New Scenario Implementing ALFRs 165
13.1 Evolution of the present scenario . . . 167
13.1.1 Introduction of an ALFR fleet . . . 167
13.2 The new scenario model . . . 168
13.2.1 Modeling the ALFR for COSI6 . . . 169

14 New Scenario Results 173
14.1 Overall environmental and economical performances . . . 175
14.2 Mass fluxes and inventories evolution . . . 177
14.3 Implied horizons . . . 185

IV Towards the Sustainable Scenario: the ELSY/ALFR Demonstrator Reactor 187

15 The Need for Demonstration in ELSY/ALFR Validation 189

15.1 The ELSY/ALFR innovation . . . 191
15.1.1 Lead technology and materials . . . 191
15.1.2 Potentially high mechanical loading . . . 193
15.1.3 Main safety functions . . . 193
15.1.4 Special operations . . . 193
15.1.5 Fuel and core design . . . 193
15.2 Research and Development strategies . . . 193
15.2.1 Lead technology and materials . . . 194
15.2.2 Potentially high mechanical loading . . . 196
15.2.3 Main safety functions . . . 197
15.2.4 Special operations . . . 197
15.2.5 Fuel and core design . . . 198

16 DEMO Characteristics for ELSY/ALFR Validation 201
16.1 Demonstration objectives uncoupling . . . 203
16.2 Criteria for DEMO parameters selection . . . 204

17 Neutronic Design of DEMO 209
17.1 Preliminary overall analysis . . . 211
17.2 DEMO computational model . . . 219
17.2.1 ERANOS model . . . 220
17.3 Engineerization of DEMO and final optimization analysis . . . 221
17.4 Results and final layout . . . 226
17.4.1 Final layout . . . 227
17.4.2 Results . . . 228

V Concluding Remarks 233

18 Conclusions 235

Appendices 240

A Summary of Materials Properties 243
A.1 Fuel . . . 244
A.2 Structural materials . . . 249
A.2.1 Ferritic-martensitic steel T91 . . . 249
A.2.2 316 stainless steels family . . . 250
A.3 Coolant . . . 251

B The "Adiabatic Concentrator" code 253
B.1 "Adiabatic Concentrator" code lists . . . 254
B.1.1 The "Nuclear" module . . . 257
B.1.2 The "Chemical" module . . . 258

C Neutron Flux Enhancement Strategies **261**
C.1 Flux heighten strategies 262
C.1.1 Via linear power increase 262
C.1.2 Via fuel pin diameter reduction 263
C.1.3 Via active height reduction 263
C.2 The FASTEF case study 264
C.2.1 Increased linear power configurations 265
C.2.2 Reduced pin diameter configurations 266
C.2.3 Reduced active height configuration 269
C.2.4 Combined strategies configurations 269

D DEMO Fuel Pin and Assembly, Absorbers and Dummy Elements Design **273**
D.1 Detailed CAD drawings 274

E Acronyms **289**

Bibliography **301**

LIST OF FIGURES

3.1 Example of material path in a typical scenario simulation. . . 17
3.2 Representation of the mass fluxes and installed facilities in the first scenario (open cycle). 21
3.3 Representation of the mass fluxes and installed facilities in the second scenario (Pu mono-recycling in LWRs). 21
3.4 Time evolution of the first scenario benchmark case (open cycle). 23
3.5 Time evolution of the second scenario benchmark case (mono-recycling of Pu). 24

4.1 Evolution of Pu and MAs in the SF inventory according to the open cycle scenario. 42
4.2 Evolution of Pu and MAs in the SF inventory according to the Pu mono-recycling scenario. 42

6.1 Evolution of nuclear power plants through different Generations. 56

7.1 Elastic cross-sections of naturally occurring lead isotopes (data from JEFF3.0 library). 72
7.2 Typical neutrons spectrum in a LFR (e.g.: ELSY). 73
7.3 (n,γ) absorption cross-sections of naturally occurring lead isotopes (data from JEFF3.0 library). 74
7.4 ELSY primary system arrangement and coolant flow path. . . 81

8.1 Cross-cut view of the preliminary ELSY FA and fuel pin. Grey positions represent structural uprights. 89
8.2 Cross-cut view of the preliminary ELSY core scheme. 89
8.3 Simplified 2D cylindrical computational scheme of ELSY for preliminary parametric analysis. 91
8.4 MCNP plot of the ELSY mid-plane cross-cut according to the Monte Carlo simulation model. 92

8.5 Dependence of the clad wall temperature on the power/FA distribution Factor (FADF). 93
8.6 Simplified 2D cylindrical computational scheme of ELSY including absorber regions. 94
8.7 Core zoning for the preliminary ELSY configuration as resulting from the criticality and power/FA distribution flattening analysis. 95
8.8 Power/FA distribution for the preliminary ELSY configuration. 95
8.9 Criticality swing during operation for the preliminary ELSY configuration. 96
8.10 Absolute and relative U, Pu and MAs mass evolution during operation for the preliminary ELSY configuration. 97

9.1 The core general layout and FAs arrangement for the final configuration of ELSY. 103
9.2 FA and pin layout for the ELSY final configuration. 104
9.3 Detailed view of a Finger Absorber Rod (FAR) inserted in the FA box beam channel. 104
9.4 Scratch design of the Control Rod and pin layout. 105
9.5 ECCO representations of the 9 central positions for a FA with (right frame) and without (left frame) a FAR. 106
9.6 Cross-cut view of the ELSY simulation domain with TGV, in which are shown the FAs (red), CRs (green) and dummy elements (blue) positions. 107
9.7 Horizontal cross-cut view of the ELSY simulation domain with MCNP. 108
9.8 Vertical cross-cut views of the ELSY simulation domain with MCNP, at different intersection planes to highlight the DHR and SG positioning. 109
9.9 Core zoning for the final ELSY configuration as resulting from the criticality and power/FA distribution flattening analysis. . 111
9.10 Power/FA distribution for the final ELSY configuration at EoC. 112
9.11 Positioning of the passive (magenta circles) and motorized (cyan circles) FARs on the final ELSY core map. 113
9.12 Criticality swing during operation for the final ELSY configuration. 114
9.13 Absolute and relative U, Pu and MAs mass evolution during operation for the final ELSY configuration. 115

10.1 Scheme of the closed fuel cycle resulting by the introduction of adiabatic reactors. 122

11.1 Temperature profiles in the fuel pin and coolant channel. . . . 135
11.2 Scheme of the dependencies for dimensioning the fuel pin radius. 138

11.3 Scheme of the dependencies for dimensioning the fuel pins lattice pitch. 139
11.4 Classical scheme of the dependencies between the main parameters for the core design. 141
11.5 Scheme of the core design approach according to the 2NP logic. 143
11.6 Scheme of the dependencies between the main parameters for the core design according to the New Paradigm for Nuclear Power. 144

12.1 Cross-cut view of the preliminary ALFR FA and pin layout. . 148
12.2 The core general layout and FAs arrangement of the ALFR. . 152
12.3 Cross-cut view of the ALFR simulation domain with TGV. . 154
12.4 Horizontal cross-cut view of the ALFR core model with MCNP. 155
12.5 Cross-cut view of the fuel pins belonging to the intermediate and outer core zones in the ALFR final configuration. 157
12.6 Local-to-average power/FA ratio for the final ALFR configuration. 158
12.7 Positioning of the control (magenta circles) and regulation (cyan circles) FARs on the ALFR core map. 161
12.8 Criticality evolution for the final ALFR configuration. 161
12.9 Evolution of ^{239}Pu and ^{238}U inventory during the whole irradiation and decay period. 162
12.10 Evolution of ^{241}Pu and ^{241}Am inventory during the whole irradiation and decay period. 163
12.11 Evolution of ^{239}Np and ^{242}Cm inventory during the whole irradiation and decay period. 163

13.1 Time evolution of the final scenario (fuel cycle closure). . . . 168
13.2 Representation of the mass fluxes and installed facilities in the final scenario (closed cycle). 170

14.1 Evolution of Pu and MAs in the SF inventory according to the closed fuel cycle scenario. 183

17.1 Simplified 2D cylindrical ERANOS computational domain for DEMO design. 223
17.2 DEMO final ("GPS10") core configuration: inner (yellow) and outer (red) FAs arrangement. 228
17.3 Control (magenta) and regulation (green) FARs positioning in the DEMO core (GPS10 configuration). 229
17.4 Criticality swing during irradiation for the final DEMO configuration. 230
17.5 DEMO regulation FARs anti-reactivity vs insertion curve. . . 231

A.1 Scheme of the cubic, face centered lattice of actinides dioxide. 246

A.2 Comparison of different thermal expansion laws for UO_2. . . . 248
A.3 Thermal expansion of PuO_2. 248

CAD drawing of the DEMO core layout. 276
CAD drawing of the DEMO fuel pin. 278
CAD drawing of the DEMO Finger Absorber Rod. 280
CAD drawing of the DEMO Fuel Assembly frame. 282
CAD drawing of the DEMO FAR positioning relative to the FA frame. 284
CAD detail drawing of the DEMO spacer grids. 286
CAD drawing of the DEMO dummy element. 288

LIST OF TABLES

2.1 Grouping of European countries according to their national nuclear policy . . . 12
2.2 Initial spent fuel inventories (tons) . . . 13

3.1 Standardized reactors data for the scenarios study . . . 20
3.2 Initial composition for UOX fuel . . . 20
3.3 Initial composition for MOX fuel . . . 20
3.4 Number of NPPs installed in the selected countries and corresponding electric capacity . . . 22
3.5 Installed capacity for different reactors during Scenario II . . . 23

4.1 NU and SWUs annual needs for the open cycle scenario . . . 27
4.2 HM annual fluxes for UOX enrichment and fabrication plants in the open cycle scenario . . . 29
4.3 NU and SWUs annual needs for the Pu mono-recycling scenario 30
4.4 Fabricated UOX and MOX annual fluxes for the Pu mono-recycling scenario . . . 31
4.5 UOX fuel isotopic evolution in a PWR . . . 33
4.6 MOX fuel isotopic evolution in a PWR . . . 34
4.7 Heavy Metals (HM) inventory for the Spent Fuel (SF) interim storage in the open cycle scenario . . . 34
4.8 Spent UOX and MOX Fuel inventories generated during the Pu mono-recycling scenario . . . 35
4.9 Reprocessed UOX and recycled Pu annual fluxes for the Pu mono-recycling scenario . . . 36
4.10 Wastes inventory characterized for Pu and MAs produced by a once through fuel management strategy . . . 37
4.11 Wastes inventory characterized for Pu and MAs produced by mono-recycling of Pu scenario evolution . . . 39
4.12 Reprocessed and lost U during the Pu mono-recycling scenario 43

5.1 Estimated world's natural Uranium resources (below 130 USD kg^{-1}) 48

6.1 Goals, Criteria and Metrics for Generation-IV candidates selection 63

7.1 Average lethargy change per elastic collision and moderating power for some typical coolants/moderators 72
7.2 Typical microscopic cross-sections of main fuel isotopes in a LFR compared to the ones of LWRs 74
7.3 Main parameters of the ELSY plant 82

8.1 Preliminary parametric analysis of pin dimension influence on the performances of a 1.10 m high core 88
8.2 Preliminary parametric analysis of pin dimension influence on the performances of a 0.90 m high core 88
8.3 Evolution of the Breeding Ratio (BR) during irradiation in the preliminary ELSY configuration 96
8.4 Equivalent Pu mass during irradiation in the preliminary ELSY configuration 96
8.5 Control systems worth in the ELSY preliminary configuration (at BoL) 98

9.1 Scheme of the 4-batches refueling strategy adopted for ELSY 109
9.2 Plutonium enrichment in the three radial zones of the final ELSY configuration 111
9.3 Criticality evaluations at BoL with MCNP and ERANOS, using JEFF3.1 and ERALIB1 libraries, for the ELSY final configuration 113
9.4 Equivalent Pu mass during irradiation in the final ELSY configuration 114
9.5 Worth of control systems in the ELSY final configuration (at BoL) 116

10.1 Resume of target (T) and source (S) nuclides in the decay and transmutation map of a generic nuclide X_Z^A 123

12.1 One group microscopic cross-sections for the ALFR fuel isotopes 149
12.2 Atom densities in the extended equilibrium ALFR fresh fuel . 150
12.3 Fuel pellet dimensions and corresponding volume fractions in the three zones of the ALFR final configuration 157
12.4 Local-to-average power/FA and coolant outlet temperature for the final ALFR configuration 159
12.5 Scheme of the 3-batches refueling strategy adopted for the ALFR 162
12.6 Worth of ALFR control systems (at BoL) 164

13.1 Installed capacity for different reactors during the final scenario 168
13.2 Standardized reactors data for the scenarios study 169

14.1 NU and SWUs annual needs for the closed fuel cycle scenario 175
14.2 Fabricated UOX and MOX annual fluxes for the closed fuel cycle scenario 176
14.3 MOX fuel isotopic evolution in a ALFR 178
14.4 Spent UOX and MOX Fuel inventories generated during the closed fuel cycle scenario 179
14.5 Reprocessed UOX and recycled MOX annual fluxes for the closed fuel cycle scenario 180
14.6 Wastes inventory characterized for Pu and MAs produced by the closed fuel cycle scenario evolution 181
14.7 Reprocessed and lost U during the Pu mono-recycling scenario 184

15.1 Summary of LFR key issues 192

16.1 Initial and guessed DEMO core parameters 208

17.1 DEMO-600 first option core parameters 212
17.2 DEMO-600 second option core parameters 213
17.3 DEMO-600 third option core parameters 214
17.4 DEMO-600 fourth option core parameters 215
17.5 DEMO-600 fifth option core parameters 216
17.6 DEMO-600 sixth option core parameters 217
17.7 DEMO-600 seventh option core parameters 218
17.8 DEMO-500 first option core parameters 219
17.9 DEMO-500 second option core parameters 220
17.10 DEMO-500 third option core parameters 221
17.11 DEMO-500 fourth option core parameters 222
17.12 Resume of GPS1-2 core configurations main core characteristics and performances 224
17.13 Resume of GPS3-4 core configurations main core characteristics and performances 224
17.14 Scheme of a three-batches cycle hypothesis 225
17.15 Resume of GPS5-6 core configurations main core characteristics and performances 226
17.16 Resume of GPS7-8 core configurations main core characteristics and performances 226
17.17 GPS10 configuration main core characteristics and performances 229
17.18 Control and regulation systems worth 230

A.1 Isotopic composition of actinide vectors 244
A.2 Main actinide dioxides lattice parameters 246
A.3 Chemical composition of the T91 FMS 250

A.4 Chemical compositions of the 316L and 316LN SS 251
A.5 Isotopic compositions of pure Lead 251

C.1 Technological constraints for FASTEF and present values for the XT-ADS-HF configuration 265
C.2 HFC-P1 main core parameters 266
C.3 HFC-P2 main core parameters 267
C.4 HFC-P3 and HFC-P4 main core parameters 267
C.5 HFC-D1 main core parameters 268
C.6 HFC-D2 main core parameters 268
C.7 HFC-D3 main core parameters 269
C.8 HFG-H1 main core parameters 270
C.9 Pros and cons of the proposed flux heighten strategies 270
C.10 HFG-P4D2 main core parameters 271
C.11 HFG-D2H1 main core parameters 271
C.12 HFG-P4D2H1 main core parameters 272

PREFACE

The present thesis describes the work performed during the three-years PhD course in Nuclear Engineering held by the Author at the University of Bologna, in collaboration with the Italian Agency for the New Technologies, Energy and Sustainable Economic Development (ENEA).

Besides the main results here presented, many important concepts have been analyzed, which led the Author far beyond the aimed goals. A thorough reflexion concerning the sustainability issues related to nuclear energy production allowed to formalize the s.c. Adiabatic Reactor Theory – for the definition of a zero-impact reactor to what concerns both the optimal exploitation of Uranium resources and the minimization of the Long Lived Radioisotopes in the High Level Wastes produced by the related fuel cycle – and, consequently, a New Paradigm for Nuclear Power, aimed at designing the core of a nuclear reactor around its adiabaticity feature.

The whole work has been consequently organized so as to guide the reader through the forming process of these innovative concepts. The whole intellective path has been included within the frame of the scenario studies demonstrating the need for adiabatic reactors in order to actually candidate nuclear energy as the most charming and effective energy source for the future, thus making the forthcoming nuclear renaissance come true.

CHAPTER 1

INTRODUCTION

Not fact-finding, but attainment to philosophy is the aim of science.

Martin H. Fischer (1879-1962)

An historical analysis of the human society evolution reveals how the main revolutions followed the discovery of new energy sources: the very first settlements of people started when men learned how to domesticate animals and use these for farming; also the main cities grew where rivers could power the first machines. The industrial revolution, still influencing the present structure of society, has been possible because of the discovery of the steam engine, exploiting directly the power coming from heat generation.

Besides the discovery of new power supplies, energy availability is a main issue for the stability of society: as far as energy provision is not in question, Manhood can rely on all the previous evolution, facing the population increase coupled to the as irrepressible as right aspiration to high wellness standard.

On the other hand, the last decades of the passed century brought up a crucial problem for humanity: to survive despite itself. This "surviving problem", mainly due to the wild usage of natural resources, spoiled the certainties on the indefinite availability of the present energy supplies. Together with the latter, another aspect contributes to the surviving problem: the superficial care spent for wastes management and disposal.

In almost every field many measures have been taken, or at least proposed, to overcome the "surviving problem". The very significant of them are referred to a new way of conceiving, approaching and solving problems instead of continuously trying to improve the "old" ways. In other words, the scientific evolution must be preferred to the merely technological one.

The same scientific approach must be applied also to the energy problem. In this frame it is evident as nuclear energy, with its enormous energy concentration, can (or even must) play a major role, provided it is able to match the environmental requirement embedded in the previous lines, which is what we call sustainability.

Focusing on the surviving questions arising from energy production, two main issues must be faced:

- the limited availability of fossil fuels, which represent the main energy source providing about 81% of the total energy production (2007 data [1]);
- the huge production of greenhouse gases, mainly due to the burning of fossil fuels (about $2.9 \cdot 10^{10}$ t of CO_2, 2007 data [1]).

A combined approach can be envisaged, targeting to an increase of the electricity production for use also in transport and industry, so as to replace the direct use of fossil fuels, together with a stronger penetration of both nuclear (for concentrate electricity production) and renewable (for a distributed production of local electricity needs) energy supplies.

According to world energy production statistics [1], the world production of electric energy (19771 TWh in 2007) corresponds to about 4350 Mtoe,

which is about 36% of the total world energy production. About 68% of this is produced by fossil fuels, 13.8% by nuclear and the remaining fraction (18.2%) by renewables (mainly hydroelectric).

If a stronger penetration of electric energy can be attained, for instance by replacing some 80% of the actual energy consumption for transport (which represents about 28% of the total energy consumption) by electric energy[1], and increasing the nuclear penetration in electric energy production to some 50%, to the detriment of fossil fuels, an overall reduction of about one third of the total greenhouse gases production could be achieved.

Aiming at a significant reduction of greenhouse gases, even claiming the highest renewables availability as possible, nuclear energy represents the only reliable solution to implement such a scenario, provided it is able in its turn to guarantee the required sustainability.

Reactors operating nowadays, mainly Light Water Reactors (LWRs) such as Pressurized Water Reactors (PWRs) and Boiling Water Reactors (BWRs), rely on the s.c. direct fuel cycle. In this scheme, two main issues arise for the sustainability of the present scenario:

- LWRs require Low-Enrichment Uranium (LEU) as input, which is obtained by selectively increasing the content of the ^{235}U fissile isotope with respect to its natural abundance, resulting in a high drawn on the resources because of the wastage of the unused ^{238}U isotope;
- the whole spent fuel is outputted to the final disposal, containing, together with the unused, depleted fuel, both Fission Products (FPs) and TRansUranics (TRUs, *i.e.*, Plutonium and Minor Actinides, MAs).

The former represent the Short-Lived component of High-Level Radioactive Wastes (HLRWs), thus could be easily confined in temporary storages for a reasonable time span (few hundreds years) before being released to the environment as not harmful waste; on the other hand, the latter, characterized by a low decay rate, represent the most problematic component of the waste, to be confined for some hundred thousands years in a geologic repository.

New concept reactors must be therefore envisaged, exploiting an efficient use of Uranium natural resources also by recycling the valuable components of the spent fuel coming from existing reactors, and minimizing - at the same time - the Long-Lived Waste, LLW (*i.e.*, TRUs). According to this, the footprint of such innovative systems would be greatly reduced, extending the availability of this "new-clear" energy source for a longer time horizon, with negligible environmental impact.

[1] For instance, by stimulating rail rather than road transport, and converting the automotive propulsion to electricity or (even if more difficult) hydrogen.

Part I

The Present European Nuclear Scenario

CHAPTER 2

THE NUCLEAR LEGACIES

Il rimorso è per ciò che siamo e fatalmente saremo: non riguarda il passato, ma anche il futuro.

Mario Soldati (1906-1999)

Abstract. The frame for the present scenario studies can be defined only accounting for the availability of detailed information on the nuclear policies and the spent fuel stock inventories.
The definition of representative scenarios can be envisaged only if national policies regarding the penetration of nuclear electricity generation are known. Starting from this data, it is therefore possible to point out the number and typology of reactors to be built and operated, together with the required capacities for national or regional facilities supporting the nuclear fleet.
The stocktaking of the spent fuel legacies also represents a fundamental milestone for scenario studies, defining the amount of waste already collected that can be exploited in a possible scenario envisaging advanced reactors able to fission all the TransUranics, which represent the long lived components of the waste, thus extending the availability of nuclear fuel far beyond the current estimates.

Introduction

Aiming at proving the inadequacy of the present scenario for proposing the nuclear option as the most fascinating candidate for the sustainability of the World's production of energy, the consequences of persevering on the present scenario in the far future (e.g.: up to 2200) will be examined at first.

A detailed preliminary analysis is therefore required, forecasting the evolution of the electric energy demand and accounting for the different nuclear policies dictating the penetration of nuclear power production in every state involved in the analysis.

The legacies accumulated up to now by the operation of the present nuclear reactors will be also accounted for initializing the spent fuel stocks, so as to allow the scenario study for starting from nowadays without missing any information regarding the past nuclear activities.

The western European region will be taken into account as reference frame for the present analysis, mainly because of the easier availability of detailed and reliable data regarding both the past energy production by nuclear, and the future nuclear aims.

2.1 National policies within the western European frame

In order to correctly set up the simulation for the current nuclear scenario, it is required to examine the nuclear policies of the involved countries in the forthcoming future, trying to foresee the penetration of electricity generation by nuclear option according to the present national aims, as well as the necessities coming by the agreement to greenhouse gases emission reduction programs such as the Kyoto protocol.

According to this general scheme, four groups of countries can be therefore identified:

group A refers to countries in a stagnant or phase-out scenario for nuclear energy, which have to manage their spent fuel, and especially the Plutonium and Minor Actinides inventories;

group B refers to countries in a continuation scenario for the nuclear energy, which have to optimize the use of their resources in Plutonium for the future deployment of fast reactors or ADS;

group C (a subset of group A) refers to countries which, after stagnation, envisages a nuclear "renaissance";

group D refers to countries initially with no NPP, which decide to go nuclear.

Among the western European countries, six candidates have been selected for defining the scenario framework because of the availability of detailed information on their nuclear activity (mainly due to their participation to European research programs on Partitioning and Transmutation, P&T). Their grouping according to the nuclear policy they envision is presented in Table 2.1.

Table 2.1: Grouping of European countries according to their national nuclear policy

Country	Group
Belgium	A (C)
France	B
Germany	A
Italy	D
Spain	A
Sweden	A (C)

2.2 Spent Fuel stocks inventory

From the sustainability point of view, a detailed stocktaking of spent fuel legacies is fundamental to point out the mass and radio-toxicity of the waste already accumulated, as well as to detail the inventories in terms of abundances of each isotope: the spent fuel of the present LWRs contains indeed very valuable materials, typically 95% of the Uranium of the fresh fuel and Plutonium with as much energy potential as 25% of the fissile part (^{235}U) of the fresh fuel.

A standard LWR of 1 GWe discharges about 23 t of actinides each year; cumulatively 900 t in 40 years lifetime of the reactor. One ton of spent fuel of average burn-up of 40 GWd t^{-1} contains about 10 kg of Pu and 1.5 kg of the other TransUranium elements (TRUs), mainly Neptunium, Americium and Curium [2, 3]. These TRUs are not only long-lived radiotoxic substances but also major heat sources which affect the performance of the repository. It is predicted that without partitioning and transmutation of transuranium elements, "repository availability may be the major constrain to nuclear energy".

The amount of spent nuclear fuel accumulated in Europe is estimated as 37000 t for year 2000, with additional 2500 t of spent fuel being produced every year [2]. By limiting the present analysis to the six countries listed in the previous section, and assuming 2010 as reference date for beginning the scenario studies, a total amount of some 35000 t can be assumed for the spent fuel stocks, the detailed inventory of which is presented in Table 2.2.

Table 2.2: Initial spent fuel inventories (tons)

	Belgium (2010)	Spain (2010)	France MOX (2010)	France UOX (2010)	France URe (2010)	Sweden (2010)	Germany (2022)
^{234}U	0,53	0,63	0,16	2,27	0,24	0,33	0,44
^{235}U	25,27	21,42	1,64	76,50	2,98	60,41	81,24
^{236}U	14,88	14,37	0,33	55,31	6,10	30,24	40,67
^{238}U	2759,37	2982,59	1177,48	10458,44	319,69	6816,41	9167,16
^{237}Np	1,86	2,10	0,26	7,06	0,49	4,49	6,04
^{238}Pu	0,85	0,72	2,13	3,22	0,27	2,26	3,04
^{239}Pu	19,73	18,84	27,65	65,49	2,08	50,96	68,54
^{240}Pu	8,91	8,29	18,60	30,96	0,94	26,50	35,64
^{241}Pu	3,26	2,17	8,77	13,87	0,44	7,19	9,67
^{242}Pu	2,30	1,91	6,60	9,63	0,27	7,40	9,95
^{244}Pu	0,00	0,00	0,00	0,00	0,00	0,00	0,00
^{241}Am	2,36	2,46	3,99	5,29	0,17	8,88	11,94
^{242}Am^{m}	0,01	0,01	0,03	0,01	0,00	0,02	0,03
^{243}Am	0,55	0,47	1,69	2,19	0,07	1,73	2,32
^{242}Cm	0,00	0,00	0,01	0,02	0,00	0,00	0,00
^{243}Cm	0,00	0,00	0,01	0,01	0,00	0,01	0,01
^{244}Cm	0,16	0,10	0,68	0,70	0,02	0,43	0,58
^{245}Cm	0,02	0,01	0,11	0,05	0,00	0,06	0,08
FPs	134,95	130,93	49,86	518,98	16,22	29,68	39,91
Total	2975	3187	1300	11250	350	7047	9477

CHAPTER 3

PRESENT REGIONAL SCENARIO

I've always thought of fantasy as a genre of best-case scenarios, and horror as a genre of worst-case scenarios.

Brian K. Vaughan (1976)

Abstract. The analysis of the present scenario represents the starting point for the comparative study on the sustainability features of different fuel cycle strategies.
Therefore, a detailed and accurate scenario model has been set up so as to carefully represent the nuclear reactors fleet of interest.
The work reported in the present and in the next chapters represents also part of the ENEA contribution to the OECD/NEA (Organization for Economic Co-operation and Development/Nuclear Energy Agency) Working Party on Scientific Issues of the Fuel Cycle (WPFC).

Introduction

Scenario studies are extremely powerful and flexible tools for analyzing the evolution of the batches feeding and discharged by a real reactors fleet, including all the facilities required for correctly serving the Nuclear Power Plants (NPPs) operating.

Aiming at describing the organization of a complex system, the logic of the scenario to be simulated (scopes, features, constraints) have to be pointed out in order at first to take into account the overall environment of interest. Then, a realistic model of the reference scenario is to be set up, considering the reactors fleet, the auxiliary facilities and the specific batches exchanged among all those actors.

In detail, the facilities defining the system have to be organized following the logic of material streams: since the main object of scenario analysis is the study of the materials fluxes both needed (incoming stream) and produced (outgoing stream) by the reactors of a regional energetic system, proper paths must be identified, each one representing a specific material stream, and all the involved facilities introduced according to the paths scheme (as shown in the sample path of Figure 3.1).

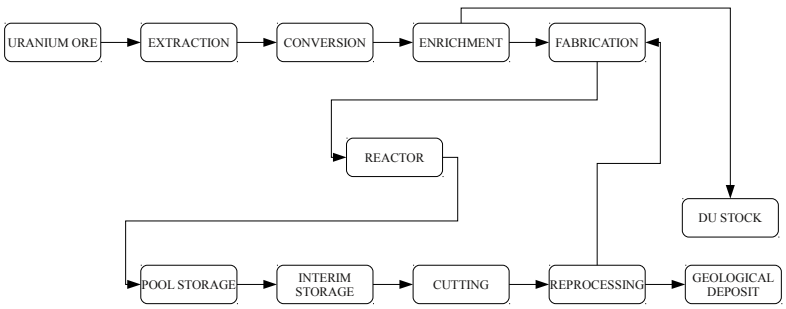

Figure 3.1: Example of material path in a typical scenario simulation.

3.1 Fuel management strategy

In order to reduce the amount of long lived radioactive materials sent to the final disposal a process of separation and recycling, typical of many other industries, has been proposed. This methodology is generically described as Partitioning and Transmutation (P&T). The first step is to separate, or partition, the spent fuel into different components according to its final use or disposal requirements. Different options are considered for combinations but the basic components are:

- the irradiated Uranium, with large mass and volume, low specific radioactivity and thermal load and large energetic potential;
- the TRUs, very small fraction of the total, very radioactive, with very long half-lives and high thermal load, high energetic potential and proliferation attractive;
- some selected short lived fission fragments, the Cs and Sr, that include the isotopes (^{137}Cs and ^{90}Sr) producing most of the thermal load of the spent fuel for the first hundred years; they are very radioactive during 300 years but of low activity and mass afterward;
- some selected long lived fission fragments, the I and Tc, representing the largest contribution to the radio-toxicity at very long term after the actinides and some of the isotopes mainly responsible for the dose at long term from the geological disposal; they are a small fraction of the total, with very low specific radioactivity and thermal load;
- the rest of fission fragments, very radioactive and with relevant thermal loads at very short times, but with small specific radioactivity and thermal load after hundred years;
- the activated structural materials and other intermediate level wastes, of high volume, low specific thermal load and a specific activity that can be low or medium depending on technological choices.

After this partitioning some of these groups will be recycled in normal or advanced reactors (including sub-critical ADS). In these reactors the actinides (U, Np, Pu, Am, Cm, ...) are fissioned becoming fission fragments or converted in other actinides, that is: they had been transmuted. The spent fuel from this transmutation normally still contains significant amounts of actinides and it is necessary to repeat the Partitioning and Transmutation steps several times. In addition, the parasitic transmutation of the selected long-lived fission fragments could be done by neutron capture in these advanced reactors.

According to the aims of the present study, no advanced reactor is envisaged, accounting therefore only for present Generation systems. In terms of

P&T strategies, this means that only limited sustainability capabilities can be exploited in MOX LWRs. Nevertheless, the use of this kind of reactors, already available, allows for both

- a reduction of the Uranium input, by substituting the ^{235}U fissile (which requires large NU fluxes for sustaining the required enrichment process) with reactor grade Pu; and
- the management of a part of the spent fuel inventories by recycling part of the Pu legacies.

3.2 Scenario model

Two scenarios have been selected for investigating the consequences due to the evolution of the present reactors fleet up to the end of the present century:

1. the first one foresees the use of standard, UOX-fueled Pressurized Water Reactors (PWRs), therefore maintaining unaltered the present open fuel cycle strategy;
2. the second scenario represents a slight evolution of the former one, foreseeing the adoption, together with the standard UOX-PWRs, also of MOX-fueled PWRs in order to implement a Pu mono-recycling strategy.

Two standardized reactors have been considered in the present analysis, representing the UOX-PWR and the MOX-PWR respectively. The exact specification parameters for each type of reactor, as required by the COSI6 code [4] used for the simulations, are presented in Table 3.1.

The UOX fuel, whose composition is presented in Table 3.2, is organized in standard 17 x 17 rods FRAGEMA type FAs, with 264 fuel rods and no extra water hole.

The MOX fuel, whose composition is presented in Table 3.3, is organized in the same standard FA type as UOX in the previous case.

The evolution of the fuel in a scenario simulation with COSI is accounted by the CESAR BU code [5]. This module implements all the routines necessary to study the evolution of a set of isotopes according to the well-known Bateman problem [6] (see also Chapter 10 for further details), both during in-pile irradiation and ex-core radioactive decay. All the specific information needed to define the peculiarities of each reactor are defined in a database of libraries ("Bibliothèque", BBL). Every library is created starting from the results of a BU calculation performed *a priori* with a compatible neutronics deterministic code (such as ERANOS [7]): the BU analysis characterizes indeed, for each specific system operating at a given power, the neutron flux and its energy spectrum as a function of time, thus all the information needed

Table 3.1: Standardized reactors data for the scenarios study

	UOX PWR	**MOX PWR**
Fuels		
Burn Up [GWd t_{HM}^{-1}]	60	60
Minimum cooling time [y]	5	5
Fabrication time [y]	2	2
Fresh fuel ^{235}U enrichment [$^{w}/_{0}$]	4.95	0.226
Fresh fuel Pu "enrichment" [$^{w}/_{0}$]	-	9.026
Moderation ratio	2	2
Cores		
Electrical nominal power [GW]	1.5	1.5
Efficiency [%]	34	34
Production factor [%]	76	76
Heavy metal mass [t]	128.9	128.9
Cycle length [EFPD]	410	410
Core management	1/4	1/4

Table 3.2: Initial composition for UOX fuel

Nuclide	[$^{w}/_{0}$]
^{234}U	0.0445
^{235}U	4.95
^{238}U	95.0055

Table 3.3: Initial composition for MOX fuel

Nuclide	[$^{w}/_{0}$]
^{235}U	0.2056
^{238}U	90.7684
^{238}Pu	0.2816
^{239}Pu	4.6565
^{240}Pu	2.1951
^{241}Pu	1.0606
^{242}Pu	0.7257
^{241}Am	0.1065

for the solution of the Bateman equations (that is: integral flux level and one-group microscopic cross-sections responsible for isotopes transmutation and fission).

In particular, the COSI6 version used (v. 2.0.4) includes the CESAR4 BU code, version 4.3. Among the available libraries to such code, the following ones have been chosen for the two fuels/reactors:

- "UOX 4" BBL for UOX PWR;
- "MOXP 800" BBL for MOX PWR.

A graphical representation of the two scenario models, highlighting the implemented facilities and the mass fluxes, is given in Figures 3.2 and 3.3.

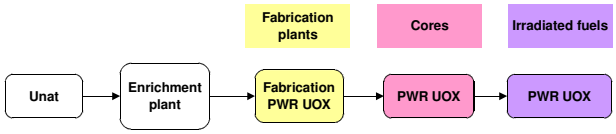

Figure 3.2: Representation of the mass fluxes and installed facilities in the first scenario (open cycle).

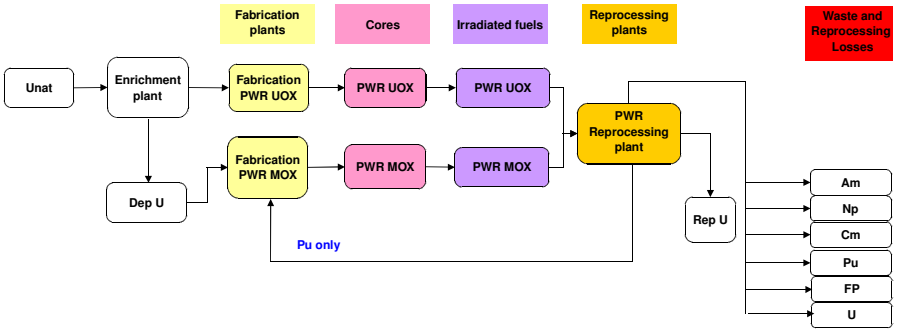

Figure 3.3: Representation of the mass fluxes and installed facilities in the second scenario (Pu mono-recycling in LWRs).

For the last scenario, the reprocessing plant required for feeding the MOX PWRs separates both the U and Pu isotopes from the spent fuel of the UOX PWRs fleet in a First-In-First-Out (FIFO) batches reprocessing order. A typical net separation efficiency of 99.9% is assumed: hence, 0.1% of the reprocessed masses is lost to the geological repository.

3.3 Energy demand forecast

In order to foresee the nuclear energy production up to the end of the present century, three main considerations have to be taken into account:

- the present nuclear capacities of the countries involved in the present analysis;

- the anticipation of the electric energy demand; and
- the national policies defining the aims of nuclear penetration in the energy frame.

Focusing on the selected reference region, a very moderate increase in the energy demand can be expected in the whole century, assumed as an average trend of strong local expansion and recession periods (that is: assuming the trend of the past 10 years as a cyclical phase, repeating quite regularly over an overall moderate expansion trend).

Combining the overall energy trend with the evolution of the installed nuclear capacity, according to the national policies, it is possible to suppose that the present installed power, *sim* 100 GWe as shown in Table 3.4, will remain constant along the century, ensuring an annual production of 670 TWhe (under the hypothesis of an average 76% constant load factor).

Table 3.4: Number of NPPs installed in the selected countries and corresponding electric capacity

Country	NPPs	Capacity [MWe]
Belgium	7	5863
France	58	63130
Germany	17	20470
Italy	0	0
Spain	8	7450
Sweden	10	8992
Total	100	105905

Under this main assumption, the temporal evolution of the first scenario can be retrieved assuming a constant number of standardized UOX PWRs are installed for the whole scenario period, as depicted in Figure 3.4.

The temporal evolution of the second scenario is depicted in Figure 3.5 and explained in Table 3.5. It is assumed that, under the same common assumption of constant installed electric capacity, a number of MOX PWRs are progressively (*i.e.*, with a linear variation) introduced during an initial transitory period. The saturation of the Pu recycling capacity has been preliminary evaluated for a fleet composed by MOX PWRs for some 10%.

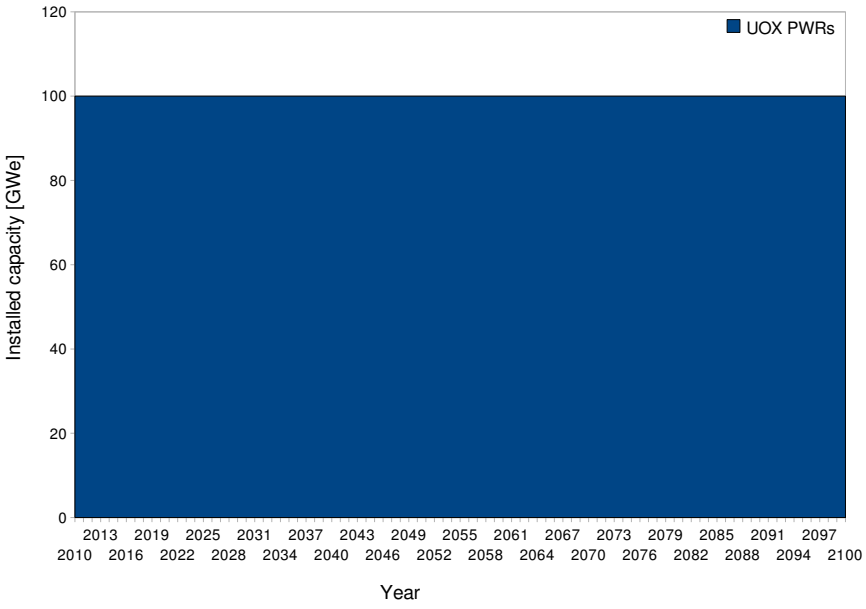

Figure 3.4: Time evolution of the first scenario benchmark case (open cycle).

Table 3.5: Installed capacity for different reactors during Scenario II

Year	UOX PWRs [GWe]	MOX PWRs [GWe]
2010	100	0
2013	90	10
2100	90	10

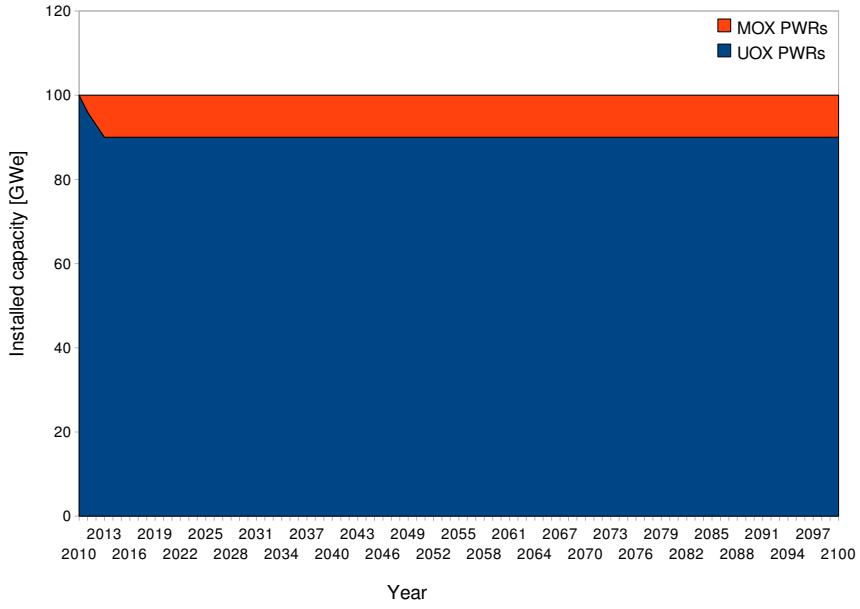

Figure 3.5: Time evolution of the second scenario benchmark case (mono-recycling of Pu).

CHAPTER 4

SCENARIO RESULTS

I believe there is no philosophical high-road in science, with epistemological signposts. No, we are in a jungle and find our way by trial and error, building our road behind us as we proceed.

Max Born (1882-1970)

Abstract. The results of the present scenario must be thoroughly analyzed in order to retrieve reference sustainability parameters for the comparative analysis of possible scenarios.
The main information on sustainability related issues have been retrieved measuring both front- and back-end observables such as the natural Uranium resources exploitation and the long-lived radioisotopes inventory in the spent fuel.
The scenario study results here presented have been also reported, on behalf of ENEA, to the OECD/NEA WPFC as benchmark cases for assessing international capabilities and code features in order to conduce collaborative advanced scenario studies.

Introduction

The sustainability performances of the present scenario, together with a possible variation achievable by means of currently available reactors, are here presented. The analysis moves from the results of the two corresponding scenario simulations to focus on some environment- and overall economy-related issues.

The exploitation of Uranium natural resources for the reference scenario are examined and compared with the ones of the second case study, implementing Pu mono-recycling in present-Generation LWRs. A similar analysis is then performed also regarding the outcomes of the two scenarios in terms of Spent Fuel (SF) masses and their isotopic characterization. Finally, within the overall scenario frame, the capacities required for the boundary facilities to support the scenario are also investigated.

The aim of this detailed analysis is the definition of the overall sustainability performances for the present scenario, to be assumed as reference for evaluating the improvements brought by more sophisticated and evolved scenarios implementing new-Generation nuclear energy systems.

4.1 Overall environmental and economical performances

For the UOX open cycle in traditional PWRs, the NU consumption (and, therefore, the corresponding enrichment Separative Working Units (SWUs) need) is the highest of the two cases. The annual NU outcome and the related SWUs required are shown in Table 4.1.

Table 4.1: NU and SWUs annual needs for the open cycle scenario

Year	NU needs [t y^{-1}]	SWU needs [SWU y^{-1}]	Year	NU needs [t y^{-1}]	SWU needs [t y^{-1}]
-2	2.192E+04	1.678E+07	7	0.000E+00	0.000E+00
-1	2.192E+04	1.678E+07	8	2.192E+04	1.678E+07
0	2.192E+04	1.678E+07	9	2.192E+04	1.678E+07
1	0.000E+00	0.000E+00	10	0.000E+00	0.000E+00
2	2.192E+04	1.678E+07	11	2.192E+04	1.678E+07
3	2.192E+04	1.678E+07	12	2.192E+04	1.678E+07
4	0.000E+00	0.000E+00	13	0.000E+00	0.000E+00
5	2.192E+04	1.678E+07	14	2.192E+04	1.678E+07
6	2.192E+04	1.678E+07	15	2.192E+04	1.678E+07

Year	NU needs [t y^{-1}]	SWU needs [SWU y^{-1}]	Year	NU needs [t y^{-1}]	SWU needs [t y^{-1}]
16	0.000E+00	0.000E+00	54	2.192E+04	1.678E+07
17	2.192E+04	1.678E+07	55	2.192E+04	1.678E+07
18	2.192E+04	1.678E+07	56	0.000E+00	0.000E+00
19	0.000E+00	0.000E+00	57	2.192E+04	1.678E+07
20	2.192E+04	1.678E+07	58	2.192E+04	1.678E+07
21	2.192E+04	1.678E+07	59	0.000E+00	0.000E+00
22	0.000E+00	0.000E+00	60	2.192E+04	1.678E+07
23	2.192E+04	1.678E+07	61	2.192E+04	1.678E+07
24	2.192E+04	1.678E+07	62	2.192E+04	1.678E+07
25	0.000E+00	0.000E+00	63	0.000E+00	0.000E+00
26	2.192E+04	1.678E+07	64	2.192E+04	1.678E+07
27	2.192E+04	1.678E+07	65	2.192E+04	1.678E+07
28	0.000E+00	0.000E+00	66	0.000E+00	0.000E+00
29	2.192E+04	1.678E+07	67	2.192E+04	1.678E+07
30	2.192E+04	1.678E+07	68	2.192E+04	1.678E+07
31	2.192E+04	1.678E+07	69	0.000E+00	0.000E+00
32	0.000E+00	0.000E+00	70	2.192E+04	1.678E+07
33	2.192E+04	1.678E+07	71	2.192E+04	1.678E+07
34	2.192E+04	1.678E+07	72	0.000E+00	0.000E+00
35	0.000E+00	0.000E+00	73	2.192E+04	1.678E+07
36	2.192E+04	1.678E+07	74	2.192E+04	1.678E+07
37	2.192E+04	1.678E+07	75	0.000E+00	0.000E+00
38	0.000E+00	0.000E+00	76	2.192E+04	1.678E+07
39	2.192E+04	1.678E+07	77	2.192E+04	1.678E+07
40	2.192E+04	1.678E+07	78	0.000E+00	0.000E+00
41	0.000E+00	0.000E+00	79	2.192E+04	1.678E+07
42	2.192E+04	1.678E+07	80	2.192E+04	1.678E+07
43	2.192E+04	1.678E+07	81	0.000E+00	0.000E+00
44	0.000E+00	0.000E+00	82	2.192E+04	1.678E+07
45	2.192E+04	1.678E+07	83	2.192E+04	1.678E+07
46	2.192E+04	1.678E+07	84	0.000E+00	0.000E+00
47	0.000E+00	0.000E+00	85	2.192E+04	1.678E+07
48	2.192E+04	1.678E+07	86	2.192E+04	1.678E+07
49	2.192E+04	1.678E+07	87	0.000E+00	0.000E+00
50	0.000E+00	0.000E+00	88	2.192E+04	1.678E+07
51	2.192E+04	1.678E+07	89	2.192E+04	1.678E+07
52	2.192E+04	1.678E+07	90	0.000E+00	0.000E+00
53	0.000E+00	0.000E+00			

The corresponding enrichment and fabrication plants mass flows are listed in Table 4.2.

Table 4.2: HM annual fluxes for UOX enrichment and fabrication plants in the open cycle scenario

Year	Enr. Plant [t y^{-1}]	Fabr. Plant [t y^{-1}]	Year	Enr. Plant [t y^{-1}]	Fabr. Plant [t y^{-1}]	Year	Enr. Plant [t y^{-1}]	Fabr. Plant [t y^{-1}]	Year	Enr. Plant [t y^{-1}]	Fabr. Plant [t y^{-1}]
-2	2.148E+03	0.000E+00	22	0.000E+00	2.148E+03	46	2.148E+03	0.000E+00	70	2.148E+03	2.148E+03
-1	2.148E+03	0.000E+00	23	2.148E+03	2.148E+03	47	0.000E+00	2.148E+03	71	2.148E+03	0.000E+00
0	2.148E+03	2.148E+03	24	2.148E+03	0.000E+00	48	2.148E+03	2.148E+03	72	0.000E+00	2.148E+03
1	0.000E+00	2.148E+03	25	0.000E+00	2.148E+03	49	2.148E+03	0.000E+00	73	2.148E+03	2.148E+03
2	2.148E+03	2.148E+03	26	2.148E+03	2.148E+03	50	0.000E+00	2.148E+03	74	2.148E+03	0.000E+00
3	2.148E+03	0.000E+00	27	2.148E+03	0.000E+00	51	2.148E+03	2.148E+03	75	0.000E+00	2.148E+03
4	0.000E+00	2.148E+03	28	0.000E+00	2.148E+03	52	2.148E+03	0.000E+00	76	2.148E+03	2.148E+03
5	2.148E+03	2.148E+03	29	2.148E+03	2.148E+03	53	0.000E+00	2.148E+03	77	2.148E+03	0.000E+00
6	2.148E+03	0.000E+00	30	2.148E+03	0.000E+00	54	2.148E+03	2.148E+03	78	0.000E+00	2.148E+03
7	0.000E+00	2.148E+03	31	2.148E+03	2.148E+03	55	2.148E+03	0.000E+00	79	2.148E+03	2.148E+03
8	2.148E+03	2.148E+03	32	0.000E+00	2.148E+03	56	0.000E+00	2.148E+03	80	2.148E+03	0.000E+00
9	2.148E+03	0.000E+00	33	2.148E+03	2.148E+03	57	2.148E+03	2.148E+03	81	0.000E+00	2.148E+03
10	0.000E+00	2.148E+03	34	2.148E+03	0.000E+00	58	2.148E+03	0.000E+00	82	2.148E+03	2.148E+03
11	2.148E+03	2.148E+03	35	0.000E+00	2.148E+03	59	0.000E+00	2.148E+03	83	2.148E+03	0.000E+00
12	2.148E+03	0.000E+00	36	2.148E+03	2.148E+03	60	2.148E+03	2.148E+03	84	0.000E+00	2.148E+03
13	0.000E+00	2.148E+03	37	2.148E+03	0.000E+00	61	2.148E+03	0.000E+00	85	2.148E+03	2.148E+03
14	2.148E+03	2.148E+03	38	0.000E+00	2.148E+03	62	2.148E+03	2.148E+03	86	2.148E+03	0.000E+00
15	2.148E+03	0.000E+00	39	2.148E+03	2.148E+03	63	0.000E+00	2.148E+03	87	0.000E+00	2.148E+03
16	0.000E+00	2.148E+03	40	2.148E+03	0.000E+00	64	2.148E+03	2.148E+03	88	2.148E+03	2.148E+03
17	2.148E+03	2.148E+03	41	0.000E+00	2.148E+03	65	2.148E+03	0.000E+00	89	2.148E+03	0.000E+00
18	2.148E+03	0.000E+00	42	2.148E+03	2.148E+03	66	0.000E+00	2.148E+03	90	0.000E+00	2.148E+03
19	0.000E+00	2.148E+03	43	2.148E+03	0.000E+00	67	2.148E+03	2.148E+03			
20	2.148E+03	2.148E+03	44	0.000E+00	2.148E+03	68	2.148E+03	0.000E+00			
21	2.148E+03	0.000E+00	45	2.148E+03	2.148E+03	69	0.000E+00	2.148E+03			

The second scenario represents a slight evolution, towards sustainability, of the previous one, with the introduction of several MOX PWRs for the mono-recycling of the Plutonium produced in the traditional UOX PWRs. As expected, the NU consumption and, therefore, the enrichment SWUs needed, can be a little reduced with respect to the open cycle case, to ensure the same electrical production. Table 4.3 summarizes the annual NU and SWUs needs for the Pu mono-recycling scenario.

Table 4.3: NU and SWUs annual needs for the Pu mono-recycling scenario

Year	NU needs [t y^{-1}]	SWU needs [SWU y^{-1}]	Year	NU needs [t y^{-1}]	SWU needs [t y^{-1}]
-2	2.192E+04	1.678E+07	35	0.000E+00	0.000E+00
-1	2.137E+04	1.638E+07	36	1.972E+04	1.511E+07
0	2.027E+04	1.553E+07	37	1.972E+04	1.511E+07
1	0.000E+00	0.000E+00	38	0.000E+00	0.000E+00
2	1.972E+04	1.511E+07	39	1.972E+04	1.511E+07
3	1.972E+04	1.511E+07	40	1.972E+04	1.511E+07
4	0.000E+00	0.000E+00	41	0.000E+00	0.000E+00
5	1.972E+04	1.511E+07	42	1.972E+04	1.511E+07
6	1.972E+04	1.511E+07	43	1.972E+04	1.511E+07
7	0.000E+00	0.000E+00	44	0.000E+00	0.000E+00
8	1.972E+04	1.511E+07	45	1.972E+04	1.511E+07
9	1.972E+04	1.511E+07	46	1.972E+04	1.511E+07
10	0.000E+00	0.000E+00	47	0.000E+00	0.000E+00
11	1.972E+04	1.511E+07	48	1.972E+04	1.511E+07
12	1.972E+04	1.511E+07	49	1.972E+04	1.511E+07
13	0.000E+00	0.000E+00	50	0.000E+00	0.000E+00
14	1.972E+04	1.511E+07	51	1.972E+04	1.511E+07
15	1.972E+04	1.511E+07	52	1.972E+04	1.511E+07
16	0.000E+00	0.000E+00	53	0.000E+00	0.000E+00
17	1.972E+04	1.511E+07	54	1.972E+04	1.511E+07
18	1.972E+04	1.511E+07	55	1.972E+04	1.511E+07
19	0.000E+00	0.000E+00	56	0.000E+00	0.000E+00
20	1.972E+04	1.511E+07	57	1.972E+04	1.511E+07
21	1.972E+04	1.511E+07	58	1.972E+04	1.511E+07
22	0.000E+00	0.000E+00	59	0.000E+00	0.000E+00
23	1.972E+04	1.511E+07	60	1.972E+04	1.511E+07
24	1.972E+04	1.511E+07	61	1.972E+04	1.511E+07
25	0.000E+00	0.000E+00	62	1.972E+04	1.511E+07
26	1.972E+04	1.511E+07	63	0.000E+00	0.000E+00
27	1.972E+04	1.511E+07	64	1.972E+04	1.511E+07
28	0.000E+00	0.000E+00	65	1.972E+04	1.511E+07
29	1.972E+04	1.511E+07	66	0.000E+00	0.000E+00
30	1.972E+04	1.511E+07	67	1.972E+04	1.511E+07
31	1.972E+04	1.511E+07	68	1.972E+04	1.511E+07
32	0.000E+00	0.000E+00	69	0.000E+00	0.000E+00
33	1.972E+04	1.511E+07	70	1.972E+04	1.511E+07
34	1.972E+04	1.511E+07	71	1.972E+04	1.511E+07

Year	NU needs [t y^{-1}]	SWU needs [SWU y^{-1}]	Year	NU needs [t y^{-1}]	SWU needs [t y^{-1}]
72	0.000E+00	0.000E+00	82	1.972E+04	1.511E+07
73	1.972E+04	1.511E+07	83	1.972E+04	1.511E+07
74	1.972E+04	1.511E+07	84	0.000E+00	0.000E+00
75	0.000E+00	0.000E+00	85	1.972E+04	1.511E+07
76	1.972E+04	1.511E+07	86	1.972E+04	1.511E+07
77	1.972E+04	1.511E+07	87	0.000E+00	0.000E+00
78	0.000E+00	0.000E+00	88	1.972E+04	1.511E+07
79	1.972E+04	1.511E+07	89	1.972E+04	1.511E+07
80	1.972E+04	1.511E+07	90	0.000E+00	0.000E+00
81	0.000E+00	0.000E+00			

The corresponding annual fluxes for both the UOX and MOX fabrication plants are collected in Table 4.4.

Table 4.4: Fabricated UOX and MOX annual fluxes for the Pu mono-recycling scenario

Year	UOX [t y^{-1}]	MOX [t y^{-1}]	Year	UOX [t y^{-1}]	MOX [t y^{-1}]
-2	0.000E+00	0.000E+00	27	0.000E+00	7.400E+01
-1	0.000E+00	0.000E+00	28	1.933E+03	1.277E+02
0	2.148E+03	1.611E+02	29	1.933E+03	1.611E+02
1	2.095E+03	2.148E+02	30	0.000E+00	7.400E+01
2	1.987E+03	1.611E+02	31	1.933E+03	1.277E+02
3	0.000E+00	1.074E+02	32	1.933E+03	1.813E+02
4	1.933E+03	1.611E+02	33	1.933E+03	1.611E+02
5	1.933E+03	1.611E+02	34	0.000E+00	7.400E+01
6	0.000E+00	1.074E+02	35	1.933E+03	1.277E+02
7	1.933E+03	1.611E+02	36	1.933E+03	1.611E+02
8	1.933E+03	1.611E+02	37	0.000E+00	7.400E+01
9	0.000E+00	3.877E+01	38	1.933E+03	1.277E+02
10	1.933E+03	0.000E+00	39	1.933E+03	1.611E+02
11	1.933E+03	1.611E+02	40	0.000E+00	7.400E+01
12	0.000E+00	9.403E+01	41	1.933E+03	1.277E+02
13	1.933E+03	1.427E+02	42	1.933E+03	1.611E+02
14	1.933E+03	1.611E+02	43	0.000E+00	7.400E+01
15	0.000E+00	7.902E+01	44	1.933E+03	1.277E+02
16	1.933E+03	1.277E+02	45	1.933E+03	1.611E+02
17	1.933E+03	1.611E+02	46	0.000E+00	7.400E+01
18	0.000E+00	7.400E+01	47	1.933E+03	1.277E+02
19	1.933E+03	1.277E+02	48	1.933E+03	1.611E+02
20	1.933E+03	1.611E+02	49	0.000E+00	7.400E+01
21	0.000E+00	7.400E+01	50	1.933E+03	1.277E+02
22	1.933E+03	1.277E+02	51	1.933E+03	1.611E+02
23	1.933E+03	1.611E+02	52	0.000E+00	7.400E+01
24	0.000E+00	7.400E+01	53	1.933E+03	1.277E+02
25	1.933E+03	1.277E+02	54	1.933E+03	1.611E+02
26	1.933E+03	1.611E+02	55	0.000E+00	7.400E+01

Year	UOX [t y^{-1}]	MOX [t y^{-1}]	Year	UOX [t y^{-1}]	MOX [t y^{-1}]
56	1.933E+03	1.277E+02	74	0.000E+00	7.400E+01
57	1.933E+03	1.611E+02	75	1.933E+03	1.277E+02
58	0.000E+00	7.400E+01	76	1.933E+03	1.611E+02
59	1.933E+03	1.277E+02	77	0.000E+00	7.400E+01
60	1.933E+03	1.611E+02	78	1.933E+03	1.277E+02
61	0.000E+00	7.400E+01	79	1.933E+03	1.611E+02
62	1.933E+03	1.277E+02	80	0.000E+00	7.400E+01
63	1.933E+03	1.813E+02	81	1.933E+03	1.277E+02
64	1.933E+03	1.611E+02	82	1.933E+03	1.611E+02
65	0.000E+00	7.400E+01	83	0.000E+00	7.400E+01
66	1.933E+03	1.277E+02	84	1.933E+03	1.277E+02
67	1.933E+03	1.611E+02	85	1.933E+03	1.611E+02
68	0.000E+00	7.400E+01	86	0.000E+00	7.400E+01
69	1.933E+03	1.277E+02	87	1.933E+03	1.277E+02
70	1.933E+03	1.611E+02	88	1.933E+03	1.611E+02
71	0.000E+00	7.400E+01	89	0.000E+00	7.400E+01
72	1.933E+03	1.277E+02	90	1.933E+03	1.277E+02
73	1.933E+03	1.611E+02			

Comparing the two tables, the net difference in the NU and enrichment SWU needs is directly imputable to the use of MOX PWRs. However, their use, desirable according to this very preliminary analysis, is limited by the availability of the Plutonium necessary to feed them. Only a limited number of traditional UOX PWRs (10% in the present simulation) can be therefore commuted in MOX PWRs, resulting in a poorly effective solution for the reduction of the NU needs.

4.2 Mass fluxes and inventories evolution

The second point for the sustainability analysis of the Pu mono-recycling scenario with respect to the traditional, open cycle present one, regards the production of long lived wastes and their accumulation in the spent fuel repositories.

At first, the evolution of both the UOX and MOX fuels during irradiation and some cooling (the results refer to 5 y cooling, which is the minimum decay period before reprocessing) is considered, assuming in both cases the same reactor (as indicated in the scenario specifications presented in the previous Chapter).

Under such hypotheses, the obtained results are presented in the following Tables 4.5 and 4.6.

Table 4.5: UOX fuel isotopic evolution in a PWR

Isotope	BoL [g t_{HM}^{-1}]	EoL [g t_{HM}^{-1}]	5 y cooling [g t_{HM}^{-1}]
^{232}U	0.000E+00	2.778E-03	3.674E-03
^{234}U	4.450E+02	2.202E+02	2.156E+02
^{235}U	4.950E+04	7.737E+03	7.592E+03
^{236}U	0.000E+00	6.828E+03	6.877E+03
^{238}U	9.501E+05	9.084E+05	9.091E+05
^{236}Pu	0.000E+00	3.804E-03	1.043E-03
^{238}Pu	0.000E+00	5.994E+02	4.915E+02
^{239}Pu	0.000E+00	6.598E+03	6.375E+03
^{240}Pu	0.000E+00	3.095E+03	3.111E+03
^{241}Pu	0.000E+00	2.032E+03	1.563E+03
^{242}Pu	0.000E+00	1.123E+03	1.127E+03
^{241}Am	0.000E+00	1.407E+02	4.711E+02
^{242}Am^{m}	0.000E+00	1.534E+00	1.352E+00
^{243}Am	0.000E+00	3.722E+02	2.938E+02
^{237}Np	0.000E+00	9.151E+02	9.018E+02
^{242}Cm	0.000E+00	1.270E+01	2.562E-02
^{243}Cm	0.000E+00	1.338E+00	1.737E+00
^{244}Cm	0.000E+00	1.720E+02	1.226E+02
^{245}Cm	0.000E+00	1.201E+01	1.046E+01
^{246}Cm	0.000E+00	3.045E+00	1.458E+00
^{247}Cm	0.000E+00	0.000E+00	0.000E+00
^{248}Cm	0.000E+00	0.000E+00	0.000E+00

Comparing the two tables two main results can be immediately pointed out:

1. about one tenth of Uranium is required to produce the MOX fuel with respect to an equivalent quantity of UOX fuel (since 1 t of a 4.95 $^{a}/_{0}{}^{235}$U-enriched UOX requires about 9.6 t of NU, assuming the associated DU has a 0.226 $^{a}/_{0}{}^{235}$U residual enrichment);

2. a higher content of MAs (in particular, higher Am and Cm contents) is present in the spent MOX fuel than in the UOX one, since the initial higher amount of Pu; including also the residual Pu in the HLW inventory, a MOX-loaded PWR discharges a quantity of HLW higher than that resulting from an equivalent UOX-loaded PWR by a factor ~ 4.45.

It is therefore clear how the adoption of MOX PWRs, even representing a possible solution for reducing the natural U resources exploitation, presents an immediate drawback concerning the production of TRUs, which are the main responsible for the long-term activity of the spent fuel to be managed.

After this preliminary evaluations, the details of the mass fluxes resulting from the two scenarios are taken into account.

Table 4.6: MOX fuel isotopic evolution in a PWR

Isotope	BoL [g t_{HM}^{-1}]	EoL [g t_{HM}^{-1}]	5 y cooling [g t_{HM}^{-1}]
^{232}U	0.000E+00	4.220E-04	8.636E-04
^{234}U	0.000E+00	1.100E+02	2.316E+02
^{235}U	2.056E+03	8.490E+02	8.563E+02
^{236}U	0.000E+00	2.530E+02	2.704E+02
^{238}U	9.077E+05	8.730E+05	8.733E+05
^{236}Pu	0.000E+00	6.920E-04	2.047E-04
^{238}Pu	2.816E+03	3.140E+03	3.174E+03
^{239}Pu	4.657E+04	1.910E+04	1.910E+04
^{240}Pu	2.195E+04	1.750E+04	1.762E+04
^{241}Pu	1.061E+04	1.000E+04	7.871E+03
^{242}Pu	7.257E+03	8.460E+03	8.463E+03
^{241}Am	1.065E+03	1.940E+03	3.789E+03
^{242}Am^{m}	0.000E+00	3.970E+01	3.875E+01
^{243}Am	0.000E+00	2.600E+03	2.601E+03
^{237}Np	0.000E+00	1.550E+02	1.965E+02
^{242}Cm	0.000E+00	1.450E+02	1.841E-01
^{243}Cm	0.000E+00	1.670E+01	1.492E+01
^{244}Cm	0.000E+00	1.620E+03	1.345E+03
^{245}Cm	0.000E+00	2.060E+02	2.060E+02
^{246}Cm	0.000E+00	2.120E+01	2.122E+01
^{247}Cm	0.000E+00	0.000E+00	0.000E+00
^{248}Cm	0.000E+00	0.000E+00	0.000E+00

Tables 4.7 and 4.8 present the Heavy Metals (HM) inventory within the UOX (and MOX) Spent Fuel (SF) interim storages during the period of scenario study.

Table 4.7: Heavy Metals (HM) inventory for the Spent Fuel (SF) interim storage in the open cycle scenario

Year	SF inventory [t]	Year	SF inventory [t]	Year	SF inventory [t]
-2	2.724E+04	11	4.443E+04	24	7.320E+04
-1	2.724E+04	12	5.601E+04	25	7.320E+04
0	2.939E+04	13	5.601E+04	26	7.535E+04
1	2.939E+04	14	5.816E+04	27	7.750E+04
2	3.154E+04	15	6.031E+04	28	7.965E+04
3	3.369E+04	16	6.031E+04	29	7.965E+04
4	3.369E+04	17	6.246E+04	30	8.180E+04
5	3.584E+04	18	6.461E+04	31	8.395E+04
6	3.798E+04	19	6.461E+04	32	8.395E+04
7	3.798E+04	20	6.676E+04	33	8.610E+04
8	4.013E+04	21	6.890E+04	34	8.825E+04
9	4.228E+04	22	6.890E+04	35	8.825E+04
10	4.228E+04	23	7.105E+04	36	9.038E+04

Year	SF inventory [t]	Year	SF inventory [t]	Year	SF inventory [t]
37	9.253E+04	55	1.183E+05	73	1.441E+05
38	9.253E+04	56	1.183E+05	74	1.462E+05
39	9.468E+04	57	1.205E+05	75	1.462E+05
40	9.683E+04	58	1.226E+05	76	1.484E+05
41	9.683E+04	59	1.248E+05	77	1.505E+05
42	9.898E+04	60	1.248E+05	78	1.505E+05
43	1.011E+05	61	1.269E+05	79	1.527E+05
44	1.011E+05	62	1.291E+05	80	1.548E+05
45	1.033E+05	63	1.291E+05	81	1.548E+05
46	1.054E+05	64	1.312E+05	82	1.570E+05
47	1.054E+05	65	1.333E+05	83	1.591E+05
48	1.076E+05	66	1.333E+05	84	1.591E+05
49	1.097E+05	67	1.355E+05	85	1.613E+05
50	1.097E+05	68	1.376E+05	86	1.634E+05
51	1.119E+05	69	1.376E+05	87	1.634E+05
52	1.140E+05	70	1.398E+05	88	1.656E+05
53	1.140E+05	71	1.419E+05	89	1.677E+05
54	1.162E+05	72	1.419E+05	90	1.677E+05

Table 4.8: Spent UOX and MOX Fuel inventories generated during the Pu mono-recycling scenario

Year	UOX [t]	MOX [t]	Year	UOX [t]	MOX [t]
-2	2.724E+04	0.000E+00	21	6.611E+04	2.954E+03
-1	2.724E+04	0.000E+00	22	6.611E+04	3.061E+03
0	2.939E+04	0.000E+00	23	6.805E+04	3.223E+03
1	2.939E+04	5.371E+01	24	6.998E+04	3.384E+03
2	3.149E+04	2.148E+02	25	6.998E+04	3.491E+03
3	3.348E+04	3.760E+02	26	7.191E+04	3.652E+03
4	3.348E+04	4.834E+02	27	7.385E+04	3.813E+03
5	3.541E+04	6.445E+02	28	7.578E+04	3.921E+03
6	3.734E+04	8.056E+02	29	7.578E+04	4.082E+03
7	3.734E+04	9.130E+02	30	7.771E+04	4.243E+03
8	3.928E+04	1.074E+03	31	7.965E+04	4.350E+03
9	4.121E+04	1.235E+03	32	7.965E+04	4.512E+03
10	4.121E+04	1.343E+03	33	8.158E+04	4.726E+03
11	4.314E+04	1.504E+03	34	8.351E+04	4.887E+03
12	5.451E+04	1.665E+03	35	8.351E+04	4.995E+03
13	5.451E+04	1.772E+03	36	8.545E+04	5.156E+03
14	5.645E+04	1.934E+03	37	8.738E+04	5.317E+03
15	5.838E+04	2.095E+03	38	8.738E+04	5.425E+03
16	5.838E+04	2.202E+03	39	8.931E+04	5.586E+03
17	6.031E+04	2.363E+03	40	9.125E+04	5.747E+03
18	6.225E+04	2.524E+03	41	9.125E+04	5.854E+03
19	6.225E+04	2.632E+03	42	9.318E+04	6.015E+03
20	6.418E+04	2.793E+03	43	9.511E+04	6.176E+03

Year	UOX [t]	MOX [t]	Year	UOX [t]	MOX [t]
44	9.511E+04	6.284E+03	68	1.280E+05	9.829E+03
45	9.705E+04	6.445E+03	69	1.280E+05	9.936E+03
46	9.898E+04	6.606E+03	70	1.299E+05	1.010E+04
47	9.898E+04	6.714E+03	71	1.318E+05	1.026E+04
48	1.009E+05	6.875E+03	72	1.318E+05	1.037E+04
49	1.028E+05	7.036E+03	73	1.338E+05	1.053E+04
50	1.028E+05	7.143E+03	74	1.357E+05	1.069E+04
51	1.048E+05	7.304E+03	75	1.357E+05	1.080E+04
52	1.067E+05	7.465E+03	76	1.376E+05	1.096E+04
53	1.067E+05	7.573E+03	77	1.396E+05	1.112E+04
54	1.086E+05	7.734E+03	78	1.396E+05	1.123E+04
55	1.106E+05	7.895E+03	79	1.415E+05	1.139E+04
56	1.106E+05	8.003E+03	80	1.434E+05	1.155E+04
57	1.125E+05	8.164E+03	81	1.434E+05	1.165E+04
58	1.144E+05	8.325E+03	82	1.454E+05	1.182E+04
59	1.164E+05	8.432E+03	83	1.473E+05	1.198E+04
60	1.164E+05	8.593E+03	84	1.473E+05	1.208E+04
61	1.183E+05	8.754E+03	85	1.492E+05	1.225E+04
62	1.202E+05	8.862E+03	86	1.512E+05	1.241E+04
63	1.202E+05	9.023E+03	87	1.512E+05	1.251E+04
64	1.222E+05	9.184E+03	88	1.531E+05	1.268E+04
65	1.241E+05	9.292E+03	89	1.550E+05	1.284E+04
66	1.241E+05	9.453E+03	90	1.550E+05	1.294E+04
67	1.260E+05	9.668E+03			

The corresponding annual fluxes for both incoming spent UOX and outgoing recycled Pu masses according to the Pu mono-recycling scenario are presented in Table 4.9.

Table 4.9: Reprocessed UOX and recycled Pu annual fluxes for the Pu mono-recycling scenario

Year	UOX [t y^{-1}]	Pu [t y^{-1}]	Year	UOX [t y^{-1}]	Pu [t y^{-1}]
-2	0.000E+00	0.000E+00	11	1.717E+03	2.233E+01
-1	0.000E+00	0.000E+00	12	1.003E+03	1.305E+01
0	1.793E+03	2.265E+01	13	1.525E+03	1.982E+01
1	2.423E+03	3.038E+01	14	1.717E+03	2.233E+01
2	1.842E+03	2.292E+01	15	8.413E+02	1.096E+01
3	1.238E+03	1.534E+01	16	1.363E+03	1.772E+01
4	1.873E+03	2.310E+01	17	1.717E+03	2.233E+01
5	1.892E+03	2.322E+01	18	7.877E+02	1.026E+01
6	1.272E+03	1.554E+01	19	1.363E+03	1.772E+01
7	1.922E+03	2.338E+01	20	1.717E+03	2.233E+01
8	1.942E+03	2.350E+01	21	7.877E+02	1.026E+01
9	4.695E+02	5.672E+00	22	1.363E+03	1.772E+01
10	0.000E+00	0.000E+00	23	1.717E+03	2.233E+01

Year	UOX [t y^{-1}]	Pu [t y^{-1}]	Year	UOX [t y^{-1}]	Pu [t y^{-1}]
24	7.877E+02	1.026E+01	58	7.877E+02	1.026E+01
25	1.363E+03	1.772E+01	59	1.363E+03	1.772E+01
26	1.717E+03	2.233E+01	60	1.717E+03	2.233E+01
27	7.877E+02	1.026E+01	61	7.877E+02	1.026E+01
28	1.363E+03	1.772E+01	62	1.363E+03	1.772E+01
29	1.717E+03	2.233E+01	63	1.933E+03	2.517E+01
30	7.877E+02	1.026E+01	64	1.717E+03	2.233E+01
31	1.363E+03	1.772E+01	65	7.877E+02	1.026E+01
32	1.933E+03	2.517E+01	66	1.363E+03	1.772E+01
33	1.717E+03	2.233E+01	67	1.717E+03	2.233E+01
34	7.877E+02	1.026E+01	68	7.877E+02	1.026E+01
35	1.363E+03	1.772E+01	69	1.363E+03	1.772E+01
36	1.717E+03	2.233E+01	70	1.717E+03	2.233E+01
37	7.877E+02	1.026E+01	71	7.877E+02	1.026E+01
38	1.363E+03	1.772E+01	72	1.363E+03	1.772E+01
39	1.717E+03	2.233E+01	73	1.717E+03	2.233E+01
40	7.877E+02	1.026E+01	74	7.877E+02	1.026E+01
41	1.363E+03	1.772E+01	75	1.363E+03	1.772E+01
42	1.717E+03	2.233E+01	76	1.717E+03	2.233E+01
43	7.877E+02	1.026E+01	77	7.877E+02	1.026E+01
44	1.363E+03	1.772E+01	78	1.363E+03	1.772E+01
45	1.717E+03	2.233E+01	79	1.717E+03	2.233E+01
46	7.877E+02	1.026E+01	80	7.877E+02	1.026E+01
47	1.363E+03	1.772E+01	81	1.363E+03	1.772E+01
48	1.717E+03	2.233E+01	82	1.717E+03	2.233E+01
49	7.877E+02	1.026E+01	83	7.877E+02	1.026E+01
50	1.363E+03	1.772E+01	84	1.363E+03	1.772E+01
51	1.717E+03	2.233E+01	85	1.717E+03	2.233E+01
52	7.877E+02	1.026E+01	86	7.877E+02	1.026E+01
53	1.363E+03	1.772E+01	87	1.363E+03	1.772E+01
54	1.717E+03	2.233E+01	88	1.717E+03	2.233E+01
55	7.877E+02	1.026E+01	89	7.877E+02	1.026E+01
56	1.363E+03	1.772E+01	90	1.363E+03	1.772E+01
57	1.717E+03	2.233E+01			

According to the SF management in the two scenarios, the detailed chemical composition evolution of the remaining waste (in terms of Pu, MAs and FPs) are shown in Tables 4.10 and 4.11, and depicted in Figures 4.1 and 4.2.

Table 4.10: Wastes inventory characterized for Pu and MAs produced by a once through fuel management strategy

Year	Pu [t]	Am [t]	Np [t]	Cm [t]
-2	0.000E+00	0.000E+00	0.000E+00	0.000E+00
-1	0.000E+00	0.000E+00	0.000E+00	0.000E+00
0	3.811E+02	3.104E+01	1.823E+01	2.825E+00
1	3.811E+02	3.104E+01	1.823E+01	2.825E+00

Year	Pu [t]	Am [t]	Np [t]	Cm [t]
2	4.100E+02	3.214E+01	2.019E+01	3.251E+00
3	4.389E+02	3.325E+01	2.216E+01	3.676E+00
4	4.389E+02	3.325E+01	2.216E+01	3.676E+00
5	4.678E+02	3.435E+01	2.412E+01	4.102E+00
6	4.967E+02	3.546E+01	2.609E+01	4.527E+00
7	4.967E+02	3.546E+01	2.609E+01	4.527E+00
8	5.255E+02	3.656E+01	2.806E+01	4.953E+00
9	5.544E+02	3.767E+01	3.002E+01	5.378E+00
10	5.544E+02	3.767E+01	3.002E+01	5.378E+00
11	5.833E+02	3.877E+01	3.198E+01	5.803E+00
12	7.391E+02	4.473E+01	4.259E+01	8.098E+00
13	7.391E+02	4.473E+01	4.259E+01	8.098E+00
14	7.680E+02	4.584E+01	4.456E+01	8.524E+00
15	7.969E+02	4.694E+01	4.652E+01	8.950E+00
16	7.969E+02	4.694E+01	4.652E+01	8.950E+00
17	8.258E+02	4.805E+01	4.849E+01	9.375E+00
18	8.547E+02	4.915E+01	5.046E+01	9.801E+00
19	8.547E+02	4.915E+01	5.046E+01	9.801E+00
20	8.837E+02	5.026E+01	5.243E+01	1.023E+01
21	9.123E+02	5.136E+01	5.438E+01	1.065E+01
22	9.123E+02	5.136E+01	5.438E+01	1.065E+01
23	9.413E+02	5.246E+01	5.635E+01	1.108E+01
24	9.702E+02	5.357E+01	5.831E+01	1.150E+01
25	9.702E+02	5.357E+01	5.831E+01	1.150E+01
26	9.991E+02	5.468E+01	6.028E+01	1.193E+01
27	1.028E+03	5.578E+01	6.225E+01	1.235E+01
28	1.057E+03	5.689E+01	6.421E+01	1.278E+01
29	1.057E+03	5.689E+01	6.421E+01	1.278E+01
30	1.086E+03	5.799E+01	6.618E+01	1.320E+01
31	1.115E+03	5.910E+01	6.815E+01	1.363E+01
32	1.115E+03	5.910E+01	6.815E+01	1.363E+01
33	1.144E+03	6.021E+01	7.012E+01	1.406E+01
34	1.173E+03	6.131E+01	7.208E+01	1.448E+01
35	1.173E+03	6.131E+01	7.208E+01	1.448E+01
36	1.201E+03	6.241E+01	7.404E+01	1.490E+01
37	1.230E+03	6.352E+01	7.600E+01	1.533E+01
38	1.230E+03	6.352E+01	7.600E+01	1.533E+01
39	1.259E+03	6.462E+01	7.797E+01	1.576E+01
40	1.288E+03	6.573E+01	7.994E+01	1.618E+01
41	1.288E+03	6.573E+01	7.994E+01	1.618E+01
42	1.317E+03	6.683E+01	8.191E+01	1.661E+01
43	1.346E+03	6.794E+01	8.387E+01	1.703E+01
44	1.346E+03	6.794E+01	8.387E+01	1.703E+01
45	1.375E+03	6.905E+01	8.584E+01	1.746E+01
46	1.404E+03	7.015E+01	8.781E+01	1.788E+01
47	1.404E+03	7.015E+01	8.781E+01	1.788E+01
48	1.433E+03	7.126E+01	8.978E+01	1.831E+01
49	1.461E+03	7.236E+01	9.174E+01	1.874E+01
50	1.461E+03	7.236E+01	9.174E+01	1.874E+01
51	1.490E+03	7.346E+01	9.370E+01	1.916E+01

Year	Pu [t]	Am [t]	Np [t]	Cm [t]
52	1.519E+03	7.457E+01	9.566E+01	1.958E+01
53	1.519E+03	7.457E+01	9.566E+01	1.958E+01
54	1.548E+03	7.567E+01	9.763E+01	2.001E+01
55	1.577E+03	7.678E+01	9.960E+01	2.044E+01
56	1.577E+03	7.678E+01	9.960E+01	2.044E+01
57	1.606E+03	7.789E+01	1.016E+02	2.086E+01
58	1.635E+03	7.899E+01	1.035E+02	2.129E+01
59	1.664E+03	8.010E+01	1.055E+02	2.171E+01
60	1.664E+03	8.010E+01	1.055E+02	2.171E+01
61	1.693E+03	8.120E+01	1.075E+02	2.214E+01
62	1.721E+03	8.231E+01	1.094E+02	2.257E+01
63	1.721E+03	8.231E+01	1.094E+02	2.257E+01
64	1.750E+03	8.342E+01	1.114E+02	2.299E+01
65	1.779E+03	8.451E+01	1.134E+02	2.341E+01
66	1.779E+03	8.451E+01	1.134E+02	2.341E+01
67	1.808E+03	8.562E+01	1.153E+02	2.384E+01
68	1.837E+03	8.673E+01	1.173E+02	2.427E+01
69	1.837E+03	8.673E+01	1.173E+02	2.427E+01
70	1.866E+03	8.783E+01	1.193E+02	2.469E+01
71	1.895E+03	8.894E+01	1.212E+02	2.512E+01
72	1.895E+03	8.894E+01	1.212E+02	2.512E+01
73	1.924E+03	9.004E+01	1.232E+02	2.554E+01
74	1.953E+03	9.115E+01	1.252E+02	2.597E+01
75	1.953E+03	9.115E+01	1.252E+02	2.597E+01
76	1.981E+03	9.226E+01	1.271E+02	2.639E+01
77	2.010E+03	9.336E+01	1.291E+02	2.682E+01
78	2.010E+03	9.336E+01	1.291E+02	2.682E+01
79	2.039E+03	9.447E+01	1.311E+02	2.725E+01
80	2.068E+03	9.557E+01	1.330E+02	2.767E+01
81	2.068E+03	9.557E+01	1.330E+02	2.767E+01
82	2.097E+03	9.667E+01	1.350E+02	2.809E+01
83	2.126E+03	9.778E+01	1.370E+02	2.852E+01
84	2.126E+03	9.778E+01	1.370E+02	2.852E+01
85	2.155E+03	9.888E+01	1.389E+02	2.895E+01
86	2.184E+03	9.999E+01	1.409E+02	2.937E+01
87	2.184E+03	9.999E+01	1.409E+02	2.937E+01
88	2.212E+03	1.011E+02	1.429E+02	2.980E+01
89	2.241E+03	1.022E+02	1.448E+02	3.022E+01
90	2.241E+03	1.022E+02	1.448E+02	3.022E+01

Table 4.11: Wastes inventory characterized for Pu and MAs produced by mono-recycling of Pu scenario evolution

Year	Pu [t]	Am [t]	Np [t]	Cm [t]
-2	0.000E+00	0.000E+00	0.000E+00	0.000E+00
-1	0.000E+00	0.000E+00	0.000E+00	0.000E+00
0	3.811E+02	3.104E+01	1.823E+01	2.826E+00

Year	Pu [t]	Am [t]	Np [t]	Cm [t]
1	3.842E+02	3.128E+01	1.824E+01	2.933E+00
2	4.219E+02	3.310E+01	2.018E+01	3.669E+00
3	4.579E+02	3.486E+01	2.202E+01	4.382E+00
4	4.642E+02	3.535E+01	2.204E+01	4.595E+00
5	4.995E+02	3.708E+01	2.383E+01	5.298E+00
6	5.349E+02	3.882E+01	2.563E+01	6.002E+00
7	5.412E+02	3.931E+01	2.564E+01	6.215E+00
8	5.765E+02	4.104E+01	2.744E+01	6.918E+00
9	6.119E+02	4.277E+01	2.923E+01	7.621E+00
10	6.182E+02	4.326E+01	2.925E+01	7.835E+00
11	6.535E+02	4.500E+01	3.104E+01	8.538E+00
12	8.158E+02	5.158E+01	4.147E+01	1.111E+01
13	8.221E+02	5.208E+01	4.149E+01	1.132E+01
14	8.575E+02	5.381E+01	4.328E+01	1.203E+01
15	8.928E+02	5.554E+01	4.508E+01	1.273E+01
16	8.991E+02	5.603E+01	4.510E+01	1.294E+01
17	9.345E+02	5.777E+01	4.689E+01	1.365E+01
18	9.698E+02	5.950E+01	4.868E+01	1.435E+01
19	9.761E+02	5.999E+01	4.870E+01	1.456E+01
20	1.011E+03	6.172E+01	5.049E+01	1.527E+01
21	1.047E+03	6.345E+01	5.229E+01	1.597E+01
22	1.053E+03	6.395E+01	5.231E+01	1.618E+01
23	1.088E+03	6.568E+01	5.410E+01	1.689E+01
24	1.124E+03	6.741E+01	5.589E+01	1.759E+01
25	1.130E+03	6.790E+01	5.591E+01	1.780E+01
26	1.165E+03	6.964E+01	5.770E+01	1.851E+01
27	1.201E+03	7.137E+01	5.950E+01	1.921E+01
28	1.233E+03	7.285E+01	6.128E+01	1.981E+01
29	1.242E+03	7.359E+01	6.131E+01	2.013E+01
30	1.278E+03	7.533E+01	6.310E+01	2.083E+01
31	1.310E+03	7.681E+01	6.489E+01	2.143E+01
32	1.319E+03	7.755E+01	6.491E+01	2.175E+01
33	1.358E+03	7.953E+01	6.672E+01	2.256E+01
34	1.393E+03	8.126E+01	6.851E+01	2.326E+01
35	1.400E+03	8.175E+01	6.853E+01	2.347E+01
36	1.435E+03	8.349E+01	7.032E+01	2.418E+01
37	1.470E+03	8.522E+01	7.212E+01	2.488E+01
38	1.477E+03	8.571E+01	7.213E+01	2.509E+01
39	1.512E+03	8.744E+01	7.393E+01	2.580E+01
40	1.547E+03	8.917E+01	7.572E+01	2.650E+01
41	1.554E+03	8.967E+01	7.574E+01	2.671E+01
42	1.589E+03	9.140E+01	7.753E+01	2.742E+01
43	1.624E+03	9.313E+01	7.933E+01	2.812E+01
44	1.631E+03	9.362E+01	7.934E+01	2.833E+01
45	1.666E+03	9.536E+01	8.114E+01	2.904E+01
46	1.701E+03	9.709E+01	8.293E+01	2.974E+01
47	1.708E+03	9.758E+01	8.295E+01	2.995E+01
48	1.743E+03	9.931E+01	8.474E+01	3.066E+01
49	1.778E+03	1.010E+02	8.654E+01	3.136E+01
50	1.785E+03	1.015E+02	8.655E+01	3.157E+01

Year	Pu [t]	Am [t]	Np [t]	Cm [t]
51	1.820E+03	1.033E+02	8.835E+01	3.227E+01
52	1.855E+03	1.050E+02	9.014E+01	3.298E+01
53	1.862E+03	1.055E+02	9.016E+01	3.319E+01
54	1.897E+03	1.072E+02	9.195E+01	3.389E+01
55	1.932E+03	1.090E+02	9.375E+01	3.460E+01
56	1.939E+03	1.095E+02	9.376E+01	3.481E+01
57	1.974E+03	1.112E+02	9.556E+01	3.551E+01
58	2.009E+03	1.129E+02	9.735E+01	3.622E+01
59	2.042E+03	1.144E+02	9.914E+01	3.681E+01
60	2.051E+03	1.151E+02	9.916E+01	3.713E+01
61	2.086E+03	1.169E+02	1.010E+02	3.784E+01
62	2.119E+03	1.184E+02	1.027E+02	3.843E+01
63	2.128E+03	1.191E+02	1.028E+02	3.875E+01
64	2.163E+03	1.208E+02	1.046E+02	3.946E+01
65	2.196E+03	1.223E+02	1.063E+02	4.005E+01
66	2.205E+03	1.231E+02	1.064E+02	4.037E+01
67	2.244E+03	1.250E+02	1.082E+02	4.118E+01
68	2.279E+03	1.268E+02	1.100E+02	4.189E+01
69	2.285E+03	1.273E+02	1.100E+02	4.210E+01
70	2.321E+03	1.290E+02	1.118E+02	4.280E+01
71	2.356E+03	1.307E+02	1.136E+02	4.351E+01
72	2.362E+03	1.312E+02	1.136E+02	4.372E+01
73	2.398E+03	1.329E+02	1.154E+02	4.442E+01
74	2.433E+03	1.347E+02	1.172E+02	4.513E+01
75	2.439E+03	1.352E+02	1.172E+02	4.534E+01
76	2.475E+03	1.369E+02	1.190E+02	4.604E+01
77	2.510E+03	1.386E+02	1.208E+02	4.675E+01
78	2.516E+03	1.391E+02	1.208E+02	4.696E+01
79	2.552E+03	1.409E+02	1.226E+02	4.766E+01
80	2.587E+03	1.426E+02	1.244E+02	4.837E+01
81	2.593E+03	1.431E+02	1.244E+02	4.858E+01
82	2.629E+03	1.448E+02	1.262E+02	4.928E+01
83	2.664E+03	1.465E+02	1.280E+02	4.999E+01
84	2.670E+03	1.470E+02	1.280E+02	5.020E+01
85	2.706E+03	1.488E+02	1.298E+02	5.090E+01
86	2.741E+03	1.505E+02	1.316E+02	5.161E+01
87	2.747E+03	1.510E+02	1.316E+02	5.182E+01
88	2.783E+03	1.527E+02	1.334E+02	5.252E+01
89	2.818E+03	1.545E+02	1.352E+02	5.323E+01
90	2.824E+03	1.550E+02	1.352E+02	5.344E+01

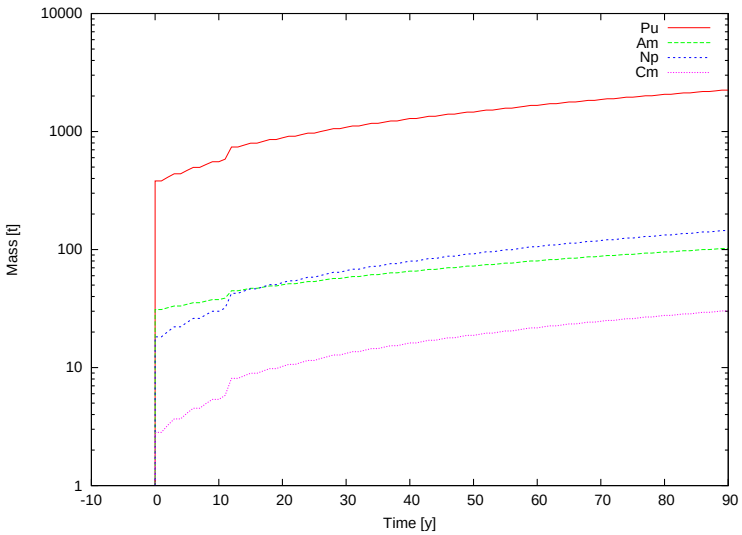

Figure 4.1: Evolution of Pu and MAs in the SF inventory according to the open cycle scenario.

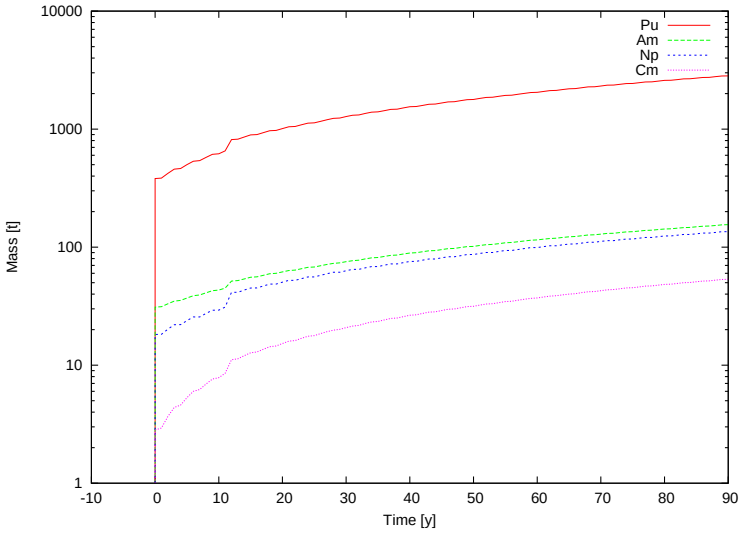

Figure 4.2: Evolution of Pu and MAs in the SF inventory according to the Pu mono-recycling scenario.

Finally, concerning the mass of U reprocessed and lost for sustaining the Pu mono-recycling scenario, the annual fluxes are listed in Table 4.12.

Table 4.12: Reprocessed and lost U during the Pu mono-recycling scenario

Year	Reprocesses [t]	Losses [t]	Year	Reprocesses [t]	Losses [t]	Year	Reprocesses [t]	Losses [t]	Year	Reprocesses [t]	Losses [t]
-2	0.000E+00	0.000E+00	22	1.363E+03	1.363E+00	46	7.877E+02	7.877E-01	70	1.717E+03	1.717E+00
-1	0.000E+00	0.000E+00	23	1.717E+03	1.717E+00	47	1.363E+03	1.363E+00	71	7.877E+02	7.877E-01
0	1.793E+03	1.793E+00	24	7.877E+02	7.877E-01	48	1.717E+03	1.717E+00	72	1.363E+03	1.363E+00
1	2.423E+03	2.423E+00	25	1.363E+03	1.363E+00	49	7.877E+02	7.877E-01	73	1.717E+03	1.717E+00
2	1.842E+03	1.842E+00	26	1.717E+03	1.717E+00	50	1.363E+03	1.363E+00	74	7.877E+02	7.877E-01
3	1.238E+03	1.238E+00	27	7.877E+02	7.877E-01	51	1.717E+03	1.717E+00	75	1.363E+03	1.363E+00
4	1.873E+03	1.873E+00	28	1.363E+03	1.363E+00	52	7.877E+02	7.877E-01	76	1.717E+03	1.717E+00
5	1.892E+03	1.892E+00	29	1.717E+03	1.717E+00	53	1.363E+03	1.363E+00	77	7.877E+02	7.877E-01
6	1.272E+03	1.272E+00	30	7.877E+02	7.877E-01	54	1.717E+03	1.717E+00	78	1.363E+03	1.363E+00
7	1.922E+03	1.922E+00	31	1.363E+03	1.363E+00	55	7.877E+02	7.877E-01	79	1.717E+03	1.717E+00
8	1.942E+03	1.942E+00	32	1.933E+03	1.933E+00	56	1.363E+03	1.363E+00	80	7.877E+02	7.877E-01
9	4.695E+02	4.695E-01	33	1.717E+03	1.717E+00	57	1.717E+03	1.717E+00	81	1.363E+03	1.363E+00
10	0.000E+00	0.000E+00	34	7.877E+02	7.877E-01	58	7.877E+02	7.877E-01	82	1.717E+03	1.717E+00
11	1.717E+03	1.717E+00	35	1.363E+03	1.363E+00	59	1.363E+03	1.363E+00	83	7.877E+02	7.877E-01
12	1.003E+03	1.003E+00	36	1.717E+03	1.717E+00	60	1.717E+03	1.717E+00	84	1.363E+03	1.363E+00
13	1.525E+03	1.525E+00	37	7.877E+02	7.877E-01	61	7.877E+02	7.877E-01	85	1.717E+03	1.717E+00
14	1.717E+03	1.717E+00	38	1.363E+03	1.363E+00	62	1.363E+03	1.363E+00	86	7.877E+02	7.877E-01
15	8.413E+02	8.413E-01	39	1.717E+03	1.717E+00	63	1.933E+03	1.933E+00	87	1.363E+03	1.363E+00
16	1.363E+03	1.363E+00	40	7.877E+02	7.877E-01	64	1.717E+03	1.717E+00	88	1.717E+03	1.717E+00
17	1.717E+03	1.717E+00	41	1.363E+03	1.363E+00	65	7.877E+02	7.877E-01	89	7.877E+02	7.877E-01
18	7.877E+02	7.877E-01	42	1.717E+03	1.717E+00	66	1.363E+03	1.363E+00	90	1.363E+03	1.363E+00
19	1.363E+03	1.363E+00	43	7.877E+02	7.877E-01	67	1.717E+03	1.717E+00			
20	1.717E+03	1.717E+00	44	1.363E+03	1.363E+00	68	7.877E+02	7.877E-01			
21	7.877E+02	7.877E-01	45	1.717E+03	1.717E+00	69	1.363E+03	1.363E+00			

CHAPTER 5

INTRODUCING REMARKS

There is no logical way to the discovery of these elemental laws. There is only the way of intuition, which is helped by a feeling for the order lying behind the appearance.

Albert Einstein (1879-1955)

Abstract. Projecting the results of the reference scenario to the World nuclear energy production, the inadequacy of the present nuclear option as optimal candidate for solving the reduction of greenhouse gases emission problem is found.
According to a open cycle fuel management strategy, the natural Uranium resources reveal to be insufficient for feeding even the present nuclear fleet beyond the current century.
At the same time, the disposal of the spent fuel legacies within geological repositories appears both an unreliable and expensive solution, unsatisfactory for a real nuclear renaissance.

Introduction

According to the initial aims, the analysis of the present scenario results proved the inadequacy of this solution to what concerns the sustainability of nuclear energy even in the short future. As evident, both front- and back-end issues are posed in managing the nuclear materials in a once-through logic (open cycle scenario).

A deep analysis of the present scenario issues can provide useful hints for conceiving new fuel management logic, as well as meters for evaluating the performances of every alternative strategy candidate at solving the sustainability problem of nuclear energy.

5.1 Implied horizons

Extending the results obtained for the western European region to the whole World, even assuming the –completely non-realistic, because of the incredible trend of the Chinese energy demand – hypothesis of no expansion of nuclear installed power, two main considerations can be brought. As discussed in Chapter 1, the World's electric energy production by nuclear power plants in 2007 has been 2728.4 TWh, 24.56% of which in the western Europe considered in the reference scenarios investigated in the present Chapters.

Taking at first into account the consumption of natural Uranium resources, the once-through scenario requires (from Table 4.1) a yearly input feed of some 14612 t. Projecting the same consumption rate for the European context to the World's nuclear energy production, the drawn of Natural Uranium increases to about 59800 t y^{-1}.

The most recent evaluations available for the natural Uranium resources (both Reasonably Assured Resources, RAR, and inferred) are presented in Table 5.1 (data taken from the 2007 "Uranium Red Book" [8]).

A preliminary evaluation of the NU availability corresponding to the given assured and inferred resources can been made by projecting the World's annual consumptions related to the nuclear electric energy production rate in 2007. According to this, the present resourced (about 5.5 mln t) can feed the present nuclear scenario – in a stagnant evolution hypothesis – for some 92 y.

Removing the optimistic assumption of no expansion of the nuclear installed power, World nuclear energy capacity is expected to grow from 372 GWe in 2007 to between 509 GWe (+37%) and 663 GWe (+78%) by 2030 [8]. To fuel this expansion, annual Uranium requirements are anticipated to rise to between 82500 t and 107600 t, based on the type of reactors in use today. Assuming the expansion of the nuclear capacity will follow a linear trend, the availability of natural Uranium resources is expected to be accordingly worked out by between 61 y and 49 y.

Table 5.1: Estimated world's natural Uranium resources (below 130 USD kg^{-1})

Country	RAR [t]	Inferred [t]	Total [t]
Australia	725000	518000	1243000
Kazakhstan	378000	439200	817200
Canada	329200	121000	450200
USA	339000		339000
South Africa	284400	150700	435100
Namibia	176400	30900	207300
Brazil	157400	121000	278400
Niger	243100	30900	274000
Russian Federation	172400	373300	545700
Uzbekistan	72400	38600	111000
India	48900	24000	72900
China	48800	19100	67900
Others	363300	263900	627200
Total	3338300	2130600	5468900

No significant change is brought by the adoption of a Pu mono-recycling scenario, reducing the NU needs by about one tenth (hence extending the resources availability by one ninth), as shown by the scenarios results of the previous Chapter (in particular, see Table 4.3).

The second point regards the masses accumulated every year in the SF stocks. Projecting the results obtained for the western European region to the whole World (under the assumption of constant installed nuclear electric energy capacity), some 5860 t of spent UOX are accumulated yearly. Apart from FPs, 78.8 t of Pu are produced every year, together with $\sim$ 3 t of Am, 5.4 t of Np and 1.2 t of Cm.

According to the open-cycle logic, all the SF is to be sent to a geological repository for final disposal. As a matter of fact, the presence of long-lived radiotoxic isotopes in the spent fuel (*i.e.*, the TRUs), whose half-lives are of the order of one hundred thousand years, imposes the need for geological repositories, since all the radiotoxic sources must be immobilized so as to prevent any environmental contamination as far as the radiologic problem exists. The immobilization of the spent fuel is typically performed by means of a vitrification process, ensuring the capability of each sample to evacuate the decay heat without compromising the structural integrity of the sample.

The partitioning of the spent fuel into vitrified forms is ruled by the aim at maximizing the SF mass per piece, without compromising the possibility of evacuating the decay heat at acceptable temperatures. It is easy to under-

stand that the lower the content of SF per piece, the smaller the form volume, hence the better the ratio surface (which is proportional to the heat transmission capability) over volume (which is proportional to the total power to be evacuated). On the other hand, small forms imply high repository volumes, that is, costs. Present cylindrical Pyrex forms typically include some 60 kg of spent UOX [9].

Every Pyrex form is then enclosed within a concrete canister, which is buried in the geological repository. The typical storage area occupied by each canister is about 44 m^2. According to this, and to provide an idea of the volumes needed for geological repositorying, the World's production of electric energy by nuclear power plants in 2007 imposed the availability of $4.3 \cdot 10^6$ m^2 new storage area.

Two main considerations can be brought concerning the possibility of geological repository. At first, the volumes of the repositories directly impact in the estimation of the back-end component of the overall kWhe cost, reducing the competitiveness of nuclear energy with respect to other energy sources. The second point concerns the reliability of the containment in terms of guaranteeing the integrity of the storage (not to release radiotoxic sources into the environment) for periods far behind human experience. A possible solution to the last question could be propose by wisely choosing the siting for the repositories; on the other hand, this could pose a problem in guaranteeing the availability of suitable sites for the entire mass of the World's spent nuclear fuel.

5.2 Desirable scenario features

Two main questions rose from the analysis of the present nuclear scenario:

- how to extend the natural Uranium resources in order to feed the World electric energy demand beyond the present century; and
- how to manage the spent fuel legacies so as to guarantee their safe burial at acceptable costs and with full repository reliability for the whole period of radiologic hazard.

Both issues are crucial in order to promote nuclear energy as safe, reliable and indefinite carbon-free energy source: as a matter of fact, the breaking need for reducing greenhouse gases emissions must be faced by fully-developed technologies able to solve the sustainability problem once and for all. The aimed nuclear renaissance must be therefore leaded by a new Generation power plants, operating according to a new fuel management strategy rather than the open-cycle one.

Concerning the natural Uranium resources issue, such new energy systems must be envisaged to operate as breeders, so as to autonomously generate

new fuel for their own need and - eventually - in order to feed even other reactors.

At the same time, effective strategies must be conceived and implemented in brand new scenarios for the management of the long-lived component of the SF: according to this, the radiotoxicity of the remaining spent fuel (once the long-lived isotopes have been separated) could be limited to a reasonable time span (*i.e.*, few centuries), allowing for the elimination of the geological repository option at all.

Part II

The Nuclear Reactors Generation-IV

CHAPTER 6

THE GENERATION-IV INITIATIVE

Now, my own suspicion is that the universe is not only queerer than we suppose, but queerer than we can suppose. I have read and heard many attempts at a systematic account of it, from materialism and theosophy to the Christian system or that of Kant, and I have always felt that they were much too simple. I suspect that there are more things in heaven and earth that are dreamed of, or can be dreamed of, in any philosophy. That is the reason why I have no philosophy myself, and must be my excuse for dreaming.

John Burden Sanderson Haldane (1892-1964)

Abstract. The nuclear power industry has been developing and improving reactor technology for more than five decades. Starting from 1950s, three Generations of nuclear power systems had been developed, built and operated. Each Generation represented an evolution of the previous one, mainly by implementing several revisions of the same concept systems, so as to improve fuel technology, increase thermal efficiency, introduce passive safety systems and standardize design for reduced maintenance and capital costs. According to the recent interest in relaunching the nuclear option worldwide, the Generation IV International Forum has been settled, representing an international endeavor intended for defining the criteria for a new Generation of nuclear energy systems. Challenging technology goals for Generation IV nuclear energy systems have been defined by the GIF in four general areas: sustainability, economics, safety and reliability, and proliferation resistance and physical protection. By striving to meet the technology goals, new nuclear systems can achieve a number of long-term benefits that will help nuclear energy play an essential role worldwide.

Introduction

The Generation IV International Forum (GIF) is a cooperative international endeavor organized to carry out the Research and Development (R&D) needed to establish the feasibility and performance capabilities of the next generation nuclear energy systems.

Its founding document, the GIF Charter, has been originally signed in July 2001 by the former nine members of the GIF: Argentina, Brazil, Canada, France, Japan, the Republic of Korea, the Republic of South Africa, the United Kingdom and the United States of America. Subsequently, it was signed by Switzerland (2002), Euratom (2003), and the People's Republic of China and the Russian Federation, both in 2006. The GIF charter provides also for the participation of the International Atomic Energy Agency (IAEA) and the Organisation for Economic Co-operation and Development Nuclear Energy Agency (OECD/NEA) as permanent observers, to provide a wider understanding of the opportunities coming from interests and possible collaborations with countries not represented in the GIF.

The goals adopted by GIF provided the basis for identifying and selecting six nuclear energy systems for further development. The six selected systems employ a variety of reactor, energy conversion and fuel cycle technologies. Their designs feature thermal and fast neutron spectra, closed and open fuel cycles and a wide range of reactor sizes from very small to very large. Depending on their respective degrees of technical maturity, the Generation IV systems are expected to become available for commercial introduction in the period between 2015 and 2030 or beyond.

Discussions on international collaboration in the development of Generation IV nuclear energy systems began in 2000, when the US Department of Energy's (DOE) Office of Nuclear Energy, Science and Technology convened a group of senior governmental representatives from the original nine countries. The group, subsequently named the Policy Group of the GIF, also decided to form a group of senior technical experts to explore areas of mutual interest and make recommendations regarding both research and development areas to be explored and processes by which collaboration could be conducted and assessed.

6.1 The present generation reactors

The nuclear power industry has been developing and improving reactor technology for more than five decades (Figure 6.1 resumes the evolution of nuclear power plants during the whole nuclear era). Starting from 1950s, a first Generation of nuclear power systems had been developed, built and operated, mainly derived from designs originally developed for naval use (Pressurized and Boiling Water Reactors, PWRs and BWRs). Except for the United

Kingdom, none of these are still running today.

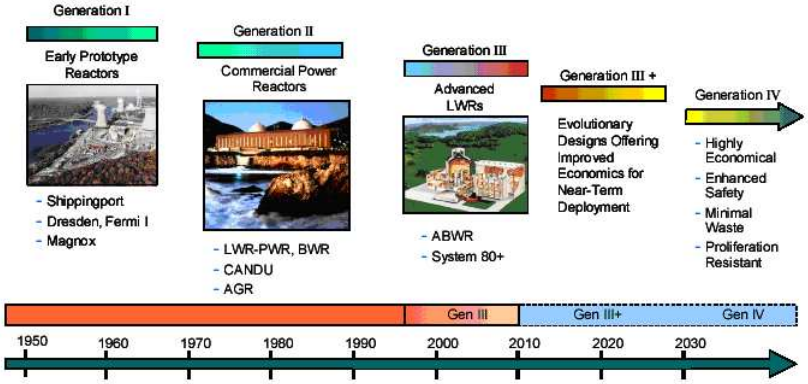

Figure 6.1: Evolution of nuclear power plants through different Generations.

After this early generation of NPP prototypes, an evolution of the Generation I systems had been developed, mainly by implementing several revisions of the same concept systems. The second Generation of nuclear systems can be considered as characterized by true commercial power reactors come to maturity thanks to the experience collected in operating the first generation reactors. Generation II reactors, typified by the present US fleet, represent the largest portion of the nuclear systems currently operating worldwide.

Generation II nuclear power units, even if found to be safe and reliable, are being superseded by better designs to fill orders now materializing. These advanced reactors represent the third Generation of NPPs. The first are already in operation in Japan since 1996 and others are under construction or ready to be ordered worldwide.

A Generation III reactor incorporates evolutionary improvements in design developed during the lifetime of the Generation II reactors, such as

- a standardized design for each type to expedite licensing, reduce maintenance and capital cost and reduce construction time,
- a simpler and more rugged design, making them easier to operate and less vulnerable to operational upsets,
- higher availability and longer operating life - typically 60 years,
- further reduced possibility of core melt accidents,
- resistance to serious damage that would allow radiological release from an aircraft impact,

- higher burn-up to reduce fuel use and the amount of waste,
- burnable absorbers ("poisons") to extend fuel life.

The greatest departure from second Generation designs is that many of the Generation III systems incorporate passive or inherent safety features[1] which require no active controls or operational intervention to avoid accidents in the event of malfunction, and may rely on gravity, natural convection or resistance to high temperatures.

Another important departure is that some of these systems will be designed for load-following. While most French reactors today are operated in that mode to some extent, the EPR design (for instance) has better capabilities. It will be able to maintain its output at 25% and then ramp up to full output at a rate of 2.5% of rated power per minute up to 60% output and at 5% of rated output per minute up to full rated power. This means that potentially the unit can change its output from 25% to 100% in less than 30 minutes, though this may be at some expense of wear and tear.

The main systems belonging to the Generation III are:

- the Advanced Boiling Water Reactor (ABWR), a GE design which first went on-line in Japan in 1996;
- the Advanced Pressurized Water Reactor (APWR), developed by Mitsubishi Heavy Industries;
- the Enhanced CANDU 6 (EC6), developed by Atomic Energy of Canada Limited.

A further slight evolution brought to an internal distinction among Generation III systems. Since the evolved systems do not represent a proper conceptual evolution, but rather an improvement over the Generation III advanced reactor designs certified by the NRC in the 1990s, mainly to what concerns safety and economics, they are commonly referred to as Generation III+ systems. Among these are:

- the Advanced CANDU Reactor (ACR-1000);
- the AP1000, based on the AP600 with increased power output;
- the European Pressurized Reactor (EPR), an evolutionary descendant of the Framatome N4 and Siemens Power Generation Division KONVOI reactors;

[1] Traditional reactor safety systems are “active” in the sense that they involve electrical or mechanical operation on command. Some engineered systems operate passively, e.g.: pressure relief valves. They function without operator control and despite any loss of auxiliary power. Both require parallel redundant systems. Inherent or full passive safety depends only on physical phenomena such as convection, gravity or resistance to high temperatures, not on functioning of engineered components.

- the Economic Simplified Boiling Water Reactor (ESBWR), based on the ABWR;
- the APR-1400, an advanced PWR design evolved from the U.S. System 80+ which is the basis for the Korean Next Generation Reactor or KNGR;
- the mPower, an Advanced Light Water Reactor to be developed by Babcock and Wilcox;
- the EU-ABWR, based on the ABWR with increased power output and compliance with EU safety standard;

6.2 The Generation-IV philosophy

The recent interest in relaunching the nuclear option worldwide has formed the wish to define the criteria for a new Generation of nuclear energy systems.

Over 100 experts from the GIF member countries and international organizations began working on the compilation of a technology roadmap for Generation IV systems, ultimated in 2002. Challenging technology goals for Generation IV nuclear energy systems are defined in this roadmap in four areas: sustainability, economics, safety and reliability, and proliferation resistance and physical protection. By striving to meet the technology goals, new nuclear systems can achieve a number of long-term benefits that will help nuclear energy play an essential role worldwide.

Eight goals for Generation IV nuclear energy systems have been pointed out in the four areas:

Sustainability-1 Generation IV nuclear energy systems will provide sustainable energy generation that meets clean air objectives and promotes long-term availability of systems and effective fuel utilization for worldwide energy production.

Sustainability-2 Generation IV nuclear energy systems will minimize and manage their nuclear waste and notably reduce the long-term stewardship burden, thereby improving protection for the public health and the environment.

Economics-1 Generation IV nuclear energy systems will have clear lifecycle cost advantage over other energy sources.

Economics-2 Generation IV nuclear energy systems will have a level of financial risk comparable to other energy projects.

Safety and Reliability-1 Generation IV nuclear energy systems operations will excel in safety and reliability.

Safety and Reliability-2 Generation IV nuclear energy systems will have a very low likelihood and degree of reactor core damage.

Safety and Reliability-3 Generation IV nuclear energy systems will eliminate the need for off-site emergency response.

Proliferation Resistance and Physical Protection Generation IV nuclear energy systems will increase the assurance that they are a very unattractive and the least desirable route for diversion or theft of weapons-usable materials, and provide increased physical protection against acts of terrorism.

6.2.1 Sustainability

Sustainability is the ability to meet the needs of the present generation while enhancing the ability of future generations to meet society's needs indefinitely into the future. There is a growing desire in society for the production of energy in accordance with sustainability principles: sustainability requires indeed the conservation of resources, protection of the environment, preservation of the ability of future generations to meet their own needs, and the avoidance of placing unjustified burdens upon them.

Since existing and future nuclear power plants meet current and increasingly stringent clean air objectives, their energy being produced without combustion processes, the two sustainability goals pointed out in the Generation IV technology roadmap, encompass the interrelated needs of improved waste management, minimal environmental impacts, effective fuel utilization, and development of new energy products that can expand nuclear energy's benefits beyond electrical generation. The benefits of meeting the reported sustainability goals therefore include:

- extending the nuclear fuel supply into future centuries by recycling used fuel to recover its energy content, and by converting ^{238}U to new fuel;
- having a positive impact on the environment through the displacement of polluting energy and transportation sources by nuclear electricity generation and nuclear-produced hydrogen;
- allowing geologic waste repositories to accept the waste of many more plant-years of nuclear plant operation through substantial reduction in the amount of wastes and their decay heat;
- greatly simplifying the scientific analysis and demonstration of safe repository performance for very long time periods (beyond 1000 years), by a large reduction in the lifetime and toxicity of the residual radioactive wastes sent to repositories for final geologic disposal.

6.2.2 Safety and reliability

Maintaining and enhancing the safe and reliable operation is an essential priority in the development of next-generation systems. Nuclear energy systems must be designed so that during normal operation or anticipated transients safety margins are adequate, accidents are prevented, and off-normal situations do not deteriorate into severe accidents. At the same time, competitiveness requires a very high level of reliability and performance.

Despite the fact that there has been a definite trend over the years to improve the safety and reliability of nuclear power plants, reducing the frequency and degree of off-site radioactive releases, as well as the possibility of significant plant damage – resulting in the design of Generation III systems –, Generation IV systems will have to face, through further improvements, new challenges to their reliability at higher temperatures and other anticipated conditions.

The three safety and reliability goals pointed out in the Generation IV technology roadmap continue the past trend and seek simplified designs that are safe and further reduce the potential for severe accidents, and minimize their consequences to both protect the investment and reduce the need for off-site emergency response. The achievement of these ambitious goals cannot rely only upon technical improvements, but will also require systematic consideration of human performance as a major contributor to the plant availability, reliability, inspectability, and maintainability. The benefits envisaged in meeting these goals include:

- increasing the use of inherent safety features, robust designs, and transparent safety features that can be understood by non-experts; and
- enhancing public confidence in the safety of nuclear energy.

6.2.3 Economics

Economic competitiveness is a requirement of the marketplace and is therefore essential for Generation IV nuclear energy systems. In today's environment, nuclear power plants are primarily base-load units that were purchased and operated by regulated public and private utilities. A transition is taking place worldwide from regulated to deregulated energy markets, which will increase the number of independent power producers and merchant power plant owner/operators. Future nuclear energy systems should accommodate a range of plant ownership options and anticipate a wider array of potential roles and options for deploying nuclear power plants, including load following and smaller units. While it is anticipated that Generation IV nuclear energy systems will primarily produce electricity, they will also help meeting anticipated future needs for a broader range of energy products beyond electricity. For example, hydrogen, process heat, district heating, and drinking

water will likely be needed to keep up with increasing worldwide demands and long-term changes in energy use.

Economics goals broadly consider competitive costs and financial risks of nuclear energy systems, for ensuring Generation IV systems are economically attractive while meeting changing energy needs. In particular, the benefits of meeting economics goals include:

- achieving economic life-cycle and energy production costs through a number of innovative advances in plant and fuel cycle efficiency, design simplifications, and plant sizes;
- reducing economic risk to nuclear projects through the development of plants built using innovative fabrication and construction techniques, and possibly modular designs;
- allowing the distributed production of hydrogen, fresh water, district heating, and other energy products to be produced where they are needed.

6.2.4 Proliferation resistance and physical protection

Proliferation Resistance and Physical Protection (PR&PP) are also essential priorities in the expanding role of nuclear energy systems: they consider means for controlling and securing nuclear materials (both source materials and special fissionable materials) and nuclear facilities (all the ones involved in enrichment, conversion, fabrication, power production, recycling, and waste disposal), preventing the use of civilian nuclear energy systems for nuclear weapons proliferation.

In addition, despite the fact that existing nuclear plants are highly secure and designed to withstand external events such as earthquakes, floods, tornadoes, plane crashes, and fires, their many protective features considerably reducing the impact of external or internal threats through the redundancy, diversity, and independence of the safety systems, the Generation IV technology roadmap points out the need to increase public confidence in the security of nuclear energy facilities against terrorist attacks. Advanced systems need therefore to be designed from the start with improved physical protection against acts of terrorism, to a level commensurate with the protection of other critical systems and infrastructure.

According to the GIF, the benefits of meeting the PR&PP goals include:

- providing continued effective proliferation resistance of nuclear energy systems through improved design features and other measures; and
- increasing physical protection against terrorism by increasing the robustness of new facilities.

6.3 The candidates typologies

The Generation IV technology roadmap also reports the work performed in identifying and evaluating the Generation IV candidate systems, together with the necessary R&D planning to support the six most promising solutions. The six systems feature increased safety, improved economics for electricity production and new products such as hydrogen for transportation applications, reduced nuclear wastes for disposal, and increased proliferation resistance.

In a first step, an Evaluation Methodology Group (EMG) was formed to develop a common evaluation methodology to systematically evaluate the potential of proposed Generation IV nuclear energy systems to meet the Generation IV goals. The basic approach is to formulate a number of factors that indicate performance relative to the goals, called criteria, and then to evaluate concept performance against these criteria using specific measures, called metrics. At the same time, a solicitation was issued worldwide, requesting that concept proponents submit information on nuclear energy systems that they believe could meet some or all of the Generation IV goals. Nearly 100 concepts and ideas were received from researchers in a dozen countries.

Technical Working Groups (TWGs) were formed – covering nuclear energy systems employing water-cooled, gas-cooled, liquid-metal-cooled, and non-classical reactor concepts – to review the proposed systems and evaluate their potential using the tools developed by the EMG. Because of the large number of system concepts submitted, the TWGs collected their concepts into sets of concepts with similar attributes. The TWGs conducted an initial screening, termed screening for potential, to eliminate those concepts or concept sets that did not have reasonable potential for advancing the goals, or were too distant or technically infeasible. Following the screening for potential, the TWGs conducted a final screening to assess quantitatively the potential of each concept or concept set to meet the Generation IV goals.

This final screening employed a more detailed and quantitative set of evaluation criteria than the screening for potential. Numerical scales were employed for a number of the criteria, and weights were assigned to the criteria associated with each goal. The scales were established relative to a representative advanced light water reactor baseline. The four goal areas, with the eight goals arranged under them, and the 15 criteria assigned to the various goals together with their 24 metrics are shown in Table 6.1.

For each criterion, the TWGs evaluated each concept and specified a probability distribution for its performance potential to reflect both the expected performance and performance uncertainty. The Crosscut Groups and the Roadmap Integration Team reviewed these evaluations and recommended changes to make them consistent. For a goal evaluated with several criteria, the goal evaluation was combined using criteria weights suggested by the

Table 6.1: Goals, Criteria and Metrics for Generation-IV candidates selection

Goal Areas	Goals	Criteria	Metrics
Sustainability	Resource Utilization	Fuel Utilization	Use of fuel resources
	Waste Minimization and Management	Waste Minimization	Mass
			Volume
			Heat load
			Radiotoxicity
		Impact of Waste Management and Disposal	Environmental impact
Economics	Life Cycle Cost	Overnight construction costs	Overnight construction costs
		Production costs	Production costs
		Construction duration	Construction duration
	Risk to Capital	Overnight construction costs	Overnight construction costs
		Construction duration	Construction duration
Safety and Reliability	Operational	Reliability	Forced outage rate
		Worker/public - routine exposure	Routine exposures
		Worker/public - accident exposure	Accident exposures
	Core Damage	Robust safety features	Reliable reactivity control
			Reliable decay heat removal
		Well-characterized models	Dominant phenomena-uncertainty
			Long fuel thermal response time
			Integral experiments scalability
	Offsite Emergency Response	Well-characterized source term/energy	Source term
			Mechanisms for energy release
		Robust mitigation features	Long system time constants
			Long and effective hold-up
Proliferation Resistance and Physical Protection	Proliferation Resistance and Physical Protection	Susceptibility to diversion or undeclared production	Separated materials
			Spent fuel characteristics
		Vulnerability of installations	Passive safety features

EMG. Comparisons of Generation IV candidates were mostly done at the goal level. A central feature of the roadmap is that the eight goals of Generation IV are all equally important. That is, a promising concept should ideally advance each, and not create a weakness in one goal to gain strength in another.

A number of Crosscut Groups were also formed to explore the impact of each concept on major elements of sustainability, economics, risk and safety, fuels and materials, and energy products. The Crosscut Groups reviewed the TWG reports for consistency in the technical evaluations and subject treatment, and continued to make recommendations regarding the scope and priority for cross-cutting R&D in their subject areas. Finally, the TWGs and Crosscut Groups worked together to select the six concepts found to be the most promising and worthy of collaborative development to become the basis for Generation IV, and to report on their R&D needs and priorities.

The six candidate typologies are briefly presented in the following subsections.

6.3.1 Gas-cooled Fast Reactor

The Gas-cooled Fast Reactor (GFR) system features a fast-neutron spectrum and closed fuel cycle for efficient conversion of fertile uranium and management of Actinides. A full Actinide recycle fuel cycle with on-site fuel cycle facilities is envisioned. The fuel cycle facilities can minimize transportation of nuclear materials and will be based on either advanced aqueous, pyrometallurgical, or other dry processing options. The reference reactor is a 600 MWth / 288 MWe, helium-cooled system operating with an outlet temperature of 850 °C using a direct Brayton cycle gas turbine for high thermal efficiency. Several fuel forms are being considered for their potential to operate at very high temperatures and to ensure an excellent retention of fission products: composite ceramic fuel, advanced fuel particles or ceramic clad elements of Actinide compounds. Core configurations are being considered based on pin- or plate-based fuel assemblies or prismatic blocks.

The GFR system is top-ranked in sustainability because of its closed fuel cycle and excellent performance in Actinide management. It is rated good in safety, economics, and in proliferation resistance and physical protection. It is primarily envisioned for missions in electricity production and Actinide management, although it may be able to also support hydrogen production. Given its R&D needs for fuel and recycling technology development, the GFR is estimated to be deployable by 2025.

6.3.2 Very-High-Temperature Reactor

The Very-High-Temperature Reactor (VHTR) system uses a thermal neutron spectrum and a once-through uranium cycle. The VHTR system is pri-

marily aimed at relatively faster deployment of a system for high-temperature process heat applications, such as coal gasification and thermochemical hydrogen production, with superior efficiency. The reference reactor concept has a 600 MWth helium-cooled core based on either the prismatic block fuel of the Gas Turbine-Modular Helium Reactor (GT-MHR) or the pebble fuel of the Pebble Bed Modular Reactor (PBMR). The primary circuit is connected to a steam reformer/steam generator to deliver process heat. The VHTR system has coolant outlet temperatures above 1000 °C. It is intended to be a high-efficiency system that can supply process heat to a broad spectrum of high-temperature and energy-intensive, nonelectric processes. The system may incorporate electricity generation equipment to meet co-generation needs. The system also has the flexibility to adopt U/Pu fuel cycles and offer enhanced waste minimization. The VHTR requires significant advances in fuel performance and high-temperature materials, but could benefit from many of the developments proposed for earlier prismatic or pebble bed gas-cooled reactors. Additional technology R&D for the VHTR includes high-temperature alloys, fiber-reinforced ceramics or composite materials, and zirconium-carbide fuel coatings.

The VHTR system is highly ranked in economics because of its high hydrogen production efficiency, and in safety and reliability because of the inherent safety features of the fuel and reactor. It is rated good in proliferation resistance and physical protection, and neutral in sustainability because of its open fuel cycle. The VHTR system is the nearest-term hydrogen production system, estimated to be deployable by 2020.

6.3.3 Supercritical-Water-cooled Reactor

The Supercritical-Water-cooled Reactor (SCWR) system features two fuel cycle options: the first is an open cycle with a thermal neutron spectrum reactor; the second is a closed cycle with a fast-neutron spectrum reactor and full Actinide recycle. Both options use a high-temperature, high-pressure, water-cooled reactor that operates above the thermodynamic critical point of water (22.1 MPa, 374 °C) to achieve a thermal efficiency approaching 44%. The fuel cycle for the thermal option is a once-through uranium cycle. The fast-spectrum option uses central fuel cycle facilities based on advanced aqueous processing for Actinide recycle. The fast-spectrum option depends upon the materials' R&D success to support a fast-spectrum reactor. In either option, the reference plant has a 1700 MWe power level, an operating pressure of 25 MPa, and a reactor outlet temperature of 550 °C. Passive safety features similar to those of the simplified boiling water reactor are incorporated. Owing to the low density of super-critical water, additional moderator is added to thermalize the core in the thermal option. Note that the balance-of-plant is considerably simplified because the coolant does not change phase in the reactor.

The SCWR system is highly ranked in economics because of the high thermal efficiency and plant simplification. If the fast-spectrum option can be developed, the SCWR system will also be highly ranked in sustainability. The SCWR is rated good in safety, and in proliferation resistance and physical protection. The SCWR system is primarily envisioned for missions in electricity production, with an option for Actinide management. Given its R&D needs in materials compatibility, the SCWR system is estimated to be deployable by 2025.

6.3.4 Sodium-cooled Fast Reactor

The Sodium-cooled Fast Reactor (SFR) system features a fast-neutron spectrum and a closed fuel cycle for efficient conversion of fertile uranium and management of Actinides. A full Actinide recycle fuel cycle is envisioned with two major options: one is an intermediate size (150 to 500 MWe) sodium-cooled reactor with a Uranium-Plutonium-minor-Actinide-Zirconium metal alloy fuel, supported by a fuel cycle based on pyrometallurgical processing in collocated facilities. The second is a medium to large (500 to 1500 MWe) sodium-cooled fast reactor with mixed uranium-plutonium oxide fuel, supported by a fuel cycle based upon advanced aqueous processing at a central location serving a number of reactors. The outlet temperature is approximately 550 °C for both. The primary focus of the R&D is on the recycle technology, economics of the overall system, assurance of passive safety, and accommodation of bounding events.

The SFR system is top-ranked in sustainability because of its closed fuel cycle and excellent potential for Actinide management, including resource extension. It is rated good in safety, economics, and proliferation resistance and physical protection. It is primarily envisioned for missions in electricity production and Actinide management. The SFR system is the nearest-term Actinide management system. Based on the experience with oxide fuel, this option is estimated to be deployable by 2015.

6.3.5 Lead-cooled Fast Reactor

The Lead-cooled Fast Reactor (LFR) system features a fast-neutron spectrum and a closed fuel cycle for efficient conversion of fertile uranium and management of actinides. A full Actinide recycle fuel cycle with central or regional fuel cycle facilities is envisioned. The system uses a lead or lead-/bismuth eutectic liquid-metal-cooled reactor. Options include a range of plant ratings, including a battery of $50 \div 150$ MWe that features a very long refueling interval, a modular system rated at $300 \div 400$ MWe, and a large monolithic plant option at 1200 MWe. The term battery refers to the long-life, factory-fabricated core, not to any provision for electrochemical energy conversion. The fuel is metal or nitride-based, containing fertile uranium

and Transuranics. The most advanced of these is the Pb/Bi battery, which employs a small size core with a very long ($10 \div 30$ year) core life. The reactor module is designed to be factory-fabricated and then transported to the plant site. The reactor is cooled by natural convection and sized between $120 \div 400$ MWth, with a reactor outlet coolant temperature of 550 °C, possibly ranging up to 800 °C, depending upon the success of the materials R&D.

The system is specifically designed for distributed generation of electricity and other energy products, including hydrogen and potable water. The LFR system is top-ranked in sustainability because a closed fuel cycle is used, and in proliferation resistance and physical protection because it employs a long-life core. It is rated good in safety and economics. The safety is enhanced by the choice of a relatively inert coolant. It is primarily envisioned for missions in electricity and hydrogen production and Actinide management with good proliferation resistance. Given its R&D needs for fuel, materials, and corrosion control, the LFR system is estimated to be deployable by 2025.

6.3.6 Molten Salt Reactor

The Molten Salt Reactor (MSR) system features an epithermal to thermal neutron spectrum and a closed fuel cycle tailored to the efficient utilization of plutonium and minor actinides. A full Actinide recycle fuel cycle is envisioned. In the MSR system, the fuel is a circulating liquid mixture of sodium, zirconium, and uranium fluorides. The molten salt fuel flows through graphite core channels, producing a thermal spectrum. The heat generated in the molten salt is transferred to a secondary coolant system through an intermediate heat exchanger, and then through another heat exchanger to the power conversion system. Actinides and most fission products form fluorides in the liquid coolant. The homogeneous liquid fuel allows addition of Actinide feeds with variable composition by varying the rate of feed addition. There is no need for fuel fabrication. The reference plant has a power level of 1000 MWe. The system operates at low pressure (< 0.5 MPa) and has a coolant outlet temperature above 700 °C, affording improved thermal efficiency.

The MSR system is top-ranked in sustainability because of its closed fuel cycle and excellent performance in waste burn-down. It is rated good in safety, and in proliferation resistance and physical protection, and it is rated neutral in economics because of its large number of subsystems. It is primarily envisioned for missions in electricity production and waste burn-down. Given its R&D needs for system development, the MSR is estimated to be deployable by 2025.

CHAPTER 7

LEAD FAST REACTORS AND THE ELSY PROJECT

We know very little, and yet it is astonishing that we know so much, and still more astonishing that so little knowledge can give us so much power.

Bertrand Russell (1872-1970)

Abstract. Among the Generation IV candidate typologies, both the Lead-cooled and Gas-cooled Fast Reactors have been top-ranked in sustainability, because of the very hard neutron spectrum they employ. However, the LFR has been preferred to the GFR for investigating the sustainability potentialities of nuclear energy, because of the higher rating in proliferation resistance and physical protection with respect to the latter, and the simpler and favorable technological solutions implemented which allow a further enhancement both in safety and economics.
The LFR system assumed as reference for this investigative analysis is the European Lead-cooled SYstem (ELSY), the Generation IV LFR European candidate. The ELSY project has been submitted to the European Commission in the third call of the 6^{th} EURATOM Framework Programme by seventeen European organizations (including research institutes and industries), two organizations from the United States of America and one from the Republic of Korea.
The general objective of the ELSY project was to demonstrate the feasibility of designing an innovative, competitive and safe lead-cooled fast reactor – complemented by an analytical effort to assess the existing knowledge base in the field of lead-alloy coolants – based on simple technical engineered features that achieves all of the Generation IV goals and gives assurance of investment protection. As a result of this investigative analysis, ELSY constitutes the reference system for the large lead-cooled reactor of Generation IV.

Introduction

The idea of developing fast spectrum reactors with molten lead (or lead alloy) as a coolant is in the 1950s. Although initially considered also in the West, where such technology was abandoned because of anticipated difficulties associated with the corrosive nature of these coolant materials, LFR technology was actively pursued in the Soviet Union for the specialized role of submarine propulsion. More recently, there has been a renewal of interest in the West for such technology, both for critical systems as well as for Accelerator Driven Subcritical (ADS) systems. Meanwhile, interest in the former Soviet Union, primarily Russia, has remained strong and has expanded well beyond the original limited mission of submarine propulsion.

The present interest derives from the GEN IV technology evaluation of the LFR: this system was top-ranked indeed in sustainability because it can embed a closed fuel cycle, and top-ranked in proliferation resistance and physical protection because it can employ a long-life core. It was rated good in safety and economics. Safety was considered to be enhanced by the choice of a relatively inert coolant. The LFR was primarily envisioned for missions in electricity and hydrogen production and Actinide management.

7.1 General neutronic properties of LFR

In order to investigate the peculiarities of a LFR (for comparison with other reactor types) it is important to consider the range of neutronic properties of the coolant including moderation (slowing down) and absorption affinity.

7.1.1 Lead properties

Moderation

Fast reactors cooled by HLMs such as lead or LBE rely primarily on the physics of the high energy portion of the neutron spectrum.

The main responsible mechanism for neutrons slowing down is elastic scattering. The elastic cross-section of naturally occurring lead isotopes is shown in Figure 7.1.

Despite its high[1] elastic cross-section, the high mass number A of lead strongly reduces the average lethargy change per elastic collision,

$$\xi = 1 - \frac{(A-1)^2}{2A} \ln\left(\frac{A+1}{A-1}\right).$$

The latter, combined with the macroscopic elastic cross section Σ_s provides an estimate for the moderating power of lead. Table 7.1 resumes typical

[1] Here high refers to the fission and capture cross-sections of the main isotopes in the fuel, see section 7.1.2.

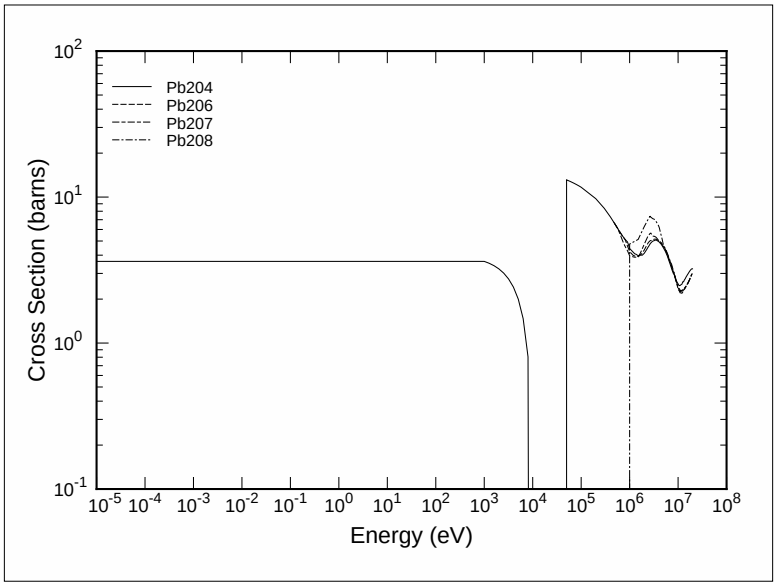

Figure 7.1: Elastic cross-sections of naturally occurring lead isotopes (data from JEFF3.0 library).

values of the average lethargy change per elastic collision and the moderating power for lead and other main coolants/moderators.

Table 7.1: Average lethargy change per elastic collision and moderating power for some typical coolants/moderators

	ξ	$\xi\Sigma_s$
H_2O	0.920	1.425
D_2O	0.509	0.177
Helium	0.425	9.0E-6
Graphite	0.158	0.083
Sodium	0.0825	0.0176
Lead	0.00963	0.00284

The low moderating power justifies the typical neutron energy distribution of a LFR shown in Figure 7.2. The mean neutron energy in a typical LFR lies in the range of 400 to 450 keV (depending also on the fuel type, *i.e.*, oxide, nitride or metallic).

The mean free path associated to the given spectrum, for a typical LFR, is of the order of 2 to 3 cm.

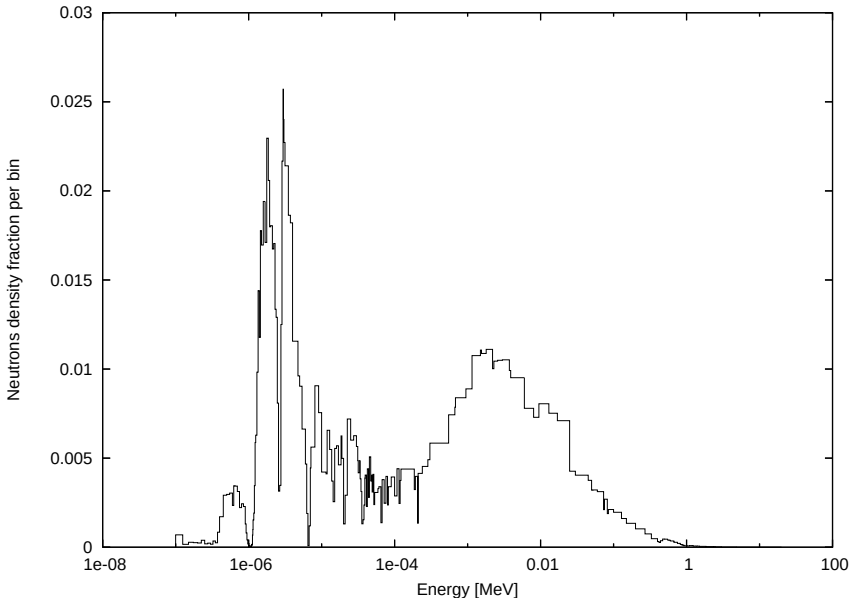

Figure 7.2: Typical neutrons spectrum in a LFR (e.g.: ELSY).

Absorption

The lead coolant affects the neutron balance in the core: as a matter of fact, captures in the coolant directly impact the reactivity of the unit cell of the system, and thus the neutronic design of the whole core (see chapter 11).

The (n,γ) absorption cross-section of naturally occurring lead isotopes is shown in Figure 7.3.

It is to be pointed out that the most highly absorbing isotope (^{204}Pb) has a natural abundance of only 1.4%, sustaining the low total absorption rate of lead.

7.1.2 Fuel properties

Whilst a variety of fuels is accounted worldwide for LFRs (e.g.: oxide in the European concept, nitride in the American one), their typical composition is a mixture of reactor-grade Plutonium (referring to an isotopic vector as if extracted from the spent fuel of a typical LWR after a mean BU of some 50 GWd t_{HM}^{-1} and a cooling period of 10 y) and DU, eventually doped by the inclusion of some MAs.

Besides the peculiarities of oxide *vs.* metallic fuels (mainly influencing the thermal design of the pin, such as the fuel thermal conductivity and its melting temperature), a series of common properties can be pointed out referring to the overall performances of fissile and fertile isotopes in a LFR.

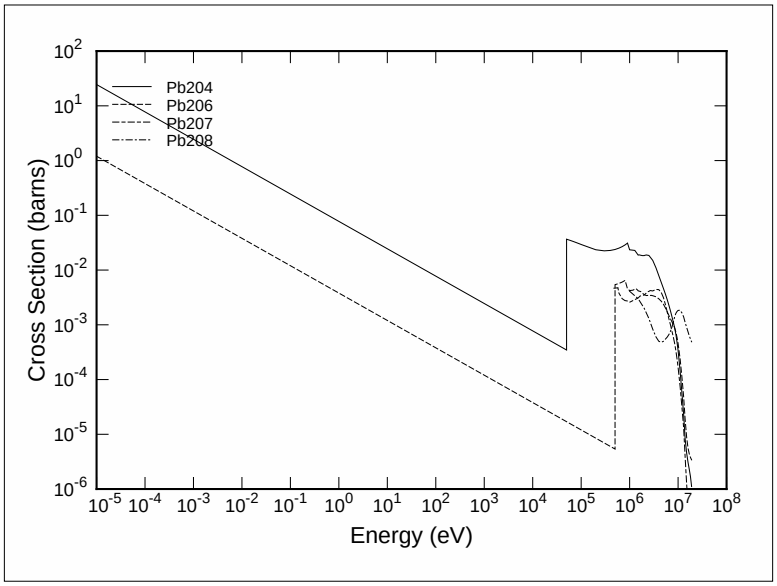

Figure 7.3: (n,γ) absorption cross-sections of naturally occurring lead isotopes (data from JEFF3.0 library).

Fission cross-sections

An immediate drawback related to the hard neutron spectrum can be found in what concerns the fission cross-sections of odd nuclides (about one to two orders of magnitude less than in thermal reactors): typical values are shown in Table 7.2 compared to corresponding capture cross-sections. Despite the fact that an increase of the fission rates for even nuclides can be gained, resulting in a wider contribution to criticality among nuclides in the fuel inventory, the reduction of the fission cross-sections implies larger inventories of fissile material to maintain criticality.

Table 7.2: Typical microscopic cross-sections of main fuel isotopes in a LFR compared to the ones of LWRs

	Capture [barns]			Fission [barns]		
	ELSY	ENHS	LWR	ELSY	ENHS	LWR
^{238}U	0.282	0.210	1.03	0.035	0.030	0.107
^{239}Pu	0.487	0.297	42.23	1.753	1.640	101.02
^{241}Pu	0.475	0.313	37.89	2.501	2.110	109.17

Average number of fission neutrons

The hard spectrum represents a positive contribution in what concerns the average number of neutrons per fission, $\overline{\nu}$, which is higher (about 2.93 for almost all the systems considered in the present chapter) than in thermal reactors. The higher number of neutrons available in the system, once criticality has been achieved, can be exploited for captures in fertile material to provide a higher breeding.

Fuel utilization

Supported also by the increase of $\overline{\nu}$, the fertility factor, η, increases monotonically above 100 keV: the main reason for this can be ascribed to the lower capture rate due to the higher separation of the bulk of the neutron spectrum from the absorption resonance energy range. LFRs therefore can rely on a more efficient fuel utilization, allowing a higher relative arrangement of fertile material in the fuel, thus resulting in a higher BR.

Spectrum evolution with Burn Up

The particularly hard spectrum of LFRs is poorly affected by the build up of FPs during operation. Hence the neutronic properties of the system can be assumed to remain approximately constant during the whole core life (e.g.: the error introduced on criticality evaluation is few tens of pcm after complete irradiation of the fuel).

Effective delayed neutron fraction and prompt neutrons lifetime

In a typical LFR with iso-breeding Pu content (such as ELSY or ENHS), the value of the effective delayed neutron fraction β_{eff} is in the range 370 (ELSY) to 420 (ENHS) pcm. This value is smaller than that of LWRs ($\sim$ 650 pcm) because of the lower fraction of delayed neutrons per fission of a ^{239}Pu isotope than for ^{235}U. In case of MA-doped fuel (with equilibrium concentrations, *i.e.*, some $1^{\text{a}}/_{0}$ of HM) the value of β_{eff} is further reduced to some 325 pcm because of the small delayed neutron fraction associated to the fission of MA isotopes.

The impact of more highly energetic neutrons also implies a lower prompt neutrons lifetime, λ, (of the order of 10^{-6} to 10^{-7} s) in comparison with thermal reactors (about two orders of magnitude higher).

The direct drawbacks related to the values of these parameters are the narrower margin to prompt-criticality and the lower capabilities for reactor control in case of prompt-criticality accident.

LFR capabilities of MAs transmutation

Finally, the harder the spectrum, the higher the fission cross sections of MAs (triggering the highest level of threshold fission reactions among even nuclides). As far as MA transmutation is concerned, this implies that the balancing of production and removal rates for the latter (which represents the frontier between MA breeders and burners) is attained by a low content of MAs in the fuel. The possibility of relying on a low fraction of MAs in the fuel allows more flexibility in waste transmutation for LFRs: performances being equal, the lower detriment to the total average fraction of delayed neutrons (since the low contribution associated to MAs) represents a larger operability margin to what concerns such a stringent constraint for reactor control.

7.2 Lead cooling choice

The members of the GIF PSSC have evaluated technology options and support the LFR based on its promise in meeting the Generation IV objectives. In particular, the GIF PSSC members have evaluated the two selected small and medium-size LFR conceptual designs by considering the four goal areas and eight specific goals of Generation IV. The main features that the members have identified in order to achieve the GEN IV goals are discussed below. These features are based either on the inherent features of lead as a coolant or on the specific designs to be engineered for LFR projects [10].

Sustainability

Resource utilization Because lead is a coolant with very low neutron absorption and moderation properties, it is possible to maintain a fast neutron flux even with a large amount of coolant in the core. This allows an efficient utilization of excess neutrons and reduction of specific uranium consumption. The reactor can be designed to achieve a Conversion Ratio of 1 (without the need for a blanket), along with long core life and a high fuel burn-up.

Waste minimization and management A fast neutron flux significantly reduces waste generation, Pu recycling in a closed cycle being the first condition recognized by Generation IV for waste minimization. The capability of the LFR systems to safely burn recycled MAs within the fuel will add to the attractiveness of the LFR and meet another important Generation IV condition.

Economics

Life cycle cost The cost advantage features of the LFR must include low capital cost, short construction duration and low fuel and production cost. The economic utilization of MOX fuel in a fast spectrum has been already demonstrated in the case of the SFR, and no significantly different conclusion can be expected for the LFR except for improvement due to the harder spectrum.
Because of the favorable characteristics of molten lead, it will be possible to significantly simplify the LFR systems in comparison with the well known designs of the SFR, and hence to reduce its overnight capital cost, which is a major cost factor for the competitive generation of nuclear electricity.
A simple plant will be the basis for reduced capital and operating cost. A pool-type, low-pressure primary system configuration offers great potential for plant simplification.
The use of in-vessel SGUs and the consequent elimination of the intermediate circuit, typical of sodium technology, are expected to provide competitive generation of electricity in the LFR. This approach is possible because of the absence of fast chemical reactions between lead and water, although the SGTR accident (*i.e.*, pressure waves inside the SGU) must be considered in the design.
The configuration of the reactor internals will be as simple as possible. The very low vapor pressure of molten lead should allow relaxation of the otherwise stringent requirements of gas-tightness of the reactor head and possibly allow the adoption of simple fuel handling systems.
Corrosion by molten lead of candidate structural steels for the primary system will be minimized by limiting the core outlet temperature. Considering that there will be no intermediate circuit to degrade the thermal cycle and that the expected core inlet temperature of about 400 °C is relatively high, the adoption of a high-efficiency water-steam super-critical cycle is possible. Additionally, a super-critical carbon dioxide Brayton cycle energy conversion system can be considered.

Risk to capital For small, transportable systems, a limitation to the risk to capital results from the small reactor size. In addition, and with particular relevance to the moderate- or large-size central station system, a reduction in the risk to capital results from the potential for removable/replaceable in-vessel components.

Safety and Reliability

Operation will excel in safety and reliability Molten lead has the advantage of allowing operation of the primary system at low (atmospheric) pressure. A low dose to the operators can also be predicted, owing to its low vapor pressure and high capability of trapping fission products and high shielding of gamma radiation. In the case of accidental air ingress, in particular during refueling, any produced lead oxide can be reduced to lead by injection of hydrogen and the reactor operation safely resumed.
The moderate ΔT between the core inlet and outlet temperatures reduces the thermal stress during transients, and the relatively low core outlet temperature minimizes the creep effects in steels.

Low likelihood and degree of core damage It is possible to design fuel assemblies with fuel pins spaced further apart than in the case of sodium and this allows a large coolant fraction as in the case of the water reactor. This results in a moderate pressure loss through the core of about 1 bar, in spite of the high density of lead, with associated improved heat removal by natural circulation and the possibility of an innovative reactor layout such as installing the primary pumps in the hot collector to improve several aspects affecting safety.
Lead allows a high level of natural circulation of the coolant; this results in less stringent requirements for the timing of operations and simplification of the control and protection systems.
In case of leakage of the reactor vessel, the free level of the coolant can be designed to maintain a level that ensures the coolant circulation through, and the safe heat removal from the core. Any leaked lead would solidify without significant chemical reactions affecting the operation or performance of surrounding equipment or structures.

No need for off site emergency response With lead as a coolant, fuel dispersion dominates over fuel compaction, preventing severe re-criticality. In fact lead, with its higher density than oxide fuel or low-density metal fuel, and its natural convection flow, does not permit fuel aggregation with subsequent formation of a secondary critical mass in the event of postulated fuel failure.

Proliferation Resistance and Physical Protection

Unattractive route for diversion of weapon-usable material The use of a MOX fuel containing MA increases proliferation resistance. The use of a coolant chemically compatible with air and

water and operating at ambient pressure enhances PP. There is reduced need for robust protection against the risk of catastrophic events, initiated by acts of sabotage because there is a little risk of fire propagation and because of the passive safety functions. There are no credible scenarios of significant containment pressurization.

Finally, in a future expanded market of nuclear energy it is expected that additional uses of nuclear energy will be sought. For example, low temperature heat for water desalination or district heating can be readily envisioned. In this respect, the LFR can play a role similar to other nuclear power reactors and, in particular, it will favor modular applications. In the case of large hydrogen demand, the LFR could provide electricity for hydrogen generation by water electrolysis. The high boiling temperature of lead is potentially exploitable for hydrogen generation by high temperature chemical processes.

7.3 The ELSY project

The approach of the GIF plan is to consider the research priorities of each member country in proposing an integrated, coordinated R&D program to achieve common objectives, while avoiding duplication of effort. The integrated plan recognizes two principal technology tracks:

- a small, transportable system of 10÷100 MWe size that features a very long refueling interval, and
- a larger-sized system rated at about 600 MWe, intended for central station power generation.

According to this, in the third call of the FP6, sixteen European organizations joined to take the initiative to submit to the European Commission the proposal for a STREP, devoted to the development of a European Lead-cooled System, known as the ELSY project [11, 12]. Two additional organizations from the US, one from the Republic of Korea and one Italian small private industry have joined the project. Consequently, ELSY constituted the reference system for the large lead-cooled reactor of Generation IV.

The general objective of the ELSY project was to design an innovative lead-cooled fast reactor complemented by an analytical effort to assess the existing knowledge base in the field of lead-alloy coolants (*i.e.*, LBE and also lead/lithium) in order to extrapolate this knowledge base to pure lead. This analysis effort had been complemented with some limited R&D activities to acquire missing or confirmatory information about fundamental topics for ELSY that had not been sufficiently covered by the European ADS program or elsewhere.

The ELSY project aimed at demonstrating the feasibility of designing a competitive and safe lead-cooled fast power reactor based on simple technical engineered features that achieves all of the Generation IV goals and gives assurance of investment protection.

The use of compact, in-vessel steam generators and a simple primary circuit with possibly all internals being removable have been recognized among the reactor features needed for competitive electric energy generation and long-term protection of investment.

7.3.1 Expected ELSY features

ELSY is an innovative project intended to globally address several of the most important technical challenges related to the use of lead technology in general, issues that have for the most part been only partially addressed in previous projects, namely:

- How to extend the LBE experience with LBE to pure lead as a coolant?
- How to mitigate the seismic issue?
- How to design a highly compact primary system?
- How to avoid in-vessel storage of spent fuel?
- How to cool high power spent fuel elements during refueling?
- How to design a compact SG?
- How to avoid the risk of catastrophic primary system pressurization associated with water or steam collector failure?
- How to mitigate the effect of a SGTR?
- How to make the reactor internals removable?
- How to handle fuel elements while maintaining a temperature of 400 °C in lead?
- How to support the fuel elements in lead?
- How to design a simple and reliable safety-related DHR system?

The elimination of an intermediate cooling system and the development of a compact and simple primary circuit with all internal components removable, are among the features needed to assure reduced capital cost and construction time, competitive electric energy generation and long-term investment protection.

The relatively small size of the reactor vessel results from advanced solutions adopted for the primary system which features a cylindrical inner vessel, primary pumps installed in the inner zone of innovative flat-spiral-tube steam generators, and fuel elements substantially supported by buoyancy. In addition, the heads of the fuel elements extend above the vessel fixed roof as they are provided with long stems to allow fuel handling from the above reactor hall under full visibility.

In spite of the reduced coolant speed and of the moderate power density core, the innovative solutions adopted for ELSY allow reduced primary system dimensions (main vessel preliminary dimensions of 12.5 m diameter and 8.7 m height) which are similar to or even smaller than those of advanced pool-type SFRs.

Safety relies on the beneficial physical characteristics of lead, redundant and diverse DHR systems and other innovative features which make the primary system more tolerant to the effects of a SGTR accident.

The resulting primary system arrangement is shown in Figure 7.4 [13]. The coolant flow path is also indicated by blue (cold-leg) and red (hot-leg) arrows.

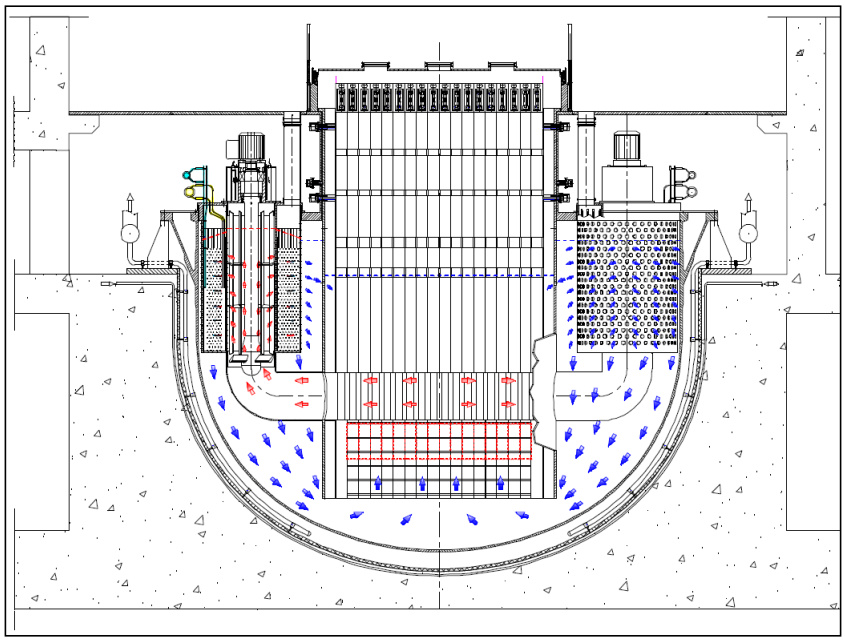

Figure 7.4: ELSY primary system arrangement and coolant flow path.

Table 7.3 provides the main parameters of ELSY.

Table 7.3: Main parameters of the ELSY plant

Parameter	Value
Power	600 MWe
Thermal efficiency	40%
Primary coolant	Pure lead
Primary system	Pool type, compact
Primary coolant circulation	Forced at power, natural circulation and pony motors for DHR
Primary pressure loss	$\sim$ 1.5 bar
Core inlet temperature	$\sim$ 400 °C
Core outlet temperature	$\sim$ 480 °C
Fuel	MOX with consideration also of nitrides and dispersed MAs
Fuel cladding material	T91 (aluminized)
Fuel cladding temperature (max)	$\sim$ 550 °C
Main vessel	Austenitic stainless steel, hung height $\sim$ 9 m, diameter $\sim$ 12.5 m
Safety vessel	Anchored to the reactor pit
Steam generators	8, integrated in the main vessel
Secondary cycle	Superheated steam at 180 bar, 450 °C
Primary pumps	8 mechanical, integrated in the SGs
Internals	Removable
Inner vessel	Cylindrical
Hot collector	Small-volume, above the core
Cold collector	Annular, free level higher than free level of hot collector
DHR coolers	4 DRC loops and 1 RVACS
Seismic design	2D isolators supporting the reactor building

CHAPTER 8

NEUTRONIC DESIGN OF ELSY: PRELIMINARY CONFIGURATION

... scientific research is compounded of ... empirical procedures, general speculative ideas, and mathematical or abstract reasoning.

James Bryant Conant (1893-1978)

Abstract. The whole neutronic design of ELSY has been carried out within the ELSY STREP as agreed in the FP6 call ELSY project. In the ELSY neutronic design two options have been investigated in parallel. The first one is based on conventional wrapped hexagonal Fuel Assemblies (FAs), typical of SFRs, where pins and FAs are arranged in a triangular lattice. The second option consists of open square FAs, typical of PWRs, where the pins and FAs are arranged in a square lattice.
This thesis refers to the open square option, developed in ENEA. In particular, the preliminary configuration of the ELSY core is here presented. Aiming at investigating the technical and economical feasibility of ELSY, the fast neutron spectrum feature of LFRs has been exploited in the core design in order to candidate ELSY for its insertion in a closed fuel cycle by means of a suitable conversion of fertile Uranium. Furthermore, the MAs burning properties of the proposed configuration has been also evaluated in order to investigate the ELSY capability to operate also as a MA burner.
The matter of this work, conducted in collaboration with ENEA, is also reported in the ELSY Deliverable 6 of EURATOM.

Introduction

As widely mentioned in the previous chapter, the ELSY STREP aimed at investigating the technical and economical feasibility of a 600 MWe LFR. According to this, common efforts from the participating organizations have spawned among the various research fields to provide an as complete as possible characterization of the system. Among the main issues, the neutronics of ELSY had to be carefully investigated to conceive the most effective core to what concerns the fuel utilization and the MA burning capabilities, so as to propose ELSY as a fully complying Generation IV candidate.

In the ELSY STREP, two different core configurations, distinguished to what concerns the FA layout, have been independently developed: the first one, proposed and investigated mainly by SCK-CEN, explicated about an hexagonal FA (typical of traditional concept SFRs), with pins organized in a triangular lattice and enclosed in a structural wrapper differentiating every FA channel so as to tune the coolant flow rate according to the power actually generated in every FA, by properly gagging the corresponding inlet nozzle. The second configuration, proposed and developed by ENEA, explicated on the other hand about the square FA concept (typical of LWRs), with pins organized in a square lattice. Furthermore, no wrapper has been envisaged for this configuration to facilitate the possibility of cooling during refueling in gas, even if to the detriment of a fine tuning of the coolant outlet temperature among the FAs.

In order to compare the two different configurations, a number of common assumptions has been pointed out by the WP devoted to core design to provide a common development frame: on the other hand, all the parameters able to exploit and show the differences between the two final configurations have been left as freedom degrees to core designers.

The common characteristics identified by the WP2, mainly regarding the desired goals and constructional constraints, are:

- the total power of the system, about 1500 MWth;
- the kind of fuel (MOX with reactor grade Pu), with its allowed peak linear rating of 320 W cm^{-1};
- the main goal of a unitary BR without blankets to respect the Generation IV requirements on sustainability and proliferation resistance;
- the in pile fuel residence time, 5 y (10 y as futuristic option);
- the minimum fuel sub-cycle duration, 1 y;
- the maximum fuel burn-up, 100 GWd t^{-1} on Heavy Metal (HM) with a corresponding peak clad damage of 100 dpa (150 GWd t^{-1} and 200 dpa have been assumed as a futuristic option);

- the maximum clad temperature, 550 °C because of corrosion[1];
- the coolant inlet and outlet temperatures in the core, 400 °C and 480 °C;
- the coolant velocity in the active region, lower than 2 m s^{-1} in order to keep structures erosion and pressure drop through the core in.

Starting from this common basis, each organization is free to conceive an optimized configuration, according to the respective FA design, by tuning the fuel pin diameter, the active height, the overall core diameter, the coolant velocity, the fuel enrichment (in Pu) and its Volumetric Fraction (VF) in the cell. The possibility of eventually relying on an axial blanket for reaching the required BR, as well as the number and positions of CRs (both for reactivity swing and safety purposes) represent other freedom degrees in the core design.

In order to get to an optimized core design for the ELSY wrapper-less square option, a preliminary scoping analysis has been conducted to assess the design of the fuel pin, the FA and the CRs. This scoping analysis required the complete characterization of a preliminary core configuration so as to investigate the neutronic features of a LFR core by a parametric and intuitive analysis on the influence of the main parameters.

8.1 Geometric and material description

In the preliminary ELSY design phase, a pure MOX fuel (*i.e.*, without any MA content) has been envisaged because of its reliability for use in fast spectrum (even if demonstrated in the case of SFRs, no significant differences are expected for LFRs). The reference MOX (whose properties are collected in Appendix A) has been assumed with 1.95 stoichiometric ratio and 95% of the theoretical density.

Limiting the preliminary analysis to the core region only, all structures are envisaged to be made of Ferritic-Martensitic Steel T91. ELSY capitalizes indeed the strong synergy with other two EU projects, IP EUROTRANS [14] and VELLA (The integrated Infrastructure initiative devoted to the dissemination of knowledge in the field of Lead and Lead-alloys technology [15]), in

[1] Actually, the maximum clad temperature limit of 550 °C has been assumed as reference since it represents a compromise between the limiting temperature for preserving from lead corrosion either bare T91 FMS (500 °C) and aluminized T91 (600 °C). It is clear that this temperature has to be considered nothing but a reference rather than an actual constraint: as a matter of fact, if aluminization techniques can be successfully validated, a limit on the maximum clad temperature assumed 50 °C below the actual technological constraint implies a non optimized core design, to the detriment of economics; on the other hand, if aluminization techniques cannot be implemented, the assumed limit is 50 °C above the safety limits, thus not acceptable.

both of which the T91 FMS has been considered as first option for structural materials, since its high irradiation resistance and promising ongoing R&D on corrosion protection technology [16].

The preliminary design of the fuel pin and fuel assembly has been then performed by means of some parametric evaluations, obtained combining few general conceptualization estimates made by paper and pencil together with some "rough" computational evaluations of main core performances.

Several configurations have been therefore evaluated, explicating about two main hypotheses: an active core height of 1.10 m to increase the reactivity of a more compact core, thus favoring the breeding, or an active core height of 0.90 m to keep both the pressure drop and the void effect in. All configurations have been preliminary assessed to guarantee the respect of the maximum linear power and clad temperature constraints (see previous section), by varying the pitch and the coolant velocity. For each analyzed configuration, the core volume and the fuel enrichment have been determined in order to obtain the desired power and reactivity.

According to the main hypothesis, different combinations of fuel pin diameter, pins lattice pitch and coolant velocity have been evaluated, estimating for each one the reactivity of the resulting core, the void effect, the breeding gain and the pressure drop in active zone. Tables 8.1 and 8.2 summarize the main results of this parametric investigation.

According to this investigative analysis, the reduction of the void coefficient has been assumed as leading choice, implying therefore the establishment of the shorter core option: it is clear indeed how a shorter active zone implies both a higher axial leakage and a smaller coolant VF (since the concurrent reduction of the total power the coolant receives through the channel and of the reduction of the pressure drops which allows a further margin for increasing the coolant flow velocity).

Aiming also at preserving some margin from the limiting coolant velocity in order to design wider channels favoring natural circulation in case of accident, the third configuration in the 90 cm active height set has been chosen as reference. According then to the idea of a PWR-like FA, the selected fuel pin has been arranged in a square 17 x 17 lattice to define the reference fuel element. A sketch of the FA cross-cut is represented in Figure 8.1.

According to the size resulting for the final FA layout, 284 positions have been identified in a square lattice to form a pseudo-cylindrical core (446 cm equivalent diameter) fitting the inner vessel with sufficient margin for hosting shielding elements all around the active zone, as shown in Figure 8.2. Within this core scheme must be placed also the CRs, reducing the number of available positions for FAs.

Table 8.1: Preliminary parametric analysis of pin dimension influence on the performances of a 1.10 m high core

v_{coolant} [m s^{-1}]	$2r_{\text{fuel}}$ [mm]	$2r_{\text{clad}}$ [mm]	p [mm]	R_{core} [cm]	Pu enrichment [$^{\text{v}}/_{0}$]	$\Delta\rho_{\text{void}}$ [pcm]	BG
1.57	7.2	8.7	13.3	195	16.2	5652	0.01
1.60	8.0	9.5	13.6	200	15.0	5730	0.06
1.65	7.6	9.1	13.3	195	15.4	5657	0.04
1.69	8.4	9.9	13.6	200	14.4	5600	0.09
1.72	7.8	8.7	12.8	190	15.7	5543	0.02
1.73	7.6	9.1	13.3	190	15.4	5576	0.03
1.75	8.0	9.5	13.2	195	14.6	5571	0.07
1.77	8.7	10.2	13.6	200	14.0	5490	0.11
1.81	7.2	8.7	12.8	185	15.7	5460	0.01
1.82	7.6	9.1	12.8	190	15.0	5495	0.05
1.86	8.4	9.9	13.2	195	14.0	5400	0.10
1.86	9.0	10.5	13.6	200	13.6	5330	0.13
1.88	7.2	8.7	12.4	185	15.3	5417	0.03
1.92	7.6	9.1	12.8	185	15.0	5426	0.04
1.93	8.0	9.5	12.8	190	14.3	5400	0.08
1.96	6.8	8.3	12.0	180	15.7	5309	0.01
1.96	8.4	9.9	12.8	195	13.7	5250	0.12
1.96	8.7	10.2	13.2	195	13.6	5264	0.12
1.96	9.0	10.5	13.6	195	13.6	5284	0.13
1.97	9.0	10.5	13.2	200	13.3	5154	0.15
1.99	7.2	8.7	12.4	180	15.3	5338	0.02
2.00	7.6	9.1	12.4	185	14.6	5332	0.06
2.08	8.7	10.2	12.8	195	13.3	5100	0.14
2.10	9.0	10.5	12.8	200	13.0	4910	0.17

Table 8.2: Preliminary parametric analysis of pin dimension influence on the performances of a 0.90 m high core

v_{coolant} [m s^{-1}]	$2r_{\text{fuel}}$ [mm]	$2r_{\text{clad}}$ [mm]	p [mm]	R_{core} [cm]	Pu enrichment [$^{\text{v}}/_{0}$]	$\Delta\rho_{\text{void}}$ [pcm]	BG
1.48	8.4	9.9	13.3	217	14.6	4830	0.04
2.00	8.4	9.9	12.3	201	13.7	4263	0.07
1.48	9.0	10.5	13.7	223	14.3	4564	0.05
2.00	9.0	10.5	12.7	207	13.2	4120	0.10

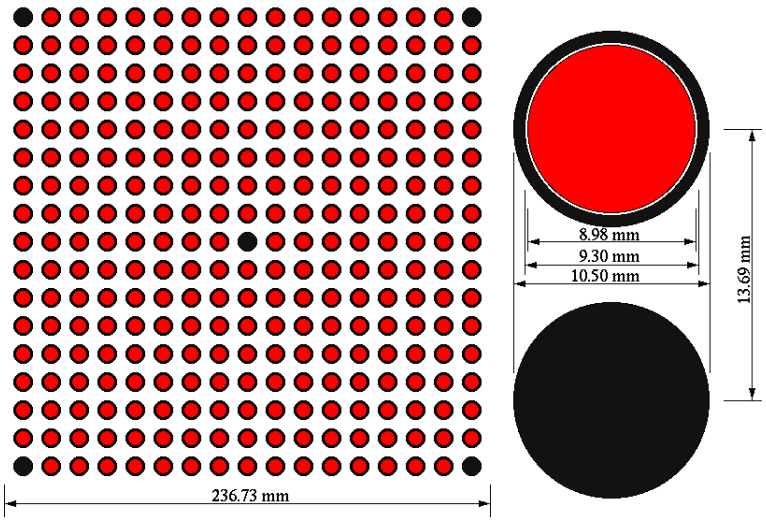

Figure 8.1: Cross-cut view of the preliminary ELSY FA and fuel pin. Grey positions represent structural uprights.

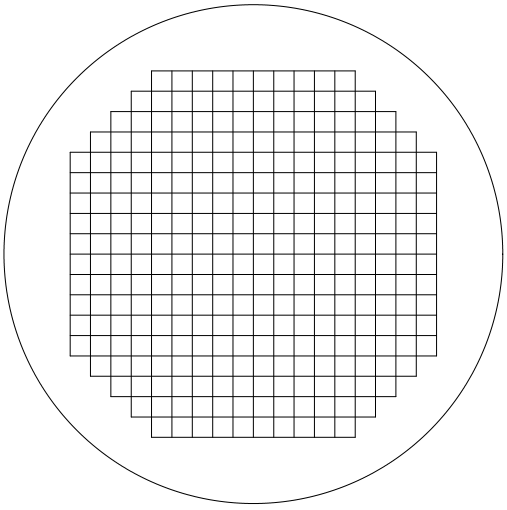

Figure 8.2: Cross-cut view of the preliminary ELSY core scheme.

8.2 ELSY computational model

All neutronics computations have been performed in parallel by both deterministic and Monte Carlo methods. Two main rationales have been envisaged

indeed in following this choice: the assessment of the results according to the specific pros and cons of each method and the acquisition of the needed confidence on the origin and entity of the unavoidable discrepancies.

In detail, deterministic analysis has been performed by means of the ERANOS (European Reactor ANalysis Optimized System) formulary [7], while Monte Carlo one has been conducted by the general purpose, continuous energy Monte Carlo N-Particle transport code MCNP5 [17].

8.2.1 ERANOS model

For the parametric analysis, a simplified cylindrical model of ELSY has been considered, where the whole core has been represented by a single homogenized cell. The simulation domain has been extended to account also for the structural regions surrounding the core, acting as a neutron reflector. A cross-cut view of the simulation domain is depicted in Figure 8.3. The parametric analysis has been carried out with the ERANOS 2.0 code [7], by adopting for cell calculations [18] an heterogeneous 2D description for the active region only (the remaining regions have been considered homogeneous) and by using the JEF2.2 nuclear data library [19].

The obtained multigroup (33 energy groups [20] in P_1 approximation) constants have been used for reactor spatial calculations, performed assuming cylindrical symmetry, in S_4 transport approximation [21].

The final characterization of the system has been performed by refining the simulation model in order to discriminate each FA for evaluating the actual power/FA distribution. It is necessary therefore to adopt a 3D Cartesian model of the domain, for which the variational-nodal TGV module of ERANOS [22] has been envisaged. The cell calculations have been performed adopting the same logic approach followed for the preliminary evaluations, since the lack of detailed information on the sub-critical cells layout. All cell calculations have been performed starting from the ERALIB1 [20] base data library, an evolution of the JEF2.2 data set [19] corrected, for the main isotopes, on the basis of a number of integral experiments conducted on the MASURCA facility [23].

8.2.2 MCNP model

By exploiting the powerful MCNP capabilities of real geometry representation, a detailed model of the core region has been set up to simulate as precisely as possible the neutronics of ELSY. Because of the lack of detailed CAD drawings for the FA, a real model of the core has been possible only for the pins region ("Fuel" and "Plenum" regions of Figure 8.3). The rest of the domain, extended - as for the ERANOS model - around the core to account for neutrons reflection, has been modeled with homogeneous regions equivalent to the ones used in ERANOS cell calculations, for the consistency of

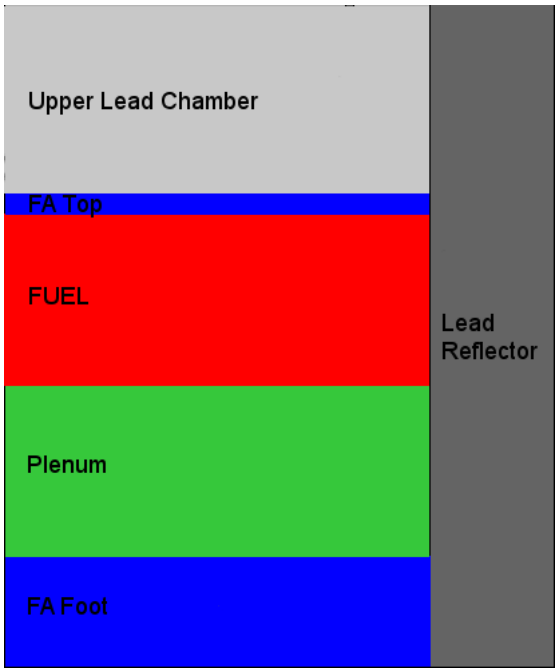

Figure 8.3: Simplified 2D cylindrical computational scheme of ELSY for preliminary parametric analysis.

the two simulations. The error introduced by this approximation is expected not to overcome the known uncertainties affecting nuclear data.

A plot of the MCNP simulation domain at core mid-plane is shown in Figure 8.4 together with a detail of the FA layout.

All MCNP simulations have been performed with JEF2.2 [19] cross-sections data library, processed at the correct operating temperatures by means of the NJoy code [24, 25] through the use of a dialog-based script [26] developed to automatize the processing of a number of cross-sections at a given temperature.

8.3 Results and final layout

The wrapper-less design implies that no gagging can be used for tuning the coolant flow rate to the actual FA power, as usually done for wrapped FAs. The aimed smoothing of the FAs T_{outlet} must be therefore pursued by carefully flattening the power/FA distribution. The choice of realizing hydraulically different FAs (e.g.: with different pin diameters) to tune the flow rates to the actual power without any trough mass transport has been discarded since the higher manufacturing costs.

To guarantee the limit on the maximum clad temperature (550 °C), in

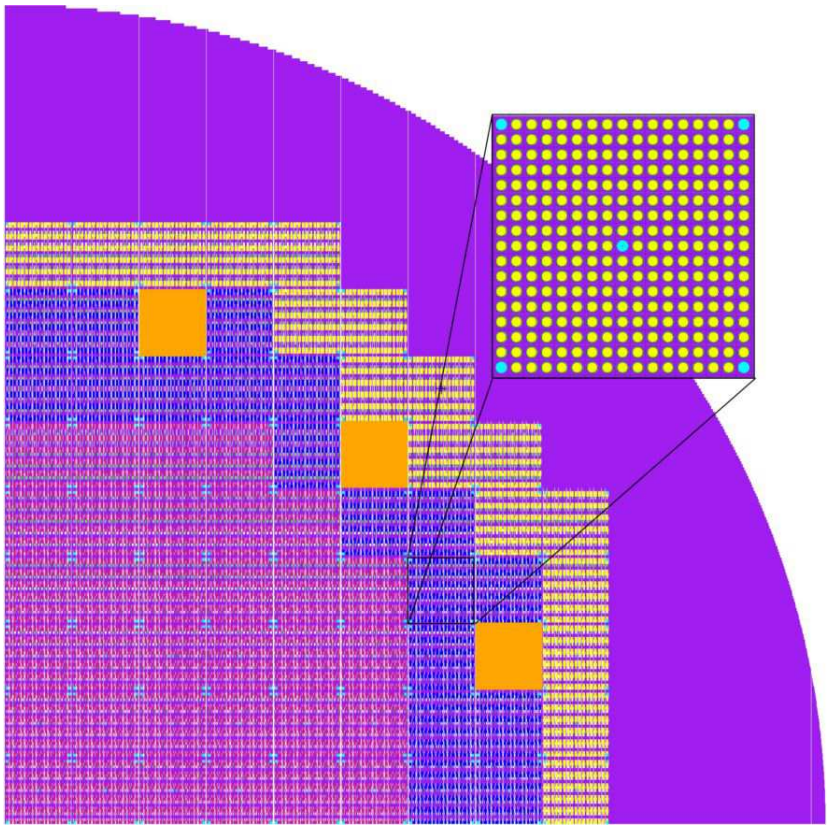

Figure 8.4: MCNP plot of the ELSY mid-plane cross-cut according to the Monte Carlo simulation model.

accordance with the design average coolant outlet temperature of 480 °C, it results necessary to segment the core into radial zones with different enrichments (*i.e.*, different Pu contents). By means of a preliminary thermal-hydraulic evaluation carried out by means of the RELAP code [27], it has been possible to represent the clad temperature as a function of the power/FA distribution factor (FADF), as shown in Figure 8.5. According to this preliminary investigation, the maximum allowed FADF has been fixed to 1.2 in order to not exceed the maximum clad temperature (along with a coolant velocity of about 1.5 m s^{-1} and according to the Zhukov's heat transfer relation for lead in square ducts [28]).

An iterative process followed for assessing the core zoning and proper enrichments selection in order to ensure both the design FADF and the criticality for the resulting core. Twelve FAs among the 284 positions in the core map have been selected for replacement with traditional concept Control Rods to provide the required anti-reactivity for reactor control, regulation and safety. The CRs, made of $90^{a}/_{0}$ ^{10}B-enriched B_4C pins arranged in a square lattice

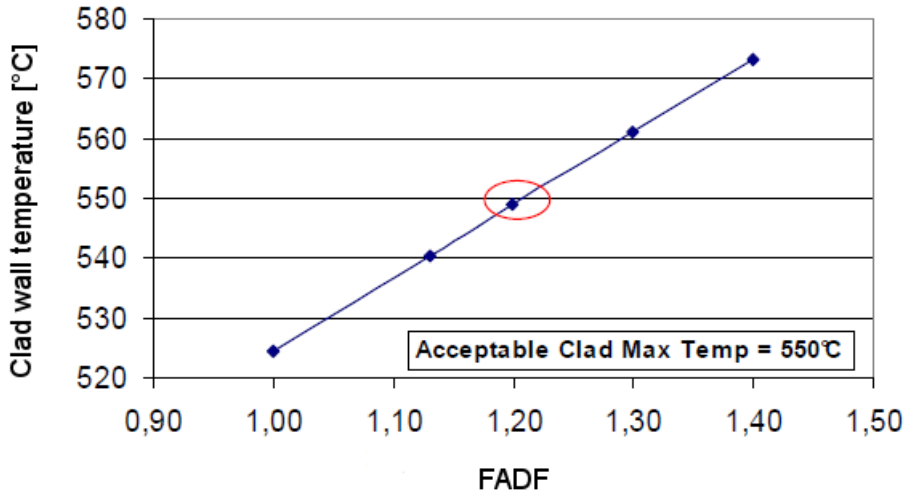

Figure 8.5: Dependence of the clad wall temperature on the power/FA distribution Factor (FADF).

so as to occupy 70% of the whole CR cross-section area, are intended to be placed within the outermost FAs ring in order to optimize their effectiveness by maximizing the neutron paths intersection area, as demonstrated in [29]. The CRs are intended to be moved in empty channels for a fast and reliable passive insertion within the core in case of scram.

A further absorbers system has been envisaged, intended for reactivity swing compensation along the cycle. This additional system is made of $90^{a}/_{0}$ ^{10}B-enriched B_4C cylinders hung on the top of the FAs in the upper lead chamber, occupying 15% of the FA cross-section area. These cylinders are intended to be actioned outside the core, by moving along the upper lead chamber, in order to minimize the perturbation on the radial power shape. Since the reduced thickness of the FA head, this system can be moved up to 10 cm above the core region to compensate the highest reactivity swing. This solution allows also to rely on the presence of neutron absorbers at the top of the lead chamber to prevent any critical rearrangement of the fuel in case of core melt.

The criticality of the core must be guaranteed along the whole cycle, so as to obtain $k_{\text{eff}} = 1$ at End of Cycle (EoC) with all absorbers withdrawn. The modified cylindrical core scheme, accounting for the presence of the two different absorbers system, is shown in Figure 8.6.

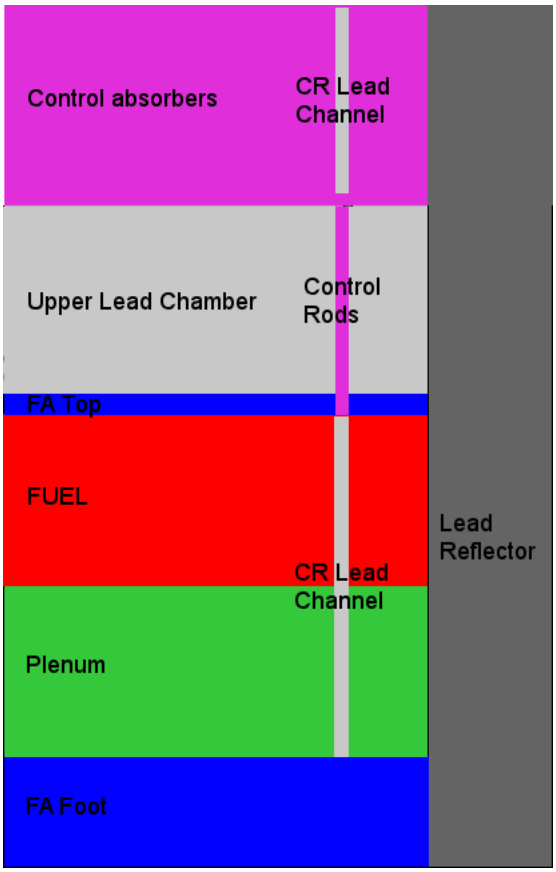

Figure 8.6: Simplified 2D cylindrical computational scheme of ELSY including absorber regions.

8.3.1 Final layout

The burn up calculations performed with ERANOS, together with static analysis at Beginning of Life (BoL), Beginning of Cycle (BoC) and EoC performed by means of MCNP, assessed the final 3-zones core layout shown in Figure 8.7. 132, 72 and 68 FAs have been arranged in the inner, intermediate and outer zone respectively, with a Pu content of 13.4, 15.0 and 18.5$^{v}/_{0}$ in the pellet.

Such a configuration allows a FADF of 1.15 at BoL, as shown in Figure 8.8, well below the postulated limit of 1.2.

8.3.2 Results

The reactivity swing along the 5 years in-pile residence has been evaluated in order to retrieve indications about the operation cycle and to define the

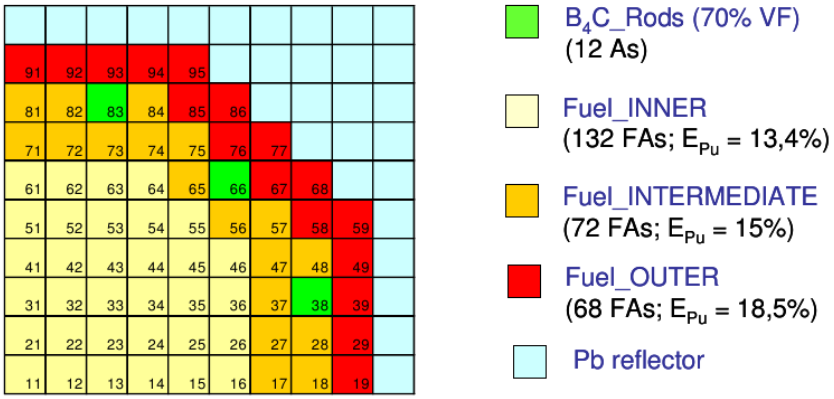

Figure 8.7: Core zoning for the preliminary ELSY configuration as resulting from the criticality and power/FA distribution flattening analysis.

106,3	100,1	92,8	90,4	85,8				
109,0	101,0		93,2	109,7	97,0			
119,6	113,8	106,8	105,8	102,9	111,7	97,7		
112,9	110,1	106,2	102,7	106,1		111,7	97,0	
115,6	113,8	110,7	106,9	101,8	106,1	102,9	109,7	85,8
118,6	117,1	114,5	111,0	106,9	102,7	105,8	93,2	90,4
121,2	120,0	117,7	114,5	110,7	106,2	106,8		92,8
123,2	122,1	120,0	117,1	113,8	110,1	113,8	101,0	100,1
124,2	123,2	121,2	118,6	115,6	112,9	119,6	109,0	106,3

Figure 8.8: Power/FA distribution for the preliminary ELSY configuration.

reactivity to be compensated from absorbers. A swing as small as possible has been targeted for avoiding any significant compensating rod insertion

and, therefore, a significant flux distortion.

Figure 8.9 shows the k_{eff} swing according to a 5 years cycle at full power and without any refueling. The maximum k_{eff} excursion results of about 700 pcm, mainly because of the breeding (almost unitary BR along the entire period, Table 8.3). It has to be noted that both the k_{eff} and the BR increase in the first three years and decrease in the last two. This behavior is coherent with the ^{239}Pu equivalent mass behavior, resumed – for the entire core – in Table 8.4.

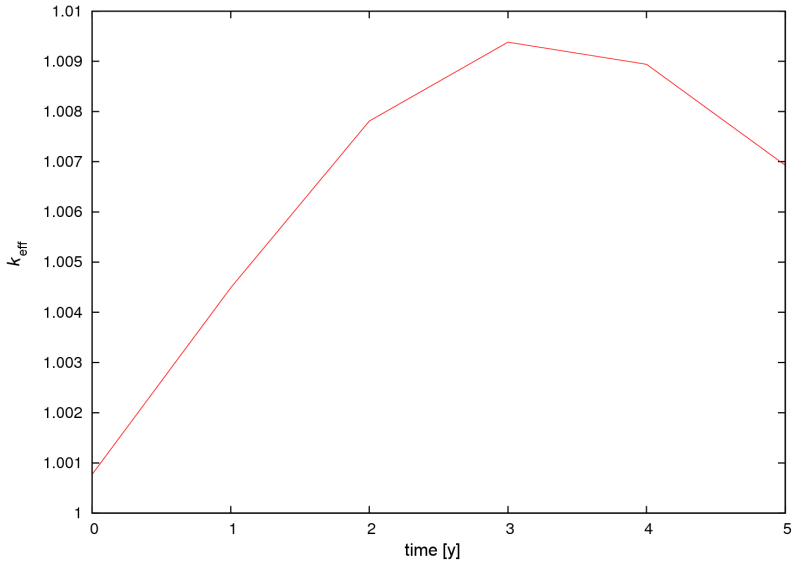

Figure 8.9: Criticality swing during operation for the preliminary ELSY configuration.

Table 8.3: Evolution of the Breeding Ratio (BR) during irradiation in the preliminary ELSY configuration

Time [y]	1	2	3	4	5
BR	1.045	1.033	1.019	1.005	0.992

Table 8.4: Equivalent Pu mass during irradiation in the preliminary ELSY configuration

Time [y]	0	1	2	3	4	5
M(^{239}Pu$_{\text{eq}}$ [kg]	4601.9	4618.3	4632.9	4638.9	4636.3	4625.6

Figure 8.10 shows the associated evolution of the U, Pu and MAs mass within the entire core during burn up. At End of Life (EoL) the mass inventory shows:

- a decrease of the U amount by some 9 $^{w}/_{0}$;
- an increase of the Pu amount by some 3 $^{w}/_{0}$;
- a build up of MA according to an almost exponential behavior toward an equilibrium content of some 400 kg, *i.e.*, about 6% of the Pu mass and 1% of the total HM inventory. The time constant of this exponential is about 12 years.

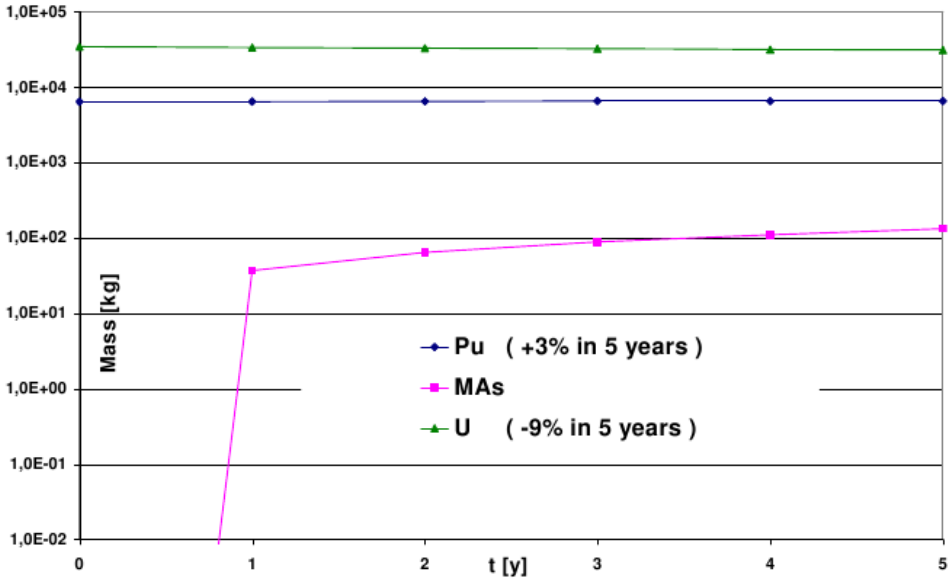

Figure 8.10: Absolute and relative U, Pu and MAs mass evolution during operation for the preliminary ELSY configuration.

Finally, the anti-reactivity of the two control systems envisioned for the preliminary ELSY configuration has been evaluated at BoL. According to the safety requirements, at least 15 $ (evaluated in some 5000 pcm) anti-reactivity must be made available to the system for the cold arrest of the reactor.

The reactivity worth of the two systems are resumed in Table 8.5: the control absorbers above the active zone have been found to provide some 2300 pcm anti-reactivity at full stroke, well above the required worth for compensating the k_{eff} swing. When inserted together with the CRs system, a total anti-reactivity of some 6300 pcm is inserted into the core, ensuring the respect of the safety worth requirement.

Table 8.5: Control systems worth in the ELSY preliminary configuration (at BoL)

Case	k_{eff}	worth [pcm]
Reference	1.00077	–
Regulation system inserted	0.97761	-2316
Control Rods inserted	0.96656	-3421
Both systems inserted	0.93755	-6322

CHAPTER 9

NEUTRONIC DESIGN OF ELSY: FINAL CONFIGURATION

Why are things as they are and not otherwise?

Johannes Kepler (1571-1630)

Abstract. An evolution in the conceptual design of ELSY required a new neutronic design of the core in order to outline the system new layout.
New neutronics calculations are needed indeed to point out both the FA zoning and fuel enrichments guaranteeing the aimed power distribution flattening: the open square configuration under investigation strictly requires indeed rather flat power production by each fuel assembly in order to achieve the economics requirement among Generation-IV specimens.
Both deterministic and Monte Carlo calculations, here presented, have been performed then to assess the reference layout concerning criticality and power distribution. The effectiveness of the three independent systems conceived for reactor shutdown has been also investigated, together with an introductory study for the positioning of the regulation system for criticality swing during the cycle, by means of the general purpose Monte Carlo N-Particles transport code MCNP5.
The matter of this work, conducted in collaboration with ENEA, is also reported in the ELSY Deliverable 8 of EURATOM.

Introduction

Within the ELSY project, after the preliminary investigations on the two alternative core configurations (the hexagonal wrapped and the square wrapper-less), the Council decided to promote the square wrapper-less option as the reference one thanks to the thorough analysis conducted, well highlighting the merits of the LFR.

The second and final step in the optimization of the ELSY core design for the wrapper-less square option has been performed accounting for the results of the safety analysis on the scoping configuration, as well as the overall system rearrangement due to the two concurrent needs of reducing the core dimensions and reinforcing the structures of the Fuel Assembly (FA). Further changes have been also brought to the control systems (two innovative solutions have been also introduced) in order to guarantee their effectiveness for shutdown, and to reduce the smeared density of the fuel pellet in the gap, in order to achieve the desired Burn Up (BU).

Taking advantage of the results obtained by the performances scoping analysis on such a system, a new, optimized core configuration has been drawn from scratch: the criticality of the system has been tuned according also at the stringent need of flattening the power/FA distribution, as well as guaranteeing the aimed peak BU.

9.1 Geometric and material description

With respect to the geometry configuration presented in the previous Chapter and reported in the EURATOM deliverable 6 [29], the overall dimensions of the core have been reduced in order to fit the inner vessel together with a sufficient number of dummy elements shielding the active region, resulting in a reduction of the total FAs number [13]. On the other hand, since the total active height had to be fixed not to undermine the natural circulation, by reducing the total pins number a higher power density is achieved by each fuel pin: it was required therefore to increase the pin pitch from 13.69 mm to 13.9 mm to allow a sufficient lead flow rate in order to guarantee the same heat removal.

The second main change involved the structural layout of the FA. Aiming at the possibility of guaranteeing an easy replacement for all the internals during the plant life, the design idea was to eliminate the lower diagrid for the FAs support and positioning, representing the most difficult element to remove. In order to achieve the diagrids removal, three structural interventions had been necessarily brought to reinforce the FA:

1. an axial extension of the FA height to more than 10 m, to permit the FAs to be hang up to an array of support beams (the dimensioning of the FA height and the positioning of the support beam follow the

criterion of compensating the weight of the FA by floating in Lead);

2. the substitution of the central structural pin with a higher-inertia element ensuring the required stiffness: 9 positions in the pins lattice have been therefore replaced with a T91 FMS, 38.3 mm wide - 1.5 mm thick box beam (the removal of further 8 fuel pins per assembly suggested also to move to larger FAs in order to minimize the critical mass reduction);

3. the reinforcement of the FA foot by introducing a rigid square box along with two diagonal beams: the new foot design could guarantee the mechanical stiffness for the creation of a continuous lattice with the other assemblies, replacing the bottom diagrid.

As a consequence of these two changes, a new 21x21 pins lattice has been proposed for the FA, resulting in 170 positions (with respect to the 284 ones of the previous configuration) fitting the required core area in a staggered square (*i.e.*, triangular-like) arrangement, with 294 mm pitch. The whole core layout is depicted in Figure 9.1.

The goal of high BU (100 GWd t^{-1}) imposes to reduce the smeared density of the fuel (*i.e.*, the area of fuel over the area of fuel and gap within the cladding) at about 0.84. This was obtained by substituting the solid pin with an hollowed one. The pin radius moved from 4.49 mm to 4.5 mm with a 2 mm diameter hole. A cross-cut view of the resulting FA and pin, showing also the central box beam, is presented in Figure 9.2.

The introduction of the box beam suggested the idea to exploit it as thimble guide for the insertion of "finger" absorbers in a properly selected subset of FAs for the system control. The effectiveness of such a solution is suggested, despite the small volumetric fraction associated with the fingers, since the small self-shielding each absorber would present to the others. A preliminary evaluation by C. Artioli and L. Cinotti envisaged the viability of this solution by providing some 70% of the FAs with finger absorbers.

Three different mechanisms were initially pointed out:

1. motorized pins with ^{10}B-enriched B_4C (solid) in box beams properly closed to lead, to be moved from the top during operation[1] and, eventually, let fall by gravity into the active zone for scram;

2. passive pins with ^{10}B-enriched B_4C (solid) in open box beams (thus flooded by lead), to be released from the bottom and let float into the active zone for scram;

[1] The small anti-reactivity associated to each finger absorber suggested also their use for regulating the system criticality during the fuel cycle, acting on the hottest FAs to further flatten the power distribution.

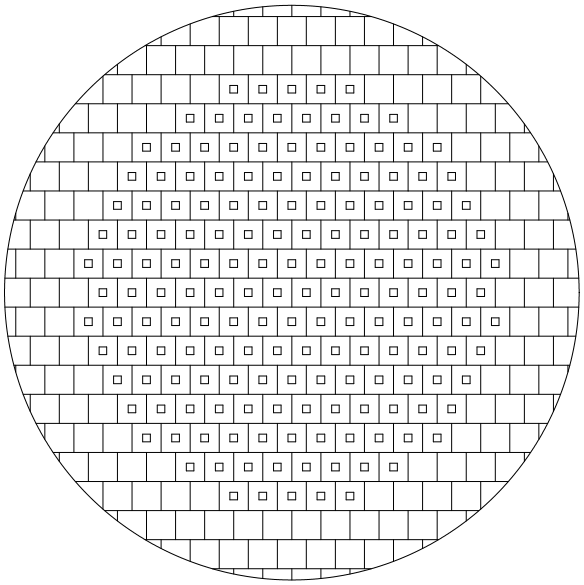

Figure 9.1: The core general layout and FAs arrangement for the final configuration of ELSY.

3. static empty pins, positioned in the active region, to be filled by pouring a liquid In-Cd eutectic from the top, as an *extrema ratio* for scram (representing also the only solution able to intervene in case of structural integrity loss of the channel).

After some scoping calculations, the rigid finger absorber has been selected as the only practical solution: despite the attractiveness of the liquid solution, it had to be rejected indeed because of the small anti-reactivity of indium and cadmium in the fast spectrum of ELSY (some 14% of that of B_4C). Furthermore, it was chosen to move the passive set to the top of the system, thus in empty channels, to prevent any perforation of the reactor vessel. This allows also a standardization of both the box beam and the Finger Absorber Rod (FAR), a cross-cut detail of which is shown in Figure 9.3.

The leading criterion for the actual dimensioning and placement of the FARs on the core map, is the reactivity worth to be ensured for the cold arrest of the system: some 3000 pcm must be provided by each of the two control

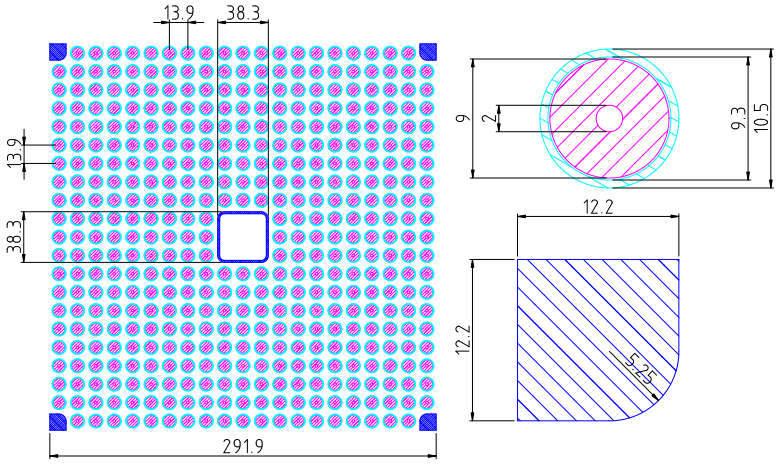

Figure 9.2: FA and pin layout for the ELSY final configuration.

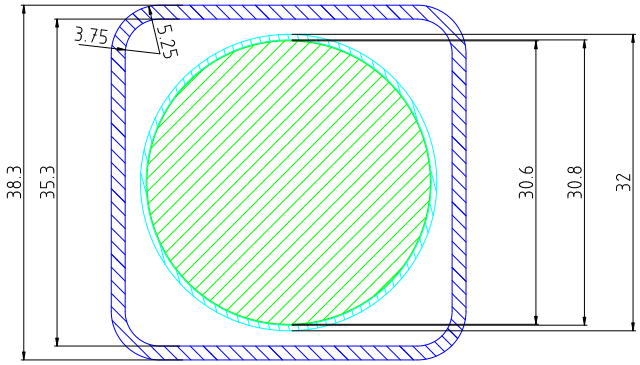

Figure 9.3: Detailed view of a Finger Absorber Rod (FAR) inserted in the FA box beam channel.

FAR systems. Furthermore, the FARs set devoted also to the criticality swing compensation during the cycle, must worth a supplementary anti-reactivity preliminary evaluated in some 1000 pcm.

Due to the innovation represented by this solution, the reliability of such a shutdown system could not be claimed to the certification authority, therefore a traditional control mechanism had to be added for security. As found by preliminary calculations [29], 8 of the 170 assembly positions (among the ones adjacent to the outer ring to maximize the interception area) have been chosen for replacement with massive B_4C Control Rods (CRs). For a passive insertion of the CRs by gravity, the positions occupied by the CRs have

been closed to Lead by introducing within the FAs lattice stiff steel boxes. A cross-cut of the ELSY CR is presented in Figure 9.4.

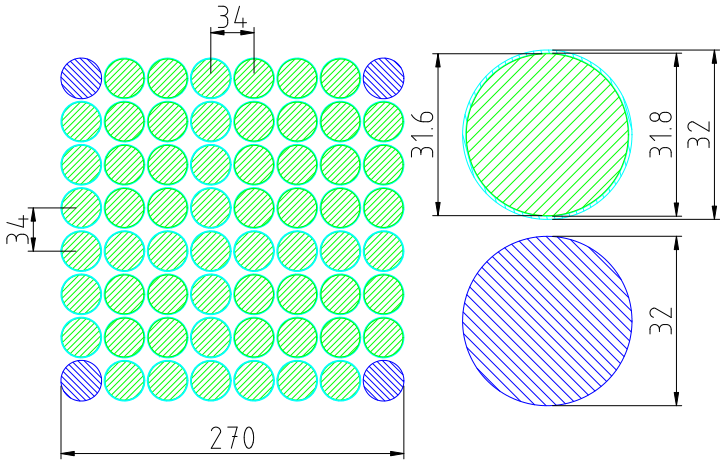

Figure 9.4: Scratch design of the Control Rod and pin layout.

Also in the final ELSY design phase, a pure MOX fuel (*i.e.*, without any MA content) with 1.97 stoichiometric ratio and 95% of the theoretical density has been considered (see Appendix A for fuel properties). All the structures within the inner vessel are made of FMS T91; on the other hand, the Stainless Steel 316LN has been chosen for the reactor vessel, while all the remaining internals are made of SS 316L.

9.2 ELSY computational model

The neutronic design of the final ELSY configuration has been carried out, as for the preliminary one, by both deterministic and stochastic methods, once again according to the aim at compensating the specific pros and cons of each method and at acquiring the needed confidence on the origin and entity of the unavoidable discrepancies.

The deterministic calculations (performed by means of the ERANOS formulary [7]) have been assumed as reference for the assessment of the core zoning into three different Pu-enrichment rings. On the other hand, the stochastic calculations (by means of the general purpose, continuous energy Monte Carlo N-Particle transport code MCNP5 [17]) provided the reference values for the critical mass and for the FARs effectiveness. The same calculations have been also used to cross check the deterministic analysis in terms of power distribution.

Both deterministic and Monte Carlo calculations have been carried out by adopting very detailed 3D geometry models of the reactor, compatibly with the specific domain representation capabilities of each code.

9.2.1 ERANOS model

As for the preliminary design of ELSY, the deterministic analysis has been carried out by means of the ERANOS v. 2.1 code [7], by a two-step process:

1. a transport calculation to evaluate the multi-group cross-sections (both microscopic and macroscopic) for every cell defined in the problem, and

2. a variational-coarse mesh nodal transport calculation to solve the multi-group Boltzmann equation in the whole reactor system.

The multigroup cross-sections set has been produced by means of ECCO [18], starting from rough nuclear data taken by both the ERALIB1 [20] and JEFF3.1 [30] data libraries, treating the main nuclides with a fine energy structure (1968 groups) and condensing the obtained cross-sections in a 33 groups scheme for reactor calculations. Very refined cell descriptions – according to ECCO capabilities – have been adopted for the main cells (*i.e.*,for the cells surrounding the active zone), with particular attention to the FAs provided with a FAR.
In particular, since the possibility of representing only cylindrical or homogeneous regions in the FA lattice, the 9 inner positions (containing the structural box beam and – eventually – the FAR) have been specifically modeled in order to preserve – as far as possible – the heterogeneity of the cell, as shown in Figure 9.5.

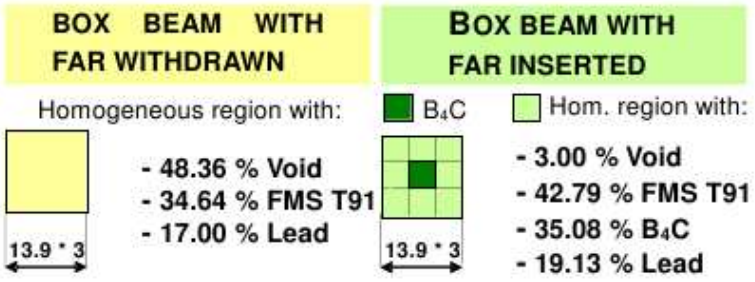

Figure 9.5: ECCO representations of the 9 central positions for a FA with (right frame) and without (left frame) a FAR.

Two different arrangements of homogeneous regions have been envisaged to distinguish FAs provided of a FAR from the remaining ones:

- for the FA without a FAR (or with the FAR withdrawn), the central position is only filled by cover gas (Argon), while the remaining 8 cells are represented by an homogeneous mixture of the remaining void, the steel the box beam is made of, the Lead flowing outside the box beam and the steel representing the three spacer grids placed along

the active height (in order to preserve the total amount of steel in the active zone);

- an analogous description has been adopted also for the FAs with a FAR inserted, substituting the void with the materials the FAR is made of, that is, B_4C in the central position and the remaining B_4C, the Helium in the absorber-clad gap and the clad steel in the 8 surrounding positions.

For the reactor spatial calculation, as for the preliminary ELSY design, the three-dimensional XYZ geometry capabilities of the ERANOS TGV [22] module have been exploited to account for different FAs depletion during BU and actual power/FA distribution. A cross-cut view of the simulation domain for TGV is shown in Figure 9.6.

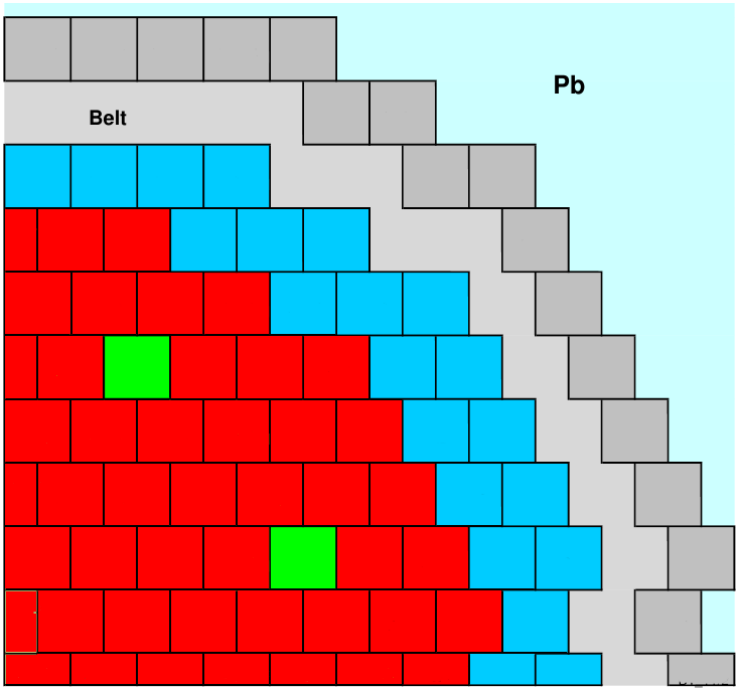

Figure 9.6: Cross-cut view of the ELSY simulation domain with TGV, in which are shown the FAs (red), CRs (green) and dummy elements (blue) positions.

9.2.2 MCNP model

A complete Monte Carlo analysis has been also performed, concerning the design route for the core neutronics through the many successive refinements that have been necessary to outline the final arrangement of the core zoning

and the relative Pu enrichments, as well as for the optimal positioning of the control and the regulation systems.

Exploiting the MCNP ability to treat arbitrary 3D configurations, an exact geometrical model of the whole reactor (as described by the mechanical drawings reported in appendix to the EURATOM Deliverable D6 [29]) has been set up in order to correctly evaluate the effectiveness of FARs. Cross-cut views of the ELSY simulation domain are provided in Figures 9.7 and 9.8 as produced by the MCNP plot interface.

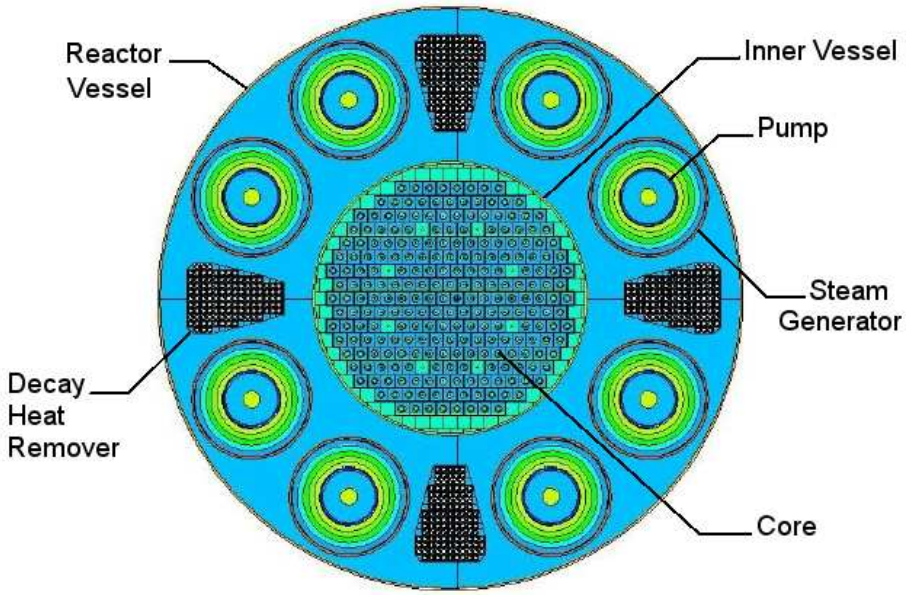

Figure 9.7: Horizontal cross-cut view of the ELSY simulation domain with MCNP.

All MCNP simulations have been performed with JEFF3.1 [30] cross-sections data library, processed at the correct operating temperatures.

9.3 ELSY design: operative parameters optimization

The scoping analysis on the preliminary ELSY configuration demonstrated that both the fuel and clad maximum temperatures (with $v_{\text{coolant}} \simeq 1.5\ \text{m s}^{-1}$) can be respected by segmenting the core into three radial zones.

In order to proceed to the neutronic design of the final ELSY configuration, it is worth notice that the aimed peak BU of 100 GWd t^{-1}, chosen even if to the detriment of the unitary BR obtained in the preliminary ELSY design (see previous Chapter), imposes the adoption of a refueling strategy

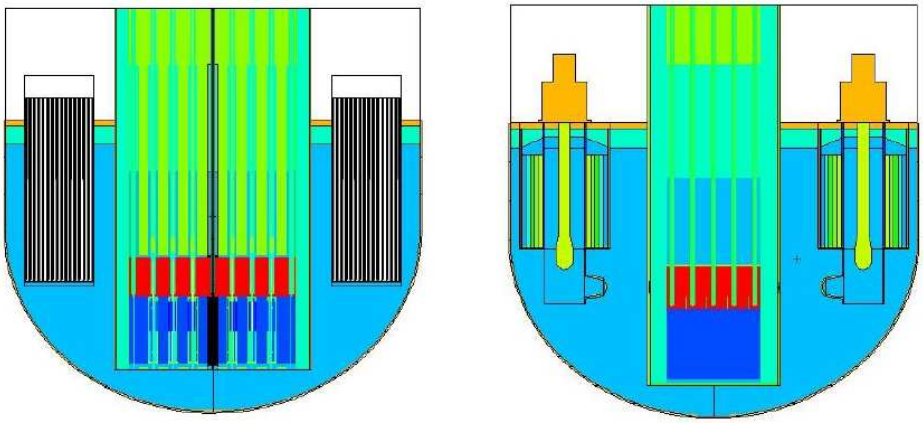

Figure 9.8: Vertical cross-cut views of the ELSY simulation domain with MCNP, at different intersection planes to highlight the DHR and SG positioning.

to mitigate the k_{eff} swing during the cycle. This operative solution has therefore to be postulated in advance – to identify the mean aging of the fuel at BoC and EoC so as to define the criteria for fixing the fuel enrichments in order to get the aimed criticality levels – and, subsequently, to be verified *a posteriori*.

The fuel cycle strategy adopted is an open 4-batch cycle with 5 years of fuel residence time: 1/4 of the core undergoes refueling every 1.25 y after being irradiated for 5 y. Table 9.1 summarizes the core loading at start-up and the subsequent equilibrium cycle: the refueling is performed in correspondence of the cells with two entries, by indicating the fuel residence time before/after it. It results that, at regime (after 3.75 y), immediately before the refueling (EoC) the mean aging of the fuel is 3.125 y, while just after refueling (BoC) the average fuel residence time in the reactor is 1.875 y.

Table 9.1: Scheme of the 4-batches refueling strategy adopted for ELSY

	Fuel residence time [y]			
Year	I quarter	II quarter	III quarter	IV quarter
0	0	0	0	0
1.25	1.25/0	1.25	1.25	1.25
2.5	1.25	2.5/0	2.5	2.5
3.75	2.5	1.25	3.75/0	3.75
5	3.75	2.5	1.25	5/0

The study of the fuel cycle can be approximated by a 1-batch simulation, that is segmenting the 5 y BU into 8 steps, 0.625 y (228 days) each long. Under such hypothesis, starting from a singular BoL configuration (step 0) of completely fresh, homogeneous core, the BoC and EoC configurations will correspond respectively to the 3^{rd} and 5^{th} BU steps. It has been demonstrated indeed [31] that the 1-batch hypothesis conservatively estimates the reactor performances (both the criticality swing and fuel maximum temperature [32]) with respect to a real 4-batches cycle evaluation with reshuffling.

According to this refueling strategy, the optimal fuel enrichments have to be pointed out so to guarantee the respect of the design FADF, as well as providing $k_{\text{eff}} = 1$ at EoC with all control rods withdrawn. The over-criticality at BoC will be therefore compensated by a proper insertion of the regulation FARs subset.

9.4 Results and final layout

As for the preliminary ELSY design, the wrapper-less option implies that no gagging can be used for tuning the coolant flow rate to the actual FA power. To guarantee the limit on the maximum clad temperature (550 °C), it is therefore needed to carefully flatten the power/FA distribution by segmenting the core into radial zones with different enrichments (*i.e.*, different Pu contents), so as to pursue the aimed smoothing of the FAs T_{outlet}. The maximum allowed FADF has been once again fixed to 1.2, according to the coolant velocity of about 1.61 m s^{-1} and to the Zhukov's heat transfer relation for lead in square ducts [28]).

An iterative process followed for assessing the core zoning and proper enrichments selection in order to ensure both the design FADF and the criticality for the resulting core. In particular, the criticality of the core must be guaranteed along the whole cycle, so as to obtain $k_{\text{eff}} = 1$ at End of Cycle (EoC) with all absorbers withdrawn. The over-criticality at BoC will be compensated by some motorized FARs, whose positioning can be, in turn, optimized in order to further flatten the radial power distribution.

9.4.1 Final layout

The burn up calculations performed with ERANOS and ERALIB1, together with static analysis at BoL performed by means of both MCNP and ERANOS with JEFF3.1, assessed the final 3-zones core layout shown in Figure 9.9. 56, 50 and 56 FAs have been arranged in the inner, intermediate and outer zone respectively, with a Pu content of 14.0, 17.0 and 19.9$^{v}/_{0}$ in the pellet.

Table 9.2 resumes the three different Pu enrichments, together with the corresponding atomic and weight fractions, and their averaged value on the whole core.

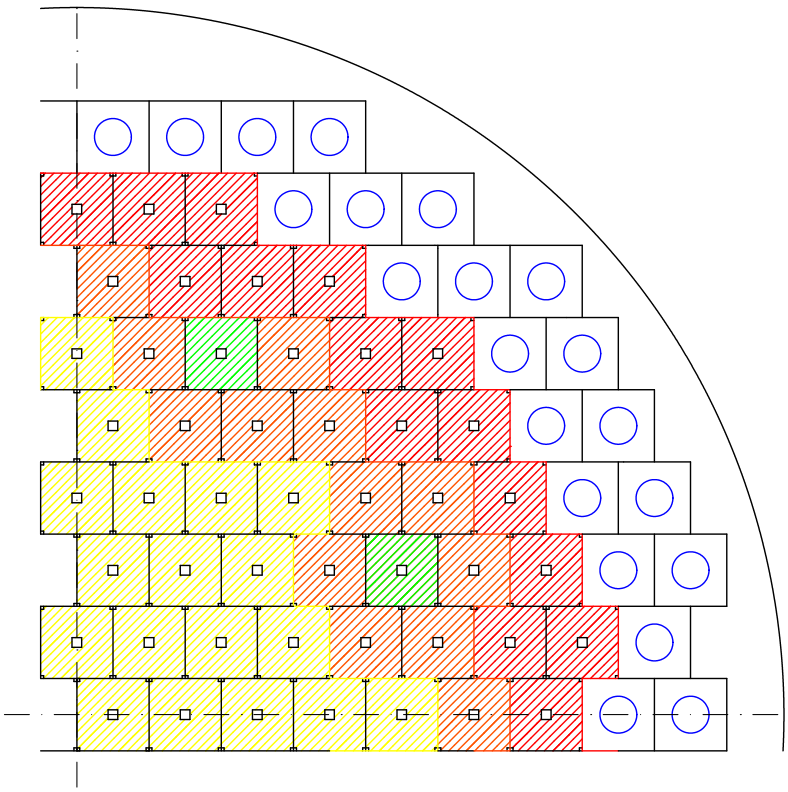

Figure 9.9: Core zoning for the final ELSY configuration as resulting from the criticality and power/FA distribution flattening analysis.

Table 9.2: Plutonium enrichment in the three radial zones of the final ELSY configuration

Region	FAs	Pu / (U + Pu)		
		[v %]	[a %]	[w %]
Inner	56	14.00	14.45	14.54
Intermediate	50	17.00	17.53	17.63
Outer	56	19.90	20.50	20.61
Whole core	162	16.97	17.49	17.59

Such a configuration allows a FADF of 1.17 at EoC, as shown in Figure 9.10, well below the postulated limit of 1.2.

According to this power/FA distribution map, and considering the different breeding figures of the three zones, useful indications have been collected for the FARs positioning (*i.e.*, for locating the FAs to be provided with a FAR),

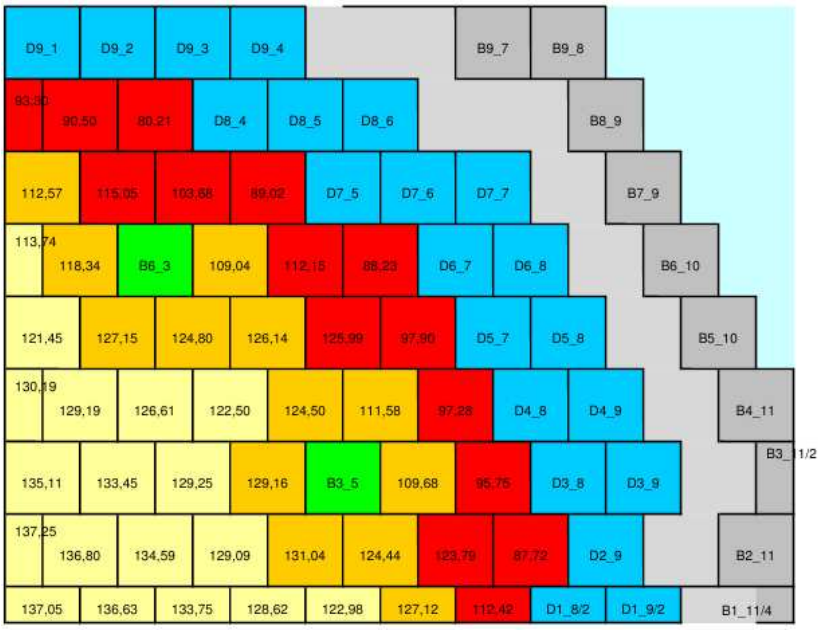

Figure 9.10: Power/FA distribution for the final ELSY configuration at EoC.

shown in Figure 9.11. The FARs have been also grouped into two different systems, each one appointed to a different task:

- 32 FARs have been foreseen for passive scram only (that is, gravity driven);
- 38 FARs have been foreseen for active (hence motor driven) control. In its turn, the motorized system can be split into two subsets, the former devoted to both criticality swing compensation during the cycle and punctual power distribution flattening, and the latter to both control and shutdown.

9.4.2 Results

The information on the reactivity swing along the 5 years in-pile residence, evaluated with ERANOS and ERALIB1, have been corrected accounting for the differences between the results obtained with different codes and libraries at BoL, resumed in Table 9.3.

The reactivity evolution during operation has been therefore corrected, assuming a constant discrepancy between the evaluations of the different codes/libraries is kept at every simulation step. The final estimated criti-

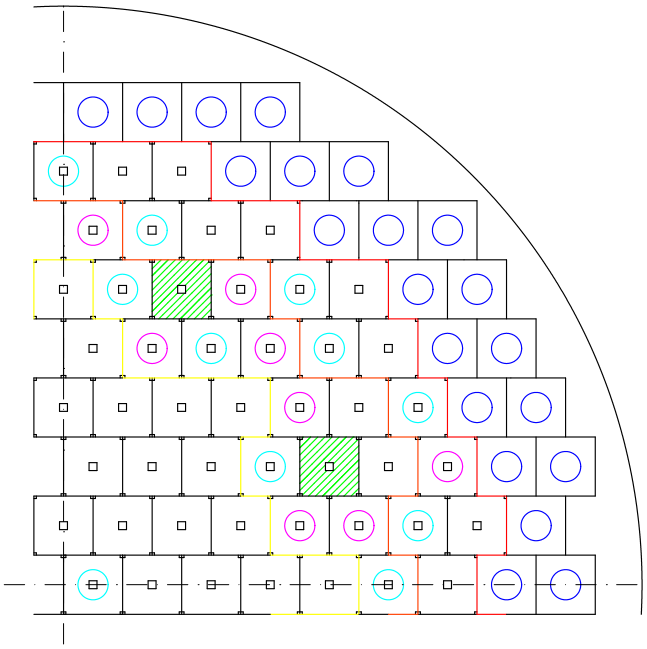

Figure 9.11: Positioning of the passive (magenta circles) and motorized (cyan circles) FARs on the final ELSY core map.

Table 9.3: Criticality evaluations at BoL with MCNP and ERANOS, using JEFF3.1 and ERALIB1 libraries, for the ELSY final configuration

Code / Library	k_{eff}	Difference [pcm]
MCNP / JEFF3.1	1.02500 ± 0.00063	–
ERANOS / JEFF3.1	1.02678	178
ERANOS / ERALIB1	1.03109	609

cality evolution for the final configuration of ELSY is therefore plotter in Figure 9.12.

As expected, a monotonic decrease of k_{eff} is observed, due to the higher enrichment reducing the breeding capabilities. Referring to the equivalent BoC - EoC interval (the green stretch in Figure 9.12), the k_{eff} excursion results of about 900 pcm. The overall criticality behavior is coherent with the ^{239}Pu equivalent mass evolution, resumed – for the entire core – in Table 9.4.

The general reduction of the ^{239}Pu equivalent mass (resulting from the combination of the fertilization in the inner region and the net depletion in the remaining ones) yields an overall BR = 0.94, as expected.

Figure 9.13 shows the associated evolution of the U, Pu and MAs mass

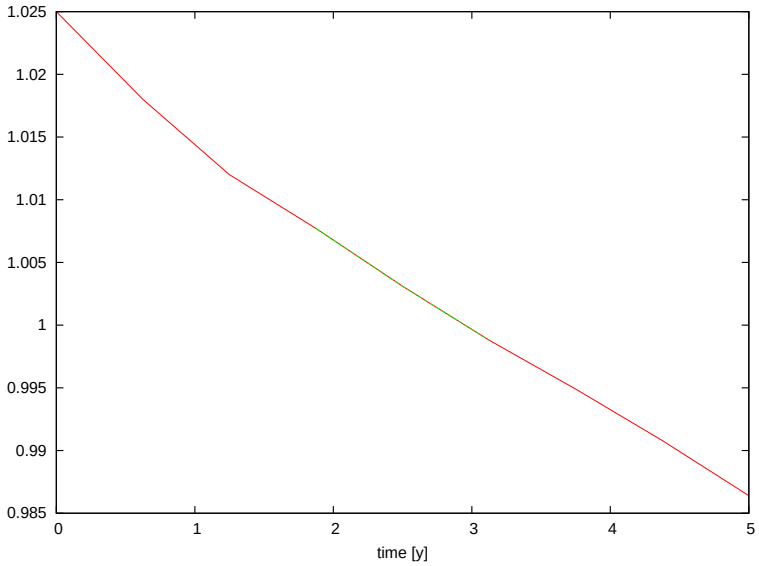

Figure 9.12: Criticality swing during operation for the final ELSY configuration.

Table 9.4: Equivalent Pu mass during irradiation in the final ELSY configuration

Time [y]	M($^{239}Pu_{eq}$) [kg]
0	4469.6
1	4415.2
2	4379.6
3	4348.0
4	4318.4
5	4290.8
6	4264.4
7	4238.4
8	4212.0

within the entire core during burn up. At End of Life (EoL) the mass inventory shows:

- a decrease of the U amount by some 9.6 $^{w}/_{0}$;
- a decrease of the Pu amount by some 1.6 $^{w}/_{0}$;
- a build up of MA according to an almost exponential behavior toward an equilibrium content of some 320 kg, *i.e.*, about 5% of the Pu mass

and 0.9% of the total HM inventory. The time constant of this exponential is about 6.5 years.

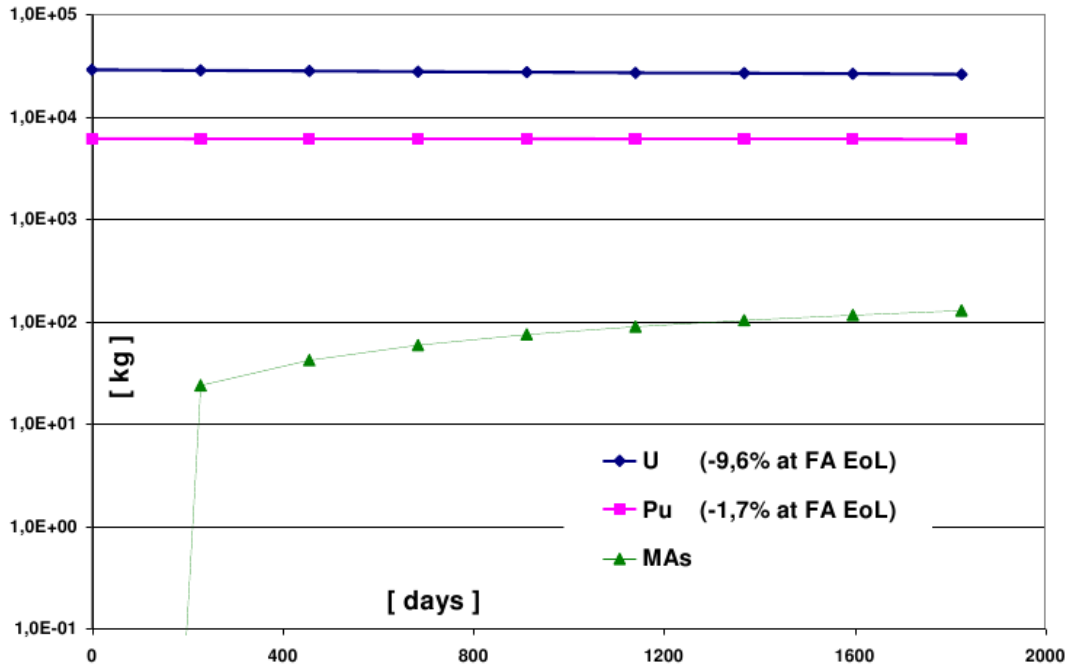

Figure 9.13: Absolute and relative U, Pu and MAs mass evolution during operation for the final ELSY configuration.

Accounting for the the average power density on the homogenized core ($\sim$ 117 W cm^{-3}), it is possible to retrieve 78.1 MWd kg^{-1} as average BU value, corresponding to the BU for the average FA. To this average value corresponds a BU for the peaked FA of about 94 MWd kg^{-1}, thus a local peak BU of 111 MWd kg^{-1}, slightly above the design limit. Nevertheless, since the evaluation of the BU for the peaked FA has been performed referring – conservatively – to the most burning FA at every step, even if corresponding to physically different positions on the core map, and considering the possibility of FAs reshuffling during refueling, it is possible to assume that the supposed 100 MWd kg^{-1} limit is respected.

Finally, the anti-reactivity of the three control systems (the two FAR sets and the CRs) envisioned for the final ELSY configuration has been evaluated at BoL. Table 9.5 resumes the results obtained with both MCNP/JEFF3.1 and ERANOS/ERALIB1.

Assuming the MCNP evaluations as the reference ones, it is possible to see that only the ERANOS estimate for the CRs worth agree within a reasonable margin to the reference one, the values of the FARs worth being much more

Table 9.5: Worth of control systems in the ELSY final configuration (at BoL)

	MCNP/JEFF3.1		ERANOS/ERALIB1	
Case	k_{eff}	worth [pcm]	k_{eff}	worth [pcm]
Reference	1.02500	–	1.03109	–
Motorized FARs inserted	0.98980	-3520	0.98632	-4477
Passive FARs inserted	0.99835	-2665	0.99247	-3862
Control Rods inserted	0.96709	-5791	0.97044	-6065

distant from those obtained by MCNP.

The large difference between the results of the two codes concerning the FAR efficacy is surely due to the approximations introduced in the deterministic analysis. In fact, even if these small absorbers have been accurately modeled in the cell analysis (for a correct treatment of the self-shielding, see subsection 9.2.1) where the intercepted area of neutrons has been correctly considered by the probability collisions method [33], their limited dimensions (a $\sim$ 40 mm side box in a 290 mm wide FA) introduce a large uncertainty in the reactor spatial calculations. As net result, the macroscopic cross-section representing the FA with FAR inserted over-estimate the captures by B_4C. The same self-shielding effect is greatly reduced for the 8 CRs worth evaluation because of the high B_4C VF in the bundle (Figure 9.4).

Referring to the results of Table 9.5, the CRs have been found able to provide far more than the aimed 3000 pcm for safety: their use can be therefore envisaged also for refueling operations, when some 5000 pcm anti-reactivity are usually requested[2].

On the other hand, the worth of the two FARs systems have been found slightly below the aimed values (by some 350 to 500 pcm). The immediate solution could be to increase their number: this results feasible because some $4 \div 8$ more FARs will yield the missing anti-reactivity and there is enough space on the plant to place them (Figure 9.11).

[2] During the refueling a wider margin of anti-reactivity is usually required for accounting, besides the cold arrest of the system, also the occurrence of accidental misplacement of highly enriched, fresh FAs in the inner core region, being the different FAs hardly distinguishable each other.

Part III

A Sustainable Nuclear Scenario Hypothesys

CHAPTER 10

THE ADIABATIC REACTOR THEORY

The most exciting phrase to hear in science, the one that heralds the most discoveries, is not "Eureka!" but "That's funny...".

Isaac Asimov (1920-1992)

Abstract. The sustainability of nuclear energy is a key point for the aimed nuclear renaissance: according to this, the next generation of Nuclear Power Plants must ensure the full closure of the fuel cycle. Besides Partitioning and Transmutation programs, a possible effective strategy is the one relying on the introduction of adiabatic reactors – that is: reactors which do not exchange any valueable material with the environment – for the closure of the fuel cycle within the reactor itself.
In this sense, the energy production can be ensured by feeding only Natural or Depleted Uranium to the system, which in turn releases to the environment only the - unavoidable - nuclear combustion outcome (Fission Products).
To do this, the nuclear equilibrium of the fuel is exploited, maintaining unaltered the total amount of TRansUranic isotopes (which represent the Long Lived Radioisotopes of the High Level Wastes) in the fuel so to continuously recycle the latter within the system.

Introduction

Since the beginning of the nuclear age, all research activities related to NPPs development were oriented at pursuing particular businesses rather than common objectives of social interest. The reflection which followed the Chernobyl accident stressed the need for stimulating nuclear research aiming at the acceptability of nuclear energy to the public opinion, with special regard to safety and sustainability. Intrinsic and passive safety concepts were developed within this frame, resulting in the technological improvements which brought from Generation-III to Generation-III+ nuclear power plants.

The issues concerning sustainability of nuclear energy as a whole up to now have been approached by defining Partitioning and Transmutation (P&T) programs to plan efficient strategies related to the management, exploitation and disposal of nuclear wastes.

The recent breaking need for the sustainability of energy production as a whole, due to the unrestrainable production of greenhouse gases following the continuously increasing worldwide energy demand, imposes the actual closure of nuclear fuel cycle in order to candidate nuclear energy as the only realistic, effective alternative to fossil fuels. Within this frame, the "adiabatic" core concept arises as an interesting and promising solution for both an efficient exploitation of Uranium resources, extending the availability of the nuclear energy feed for thousand years, and the minimization of the volumes and radiotoxicity of High Level nuclear Wastes (HLWs).

10.1 The Adiabatic core concept

The evolution of the fuel composition is ruled by radioactive decay and neutron induced transmutation: as a matter of fact, each nuclide can either transmute into another – different – one or disappear from the fuel inventory (*i.e.* removed by fission). The number of created/removed isotopes depends therefore on their abundance in the fuel: each reaction (either natural or neutron-induced) transmutes or removes an isotope at a rate which depends on the abundance of the source nuclide in the inventory.

The balancing of production and removal rates for valuable actinides can be therefore set by adjusting the mutual abundances of the isotopes in the fuel: it is possible indeed to compute proper Actinide concentrations so to exactly equilibrate the TRUs build up and burn up rates, maintaining unaltered their amount – both in quantity and vector – in the cycle within and outside the reactor.

For this equilibrium goal, the net depletion due to fission must be applied to U^{238}, the reference fertile material in the core: every fission in the system reverberates therefore through the creation/removal chain up to Uranium.

At the end of operations, a net depletion of fertile will be only observed, the inventory of TRUs being unaltered.

An adiabatic core is therefore a black box system able to convert an input feed of either Natural or Depleted Uranium (NU or DU, respectively) into energy, with FPs and Actinides reprocessing losses as only output stream (the U depletion and FPs build up rates being 238 uma/200 MeV). In detail, within an adiabatic core, Pu and MAs are introduced in the fuel according to their equilibrium concentrations. According to this, the Actinides build up and burn up rates equilibrate, maintaining unaltered their amount in the system: this allows the full closure of the fuel cycle (Fig. 10.1) within the reactor (thus the term adiabatic, because having no "valuable" exchange with the environment).

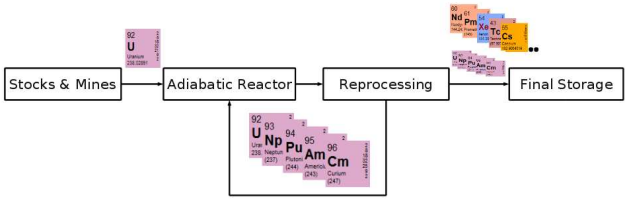

Figure 10.1: Scheme of the closed fuel cycle resulting by the introduction of adiabatic reactors.

In this frame, a new scenario with minimal impact on the environment can be proposed as a candidate to effectively eliminate the need for fossil fuels. According to this, nuclear energy represents the base-load supply for the worldwide power request. The load-following can be set by extensively introducing alternative energy distributed supplies, as well as over-dimensioning the installed nuclear capacity and modulating the fraction of power to be destined to distribution rather than to Hydrogen production for urban transport, for instance.

It is also to be pointed out that the homogeneous reprocessing of the spent fuel (for the extraction of the FPs only from the matrix), intrinsically implied by the adiabatic fuel cycle, would also represent a valuable barrier against proliferation.

10.2 The nuclear equilibrium state

The research for the equilibrium concentrations of Actinides in the fuel is therefore the key task for the design of an adiabatic reactor. The well-known Bateman equations [6] can be used to express the evolution of the

fuel within the reactor:

$$\frac{\mathrm{d}\,N_i(t)}{\mathrm{d}\,t} = \sum_j N_j(t)\sigma_{j\to i} f\varphi + \sum_j N_j(t)\lambda_j - N_i(t)\sigma_i f\varphi - N_i(t)\lambda_i\,, \quad (10.1)$$

where $N_i(t)$ is the number of atoms of isotope i at time t, $\sigma_{j\to i}$ is the one-group cross section related to the reaction transmuting isotope j into isotope i, f is the load factor of the NPP, φ is the neutron flux integrated over the whole fuel volume, $\lambda_{j\to i}$ the decay constant of isotope j into isotope i, σ_i the total, one-group transmutation cross section of isotope i and λ_i the total decay constant of isotope i.

For each isotope, the former terms are given by decay and transmutations laws for the considered isotope, while the latter terms are represented by analogous laws for the proper isotopes among the remaining ones. It is known indeed that every actinide decays radioactively into another isotope with an exponential law regulated by a proper time constant, as well as, under neutron flux, transmutes into a different nuclide by capture, (n,xn) reaction, inelastic scattering (if a metastable state exists), or disappears for fission. For each mechanism (except fission), an isotope is removed and another one is created according to the physics of the phenomenon. Table 10.1 resumes the interconnection scheme for every possible reaction a generic isotope of atomic number Z and mass number A undergoes.

Table 10.1: Resume of target (T) and source (S) nuclides in the decay and transmutation map of a generic nuclide X_Z^A

mechanism	target	source
α-decay	T_{Z-2}^{A-4}	S_{Z+2}^{A+4}
β^--decay	T_{Z+1}^{A}	S_{Z-1}^{A}
β^+-decay	T_{Z-1}^{A}	S_{Z+1}^{A}
γ-decay	T_{Z}^{A}	S_{Z}^{A*}
neutron capture	T_{Z}^{A+1}	S_{Z}^{A-1}
(n,xn) collision	T_{Z}^{A-x+1}	S_{Z}^{A+x-1}
inelastic collision	T_{Z}^{A*}	S_{Z}^{A}

It is clear that the concentration of each isotope may change (from system to system) depending only on the effective reaction rates, which in turn are determined by the integral neutron flux level and the cross sections (thus on the neutron flux energy spectrum), facing the – fixed – decay rate.

Several studies have been already conducted regarding the nuclear equilibrium steady-state [34] as well as the evolution of the fuel in a reactor according to either the Pu and Pu+MAs multi-recycling scheme [35, 36]. An alternative, theoretical approach is proposed to define *a priori* the composition of the equilibrium fuel, imposing that the net amount of TRUs to

be loaded in a hypothetical system, after cooling and refabrication (with respective radioactive decay and reprocessing losses), equals the total amount at the beginning of the cycle, in the s.c. *extended equilibrium state*.

10.2.1 Steady-state equilibrium

In steady-state equilibrium all isotope concentrations remain unaltered along operation, so the time derivative term vanishes. Physically, despite the fact that transmutation mechanisms co-operate toward equilibrium, this is not possible because of the net depletion due to fission. Since in nuclear reactors the depletion of fissile (or fertile, for breeder reactors) and the simultaneous production of FPs is compensated by refueling the core periodically, in the considered steady-state model a fictitious term of continuous feed has to be introduced in order to balance the net fission loss. Aiming at the adiabatic configuration, an Uranium (either natural or depleted) feed is conceived: the combined transmutation/decay mechanism balances the losses by fission rearranging the fuel composition according to a net depletion of the Uranium component only. For each nuclide a feed term s_i is therefore introduced[1], modifying the system (10.1) into the new

$$0 = \sum_j N_j(t)\sigma_{j\to i} f\varphi + \sum_j N_j(t)\lambda_j + s_i - N_i(t)\sigma_i f\varphi - N_i(t)\lambda_i \,. \quad (10.2)$$

10.2.2 Extended equilibrium state

The assumption of a continuous refueling introduced to justify the steady-state hypothesis is far from actual operation: the fresh fuel can be inserted within the reactor only during proper refueling periods, according to well-defined strategies that take into account the maximum admissible BU of the fuel, the criticality swing, the neutrons induced damaging on the FA structurals, etc.

A more general approach must be set in order to consider the actual closure of the fuel cycle, taking also into account the decay period out of pile, during the cooling, reprocessing and refabrication phases. Aiming at recycling continuously the same amount of TRUs within the reactor, the equilibrium condition translates by imposing that the composition of a refuel batch does not change between two successive loadings into the core. That is: the isotopic inventory of the fuel, after irradiation in pile, cooling out of pile, repro-

[1] The total feed rate (sum of the s_i terms) can be computed by converting the thermal power of the system $P_{\rm th}$ into a rate of fission events, that is

$$s = \frac{P_{\rm th}}{< Q >} \,,$$

where $< Q >$ is the mean energy released by every fission event, splitted among the isotopes the feed vector is made of, according to their abundances.

cessing (with the associated losses), integration with fresh fertile (according to the adiabatic core concept) and refabrication must remain unaltered.

The time dependent formulation of the Bateman equations has therefore to be considered, both for the irradiation period and the cooling/reprocessing one. During the latter, a simplified formulation of equation (10.1) holds, in which the transmutation term vanishes since $\varphi = 0$:

$$\frac{\mathrm{d}\, N_i(t)}{\mathrm{d}\, t} = \sum_j N_j(t)\lambda_j - N_i(t)\lambda_i \,. \tag{10.3}$$

10.3 Numerical formulations for nuclear equilibrium solution

By indexing the actinide isotopes to be considered in the model, it is possible to build two matrixes representing the transmutation operator $\underline{T}$ and the decay operator $\underline{D}$ according to the mutual relationships summarized in Table 10.1. These operators, collecting, row-by-row, the removal term (in the diagonal position) and the proper source terms (in the relative non-diagonal positions) for each isotope, are defined, respectively, by

$$t_{i,j} = \begin{cases} -\sigma_i f \varphi & i = j \\ +\sigma_{j\to i} f \varphi & i \neq j \,, \end{cases} \tag{10.4}$$

and

$$d_{i,j} = \begin{cases} -\lambda_i & i = j \\ +\lambda_{j\to i} & i \neq j \,. \end{cases} \tag{10.5}$$

Equation (10.1) and (10.3) would become then

$$\frac{\mathrm{d}\, \vec{N}(t)}{\mathrm{d}\, t} = \underline{T} \cdot \vec{N}(t) + \underline{D} \cdot \vec{N}(t) \equiv \underline{O} \cdot \vec{N}(t) \tag{10.6}$$

and

$$\frac{\mathrm{d}\, \vec{N}(t)}{\mathrm{d}\, t} = \underline{D} \cdot \vec{N}(t) \,, \tag{10.7}$$

where the irradiation operator $\underline{O}$ has been introduced.

10.3.1 Steady-state equilibrium

The steady-state equilibrium can be easily solved numerically by considering the matrix form of equation (10.2):

$$0 = \underline{O} \cdot \vec{N} + \vec{S} \,, \tag{10.8}$$

where S is the feed vector, collecting the single s_i terms.

The flux level has been retrieved by normalizing the neutron flux to the reactor power, according to the density of the fuel pellet (recalculated at every iteration for the solution convergence) and the total volume of fuel in the system.

The update of the flux is based on the conservation of the reactor power P_{th} (input by the user) according to the following relation:

$$\varphi = P_{\text{th}} \frac{\sum_i N_i}{V_{\text{fuel}} \rho_{\text{fuel}} \sum_i Q_i \sigma_{i,\text{f}} N_i} , \tag{10.9}$$

where V_{fuel} and ρ_{fuel} are the total volume of the fuel in the reactor (input by the user) and the fuel density, respectively, and Q_i is the fission Q-value for isotope i. The fuel density is calculated by the code according to relation A.11 presented in Appendix A.

The "adiabatic concentrator" code has been developed in order to apply to whatever system by inputing all the peculiar properties of the latter. An iterative solver (traditional SOR) has been implemented to retrieve the equilibrium concentrations for a given integral flux, the spectrum of which being fixed by the proper cross sections, input by an external ASCII file in the code. The "adiabatic concentrator" source is listed in Appendix B.

10.3.2 Extended equilibrium state

The time discretization has to be dealt now, segmenting the total irradiation and decay periods, T_O and T_D, into successions of t_O and t_D steps respectively, Δt each long.

The evolution of the fuel composition can be then formalized by recalling the general recurrence formula for time integration:

$$\overrightarrow{N}^{(t+1)} = \underline{A} \cdot \overrightarrow{N}^{(t)} , \tag{10.10}$$

where

$$\underline{A} = \left(\frac{1}{\Delta t} \underline{I} - \vartheta \left\{ \begin{array}{c} \underline{O} \\ \underline{D} \end{array} \right\} \right)^{-1} \cdot \left(\frac{1}{\Delta t} \underline{I} + (1 - \vartheta) \left\{ \begin{array}{c} \underline{O} \\ \underline{D} \end{array} \right\} \right) . \tag{10.11}$$

In (10.11), $\underline{I}$ is the identity matrix and ϑ is a weighting factor. It can be proven that the stability of the time integration is always ensured for implicit methods, where $\vartheta > \frac{1}{2}$. For values $\vartheta < \frac{1}{2}$, the scheme becomes stable if $\Delta t < \Delta t_{\text{critical}} = \Delta t_{\text{critical}}(\vartheta)$.

According to (10.10) it results

$$\begin{aligned}
\overrightarrow{N}^{(1)} &= \underline{A}_O \cdot \overrightarrow{N}^{(0)} \\
&\dots \\
\overrightarrow{N}^{(t_O)} &= \underline{A}_O \cdot \overrightarrow{N}^{(t_O-1)} = \underline{A}_O^{t_O} \cdot \overrightarrow{N}^{(0)} \\
\overrightarrow{N}^{(t_O+1)} &= \underline{A}_D \cdot \overrightarrow{N}^{(t_O)} \\
&\dots \\
\overrightarrow{N}^{(t_O+t_D)} &= \underline{A}_D \cdot \overrightarrow{N}^{(t_O+t_D-1)} = \underline{A}_D^{t_D} \cdot \overrightarrow{N}^{(t_O)} = \underline{A}_D^{t_D} \cdot \underline{A}_O^{t_O} \cdot \overrightarrow{N}^{(0)} .
\end{aligned}$$

The adiabaticity of the system holds if the irradiated and decayed fuel, $\overrightarrow{N}^{(t_O+t_D)}$, differs from the fresh one, $\overrightarrow{N}^{(0)}$, by the only disappearance of the feed Uranium[2]:

$$\underline{A}_D^{t_D} \cdot \underline{A}_O^{t_O} \cdot \overrightarrow{N}^{(0)} + \overrightarrow{F} = \overrightarrow{N}^{(0)} , \tag{10.12}$$

that is:

$$\left(\underline{A}_D^{t_D} \cdot \underline{A}_O^{t_O} - \underline{I} \right) \cdot \overrightarrow{N}^{(0)} = -\overrightarrow{F} . \tag{10.13}$$

This problem admits an analytical solution in the form

$$\overrightarrow{N}^{(0)} = -\left(\underline{A}_D^{t_D} \cdot \underline{A}_O^{t_O} - \underline{I} \right)^{-1} \cdot \overrightarrow{F} , \tag{10.14}$$

which is the aimed equilibrium fuel vector.

[2]The feed Uranium vector can be computed by evaluating the total number of fissions occurred during operation, that is

$$\sum_i F_i = \frac{P_{\text{th}} T_O}{Q} ,$$

where P_{th} is the thermal power of the reactor and Q is the mean energy released by every fission event, splitted among the isotopes the feed vector is made of, according to their abundances.

CHAPTER 11

A NEW PARADIGM FOR CORE DESIGN

The important thing in science is not so much to obtain new facts as to discover new ways of thinking about them.

William Lawrence Bragg (1890-1971)

Abstract. In almost every field many measures have been taken, or at least proposed, to overcome the "surviving problem". The very significant of them are referred to a new way of conceiving, approaching and solving problems instead of continuously trying to improve the "old" ways.
Something similar must be done with the energy problem. It is evident as nuclear energy, with its enormous energy concentration, can (or even must) play a major role, provided it is able to match the environmental requirement embedded in the previous lines, which is what is called sustainability. This means that the acceptability of nuclear energy is subject to the possibility of proving the feasibility, with available (or almost available) technology, of reactors and cycles with a substantially negligible environmental footprint. That requires a new way of conceiving a nuclear reactor.

Introduction

Since its born, nuclear engineering has been oriented to the design of critical arrangements of fissile material to develop technologically feasible systems able to generate an aimed power. Besides the development of intrinsic and passive safety concepts, resulting in the technological improvements which brought up to Generation-III+ NPPs, the design of the core still follows the same logic: the dimensioning of both the elementary unit cell (fuel pin and coolant channel) and the whole core is determined by the neutronic and thermo-hydraulic viability of a system whose power is fixed *a priori*.

In this scheme, the only way to pursue sustainability is to face, beyond the reactor, both its front-end (availability and reliability of input materials) and back-end issues (through P&T programs). Nevertheless the derived solutions can not be considered as final: they rather represent provisional - even if effective - palliatives to the problem.

The only way to fully achieve the sustainability of nuclear energy is to move from a logic of improving the existing NPPs generation to a conceptually evolved one: the reactor design process itself must be renewed, starting from something which has, by definition, no impact on the environment and verifying afterwards whether we are able to extract energy from that. Which is not assured. This new paradigm to design a core could be called - a little bit pompously - 2NP: a New Paradigm for Nuclear Power.

Within this frame, the adiabatic core concept arises as an interesting and promising solution for both an efficient exploitation of Uranium resources, extending the availability of the nuclear energy feed for thousand years, and the minimization of the volumes and radiotoxicity of HLWs.

11.1 Present design philosophy

Core design aims at determining the main parameters which univocally define a reactor configuration providing the required neutronic features and complying with all the (mainly) thermal/hydraulic constraints. Since there is a strong inter-dependence among the core parameters, it is therefore a complex task to balance the pros and cons considering any consistent combination of these parameters. If one defines a "reactors space" as a hyper-space where the axes represent the independent core parameters, core design can be visualized as the research for an optimal operating point in this multi-parameter diagram: the technological limits introduce boundaries narrowing the viability domain, the parameter inter-dependence laws define hyper-surfaces representing the relationships between degrees of freedom and constraints, and the goal features provide the criteria to orient the choice for the most suitable operating point in the design domain.

The first thing to be considered in approaching the neutronic design of a

core is its technological viability.

With respect to LFRs, besides the traditional constraints regarding core integrity, four main aspects have to be taken into account:

1. the corrosion/erosion of the structurals due to coolant flow, resulting in both a maximum clad wall temperature and a lead flow velocity limit within the core;

2. the embrittlement of the structurals at low temperatures because of neutron irradiation, resulting in a minimum temperature limit for the coolant;

3. the solidification of the coolant in the coldest regions of the reactor, resulting in a further minimum lead temperature limit;

4. the melting of the fuel, resulting in a maximum temperature limit for the pellets.

The minimum safety characteristics in core design are related to

1. the natural circulation of the coolant in accidental conditions, so to guarantee the nominal heat removal from the core within an acceptable temperature range, and

2. the minimization of the plant (typically pool-type) size, so to reduce, in case of earthquake, the sloshing actions due to the huge mass of coolant.

Following the design constraints, the mutual relationships among the core properties are exploited in order to outline the most exhaustive working point with respect to the aimed performances:

- first, the design constraints are translated into a set of viability ranges for the directly implied parameters;

- axial and radial form factors are initially guessed (or inferred by previous analyses), corresponding to an initial hypothesis on the reactor shape;

- the remaining equations are then put together and solved, providing the complete set of core parameters.

The optimization phase follows, inferring feedback information to assess the shape factors and then repeating iteratively the system characterization step, until all parameters imply satisfactory core performances.

11.1.1 First step: viability region identification

In order to define the viability domain in the reactor space, each single constraint is translated into an equivalent inequality defining the actual range for the corresponding parameter.

In particular, the ranges for the coolant inlet temperature and the clad wall temperature are fixed according to

$$\begin{aligned} T_{\text{inlet}} &\geq \max\{T_{\text{coolant, solidification}}, T_{\text{structurals, embrittlement}}\} + \\ &\quad + \Delta T_{\text{design margin}} \\ T_{\text{clad}} &\leq T_{\text{clad, corrosion}} - \Delta T_{\text{design margin}} \,. \end{aligned} \tag{11.1}$$

The coolant flow velocity must be analogously limited according to

$$v_{\text{coolant}} \leq v_{\text{coolant, erosion}} \,. \tag{11.2}$$

The maximum fuel temperature must be accounted for to prevent (with a sufficient margin) the possibility of fuel melting. According to this, the maximum fuel temperature limit can be translated into an equivalent upper limit on the maximum linear power, according to the conductivity integral relation.

The heat flow through the fuel, where power generation occurs, is ruled by a balance equation (derived from the Fourier's law) of the form

$$\bigtriangledown \cdot (k_{\text{f}} \bigtriangledown T) + q''' = 0 \,, \tag{11.3}$$

where the nabla operator only acts along the radial direction.

For metallic fuels, the previous relation is greatly simplified since the validity of assuming k_{f} constant with temperature (thus along the radius).

For oxide fuels, the conductivity k_{f} strongly varies with temperature, thus equation (11.3) can be solved by considering a cylindrical portion of the fuel, and the thermic balance in it:

$$q''' \pi r^2 l = -k_{\text{f}}(T) \frac{\mathrm{d}\, T}{\mathrm{d}\, r} 2\pi r l \,,$$

which in turn becomes

$$q''' \frac{r}{2} = -k_{\text{f}}(T) \frac{\mathrm{d}\, T}{\mathrm{d}\, r} \,.$$

Separating the variables and integrating from the pellet boundary to its center, it results

$$\int_{r_{\text{f}}}^{0} q''' \frac{r}{2} \,\mathrm{d}\, r = -\int_{T_{\text{f-g}}}^{T_0} k_{\text{f}}(T) \,\mathrm{d}\, T \,,$$

or, equivalently (multiplying both sides by -4π):

$$q' \equiv q'''\pi r_{\mathrm{f}}^2 = 4\pi \int_{T_{\mathrm{f-g}}}^{T_0} k_{\mathrm{f}}(T)\,\mathrm{d}\,T\,.$$

According to this, the limit on the maximum fuel temperature can be fulfilled by imposing:

$$q' \leq 4\pi \int_{T_{\mathrm{f-g}}}^{T_0} k_{\mathrm{f}}(T) dT\,, \tag{11.4}$$

where $T_0 = T_{\mathrm{fuel,\,melting}} - \Delta T_{\mathrm{design\,margin}}$ is the maximum allowable temperature for the fuel (at the center of the pellet), $T_{\mathrm{f-g}}$ is the temperature at the pellet surface (*i.e.*, at the fuel-gap interface) and $k_{\mathrm{f}}(T)$ is the thermal conductivity of the fuel.

11.1.2 Second step: preliminary estimate of shape factors

Preliminary estimates for the flux axial and radial peak factors can be inferred by the general settlement of the system produced by mechanical analysis, taking into account the theoretical flux shapes for the bare core and the needed corrections due to the reflection by lead and the absorption in possible reflectors or blankets.

For economic reasons it could worth supposing a segmentation (radial or even axial) of the core by different fuel compositions (*i.e.*, enrichments) or fuel volumetric fractions (e.g.: different pin diameters), in order to flatten the power distribution among the core regions. This choice would therefore imply the reduction of the peak factors to be assumed as starting point for the core characterization.

To achieve the economy goal, the radial power flattening strategy may become crucial. In traditional concept fast reactors this is done by orificing the inlet nozzle of each FA according to its actual power generation. The typical FAs design includes indeed a wrapper delimiting a separated channel for the FA: each one can then be gagged and the respective flow rate tuned according to the pressure loss introduced. The limit on the maximum pressure loss allowed to guarantee the natural circulation in incidental conditions implies the need to reduce the power unbalancing to keep the gagging below the safety limit.

In "open" FA solutions no channel is defined since no wrapper is considered. For such systems the core zoning strategy has to be stressed, representing the only solution to enlarge the average coolant temperature gain through the core[1].

[1] Being the maximum outlet temperature fixed by design because of technological constraints, a large radial peak factor results indeed in a low average outlet temperature.

11.1.3 Third step: iterative core characterization

Once the viability domain in the reactor space has been determined, the starting point for the neutronic design of a core is represented by the thermal-hydraulics design of the fuel pin and coolant channel: as a matter of fact, both the pin radius r_c and lattice pitch p depend only on the thermal-hydraulic consistency of the system. It is possible indeed to determine those parameters according to the technological constraints represented by the allowable maximum temperatures for the coolant, the clad and the fuel as well as the maximum allowable pressure drops through the core. Since the system must be dimensioned to prevent out-of-range working everywhere in the core, the most peaked fuel pin (*i.e.*, the pin in the s.c. "hottest channel", producing the highest power) is assumed as reference for the design.

The typical temperature profile through a fuel pin (shown in Figure 11.1) is given by a sequence of temperature gains in each material, from the bulk of the coolant to the center of the fuel, determined by the thermal head necessary to evacuate the local power. All these gains depend on the geometry and the materials of the pin only.

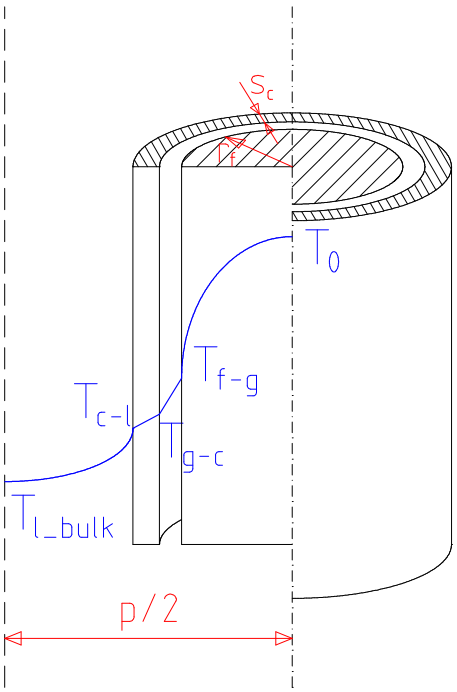

Figure 11.1: Temperature profiles in the fuel pin and coolant channel.

The general considerations presented can be formalized into a set of equa-

tions, once both radial, f_{rad}, and axial, f_{ax}[2], form factors have been evaluated.

Starting from the maximum linear power allowed[3], the axial power profile in the hottest pin can be inferred by assuming

$$q'_{\max}(z) = q'_{\max} \int_0^{h_{\mathrm{fuel}}} \cos\left(\frac{\pi}{L}\left(z - \frac{h_{\mathrm{fuel}}}{2}\right)\right) \mathrm{d}\, z\,. \tag{11.5}$$

The parameter L in equation 11.5 must be computed so that the length of the arc over which the cosine is defined provides the assumed axial distribution factor, that is:

$$\int_{-\beta}^{\beta} \cos(\alpha)\ \mathrm{d}\,\alpha = \frac{1}{f_{\mathrm{ax}}} \ \rightarrow\ \beta = \arcsin\left(\frac{1}{2f_{\mathrm{ax}}}\right) \ \Rightarrow\ L = \frac{\pi h_{\mathrm{fuel}}}{2\beta}\,.$$

The thermal analysis of the channel follows, in order to retrieve the actual temperature profile through the elementary cell (fuel pin and coolant channel) for dimensioning the fuel pellet radius. The starting point is the axial coolant temperature profile in the hottest channel, inferred by the axial power profile according to

$$T_{\mathrm{l}}(z) = T_{\mathrm{inlet}} + (T_{\mathrm{outlet}} - T_{\mathrm{inlet}})\, f_{\mathrm{rad}} \frac{\int_0^z q'_{\max}(z)\,\mathrm{d}z}{\int_0^{h_{\mathrm{fuel}}} q'_{\max}(z)\,\mathrm{d}z}\,. \tag{11.6}$$

All the temperature gains within each material the fission heat passes through from fuel to coolant, combine over the coolant temperature, raising along the channel according to equation (11.6).

$$T_0(z) - T_{\mathrm{f-g}}(z) = \frac{q'_{\max}(z)}{4\pi\langle k_{\mathrm{f}}\rangle} \tag{11.7}$$

$$T_{\mathrm{f-g}}(z) - T_{\mathrm{g-c}}(z) = \frac{q'_{\max}(z)}{2\pi k_{\mathrm{g}}} \ln\frac{r_{\mathrm{g}}}{r_{\mathrm{f}}} \tag{11.8}$$

$$T_{\mathrm{g-c}}(z) - T_{\mathrm{c-l}}(z) = \frac{q'_{\max}(z)}{2\pi k_{\mathrm{c}}} \ln\frac{r_{\mathrm{c}}}{r_{\mathrm{g}}} \tag{11.9}$$

$$T_{\mathrm{c-l}}(z) - T_{\mathrm{l\_bulk}}(z) = \frac{q'_{\max}(z)}{2\pi h_{\mathrm{l}} r_{\mathrm{c}}}\,. \tag{11.10}$$

In the previous system, single subscripts refer to materials ("f" for fuel, "g" for the gas filling the gap, "c" for clad and "l" for the coolant) while coupled subscripts refer to materials interfaces ("f-g" for fuel-gap interface,

[2]The estimate of the axial form factor almost follows - for most systems - from the preliminary assumed active height, h_{fuel}, of the core, derived from the general mechanical settlement of the system.

[3]There's no reason to assume any other admissible value but the maximum one, aiming at maximizing the economy of the system.

"g-c" for gap-clad interface and "c-l" for clad-coolant interface); k_{i} indicates the thermal conductivity of material i and h_{l} indicates the heat-transfer coefficient of the coolant.

The gap and clad thickness, s_{g} and s_{c}, as well as the plenum length h_{plenum} ($h_{\mathrm{channel}} - h_{\mathrm{fuel}}$ in equation (11.16)) are somehow fixed by performance analysis on the fuel Burn Up (BU), in order to guarantee the minimization of the Pellet-Clad Mechanical Interaction (PCMI) and the resistance to the GFPs pressure.

It is therefore possible to put together equations (11.7-11.10) in order to obtain a single expression for the dimensioning of the pin (which can be limited to r_{f}), in order to respect both the fuel and clad maximum temperature, according to relations (11.4) and (11.1):

$$T_0(z) = \frac{q'_{\max}(z)}{2\pi}\left(\frac{1}{2\langle k_{\mathrm{f}}\rangle} + \frac{1}{h_{\mathrm{g}} r_{\mathrm{f}}} + \frac{1}{k_{\mathrm{c}}}\ln\frac{r_{\mathrm{f}} + s_{\mathrm{g}} + s_{\mathrm{c}}}{r_{\mathrm{f}} + s_{\mathrm{g}}} + \right.$$
$$\left. + \frac{1}{h_{\mathrm{l}}(r_{\mathrm{f}} + s_{\mathrm{g}} + s_{\mathrm{c}})}\right) + T_{\mathrm{l\_bulk}}(z)\,. \tag{11.11}$$

The same relation holds for hollowed fuel pins too, with minor changes: said γ_{f} the ratio between the hollow and pellet radii, equation (11.11) becomes

$$T_0(z) = \frac{q'_{\max}(z)}{2\pi}\left(1-\gamma_{\mathrm{f}}^2\right)\left[\frac{1}{2\langle k_{\mathrm{f}}\rangle}\left(1 + \frac{\gamma_{\mathrm{f}}^2 \cdot \ln\gamma_{\mathrm{f}}^2}{1-\gamma_{\mathrm{f}}^2}\right) + \frac{1}{h_{\mathrm{g}} r_{\mathrm{f}}} + \right.$$
$$\left. + \frac{1}{k_{\mathrm{c}}}\ln\frac{r_{\mathrm{f}} + s_{\mathrm{g}} + s_{\mathrm{c}}}{r_{\mathrm{f}} + s_{\mathrm{g}}} + \frac{1}{h_{\mathrm{l}}(r_{\mathrm{f}} + s_{\mathrm{g}} + s_{\mathrm{c}})}\right] + T_{\mathrm{l\_bulk}}(z)\,. \tag{11.12}$$

The logical process for the fuel pin dimensioning can be represented by the dependencies scheme of Figure 11.2.

Once the fuel radius (and the eventual hollow one) has been defined, the coolant channel must be dimensioned. The pitch of the pins lattice, p, is to be chosen according to the average coolant temperature gain along the average channel. The increase of the coolant temperature in the channel is derived from the enthalpy balance equation

$$\rho_{\mathrm{l}} A v_{\mathrm{coolant}} c_p \Delta T = \frac{q'_{\max}}{f_{\mathrm{rad}}\, f_{\mathrm{ax}}} h_{\mathrm{fuel}}\,, \tag{11.13}$$

where ρ_{l} and c_p are the coolant average density in the channel and heat capacity respectively (for lead see [37]) and A, the flow area of the channel, depends on the fuel pin radius and lattice pitch according to

$$A = \begin{cases} \frac{p^2\sqrt{3}}{2} - \pi r_{\mathrm{c}}^2 & \text{hexagonal lattices} \\ p^2 - \pi r_{\mathrm{c}}^2 & \text{square lattices}\,. \end{cases}$$

The reference pitch value must be set by taking into account also the maximum allowed coolant velocity, eq. (11.2), and the pressure drops through the channel.

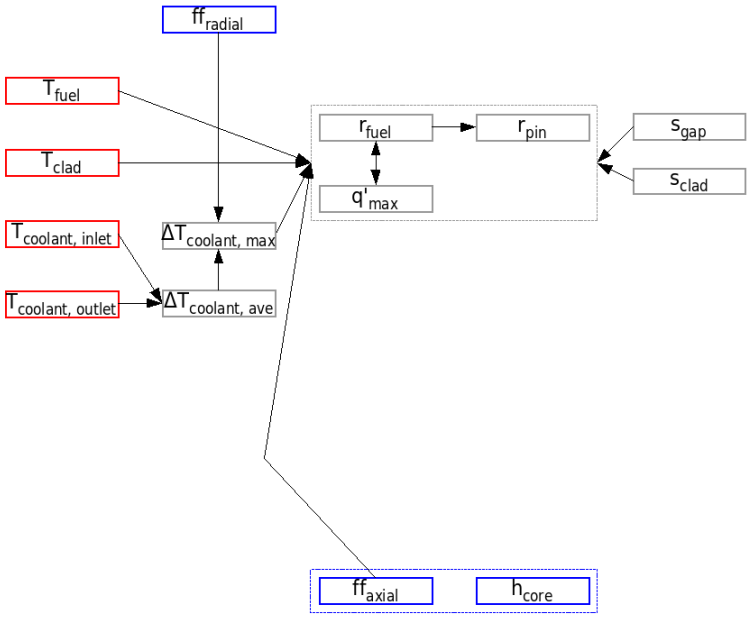

Figure 11.2: Scheme of the dependencies for dimensioning the fuel pin radius.

The latter comes from the requirement of providing a sufficient natural circulation, in case of ULOF accident, so as to guarantee nominal heat removal from the core within an acceptable temperature range ΔT_{ULOF}[4]. According to this, the channel must be dimensioned so as to keep the pressure losses in.

The thermal head assessing in natural circulation can be easily determined as

$$\Delta p = \Delta\rho_{\mathrm{l}} g h_{\mathrm{buoyancy}} \simeq 3\alpha\Delta T_{\mathrm{ULOF}}\, \rho_{\mathrm{inlet}} g h_{\mathrm{buoyancy}}\,, \tag{11.14}$$

where g is the strength of the gravitational field, h_{buoyancy} is the buoyancy height (*i.e.*, the height of the primary circuit hot-leg, from core midplane to SGs midplane) and α is the LTE coefficient of the coolant (for lead see [37]).

This forcing term must overtake the pressure drop through the whole primary circuit, expressed, separating the contribution within and outside the

[4] ΔT_{ULOF} is the temperature gain along the channel which establishes in order to provide the required prevalence for natural circulation. According to core integrity, it is important that ΔT_{ULOF} settles so as to keep T_{c} below the critical clad failure temperature: as a matter of fact, the allowed temperature gain in accidental condition is higher than the normal one because the higher temperature range is supposed to last for a limited time span (typically 30 minutes before human intervention), during which the clad must mechanically resist to the stresses due to the internal GFP pressure for all surface corrosion at the time of the accident, erosion/corrosion constraints being negligible.

core, as

$$\Delta p = \Delta p_{\text{core}} + \Delta p_{\text{system}} = f \frac{h_{\text{channel}}}{D_h} \frac{\rho_{\text{l}} v_{\text{coolant}}^2}{2} + \Delta p_{\text{system}} \,, \tag{11.15}$$

where f is the effective friction term in the channel, D_h and h_{channel} are, respectively, the hydraulic diameter and the length of the channel.

Putting together equations (11.14) and (11.15), and applying eq. (11.13) to the ULOF case, the following expression involving the geometry of the channel can be extracted

$$3\alpha \Delta T_{\text{ULOF}}\, \rho_{\text{inlet}} g h_{\text{buoyancy}} = \tag{11.16}$$
$$= f \frac{h_{\text{channel}}}{D_h \rho_{\text{inlet}} (2 - 3\alpha \Delta T_{\text{ULOF}})} \left(\frac{q'_{\text{max}} h_{\text{fuel}}}{f_{\text{rad}} f_{\text{ax}} A c_p \Delta T_{\text{ULOF}}} \right)^2 + \Delta p_{\text{system}} \,,$$

for testing whether the temperature gain set up for coolant circulation is acceptable.

The overall logical process of coolant channel dimensioning can be represented by the dependencies scheme of Figure 11.3.

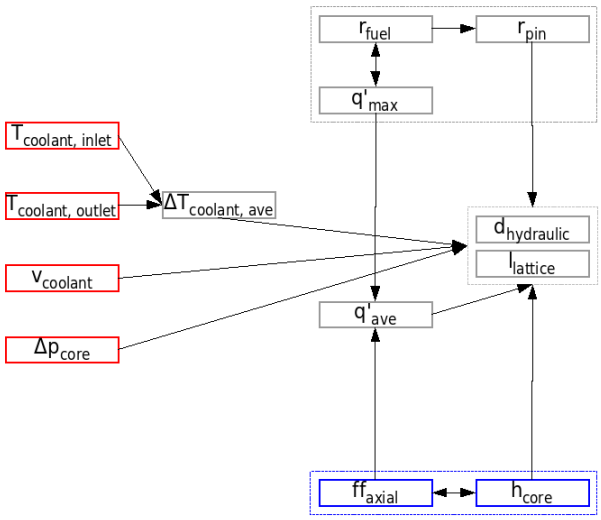

Figure 11.3: Scheme of the dependencies for dimensioning the fuel pins lattice pitch.

11.1.4 Fourth step: whole core design

Once the elementary cell has been determined, the axial and radial form factors are used to infer the average linear power in the core:

$$\langle q' \rangle = \frac{\max\{q'\}}{f_{\text{rad}} f_{\text{ax}}} \,. \tag{11.17}$$

This can be used in turn to calculate the total development of the fuel needed to achieve the nominal power desired:

$$H = \frac{P_{\text{th}}}{\langle q' \rangle} \,. \tag{11.18}$$

Combining the total development of the fuel H with the preliminary core height h_{fuel} to retrieve the number of fuel pins n_{pins}, the radius of the core equivalent cylinder results

$$R_{\text{core}} = \sqrt{\frac{1}{\pi} n_{\text{pins}} A_{\text{lattice}}} = \begin{cases} \sqrt{\frac{H}{\pi h} \frac{p^2\sqrt{3}}{2}} & \text{hexagonal lattices} \\ \sqrt{\frac{H}{\pi h} p^2} & \text{square lattices} \,. \end{cases}$$

The aimed BU performances allow also to preliminary evaluate the in-pile residence time for the fuel. According to this, the core can be also segmented into batches for refueling, so to define the mean fuel ageing at BoC and EoC, averaging the in-pileresidence time of the FAs belonging to different batches just before (EoC) and immediately after (BoC) the refueling. This approach leads to a 1-batch approximation (which has been proven [32] to be equivalent - in terms of criticality swing along the cycle - to the real n-batches refueling strategy) for the criticality analysis of the core.

The assessment of criticality can be performed taking into account that the overall shape of the system fixes the geometrical buckling of the reactor. Considering the system as a homogeneous volume V, the neutrons net balance, expressed as the ratio of the material buckling upon the geometrical one, can be translated into a balance between the net production in the reactor over the net leakage from the latter:

$$\frac{Prod}{Leak} = 1 \quad \Longrightarrow \quad \frac{\int_V \nu\Sigma_f \Phi \, \mathrm{d}\, V - \int_V \Sigma_a \Phi \, \mathrm{d}\, V}{\int_V \nabla \cdot \vec{J} \, \mathrm{d}\, V} = 1 \,. \tag{11.19}$$

The volumes in the cells are fixed by the thermohydraulic analysis of the channel. The neutron spectrum is therefore also fixed by the volumetric fraction of coolant, fuel and structurals in the cell. For criticality, neutronic calculations must be performed to assess the composition of the fuel (*i.e.*, its enrichment), which is used as an almost free parameter to match the required reactivity during the cycle and the power distribution flattening: as a matter of fact, the fuel must be enriched so to adjust the material buckling coherently with the geometrical one. The increase of the fuel enrichment both acts in increasing the fission term and in reducing the absorption one (*i.e.*, the fissile is added to the detriment of the absorbing fissile).

It is clear that modifying the mutual abundances of fissile and fertile also changes the breeding capacity of the system, which could represent a design goal acting as feedback parameter in the design process; the same is valid for the eventual dispersion of MAs in the fuel.

Furthermore, it is to be noticed that the enrichment also determines the flux level, according to the fixed power density in the fuel: the higher the enrichment, the lower the flux needed to achieve the same power density,

$$q' = \pi r_{\mathrm{f}}^2 \Phi Q \rho_{\mathrm{fuel}} \sigma_f \,. \tag{11.20}$$

For instance, in designing experimental reactors, the flux level could represent a binding criterion: again, also the peak neutron flux can be used as a feedback parameter for core design.

As a matter of fact, the collection of output performances resulting by the present core configuration should be used as feedback to adjust the core design in order to achieve completely all the aimed goals, in an iterative process. The overall dependencies scheme for core design is shown in Figure 11.4.

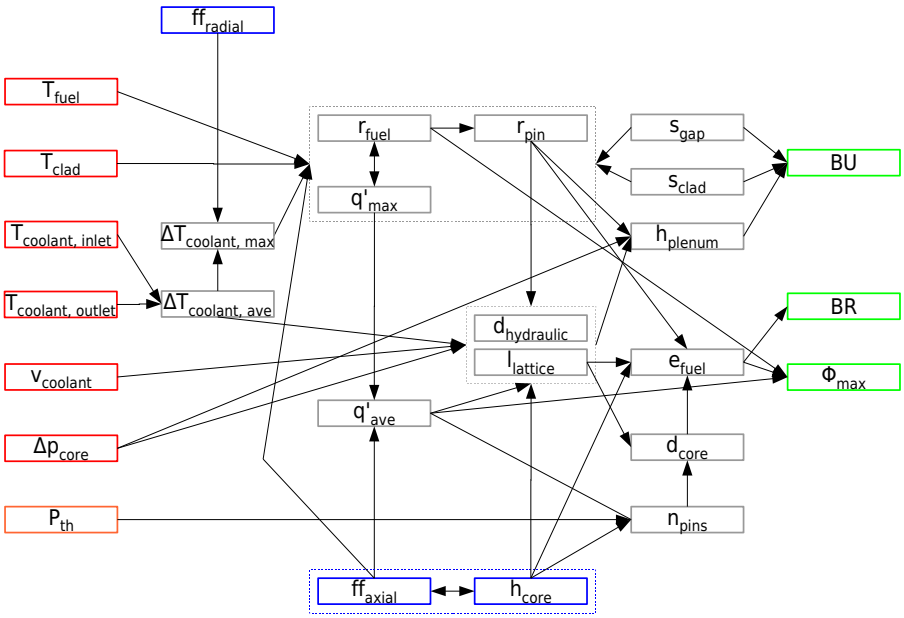

Figure 11.4: Classical scheme of the dependencies between the main parameters for the core design.

11.2 The New Paradigm for Nuclear Power

Aiming at designing adiabatic reactors, to ensure the sustainability of nuclear energy through the closure of the fuel cycle within the reactor itself, it is fundamental to clearly point out the parameters univocally defining the

goal. Something similar has been already done - *mutatis mutandis* - for the Accelerator Driven System (ADS) EFIT (European Facility for Industrial Transmutation) [38, 39], where the Pu/MA parameter has been determined beforehand to get the most effective MA burning goal, rather than used to set the core multiplication.

In order to design an adiabatic reactor, as a first step the equilibrium isotopic composition of the fuel must be fixed. This constraint in turn determines the intrinsic reactivity of the fuel: hence, the core designer is no more allowed to design nuclear reactors to achieve an aimed power by setting the core size, and consequently adjusting criticality by tuning the fissile content in the fuel; he must rather set up a critical arrangement for the given fuel. According then to the thermal-hydraulic feasibility of the resulting core, and exploiting its viability, the system power will be univocally determined.

This acts as - *si parva licet* - a "Copernican" revolution in the way of conceiving reactors, reversing the mental approach of subordinating the core design to its power: the whole design will be based on the fuel enrichment, fixed for the adiabaticity of the system; it will be possible then to tune the power by iteratively adjusting the elementary cell and the corresponding fuel vector acting on the fuel volume fraction. A logical scheme for the design of an adiabatic core, according to the New Paradigm for Nuclear Power, is shown in Figure 11.5.

The starting point for the whole process is the definition of the equilibrium vector. In order to retrieve the volume fractions of the materials in the elementary cell (which determine the neutrons spectrum), a preliminary dimensioning of the fuel pin and coolant channel, *i.e.*, both the pin radius and lattice pitch, is needed. As described in the previous section, it is possible indeed to determine those parameters *a priori*, by investigating the thermal-hydraulic consistency of the system according to the technological constraints represented by the allowable maximum temperatures for the coolant, the clad and the fuel as well as the maximum allowable coolant velocity and pressure drops through the core.

Once the fuel vector has been determined, whether its reactivity (*i.e.*, the k_∞ of the elementary cell) is enough higher than 1, the number of pins to be arranged in the core to get the criticality of the system is univocally determined, balancing the material buckling with the geometrical one. The number of pins in turn defines the corresponding core power. According to this reverted scheme, the dependency among the core parameters can be represented by the scheme of Figure 11.6.

Hence, in an adiabatic core the dimensioning of the elementary cell uneqivocally determines a core power. The matching between the aimed power and the criticality of the system can be set by acting on the fuel volume fraction (see [39]), thus redefining from scratches the elementary cell in an iterative process (since the latter affects the neutron spectrum).

It is worth noticing that the 2NP scheme is conceived for the design of

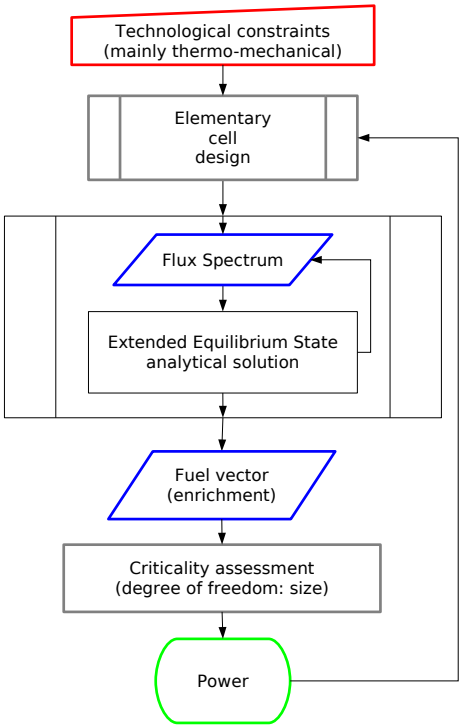

Figure 11.5: Scheme of the core design approach according to the 2NP logic.

a zero-impact core but, given the U/Pu/MAs equilibrium concept, it also allows - if the case - the design of:

- a breeder reactor, if the U/Pu ratio is increased;
- a Pu burner, if the U/Pu ratio is decreased;
- a MAs burner, if the MAs/Pu ratio is increased.

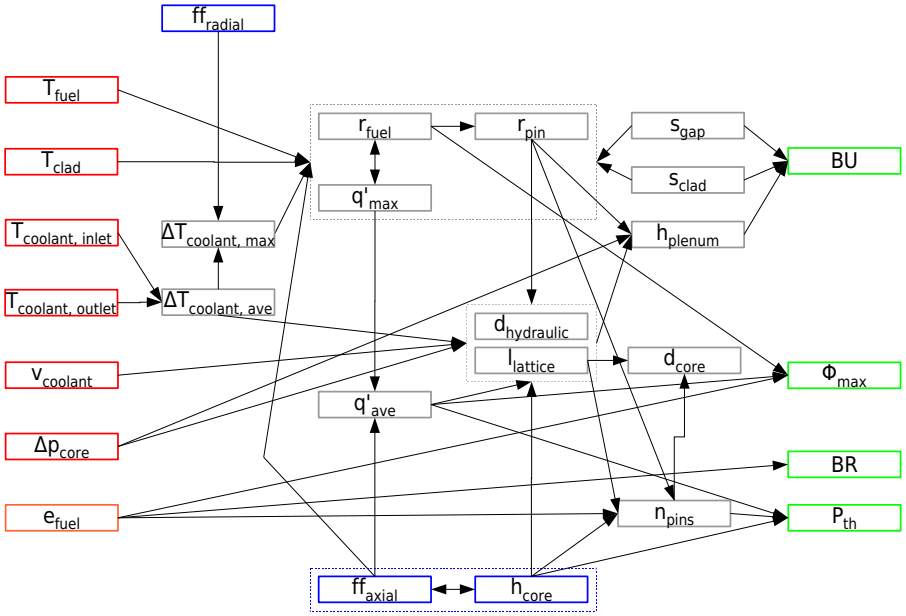

Figure 11.6: Scheme of the dependencies between the main parameters for the core design according to the New Paradigm for Nuclear Power.

CHAPTER 12

NEUTRONIC DESIGN OF AN ADIABATIC LEAD FAST REACTOR

There is no adequate defense, except stupidity, against the impact of a new idea.

Percy Williams Bridgman (1882-1961)

Abstract. The whole neutronic design of an Adiabatic Lead-cooled Fast Reactor, capitalizing the experience accrued on the ELSY project, has been carried out according to the New Paradigm for Nuclear Power.
The ALFR inherits the same overall system arrangement and design of ELSY, with several modification to the FA and pin design to accomplish for the adiabatic goal. The wrapper-less square lattice still representing the FA reference option, the adoption of a fixed fuel composition introduces the need for differentiating the core into three regions with different fuel volume fractions, in order to get the flattening of the coolant outlet temperature distribution.
A complete set of Monte Carlo neutronics calculations have been carried out to retrieve both the FA zoning and flow regimes guaranteeing the aimed power distribution corresponding to the flattening of the coolant outlet temperature.

Introduction

Aiming at designing an Adiabatic Lead-cooled Fast Reactor (ALFR) for proving the fully sustainable features of nuclear energy, the overall system layout of ELSY has been borrowed, relying on the experience accrued on the design of the latter (see Chapters 7 to 9).

On the other hand, according to the New Paradigm for Nuclear Power, the design of an Adiabatic system requires the reconfiguration of the whole core, starting from the equilibrium fuel vector corresponding to a precise elementary cell design and verifying then the possibility of arranging a critical core with the given fuel.

In order to further increment the sustainability features embedded in an adiabatic reactor, it is also envisaged to increase the fuel BU aiming at maximizing the energy production as well as at minimizing the reprocessing losses to be buried in a geological repository. It is clear indeed that, minimizing the number of average fuel reprocessing per unit energy, that is: extracting the more energy per fuel unit volume, the losses are also proportionally reduced.

According to this, it was envisaged to operate the ALFR up to 140 GWd t^{-1} peak BU (with a corresponding average BU of some 100 GWd t^{-1}), extending the in-pile fuel residence time up to 7.5 y, with a minimum cycle duration of 1.5 y.

The main characteristics identified for the ALFR therefore are:

- an adiabatic core to optimize by design the Generation IV requirements on sustainability and proliferation resistance;
- a total thermal power of the system ruled by the 2NP core design process;
- an equilibrium MAs-doped MOX fuel, with its allowed peak linear rating of 320 W cm^{-1} (solid pin);
- an in pile fuel residence time of 7.5 y;
- a minimum fuel sub-cycle duration of 1.5 y;
- a peak fuel burn-up of 140 GWd t^{-1} on Heavy Metal (HM) (average fuel BU: 100 GWd t^{-1}) with a corresponding peak clad damage of 100 dpa;
- a maximum clad temperature of 550 °C because of corrosion;
- core inlet and outlet coolant temperatures set at 400 °C and 480 °C;
- a maximum coolant velocity through the core lower than 2 m s^{-1} in order to keep structures erosion and pressure drop through the core in.

12.1 Elementary cell design

Since the elementary cell design represents the very first step in the 2NP core design logic, being subject to continue refining intended at optimizing the overall system performances, the design of the very first layout can be drawn simply by the technological constraints accounting for cell integrity.

According to this, it was decided to borrow the preliminary ALFR elementary cell design from the ELSY one – with few minor changes – for two main reasons:

- the ELSY elementary cell was designed according to the same technological constraints assumed for the ALFR;
- the ELSY design has been led by an embryonic form of the 2NP, targeted at obtaining an isobreeder reactor (which is one of the conditions for the nuclear equilibrium).

According to the aim at reaching a peak BU of 140 GWd t^{-1}, the smear density of the fuel within the clad had to be lowered with respect to the ELSY pin. In ELSY, preliminary evaluations performed by FZK showed that a 84% smear density is compatible with a peak BU of 100 GWd t^{-1}. According to this evaluation, a 71% smear density has been assumed sufficient to allow the aimed maximum BU. Being 5% the porosity of the pellet, the hollow radius has been enlarged to 2 mm. The preliminary FA and pin layout for the ALFR is represented in Figure 12.1.

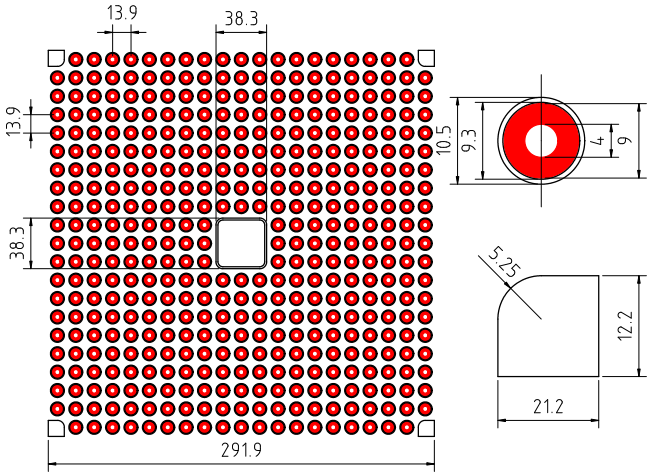

Figure 12.1: Cross-cut view of the preliminary ALFR FA and pin layout.

The MCNP model of the ALFR preliminary FA, completely defined along its axial extension, has been set up for a reactivity calculation (*i.e.*, assuming

reflexion and void boundary conditions at lateral and axial surfaces, respectively) in order to retrieve the one group microscopic cross-sections for all the nuclides intended in the equilibrium fuel (all the ones whose cross section data are available in the JEFF3.1 library). This calculation indeed, reproducing the neutron spectrum in the FA, allowed to compute the equivalent one group constants preserving the actual reaction rates in the system. The results of the iterative refining of the one group cross-section evaluation as a function of the fuel composition (since the latter affects the neutron spectrum) are listed in Table 12.1.

Table 12.1: One group microscopic cross-sections for the ALFR fuel isotopes

	n,xn	fission	inelastic	capture	total
^{226}Ra	1.87033E-3	2.35544E-5	0.00000E+0	3.61588E-1	3.63482E-1
^{228}Ra	0.00000E+0	0.00000E+0	0.00000E+0	0.00000E+0	0.00000E+0
^{229}Th	3.29809E-3	8.15333E-1	0.00000E+0	1.29239E+0	2.11103E+0
^{230}Th	1.15391E-3	2.48114E-2	0.00000E+0	2.19798E-1	2.45763E-1
^{231}Th	0.00000E+0	0.00000E+0	0.00000E+0	0.00000E+0	0.00000E+0
^{232}Th	1.22874E-3	8.48423E-3	0.00000E+0	3.98919E-1	4.08632E-1
^{233}Th	4.50191E-3	2.11395E-1	0.00000E+0	5.42495E-1	7.58392E-1
^{234}Th	1.52232E-3	3.97111E-3	0.00000E+0	3.76076E-1	3.81569E-1
^{231}Pa	7.76111E-4	2.25771E-1	0.00000E+0	3.10958E+0	3.33613E+0
^{232}Pa	1.80185E-3	1.82281E+0	0.00000E+0	7.22853E-1	2.54746E+0
^{233}Pa	3.18731E-4	5.24967E-2	0.00000E+0	1.09858E+0	1.15139E+0
^{234}Pa	0.00000E+0	0.00000E+0	0.00000E+0	0.00000E+0	0.00000E+0
^{232}U	5.67245E-4	2.20258E+0	0.00000E+0	6.98865E-1	2.90201E+0
^{233}U	2.83778E-4	2.72655E+0	0.00000E+0	2.56948E-1	2.98379E+0
^{234}U	1.85867E-4	2.93205E-1	0.00000E+0	5.77558E-1	8.70948E-1
^{235}U	8.10632E-4	1.91183E+0	0.00000E+0	5.54486E-1	2.46713E+0
^{235}U^{m}	0.00000E+0	0.00000E+0	0.00000E+0	0.00000E+0	0.00000E+0
^{236}U	5.26352E-4	8.62820E-2	0.00000E+0	4.30901E-1	5.17709E-1
^{237}U	2.56077E-3	9.38921E-1	0.00000E+0	5.93433E-1	1.53491E+0
^{238}U	1.03081E-3	3.43195E-2	0.00000E+0	2.86122E-1	3.21472E-1
^{239}U	0.00000E+0	0.00000E+0	0.00000E+0	0.00000E+0	0.00000E+0
^{240}U	0.00000E+0	0.00000E+0	0.00000E+0	0.00000E+0	0.00000E+0
^{235}Np	0.00000E+0	0.00000E+0	0.00000E+0	0.00000E+0	0.00000E+0
^{236}Np	5.37557E-4	2.74914E+0	0.00000E+0	5.83488E-1	3.33316E+0
^{237}Np	2.24195E-4	3.12049E-1	0.00000E+0	1.58939E+0	1.90166E+0
^{238}Np	1.03241E-3	3.55521E+0	0.00000E+0	1.78911E-1	3.73516E+0
^{239}Np	2.57241E-4	4.34975E-1	0.00000E+0	1.97661E+0	2.41184E+0
^{240}Np	0.00000E+0	0.00000E+0	0.00000E+0	0.00000E+0	0.00000E+0
^{241}Np	0.00000E+0	0.00000E+0	0.00000E+0	0.00000E+0	0.00000E+0
^{236}Pu	0.00000E+0	0.00000E+0	0.00000E+0	0.00000E+0	0.00000E+0
^{237}Pu	1.57363E-4	3.69404E+0	0.00000E+0	2.03668E-1	3.89787E+0
^{238}Pu	2.63104E-4	1.21329E+0	0.00000E+0	5.46851E-1	1.76040E+0
^{239}Pu	3.21750E-4	1.77197E+0	0.00000E+0	5.06791E-1	2.27908E+0
^{240}Pu	2.30360E-4	3.54902E-1	0.00000E+0	4.95052E-1	8.50184E-1
^{241}Pu	1.43475E-3	2.55178E+0	0.00000E+0	4.89644E-1	3.04286E+0

	n,xn	fission	inelastic	capture	total
^{242}Pu	4.91695E-4	2.48033E-1	0.00000E+0	5.18081E-1	7.66606E-1
^{243}Pu	3.58924E-3	8.43890E-1	0.00000E+0	3.97208E-1	1.24469E+0
^{244}Pu	1.47066E-3	1.98589E-1	0.00000E+0	2.22799E-1	4.22859E-1
^{239}Am	0.00000E+0	0.00000E+0	0.00000E+0	0.00000E+0	0.00000E+0
^{240}Am	0.00000E+0	0.00000E+0	0.00000E+0	0.00000E+0	0.00000E+0
^{241}Am	9.67610E-5	2.40477E-1	0.00000E+0	1.84018E+0	2.08076E+0
^{242}Am	3.76322E-4	3.14982E+0	3.57758E-2	4.34045E-1	3.62001E+0
^{242}Am^{m}	3.73770E-4	3.13136E+0	0.00000E+0	4.95689E-1	3.62742E+0
^{243}Am	2.67779E-4	1.73002E-1	0.00000E+0	1.65504E+0	1.82831E+0
^{244}Am	1.61873E-3	3.22165E+0	1.17337E-4	8.32185E-1	4.05557E+0
^{244}Am^{m}	1.61867E-3	3.22133E+0	0.00000E+0	7.67885E-1	3.99084E+0
^{245}Am	0.00000E+0	0.00000E+0	0.00000E+0	0.00000E+0	0.00000E+0
^{241}Cm	3.06796E-5	3.16468E+0	0.00000E+0	2.04022E-1	3.36873E+0
^{242}Cm	7.86029E-5	6.08306E-1	0.00000E+0	4.82412E-1	1.09080E+0
^{243}Cm	2.59152E-4	3.30145E+0	0.00000E+0	3.03565E-1	3.60527E+0
^{244}Cm	2.69909E-4	3.94194E-1	0.00000E+0	8.72539E-1	1.26700E+0
^{245}Cm	3.59430E-4	2.75727E+0	0.00000E+0	5.36025E-1	3.29366E+0
^{246}Cm	3.09013E-4	2.57953E-1	0.00000E+0	5.27358E-1	7.85620E-1
^{247}Cm	8.98292E-4	2.28789E+0	0.00000E+0	4.90466E-1	2.77925E+0
^{248}Cm	5.68266E-4	2.65324E-1	0.00000E+0	2.93977E-1	5.59870E-1

Starting then from the one group cross-sections, the extended nuclear equilibrium problem (see Section 10.2) has been solved by means of the "Adiabatic Concentrator" code, described in Appendix B, assuming a total in-pile irradiation time of 7.5 y and an equivalent cooling, reprocessing and fabrication time, 7.5 y, for a fuel with 1.97 stoichiometric ratio. The atom densities of each Actinide in the fuel are listed in Table 12.2, while the fuel density resulted 10.432 g cm^{-3} according to equation (A.11), presented in Appendix A.

Table 12.2: Atom densities in the extended equilibrium ALFR fresh fuel

Isotope	Concentration at BoL
^{226}Ra	6.2029789E-12
^{228}Ra	2.3332270E-20
^{229}Th	4.5058931E-12
^{230}Th	8.2940233E-09
^{231}Th	4.6181033E-17
^{232}Th	5.9694963E-11
^{233}Th	7.1123421E-18
^{234}Th	2.4071425E-13
^{231}Pa	5.2703202E-10
^{232}Pa	4.7161616E-80
^{233}Pa	6.4494278E-13
^{234}Pa	8.5347695E-36

Isotope	Concentration at BoL
^{232}U	7.0237834E-10
^{233}U	1.6507124E-09
^{234}U	2.5805440E-05
^{235}U	2.2432245E-05
^{235}U^{m}	6.0142596E-12
^{236}U	2.6601435E-05
^{237}U	3.7709482E-12
^{238}U	1.9068131E-02
^{239}U	1.4350036E-09
^{240}U	1.3665612E-18
^{235}Np	4.7790734E-19
^{236}Np	8.3815379E-78
^{237}Np	1.8743623E-05
^{238}Np	7.1472293E-13
^{239}Np	1.4104010E-09
^{240}Np	7.8784630E-14
^{241}Np	0.0000000E+00
^{236}Pu	1.8491464E-11
^{237}Pu	2.3665121E-28
^{238}Pu	8.2504352E-05
^{239}Pu	2.2021819E-03
^{240}Pu	1.3720689E-03
^{241}Pu	1.1848041E-04
^{242}Pu	1.3600992E-04
^{243}Pu	3.3645311E-17
^{244}Pu	6.8682609E-08
^{239}Am	0.0000000E+00
^{240}Am	1.2907013E-18
^{241}Am	1.3198839E-04
^{242}Am	4.8763599E-11
^{242}Am^{m}	3.7770523E-06
^{243}Am	3.9484048E-05
^{244}Am	1.1358000E-38
^{244}Am^{m}	1.6355148E-11
^{245}Am	2.2861847E-20
^{241}Cm	4.2346368E-37
^{242}Cm	9.9149835E-09
^{243}Cm	5.3010213E-07
^{244}Cm	2.2907661E-05
^{245}Cm	7.4483299E-06
^{246}Cm	4.8894047E-06
^{247}Cm	9.2772955E-07
^{248}Cm	8.1272688E-07

12.2 Geometric and material description

The ALFR inherits the same system configuration of ELSY as presented in the Chapter 9. Regarding the core layout, a shift of the same FA lattice of ELSY (staggered square), with respect to the inner vessel, has been envisaged

to center the inner vessel in correspondence to the center of a FA. This simple solution allows to arrange 173 FAs and 80 dummy elements within the same inner vessel of ELSY (instead of 170 FAs and 80 dummy elements). Eight among the 173 positions have been devoted to host a traditional concept Control Rod (identical to the ELSY ones, represented in Figure 9.4) for redundancy with the safety systems and for refueling; the rationale for their positioning is the same as for ELSY, *i.e.*, within the outermost FA ring and equidistant each other, to maximize the neutrons interception area. As for ELSY, the CRs are intended to be moved in empty channels for a fast and reliable passive insertion within the core in case of scram. The ALFR core layout is depicted in Figure 12.2.

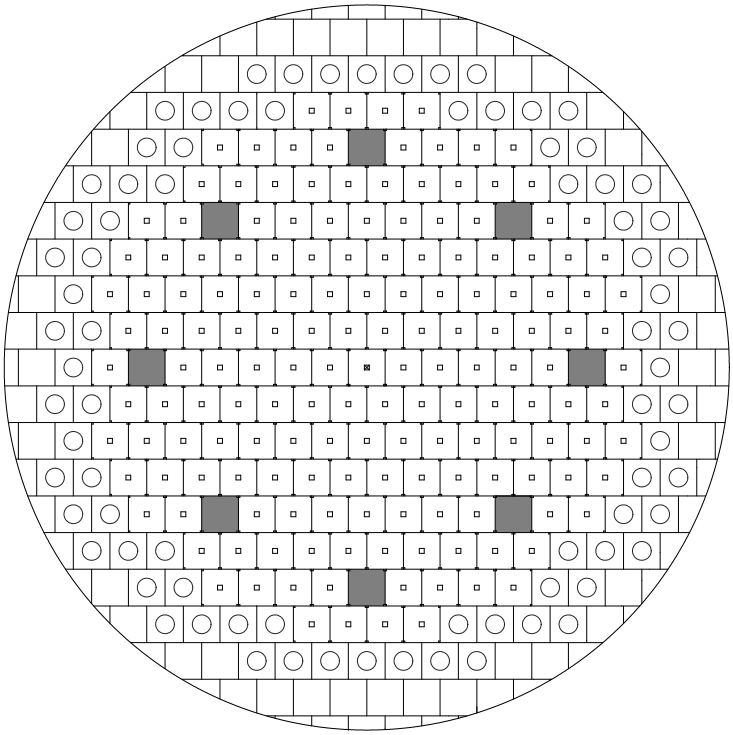

Figure 12.2: The core general layout and FAs arrangement of the ALFR.

As for ELSY, two sets of FARs, identical to the one represented in Figure 9.3, have been envisioned for the ALFR, relying on the effectiveness of such a solution, demonstrated for ELSY. The leading criterion for the actual dimensioning and placement of the FARs on the core map, is again the anti-reactivity needed for the cold arrest of the system, evaluated in some 3000 pcm, to be provided by each of the two control FAR systems. Furthermore, the FARs set devoted also to the criticality swing compensation during

the cycle, must worth a supplementary anti-reactivity preliminary evaluated in some 1000 pcm.

Since the small reactivity swing expected during operation (which is a consequence of the extended equilibrium condition imposed for the fuel), the regulation FARs have been supposed made of Europium sesquioxide (Eu_2O_3): as reported in Reference [40], even if the self-shielding reduces the effectiveness of Eu as neutrons absorber (both naturally occurring isotopes, ^{151}Eu and ^{153}Eu, have indeed (n,γ) absorption cross-sections comparable to that of ^{10}B in the fast spectrum of LFRs) to that of natural B_4C, two interesting features let the Author incline to this choice:

- no Helium is produced (since the Eu capture mechanism is radiative absorption) thus, differently from B_4C rods, no venting is required[1];
- the daughter products are also good neutron absorbers, thus the loss of anti-reactivity worth during operation is reduced with respect to B_4C rods.

Finally, all the structurals of the ALFR are supposed to be made of the same materials assumed as reference for ELSY, that is: FMS T91 for all the structures within the inner vessel, Stainless Steel 316LN for the reactor vessel and SS 316L for all the remaining internals.

12.3 ALFR computational model

The neutronic design of the ALFR has been carried out mainly by Monte Carlo calculations, evaluating by means of MCNP5 [17] the system criticality and power/FA distribution, together with the evolution of the fuel with BU and control systems dimensioning and positioning. The use of the deterministic transport code ERANOS has been limited to the modeling of the ALFR for BU calculations needed to produce the depletion libraries for use in COSI [4] (see Chapter 13 for details).

Both deterministic and Monte Carlo calculations have been carried out by adopting very detailed 3D geometry models of the reactor, compatibly with the specific domain representation capabilities of each code.

12.3.1 ERANOS model

The typical two-step process for core design has been performed by means of the two modules ECCO [18] (for cell transport calculations) and TGV [22] (for reactor spatial calculations by variational-nodal coarse-mesh transport) of the ERANOS v. 2.1 formulary [7].

[1]The removal of the plenum due to the absence of gas release is also an important simplification in the plant design, since the high operation periods envisaged for the ALFR.

The only JEFF3.1 cross-section data library [30] has been assumed as reference for cell calculations, providing the basis for the fine energy (*i.e.*, 1968 groups) calculations necessary for accounting in detail the effect of cross sections resonances.

Very refined cell descriptions – according to ECCO capabilities – have been adopted for the main cells (*i.e.*,for the cells surrounding the active zone), with particular attention to the FAs provided with a FAR. In particular, as for the ELSY final configuration, the 9 inner positions (containing the structural box beam and – eventually – the FAR) have been specifically modeled in order to preserve – as far as possible – the heterogeneity of the cell, as shown in Figure 9.5.

The successive reactor spatial calculation, as for the ELSY design, has been performed on a detailed three-dimensional XYZ model of the reactor so as to differentiate each FAs for depletion calculations. A fourth-order discrete ordinates approach (S_4) has been adopted to solve the transport equation, energetically discretized at 33 groups, obtained by condensation of the 1968 groups structure used for cell calculations. A cross-cut view of the ALFR simulation domain for TGV is shown in Figure 12.3.

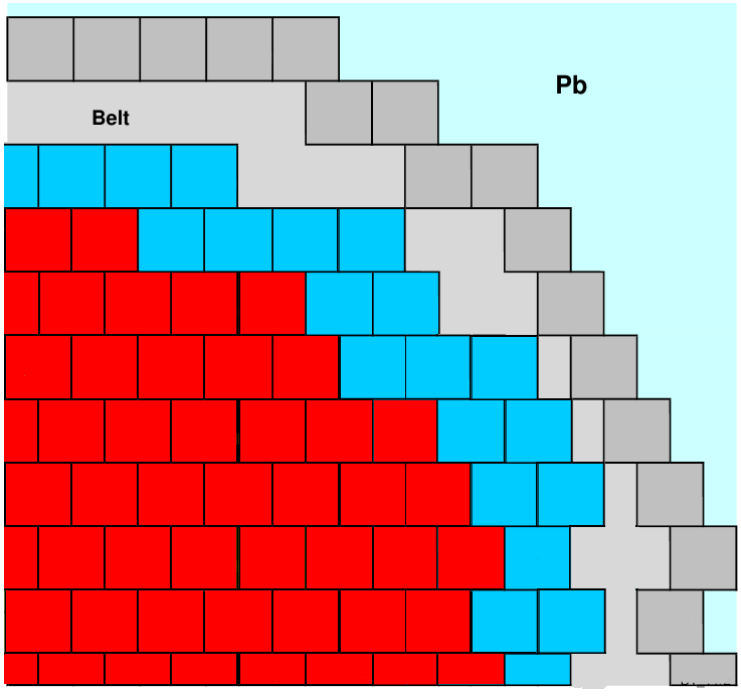

Figure 12.3: Cross-cut view of the ALFR simulation domain with TGV.

12.3.2 MCNP model

Being MCNP the reference code for the whole core design process, an exact geometrical model of the whole reactor has been set up in order to correctly evaluate the actual power/FA distribution and the effectiveness of FARs. Being the overall system arrangement similar to the ELSY one, depicted in Figures 9.7 and 9.8, a cross-cut view of the ALFR core as produced by the MCNP plot interface is presented for comparison in Figure 12.4.

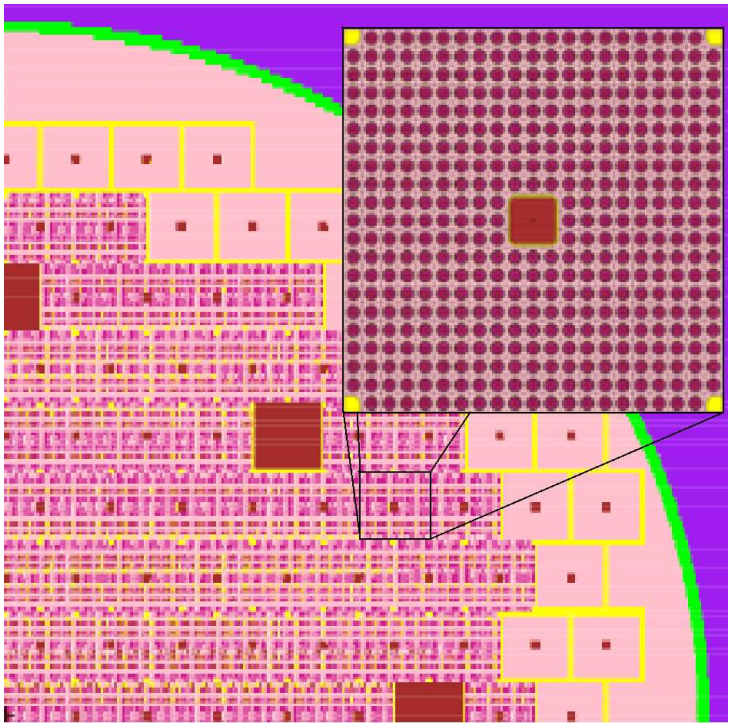

Figure 12.4: Horizontal cross-cut view of the ALFR core model with MCNP.

All MCNP simulations have been performed with JEFF3.1 [30] cross-sections data library, processed at the correct operating temperatures.

12.4 Results and final layout

The wrapper-less design implies that no gagging can be used for tuning the coolant flow rate to the actual FA power, as usually done for wrapped FAs. Furthermore, the adiabatic design excludes the possibility of different fuel enrichment to regulate the power distribution. The aimed smoothing of the FAs T_{outlet} must be therefore pursued by differentiating the fuel volume

fractions throughout core (e.g.: by different pellet areas), thus acting both on the power and the flow rate.

An iterative process followed for assessing the core zoning in order to ensure both the design FADF and the criticality for the resulting core.

It is worth notice that the criticality evolution along irradiation, ruled mainly by:

- a monotonic reduction of the ^{238}U, which is a neutron absorber;
- a ^{239}Pu content that is expected to increase during the first half of the irradiation, to decrease then to the initial value during the remaining in-pile residence time (due to the behavior of the fissile ^{238}U described above);
- a monotonic increase of the ^{241}Pu, to accumulate enough isotopes to exactly compensate its radioactive decay during the ex-core cooling period; and
- a linear increase of the fission products (neutron absorbers) during irradiation;

might impose the adoption of a refueling strategy to mitigate the k_{eff} swing during the cycle. The need for adopting a refueling strategy must be confirmed *a posteriori*, once the criticality evolution of a entirely fresh core has been evaluated.

Whether the refueling strategy is needed, the criticality study for the real core can be approximated by an equivalent 1-batch approximation [31], as done for the final ELSY configuration design, since the 1-batch hypothesis conservatively estimates the reactor performances (in terms of both criticality swing and fuel maximum temperature [32]) with respect to a real n-batches cycle evaluation with reshuffling.

12.4.1 Final layout

The very detailed preliminary criticality and power/FA distribution assessment analysis led to the definition of the final ALFR layout: three zones with different fuel volume fractions have been pointed out throughout the core in order to obtain the aimed goals, enumerating, from the central to the outermost one, 55, 48 and 62 FAs respectively.

The three zones have been characterized by fuel pins with different fuel pellet dimensions, arranged in a lattice with fixed pitch (13.9 mm). The FAs belonging to the inner region are made of the reference fuel pin shown in Figure 12.1. The fuel pins for the intermediate and outer FAs foresee different hollow and pellet radii (shown in Figure 12.5), according to a rationale of standardizing – as far as possible – the pellet design in order to minimize the manufacturing costs:

- the pellet of the intermediate region has a hollow radius of 1 mm, maintaining the same outer diameter as the reference pellet (the one in the inner FAs);
- the pellet of the outer region inherits the same hollow radius of the intermediate fuel pins, the outer diameter being increased to 9.8 mm.

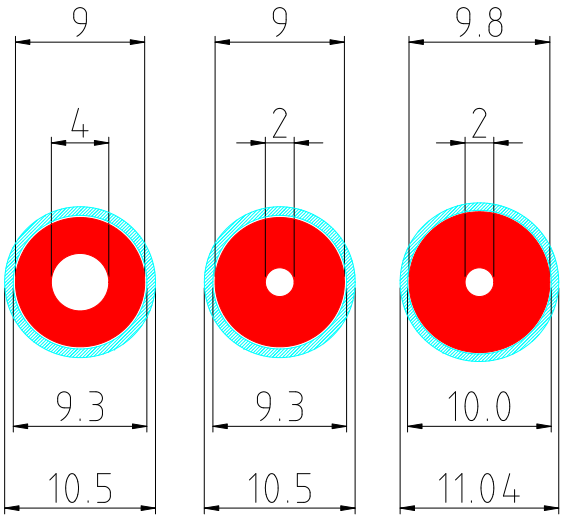

Figure 12.5: Cross-cut view of the fuel pins belonging to the intermediate and outer core zones in the ALFR final configuration.

According to this, three different fuel volume fractions in the elementary cell have been obtained by means of two pellet and hollow radii. The dimensions of the fuel pellets belonging to the three different core zones, together with the corresponding fuel volume fractions are resumed in Table 12.3.

Table 12.3: Fuel pellet dimensions and corresponding volume fractions in the three zones of the ALFR final configuration

Zone	Hollow radius [mm]	Pellet radius [mm]	Fuel volume fraction
Inner	2.0	4.5	0.264
Intermediate	1.0	4.5	0.313
Outer	1.0	4.9	0.374

The outer pin has been increased in order to rely both on a higher fuel volume fraction and on a lower coolant flow area, so as to combine the two effects

in order to obtain the aimed coolant outlet temperature. The enthalpic balance through this thinner channel allows for an additional 1.17 factor for outlet temperature: the coolant velocity v_{coolant} through the channels sets in order to uniform the pressure losses. Referring to equation (11.15), the reduction of the hydraulic diameter in the outer zone impacts on the coolant velocity which, combined with the lower flow area, results in a higher temperature rise through the channel:

$$\begin{aligned} v_{\text{coolant, outer}} &= v_{\text{coolant, inner}} \sqrt{\frac{D_{h,\,outer}}{D_{h,\,inner}}} = 0.933\, v_{\text{coolant, inner}} \\ A_{\text{outer}} &= 0.914\, A_{\text{inner}} \\ \Delta T_{\text{outer}} &= \Delta T_{\text{inner}} \frac{A_{\text{inner}} v_{\text{coolant, inner}}}{A_{\text{outer}} v_{\text{coolant, outer}}} = 1.17\, \Delta T_{\text{inner}}\,. \end{aligned} \tag{12.1}$$

12.4.2 Results

The final power/FA distribution obtained by the zoning strategy are represented in Figure 12.6, showing the local-to-average power/FA ratio in a quarter of the ALFR core.

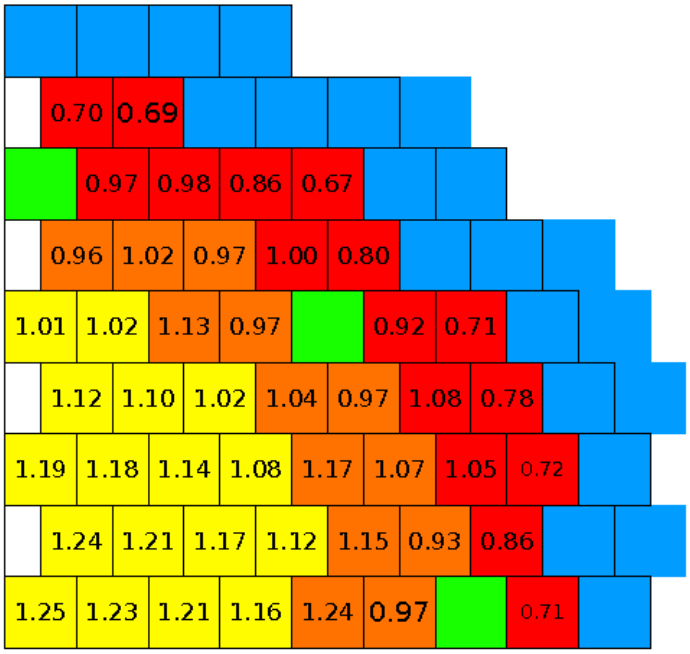

Figure 12.6: Local-to-average power/FA ratio for the final ALFR configuration.

The local-to-average coolant outlet temperature ratios for each FA are re-

sumed in Table 12.4 together with the corresponding local-to-average power/FA ratio. The capital letter indicates the zone the FA belongs to (A, B and C for the inner, intermediate and outer zones respectively), while the two numbers indicate the row and column index in the core map (one quarter of the core).

Table 12.4: Local-to-average power/FA and coolant outlet temperature for the final ALFR configuration

FA Position	Local-to-average ratio	
(zone_row-column)	power/FA	coolant outlet temperature
A_1-1	1.25	1.18
A_1-2	1.23	1.16
A_1-3	1.21	1.14
A_1-4	1.16	1.09
B_1-5	1.24	1.17
B_1-6	0.97	0.91
C_1-8	0.71	0.78
A_2-1	1.24	1.16
A_2-2	1.21	1.14
A_2-3	1.17	1.10
A_2-4	1.12	1.05
B_2-5	1.15	1.09
B_2-6	0.93	0.87
C_2-7	0.86	0.95
A_3-1	1.19	1.12
A_3-2	1.18	1.11
A_3-3	1.14	1.07
A_3-4	1.08	1.02
B_3-5	1.17	1.11
B_3-6	1.07	1.01
C_3-7	1.05	1.16
C_3-8	0.72	0.79
A_4-1	1.12	1.06
A_4-2	1.10	1.04
A_4-3	1.02	0.96
B_4-4	1.04	0.98
B_4-5	0.97	0.92
C_4-6	1.08	1.19
C_4-7	0.78	0.85
A_5-1	1.01	0.95
A_5-2	1.02	0.96
B_5-3	1.13	1.07
B_5-4	0.97	0.92
C_5-6	0.92	1.01
C_5-7	0.71	0.79
B_6-1	0.96	0.90
B_6-2	1.02	0.96
B_6-3	0.97	0.91

FA Position (zone_row-column)	Local-to-average ratio power/FA	coolant outlet temperature
C_6-4	1.00	1.11
C_6-5	0.80	0.88
C_7-2	0.97	1.06
C_7-3	0.98	1.08
C_7-4	0.86	0.95
C_7-5	0.67	0.74
C_8-1	0.70	0.78
C_8-2	0.69	0.76

The zoning strategy pointed out presents an overall FADF of 1.19, lower than the maximum value of 1.2 assumed for the design, with an excellent figure of merit to what concerns the coolant outlet temperature flattening in the three zones: the three FADF for each zone result indeed 1.18, 1.17 and 1.19 in the inner, intermediate and outer regions respectively.

According to the coolant outlet temperature distribution, useful indications have been collected for the FARs positioning (*i.e.*, for locating the FAs to be provided with a FAR), shown in Figure 12.7. The FARs have been also grouped into two different systems, each one appointed to a different task:

- 25 FARs made of Eu_2O_3 have been foreseen for regulating the criticality swing during the cycle (hence provided of motors);
- 38 FARs have been foreseen for reactor control and shutdown (hence motor driven). These FARs can be also used for passive (that is, gravity driven) scram by electromagnetic blockage release.

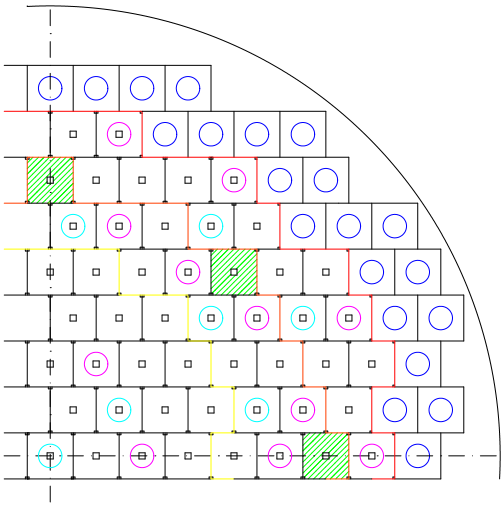

Figure 12.7: Positioning of the control (magenta circles) and regulation (cyan circles) FARs on the ALFR core map.

A $k_{\text{eff}} = 1$ has been obtained at BoL, evolving, during irradiation, as shown in Figure 12.8, mainly because of the four concurring mechanisms described in the introductory part of the present section.

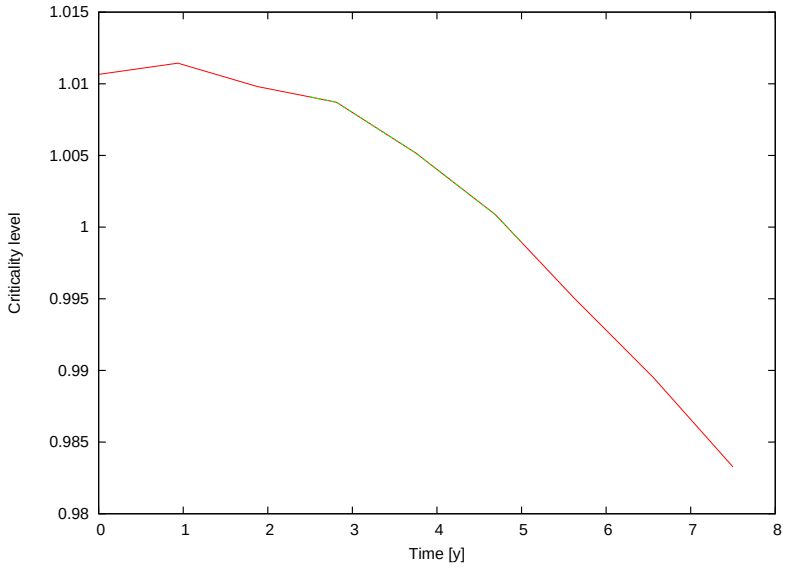

Figure 12.8: Criticality evolution for the final ALFR configuration.

Since the criticality evolution found by the burn-up calculation, a refueling

strategy must be considered to keep the reactor critical during operations. On the other hand, the tight k_{eff} swing allows for long refueling intervals, favoring the availability factor of the ALFR.

According to this, a 3-batches strategy is proposed, with a total cycle length of 2.5 y, as shown in Table 12.5. The criticality of the system at BoC and EoC (corresponding to 2.5 and 5 y time steps in the equivalent 1-batch approximated model [31]) results 1.00908 and 0.99894 respectively.

Table 12.5: Scheme of the 3-batches refueling strategy adopted for the ALFR

	Fuel aging [y]		
Year	I third	II third	III third
0	0	0	0
2.5	2.5/0	2.5	2.5
5	2.5	5/0	5
7.5	5	2.5	7.5/0

As expected, the masses evolution follows the theoretical behavior formalized by the extended equilibrium approach (see Chapter 10 for details). Figures 12.9 to 12.11 depict the mass evolution of the main isotopes (and the most representative of the effectiveness of the method) during both irradiation and decay periods.

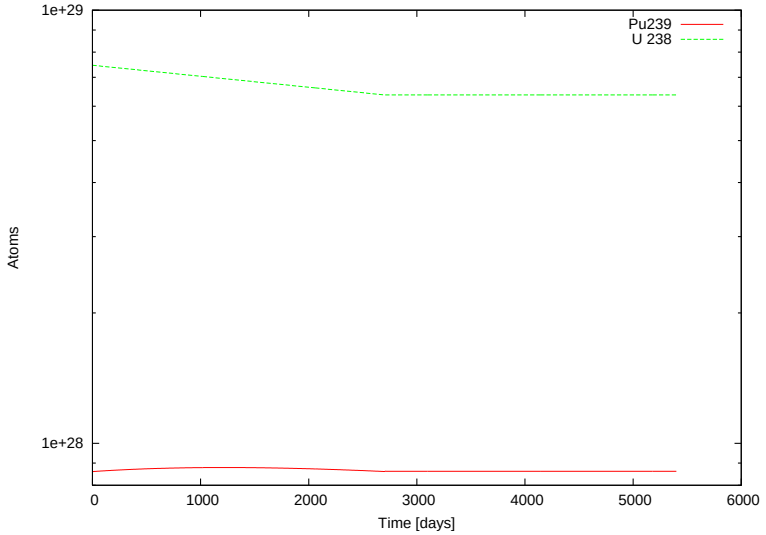

Figure 12.9: Evolution of ^{239}Pu and ^{238}U inventory during the whole irradiation and decay period.

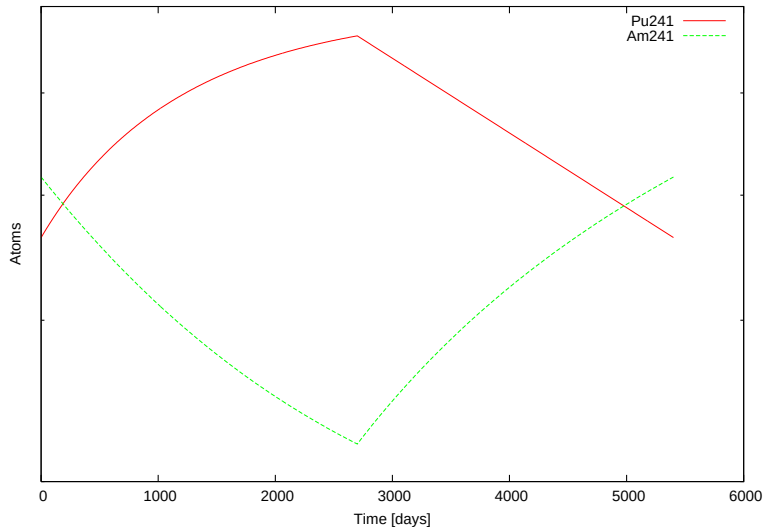

Figure 12.10: Evolution of ^{241}Pu and ^{241}Am inventory during the whole irradiation and decay period.

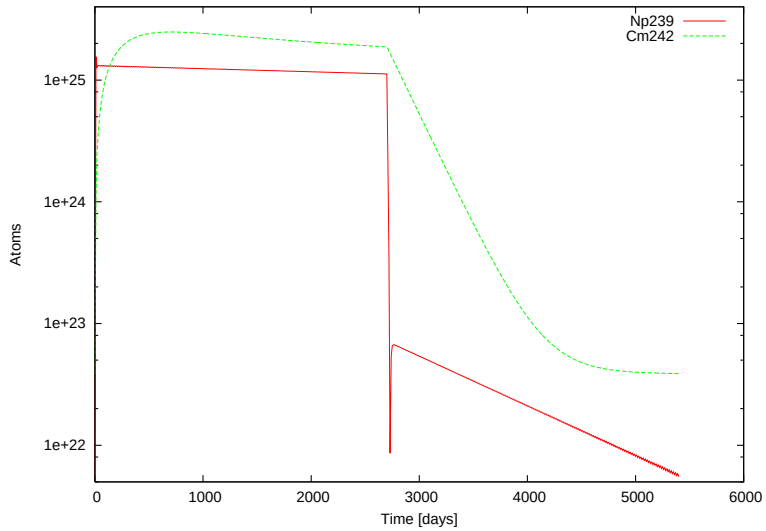

Figure 12.11: Evolution of ^{239}Np and ^{242}Cm inventory during the whole irradiation and decay period.

Concerning the reactivity worth of the three control systems, it has been evaluated at BoL to verify they are able to provide the required anti-reactivity for criticality compensation, reactor control and safety.

All the obtained results are within acceptable ranges about the required

Table 12.6: Worth of ALFR control systems (at BoL)

Case	$k_{\text{eff}} \pm \sigma$	worth [pcm]
Reference	1.00908 ± 0.00039	–
Regulation FARs	0.99927 ± 0.00041	-981
Control FARs	0.97718 ± 0.00035	-3190
Control Rods	0.98001 ± 0.00032	-2907

worth.

Finally, the delayed neutrons effective fraction, β_{eff} has been evaluated to verify whether the MA content in the fuel allows a reliable control of the system. According to MCNP evaluations at BoL, it resulted $\beta_{\text{eff}} = 328$ pcm. Comparing the latter with the corresponding one found for ELSY (which is loaded at BoL with a pure MOX fuel without MAs), a reduction of 48 pcm is found (for ELSY it was $\beta_{\text{eff}} = 376$ pcm [41]). According to some preliminary evaluations performed for ELSY, such a value is expected to fulfill the safety requirements for the ALFR.

CHAPTER 13

A NEW SCENARIO IMPLEMENTING ALFRS

In Science the credit goes to the man who convinces the world, not to the man to whom the idea first occurred.

Sir William Osler (1849-1919)

Abstract. The sustainability of a possible scenario implementing ALFRs is shown by comparison with the present scenario, proving the necessity to move towards closed fuel cycle strategies.
Therefore, a detailed and accurate scenario model has been set up so as to carefully represent the nuclear reactors fleet of interest.
The capacity of the present scenario to support the new fleet is also investigated, to what concerns the availability of spent fuel for the first load of the ALFRs to be operated.

Introduction

In order to analyze the impact on the evolution of a scenario due to the introduction of Adiabatic reactors in the associated fleet, a proper scenario model must be set up, implementing all the features of the new systems to be simulated.

These are accounted by creating a proper CESAR [5] library describing the ALFR for simulating with COSI [4].

13.1 Evolution of the present scenario

The present scenario, deeply analyzed in Chapter 3, is here supposed to evolve according to the national policies resumed in Chapter 2. A constant annual production of 670 TWh electric energy by NPPs is assumed also for this scenario, for ensuring the possibility to compare the new scenario with the reference one. On the other hand, for nations belonging to group "B" (*i.e.*, France), the present nuclear reactors fleet is supposed to be substituted by ALFRs.

According to the aims of the present study, the TRUs recycling is therefore envisaged by implementing a "double strata" fuel cycle strategy: besides traditional PWRs, a fleet of adiabatic reactors is foreseen to manage the Pu and MAs legacies. The use of this kind of reactors, available in a short future, allows for both:

- the minimization of the Uranium input, by changing the valuable U isotope from the fissile ^{235}U to the fertile ^{238}U; and
- the immobilization of the present TRU legacies, with no further net production (besides the unavoidable reprocessing losses).

13.1.1 Introduction of an ALFR fleet

The introduction of the ALFRs is supposed linear with time, starting from 2035 so as to replace the whole French fleet by 2095. This hypothesis has been posed on two assumptions:

- according to the evaluations of the GIF, LFRs will be available only after 2025 (see subsection 6.3.5);
- since the electric power of the proposed ALFR is 600 MWe (vs 1.5 GWe of a PWR), every three years two PWRs are decommissioned and replaced by an equivalent capacity provided by ALFRs, so as to keep the ALFR deploying rate below 2 units per year.

Under this overall hypothesis, the temporal evolution of the final scenario can be represented by the scheme of Figure 13.1, explained in Table 13.1.

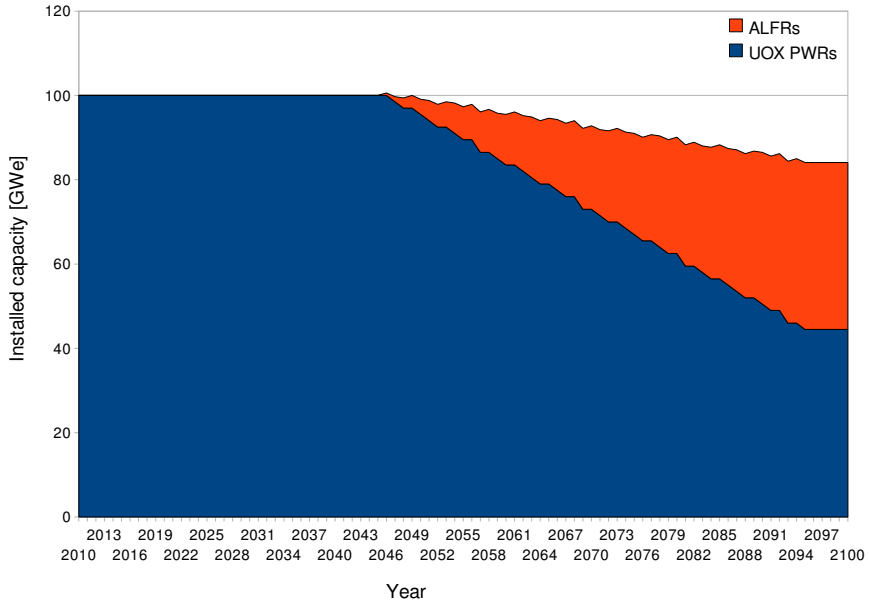

Figure 13.1: Time evolution of the final scenario (fuel cycle closure).

Table 13.1: Installed capacity for different reactors during the final scenario

Year	UOX PWRs [GWe]	ALFRs [GWe]
2010	100	0
2035	100	0
2095	40	50.4
2100	40	50.4

It is worth notice that, since the higher availability factor of ALFRs, mainly because of the longer cycle length, a lower installed capacity is required to provide the same amount of electric energy.

13.2 The new scenario model

Two standardized reactors have been considered in the present analysis, representing the UOX PWR and the ALFR respectively. The exact specification parameters for each type of reactor, as required by the COSI6 code [4] used for the simulations, are presented in Table 13.2.

Table 13.2: Standardized reactors data for the scenarios study

	UOX PWR	**ALFR**
Fuels		
Burn Up [GWd t_{HM}^{-1}]	60	140
Minimum cooling time [y]	5	5
Fabrication time [y]	2	2.5
Fresh fuel ^{235}U enrichment [$^{w}/_{0}$]	4.95	0.226
Fresh fuel Pu "enrichment" [$^{w}/_{0}$]	-	17.82
Moderation ratio	2	–
Cores		
Electrical nominal power [GW]	1.5	0.6
Efficiency [%]	34	40
Production factor [%]	76	90
Heavy metal mass [t]	128.9	40.96
Cycle length [EFPD]	410	900
Core management	1/4	1/3

The UOX fuel is the same standard 17 x 17 rods FRAGEMA type FAs, whose fresh isotopic composition is presented in Table 3.2. All specifications for the ALFR MOX fuel can be found in Chapter 12.

As for the two reference scenarios, the following BBLs have been chosen for describing the proper fuel/reactor within the CESAR module of COSI:

- "UOX 4" BBL for UOX/PWR;
- "MOXP 2403" BBL for MOX/ALFR (see next subsection).

A graphical representation of the new scenario model, highlighting the implemented facilities and the mass fluxes, is given in Figure 13.2.

For the final scenario, the reprocessing plant required for feeding the ALFRs separates homogeneously all the Actinides from the FPs of the spent fuel of the UOX PWRs fleet in a First-In-First-Out (FIFO) batches reprocessing order. A typical net separation efficiency of 99.9% is assumed: hence, 0.1% of the reprocessed masses is lost to the geological repository.

13.2.1 Modeling the ALFR for COSI6

As mentioned in section 3.2, and aiming at simulating the closed cycle by means of the COSI6 scenario code [4], all the specific information needed to define the ALFR must be collected and prepared as a proper CESAR-compatible BBL [5].

The creation of a CESAR BBL file relies on the use of APOGENE, a very simple but powerful code developed by CEA so as to dispose of an

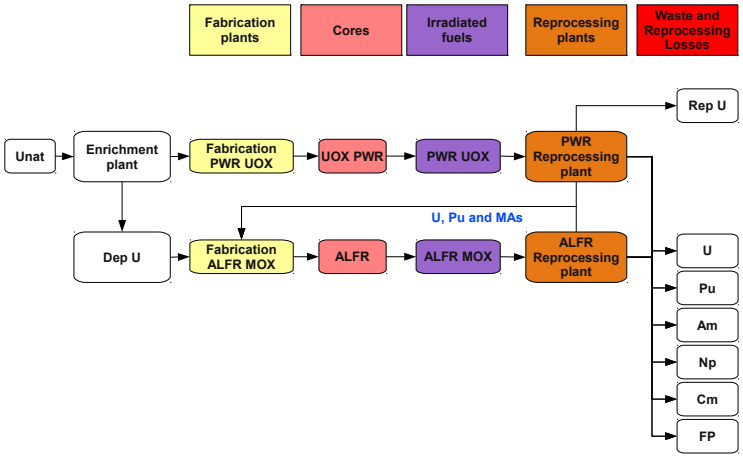

Figure 13.2: Representation of the mass fluxes and installed facilities in the final scenario (closed cycle).

automatized route for overall nuclear analysis, from reactor neutronics to scenario calculations.

In detail, APOGENE implements a list of routines for manipulating the cross-sections sets retrieved from the reference neutronics codes, *i.e.*, APOLLO [42] for the thermal spectrum systems and ERANOS for the fast spectrum systems. The cross sections sets are given as a function of burn-up and, eventually, also of the initial ^{235}U enrichment (for UOX fuel) or Pu content (for MOX fuel). The parametric analysis (regarding the burn-up and the initial fuel composition) performed by APOGENE on the cross-sections set results in a set of interpolating Legendre coefficients: the latter, collected in a single BBL file properly formatted, provide the reference depletion code CESAR with all data necessary for modeling a specific type of reactor, so as to simulate the evolution with BU of a generic fuel loaded in the latter.

In the particular case of interest, aiming at modeling an adiabatic reactor, no use can be derived from a parametric analysis on the initial fuel composition, since the initial fuel vector is uniquely determined by definition of adiabaticity. Hence, despite the wide multitude of possibilities for creating the final BBL allowed by APOGENE, the process followed for the ALFR had been articulated into three steps [43] only:

1. a first step ("APOGENE-ERANOS-DARWIN") for retrieving the neutron flux and effective cross-sections from a file created by the DARWIN interface starting from the results of the ERANOS BU calculation mentioned in section 12.3.1;

2. a second step (“LISSAGE”) in which, starting from the punctual data retrieved in the previous step, the Legendre polynomials coefficients have been computed for interpolating the effective cross-sections as a function of the BU;

3. a third and final step (“ENCRYPTAGE-BBL”) which generated the BBL by arranging the computed Legendre polynomials coefficients in CESAR format.

CHAPTER 14

NEW SCENARIO RESULTS

[Those] who have an excessive faith in their theories or in their ideas are not only poorly disposed to make discoveries, but they also make very poor observations.

Claude Bernard (1813-1878)

Abstract. The analysis of the scenario implementing adiabatic reactors has been carried out in order to confirm the improved performances implied by the ALFR design, in terms of both overall scenario features and mass fluxes.
Even if only a part of the traditional LWRs are replaced by ALFRs, a strong reduction of both the uranium consumption and the TRUs abundance in the spent fuel are obtained.
The comparison of the overall sustainability figure for the proposed futurist scenario with the reference one confirms the strong potentiality of the adiabatic reactor design in candidating nuclear energy as an interesting solution for the problem of greenhouse gases emission reduction.

Introduction

The sustainability performances of the desirable scenario are here presented, moving from the results of the corresponding scenario simulation to focus on some environment- and overall economy-related issues.

The exploitation of Uranium natural resources is examined and compared with the one of the reference scenario. A similar analysis is then performed also regarding the outcomes of the two scenarios in terms of Spent Fuel (SF) masses and their isotopic characterization. Finally, within the overall scenario frame, the capacities required for the boundary facilities to support the scenario are also investigated.

The aim of this detailed analysis is proving the desired overall sustainability performances obtained by the desirable scenario, to be proposed as possible option for presenting nuclear energy as the most mature and appealing candidate for the solution of the problem of greenhouse gases emission reduction.

14.1 Overall environmental and economical performances

The NU consumption (and, therefore, the corresponding enrichment Separative Working Units (SWUs) need) is the lowest amongst the examined cases. The annual NU outcome and the related SWUs required are shown in Table 14.1.

Table 14.1: NU and SWUs annual needs for the closed fuel cycle scenario

Year	NU needs [t y^{-1}]	SWU needs [SWU y^{-1}]	Year	NU needs [t y^{-1}]	SWU needs [t y^{-1}]
-2	2.192E+04	1.678E+07	13	0.000E+00	0.000E+00
-1	2.192E+04	1.678E+07	14	2.192E+04	1.678E+07
0	2.192E+04	1.678E+07	15	2.192E+04	1.678E+07
1	0.000E+00	0.000E+00	16	0.000E+00	0.000E+00
2	2.192E+04	1.678E+07	17	2.192E+04	1.678E+07
3	2.192E+04	1.678E+07	18	2.192E+04	1.678E+07
4	0.000E+00	0.000E+00	19	0.000E+00	0.000E+00
5	2.192E+04	1.678E+07	20	2.192E+04	1.678E+07
6	2.192E+04	1.678E+07	21	2.192E+04	1.678E+07
7	0.000E+00	0.000E+00	22	0.000E+00	0.000E+00
8	2.192E+04	1.678E+07	23	2.192E+04	1.678E+07
9	2.192E+04	1.678E+07	24	2.192E+04	1.678E+07
10	0.000E+00	0.000E+00	25	0.000E+00	0.000E+00
11	2.192E+04	1.678E+07	26	2.192E+04	1.678E+07
12	2.192E+04	1.678E+07	27	2.192E+04	1.678E+07

Year	NU needs [t y^{-1}]	SWU needs [SWU y^{-1}]	Year	NU needs [t y^{-1}]	SWU needs [t y^{-1}]
28	0.000E+00	0.000E+00	60	1.534E+04	1.175E+07
29	2.192E+04	1.678E+07	61	1.534E+04	1.175E+07
30	2.192E+04	1.678E+07	62	1.501E+04	1.150E+07
31	2.192E+04	1.678E+07	63	0.000E+00	0.000E+00
32	0.000E+00	0.000E+00	64	1.436E+04	1.099E+07
33	2.192E+04	1.678E+07	65	1.436E+04	1.099E+07
34	2.192E+04	1.678E+07	66	0.000E+00	0.000E+00
35	0.000E+00	0.000E+00	67	1.370E+04	1.049E+07
36	2.126E+04	1.628E+07	68	1.370E+04	1.049E+07
37	2.126E+04	1.628E+07	69	0.000E+00	0.000E+00
38	0.000E+00	0.000E+00	70	1.304E+04	9.986E+06
39	2.060E+04	1.578E+07	71	1.271E+04	9.734E+06
40	2.027E+04	1.552E+07	72	0.000E+00	0.000E+00
41	0.000E+00	0.000E+00	73	1.238E+04	9.483E+06
42	1.994E+04	1.527E+07	74	1.205E+04	9.231E+06
43	1.962E+04	1.502E+07	75	0.000E+00	0.000E+00
44	0.000E+00	0.000E+00	76	1.140E+04	8.727E+06
45	1.896E+04	1.452E+07	77	1.140E+04	8.727E+06
46	1.896E+04	1.452E+07	78	0.000E+00	0.000E+00
47	0.000E+00	0.000E+00	79	1.074E+04	8.224E+06
48	1.830E+04	1.401E+07	80	1.074E+04	8.224E+06
49	1.830E+04	1.401E+07	81	0.000E+00	0.000E+00
50	0.000E+00	0.000E+00	82	1.008E+04	7.720E+06
51	1.764E+04	1.351E+07	83	9.753E+03	7.469E+06
52	1.731E+04	1.326E+07	84	0.000E+00	0.000E+00
53	0.000E+00	0.000E+00	85	9.753E+03	7.469E+06
54	1.699E+04	1.301E+07	86	9.753E+03	7.469E+06
55	1.666E+04	1.276E+07	87	0.000E+00	0.000E+00
56	0.000E+00	0.000E+00	88	9.753E+03	7.469E+06
57	1.600E+04	1.225E+07	89	0.000E+00	0.000E+00
58	1.600E+04	1.225E+07	90	0.000E+00	0.000E+00
59	0.000E+00	0.000E+00			

The corresponding annual fluxes for both the UOX and MOX fabrication plants are collected in Table 14.2.

Table 14.2: Fabricated UOX and MOX annual fluxes for the closed fuel cycle scenario

Year	UOX [t y^{-1}]	MOX [t y^{-1}]	Year	UOX [t y^{-1}]	MOX [t y^{-1}]
-2	0.000E+00	0.000E+00	3	0.000E+00	0.000E+00
-1	0.000E+00	0.000E+00	4	2.148E+03	0.000E+00
0	2.148E+03	0.000E+00	5	2.148E+03	0.000E+00
1	2.148E+03	0.000E+00	6	0.000E+00	0.000E+00
2	2.148E+03	0.000E+00	7	2.148E+03	0.000E+00

Year	UOX [t y^{-1}]	MOX [t y^{-1}]	Year	UOX [t y^{-1}]	MOX [t y^{-1}]
8	2.148E+03	0.000E+00	50	1.794E+03	1.638E+02
9	0.000E+00	0.000E+00	51	1.794E+03	1.502E+02
10	2.148E+03	0.000E+00	52	0.000E+00	1.502E+02
11	2.148E+03	0.000E+00	53	1.729E+03	1.911E+02
12	0.000E+00	0.000E+00	54	1.697E+03	1.638E+02
13	2.148E+03	0.000E+00	55	0.000E+00	1.638E+02
14	2.148E+03	0.000E+00	56	1.665E+03	2.321E+02
15	0.000E+00	0.000E+00	57	1.633E+03	1.775E+02
16	2.148E+03	0.000E+00	58	0.000E+00	1.911E+02
17	2.148E+03	0.000E+00	59	1.568E+03	2.458E+02
18	0.000E+00	0.000E+00	60	1.568E+03	1.911E+02
19	2.148E+03	0.000E+00	61	0.000E+00	2.321E+02
20	2.148E+03	0.000E+00	62	1.504E+03	2.594E+02
21	0.000E+00	0.000E+00	63	1.504E+03	2.185E+02
22	2.148E+03	0.000E+00	64	1.472E+03	2.458E+02
23	2.148E+03	0.000E+00	65	0.000E+00	2.731E+02
24	0.000E+00	0.000E+00	66	1.407E+03	2.594E+02
25	2.148E+03	0.000E+00	67	1.407E+03	2.594E+02
26	2.148E+03	0.000E+00	68	0.000E+00	3.004E+02
27	0.000E+00	0.000E+00	69	1.343E+03	2.731E+02
28	2.148E+03	0.000E+00	70	1.343E+03	2.731E+02
29	2.148E+03	0.000E+00	71	0.000E+00	3.413E+02
30	0.000E+00	0.000E+00	72	1.278E+03	2.867E+02
31	2.148E+03	0.000E+00	73	1.246E+03	3.004E+02
32	2.148E+03	0.000E+00	74	0.000E+00	3.550E+02
33	2.148E+03	0.000E+00	75	1.214E+03	3.004E+02
34	0.000E+00	0.000E+00	76	1.182E+03	3.413E+02
35	2.148E+03	0.000E+00	77	0.000E+00	3.686E+02
36	2.148E+03	4.096E+01	78	1.117E+03	3.277E+02
37	0.000E+00	4.096E+01	79	1.117E+03	3.550E+02
38	2.084E+03	8.192E+01	80	0.000E+00	3.823E+02
39	2.084E+03	5.461E+01	81	1.053E+03	3.686E+02
40	0.000E+00	5.461E+01	82	1.053E+03	3.686E+02
41	2.019E+03	1.229E+02	83	0.000E+00	4.096E+02
42	1.987E+03	6.827E+01	84	9.882E+02	3.823E+02
43	0.000E+00	8.192E+01	85	9.560E+02	3.823E+02
44	1.955E+03	1.365E+02	86	0.000E+00	3.686E+02
45	1.923E+03	8.192E+01	87	9.560E+02	3.550E+02
46	0.000E+00	1.229E+02	88	9.560E+02	3.686E+02
47	1.858E+03	1.502E+02	89	0.000E+00	3.550E+02
48	1.858E+03	1.092E+02	90	9.560E+02	3.550E+02
49	0.000E+00	1.365E+02			

14.2 Mass fluxes and inventories evolution

The sustainability analysis of the closed fuel cycle is carried out also concerning the production of long lived wastes and their accumulation in the spent fuel repositories, for comparison with the reference case (traditional

open cycle scenario).

At first, the evolution of the ALFR MOX fuel during irradiation and some cooling (the results refer to 7.5 y cooling, according to the hypothesis introduced in Chapter 12) is considered, together with the associated specific reprocessing losses. For the evolution of the PWR UOX, see Chapter 4.

Under such hypotheses, the obtained results are presented in Table 14.3.

Table 14.3: MOX fuel isotopic evolution in a ALFR

Isotope	BoL [g t_{HM}^{-1}]	EoL [g t_{HM}^{-1}]	7.5 y cooling [g t_{HM}^{-1}]	losses [g t_{HM}^{-1}]
^{232}U	3.016E-02	3.225E-02	3.427E-02	3.427E-05
^{234}U	1.108E+03	1.014E+03	1.255E+03	1.255E+00
^{235}U	9.633E+02	5.216E+02	5.444E+02	5.444E-01
^{236}U	1.142E+03	1.232E+03	1.284E+03	1.284E+00
^{238}U	8.189E+05	7.949E+05	7.948E+05	7.948E+02
^{236}Pu	7.941E-04	5.421E-03	9.023E-04	9.023E-07
^{238}Pu	3.543E+03	4.027E+03	4.026E+03	4.026E+00
^{239}Pu	9.457E+04	1.073E+05	1.075E+05	1.075E+02
^{240}Pu	5.892E+04	6.664E+04	6.695E+04	6.695E+01
^{241}Pu	5.088E+03	8.285E+03	5.781E+03	5.781E+00
^{242}Pu	5.841E+03	6.636E+03	6.636E+03	6.636E+00
^{241}Am	5.668E+03	4.001E+03	6.440E+03	6.440E+00
^{242}Am^{m}	1.622E+02	1.911E+02	1.843E+02	1.843E-01
^{243}Am	1.696E+03	1.928E+03	1.927E+03	1.927E+00
^{237}Np	8.049E+02	8.494E+02	9.146E+02	9.146E-01
^{242}Cm	4.258E-01	2.337E+02	4.838E-01	4.838E-04
^{243}Cm	2.277E+01	3.085E+01	2.587E+01	2.587E-02
^{244}Cm	9.838E+02	1.484E+03	1.118E+03	1.118E+00
^{245}Cm	3.199E+02	3.637E+02	3.634E+02	3.634E-01
^{246}Cm	2.100E+02	2.389E+02	2.386E+02	2.386E-01
^{247}Cm	3.984E+01	4.527E+01	4.527E+01	4.527E-02
^{248}Cm	3.490E+01	3.966E+01	3.966E+01	3.966E-02

Comparing the previous table with Table 4.5, two main results can be immediately pointed out:

1. less than 3% of Uranium is required to produce the ALFR MOX fuel – for restoring the initial U amount after BU – with respect to an equivalent quantity of UOX fuel;

2. a higher content of TRUs is present in the fuel, but a lower amount of these ends up in the spent fuel stocks than in the UOX one (about 1.4%), because of the reprocessing losses.

It is therefore clear how a scenario adopting ALFRs, once operating at full capacity, would effectively reduce the natural U resources exploitation as well as the production of TRUs, which are the main responsible for the long-term activity of the spent fuel to be managed.

After this preliminary evaluations, the details of the mass fluxes resulting from the transition scenario towards the closed fuel cycle strategy are taken into account.

Table 14.4 presents the Heavy Metals (HM) inventory within the UOX and MOX Spent Fuel (SF) interim storages during the period of scenario study.

Table 14.4: Spent UOX and MOX Fuel inventories generated during the closed fuel cycle scenario

Year	UOX [t]	MOX [t]	Year	UOX [t]	MOX [t]
-2	1.000E+04	0.000E+00	37	6.031E+04	0.000E+00
-1	1.000E+04	0.000E+00	38	5.989E+04	0.000E+00
0	1.215E+04	0.000E+00	39	6.059E+04	4.100E+01
1	1.430E+04	0.000E+00	40	5.893E+04	4.100E+01
2	1.645E+04	0.000E+00	41	5.817E+04	1.230E+02
3	1.645E+04	0.000E+00	42	5.849E+04	8.200E+01
4	1.859E+04	0.000E+00	43	5.627E+04	1.230E+02
5	2.074E+04	0.000E+00	44	5.545E+04	1.640E+02
6	2.074E+04	0.000E+00	45	5.571E+04	1.230E+02
7	2.289E+04	0.000E+00	46	5.349E+04	2.460E+02
8	2.504E+04	0.000E+00	47	5.258E+04	2.050E+02
9	2.504E+04	0.000E+00	48	5.277E+04	2.050E+02
10	2.719E+04	0.000E+00	49	5.055E+04	2.460E+02
11	2.934E+04	0.000E+00	50	4.957E+04	2.050E+02
12	2.934E+04	0.000E+00	51	4.970E+04	2.460E+02
13	3.148E+04	0.000E+00	52	4.748E+04	2.460E+02
14	3.363E+04	0.000E+00	53	4.643E+04	2.460E+02
15	3.363E+04	0.000E+00	54	4.647E+04	1.640E+02
16	3.578E+04	0.000E+00	55	4.425E+04	2.460E+02
17	3.793E+04	0.000E+00	56	4.314E+04	2.870E+02
18	3.793E+04	0.000E+00	57	4.310E+04	1.640E+02
19	4.008E+04	0.000E+00	58	4.088E+04	2.870E+02
20	4.223E+04	0.000E+00	59	3.968E+04	2.050E+02
21	4.223E+04	0.000E+00	60	3.958E+04	1.640E+02
22	4.437E+04	0.000E+00	61	3.736E+04	3.280E+02
23	4.652E+04	0.000E+00	62	3.609E+04	2.050E+02
24	4.652E+04	0.000E+00	63	3.593E+04	2.050E+02
25	4.867E+04	0.000E+00	64	3.518E+04	2.460E+02
26	5.082E+04	0.000E+00	65	3.241E+04	2.050E+02
27	5.082E+04	0.000E+00	66	3.215E+04	2.460E+02
28	5.297E+04	0.000E+00	67	3.134E+04	2.460E+02
29	5.512E+04	0.000E+00	68	2.856E+04	2.460E+02
30	5.512E+04	0.000E+00	69	2.824E+04	1.640E+02
31	5.726E+04	0.000E+00	70	2.736E+04	2.460E+02
32	5.941E+04	0.000E+00	71	2.459E+04	2.870E+02
33	6.073E+04	0.000E+00	72	2.420E+04	1.640E+02
34	5.990E+04	0.000E+00	73	2.323E+04	2.870E+02
35	6.038E+04	0.000E+00	74	2.045E+04	2.050E+02
36	6.142E+04	0.000E+00	75	2.000E+04	1.640E+02

Year	UOX [t]	MOX [t]	Year	UOX [t]	MOX [t]
76	1.896E+04	3.280E+02	84	9.032E+03	1.640E+02
77	1.619E+04	2.050E+02	85	8.600E+03	2.460E+02
78	1.564E+04	2.050E+02	86	8.045E+03	2.870E+02
79	1.454E+04	2.460E+02	87	8.446E+03	1.640E+02
80	1.176E+04	2.050E+02	88	9.402E+03	2.870E+02
81	1.115E+04	2.460E+02	89	9.402E+03	1.230E+02
82	9.986E+03	2.460E+02	90	1.036E+04	1.230E+02
83	8.876E+03	2.460E+02			

The corresponding annual fluxes for both incoming spent UOX and outgoing recycled MOX masses according to the closed fuel cycle scenario are presented in Table 14.5.

Table 14.5: Reprocessed UOX and recycled MOX annual fluxes for the closed fuel cycle scenario

Year	UOX [t y^{-1}]	MOX [t y^{-1}]	Year	UOX [t y^{-1}]	MOX [t y^{-1}]
-2	0.000E+00	0.000E+00	29	0.000E+00	0.000E+00
-1	0.000E+00	0.000E+00	30	0.000E+00	0.000E+00
0	0.000E+00	0.000E+00	31	0.000E+00	0.000E+00
1	0.000E+00	0.000E+00	32	0.000E+00	0.000E+00
2	0.000E+00	0.000E+00	33	8.324E+02	0.000E+00
3	0.000E+00	0.000E+00	34	8.324E+02	0.000E+00
4	0.000E+00	0.000E+00	35	1.665E+03	0.000E+00
5	0.000E+00	0.000E+00	36	1.110E+03	0.000E+00
6	0.000E+00	0.000E+00	37	1.110E+03	0.000E+00
7	0.000E+00	0.000E+00	38	2.497E+03	0.000E+00
8	0.000E+00	0.000E+00	39	1.387E+03	0.000E+00
9	0.000E+00	0.000E+00	40	1.665E+03	0.000E+00
10	0.000E+00	0.000E+00	41	2.775E+03	0.000E+00
11	0.000E+00	0.000E+00	42	1.665E+03	0.000E+00
12	0.000E+00	0.000E+00	43	2.220E+03	0.000E+00
13	0.000E+00	0.000E+00	44	2.775E+03	0.000E+00
14	0.000E+00	0.000E+00	45	1.665E+03	0.000E+00
15	0.000E+00	0.000E+00	46	2.220E+03	0.000E+00
16	0.000E+00	0.000E+00	47	2.775E+03	0.000E+00
17	0.000E+00	0.000E+00	48	1.665E+03	0.000E+00
18	0.000E+00	0.000E+00	49	2.220E+03	4.100E+01
19	0.000E+00	0.000E+00	50	2.775E+03	4.100E+01
20	0.000E+00	0.000E+00	51	1.665E+03	8.200E+01
21	0.000E+00	0.000E+00	52	2.220E+03	8.200E+01
22	0.000E+00	0.000E+00	53	2.775E+03	8.200E+01
23	0.000E+00	0.000E+00	54	1.665E+03	2.050E+02
24	0.000E+00	0.000E+00	55	2.220E+03	1.230E+02
25	0.000E+00	0.000E+00	56	2.775E+03	1.640E+02
26	0.000E+00	0.000E+00	57	1.665E+03	2.460E+02
27	0.000E+00	0.000E+00	58	2.220E+03	1.640E+02
28	0.000E+00	0.000E+00	59	2.775E+03	2.870E+02

Year	UOX [t y^{-1}]	MOX [t y^{-1}]	Year	UOX [t y^{-1}]	MOX [t y^{-1}]
60	1.665E+03	2.870E+02	76	2.220E+03	5.740E+02
61	2.220E+03	2.460E+02	77	2.775E+03	6.560E+02
62	2.775E+03	3.280E+02	78	1.665E+03	6.560E+02
63	1.665E+03	3.280E+02	79	2.220E+03	6.970E+02
64	2.220E+03	3.690E+02	80	2.775E+03	6.970E+02
65	2.775E+03	3.690E+02	81	1.665E+03	7.380E+02
66	1.665E+03	4.100E+02	82	2.220E+03	7.380E+02
67	2.220E+03	4.100E+02	83	1.110E+03	7.380E+02
68	2.775E+03	4.100E+02	84	8.324E+02	8.610E+02
69	1.665E+03	5.330E+02	85	1.387E+03	7.790E+02
70	2.220E+03	4.510E+02	86	5.549E+02	8.200E+02
71	2.775E+03	4.920E+02	87	5.549E+02	9.020E+02
72	1.665E+03	5.740E+02	88	0.000E+00	8.200E+02
73	2.220E+03	4.920E+02	89	0.000E+00	9.430E+02
74	2.775E+03	6.150E+02	90	0.000E+00	9.430E+02
75	1.665E+03	6.150E+02			

According to the SF management in the closed fuel cycle strategy, the detailed chemical composition evolution of the remaining waste (in terms of Pu and MAs) is shown in Table 14.6 and depicted in Figure 14.1.

Table 14.6: Wastes inventory characterized for Pu and MAs produced by the closed fuel cycle scenario evolution

Year	Pu [t]	Am [t]	Np [t]	Cm [t]
-2	0.000E+00	0.000E+00	0.000E+00	0.000E+00
-1	0.000E+00	0.000E+00	0.000E+00	0.000E+00
0	3.811E+02	1.823E+01	3.104E+01	2.825E+00
1	3.811E+02	1.823E+01	3.104E+01	2.825E+00
2	4.100E+02	2.019E+01	3.214E+01	3.251E+00
3	4.389E+02	2.216E+01	3.325E+01	3.676E+00
4	4.389E+02	2.216E+01	3.325E+01	3.676E+00
5	4.678E+02	2.412E+01	3.435E+01	4.102E+00
6	4.967E+02	2.609E+01	3.546E+01	4.527E+00
7	4.967E+02	2.609E+01	3.546E+01	4.527E+00
8	5.255E+02	2.806E+01	3.656E+01	4.953E+00
9	5.544E+02	3.002E+01	3.767E+01	5.378E+00
10	5.544E+02	3.002E+01	3.767E+01	5.378E+00
11	5.833E+02	3.198E+01	3.877E+01	5.803E+00
12	8.659E+02	4.863E+01	5.902E+01	8.768E+00
13	8.659E+02	4.863E+01	5.902E+01	8.768E+00
14	8.949E+02	5.060E+01	6.013E+01	9.194E+00
15	9.238E+02	5.256E+01	6.123E+01	9.620E+00
16	9.238E+02	5.256E+01	6.123E+01	9.620E+00
17	9.527E+02	5.453E+01	6.234E+01	1.005E+01
18	9.816E+02	5.650E+01	6.344E+01	1.047E+01
19	9.816E+02	5.650E+01	6.344E+01	1.047E+01

Year	Pu [t]	Am [t]	Np [t]	Cm [t]
20	1.011E+03	5.847E+01	6.455E+01	1.090E+01
21	1.039E+03	6.042E+01	6.565E+01	1.132E+01
22	1.039E+03	6.042E+01	6.565E+01	1.132E+01
23	1.068E+03	6.239E+01	6.675E+01	1.175E+01
24	1.097E+03	6.435E+01	6.786E+01	1.217E+01
25	1.097E+03	6.435E+01	6.786E+01	1.217E+01
26	1.126E+03	6.632E+01	6.897E+01	1.260E+01
27	1.155E+03	6.829E+01	7.007E+01	1.302E+01
28	1.184E+03	7.025E+01	7.118E+01	1.345E+01
29	1.184E+03	7.025E+01	7.118E+01	1.345E+01
30	1.213E+03	7.222E+01	7.228E+01	1.387E+01
31	1.242E+03	7.419E+01	7.339E+01	1.430E+01
32	1.242E+03	7.419E+01	7.339E+01	1.430E+01
33	1.264E+03	7.612E+01	7.419E+01	1.467E+01
34	1.286E+03	7.806E+01	7.499E+01	1.504E+01
35	1.272E+03	7.799E+01	7.437E+01	1.493E+01
36	1.291E+03	7.990E+01	7.506E+01	1.528E+01
37	1.311E+03	8.180E+01	7.573E+01	1.563E+01
38	1.290E+03	8.170E+01	7.481E+01	1.547E+01
39	1.307E+03	8.355E+01	7.537E+01	1.579E+01
40	1.320E+03	8.536E+01	7.581E+01	1.609E+01
41	1.298E+03	8.525E+01	7.478E+01	1.591E+01
42	1.311E+03	8.701E+01	7.519E+01	1.619E+01
43	1.319E+03	8.874E+01	7.539E+01	1.644E+01
44	1.296E+03	8.863E+01	7.436E+01	1.626E+01
45	1.308E+03	9.032E+01	7.473E+01	1.653E+01
46	1.316E+03	9.200E+01	7.490E+01	1.677E+01
47	1.293E+03	9.189E+01	7.387E+01	1.659E+01
48	1.304E+03	9.352E+01	7.421E+01	1.685E+01
49	1.310E+03	9.511E+01	7.433E+01	1.706E+01
50	1.287E+03	9.500E+01	7.330E+01	1.688E+01
51	1.297E+03	9.656E+01	7.360E+01	1.713E+01
52	1.303E+03	9.809E+01	7.369E+01	1.733E+01
53	1.280E+03	9.798E+01	7.266E+01	1.715E+01
54	1.289E+03	9.947E+01	7.292E+01	1.738E+01
55	1.293E+03	1.009E+02	7.297E+01	1.757E+01
56	1.271E+03	1.008E+02	7.194E+01	1.739E+01
57	1.279E+03	1.023E+02	7.217E+01	1.760E+01
58	1.282E+03	1.037E+02	7.219E+01	1.778E+01
59	1.281E+03	1.050E+02	7.197E+01	1.791E+01
60	1.267E+03	1.049E+02	7.135E+01	1.780E+01
61	1.269E+03	1.062E+02	7.132E+01	1.796E+01
62	1.266E+03	1.075E+02	7.106E+01	1.808E+01
63	1.253E+03	1.074E+02	7.045E+01	1.797E+01
64	1.254E+03	1.087E+02	7.038E+01	1.812E+01
65	1.250E+03	1.099E+02	7.009E+01	1.822E+01
66	1.237E+03	1.098E+02	6.947E+01	1.811E+01
67	1.237E+03	1.110E+02	6.938E+01	1.824E+01
68	1.233E+03	1.122E+02	6.906E+01	1.834E+01
69	1.219E+03	1.121E+02	6.844E+01	1.823E+01

Year	Pu [t]	Am [t]	Np [t]	Cm [t]
70	1.219E+03	1.133E+02	6.831E+01	1.835E+01
71	1.213E+03	1.143E+02	6.794E+01	1.842E+01
72	1.199E+03	1.143E+02	6.732E+01	1.831E+01
73	1.198E+03	1.153E+02	6.714E+01	1.841E+01
74	1.191E+03	1.163E+02	6.674E+01	1.847E+01
75	1.177E+03	1.162E+02	6.612E+01	1.836E+01
76	1.175E+03	1.172E+02	6.591E+01	1.845E+01
77	1.167E+03	1.182E+02	6.547E+01	1.850E+01
78	1.154E+03	1.181E+02	6.486E+01	1.839E+01
79	1.150E+03	1.190E+02	6.461E+01	1.847E+01
80	1.142E+03	1.199E+02	6.414E+01	1.850E+01
81	1.128E+03	1.199E+02	6.352E+01	1.839E+01
82	1.124E+03	1.207E+02	6.324E+01	1.846E+01
83	1.128E+03	1.216E+02	6.334E+01	1.858E+01
84	1.121E+03	1.216E+02	6.303E+01	1.852E+01
85	1.123E+03	1.224E+02	6.301E+01	1.862E+01
86	1.131E+03	1.232E+02	6.330E+01	1.878E+01
87	1.126E+03	1.232E+02	6.309E+01	1.874E+01
88	1.139E+03	1.241E+02	6.358E+01	1.893E+01
89	1.152E+03	1.250E+02	6.407E+01	1.912E+01
90	1.152E+03	1.250E+02	6.407E+01	1.912E+01

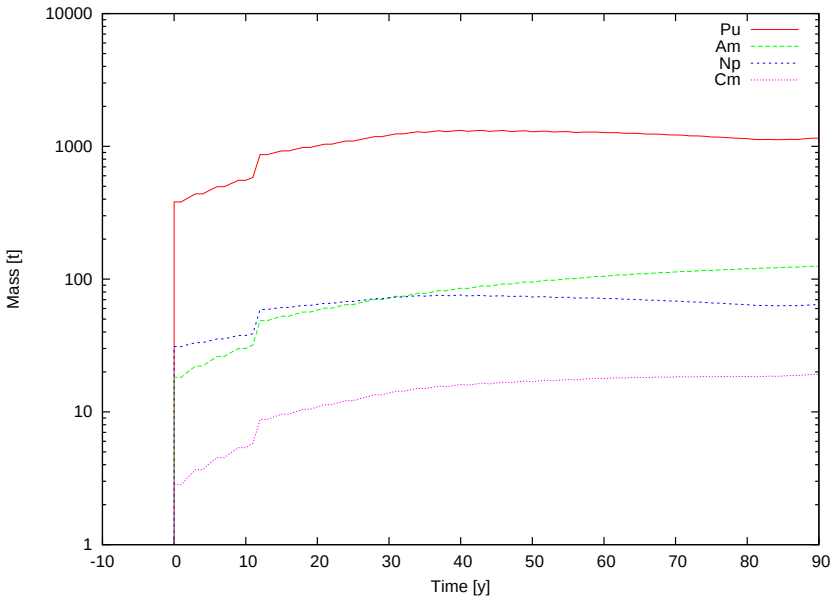

Figure 14.1: Evolution of Pu and MAs in the SF inventory according to the closed fuel cycle scenario.

Finally, concerning the mass of UOX and MOX reprocessed and lost for sustaining the ALFRs fleet, the annual fluxes are listed in Table 14.7.

Table 14.7: Reprocessed and lost U during the Pu mono-recycling scenario

Year	Reprocesses [t]	Losses [t]	Year	Reprocesses [t]	Losses [t]	Year	Reprocesses [t]	Losses [t]	Year	Reprocesses [t]	Losses [t]
-2	0.000E+00	0.000E+00	22	0.000E+00	0.000E+00	46	2.220E+03	2.220E+00	70	2.671E+03	2.671E+00
-1	0.000E+00	0.000E+00	23	0.000E+00	0.000E+00	47	2.775E+03	2.775E+00	71	3.267E+03	3.267E+00
0	0.000E+00	0.000E+00	24	0.000E+00	0.000E+00	48	1.665E+03	1.665E+00	72	2.239E+03	2.239E+00
1	0.000E+00	0.000E+00	25	0.000E+00	0.000E+00	49	2.261E+03	2.261E+00	73	2.712E+03	2.712E+00
2	0.000E+00	0.000E+00	26	0.000E+00	0.000E+00	50	2.816E+03	2.816E+00	74	3.390E+03	3.390E+00
3	0.000E+00	0.000E+00	27	0.000E+00	0.000E+00	51	1.747E+03	1.747E+00	75	2.280E+03	2.280E+00
4	0.000E+00	0.000E+00	28	0.000E+00	0.000E+00	52	2.302E+03	2.302E+00	76	2.794E+03	2.794E+00
5	0.000E+00	0.000E+00	29	0.000E+00	0.000E+00	53	2.857E+03	2.857E+00	77	3.431E+03	3.431E+00
6	0.000E+00	0.000E+00	30	0.000E+00	0.000E+00	54	1.870E+03	1.870E+00	78	2.321E+03	2.321E+00
7	0.000E+00	0.000E+00	31	0.000E+00	0.000E+00	55	2.343E+03	2.343E+00	79	2.917E+03	2.917E+00
8	0.000E+00	0.000E+00	32	0.000E+00	0.000E+00	56	2.939E+03	2.939E+00	80	3.472E+03	3.472E+00
9	0.000E+00	0.000E+00	33	8.324E+02	8.324E-01	57	1.911E+03	1.911E+00	81	2.403E+03	2.403E+00
10	0.000E+00	0.000E+00	34	8.324E+02	1.665E+00	58	2.384E+03	2.384E+00	82	2.958E+03	2.958E+00
11	0.000E+00	0.000E+00	35	1.665E+03	1.665E+00	59	3.062E+03	3.062E+00	83	1.848E+03	1.848E+00
12	0.000E+00	0.000E+00	36	1.110E+03	1.110E+00	60	1.952E+03	1.952E+00	84	1.693E+03	1.693E+00
13	0.000E+00	0.000E+00	37	1.110E+03	1.110E+00	61	2.466E+03	2.466E+00	85	2.166E+03	2.166E+00
14	0.000E+00	0.000E+00	38	2.497E+03	2.497E+00	62	3.103E+03	3.103E+00	86	1.375E+03	1.375E+00
15	0.000E+00	0.000E+00	39	1.387E+03	1.387E+00	63	1.993E+03	1.993E+00	87	1.457E+03	1.457E+00
16	0.000E+00	0.000E+00	40	1.665E+03	1.665E+00	64	2.589E+03	2.589E+00	88	8.200E+02	8.200E-01
17	0.000E+00	0.000E+00	41	2.775E+03	2.775E+00	65	3.144E+03	3.144E+00	89	9.430E+02	9.430E-01
18	0.000E+00	0.000E+00	42	1.665E+03	1.665E+00	66	2.075E+03	2.075E+00	90	9.430E+02	9.430E-01
19	0.000E+00	0.000E+00	43	2.220E+03	2.220E+00	67	2.630E+03	2.630E+00			
20	0.000E+00	0.000E+00	44	2.775E+03	2.775E+00	68	3.185E+03	3.185E+00			
21	0.000E+00	0.000E+00	45	1.665E+03	1.665E+00	69	2.198E+03	2.198E+00			

14.3 Implied horizons

The same evaluations for the reference scenario, presented in Chapter 5 are here borrowed also for the closed fuel cycle scenario.

Extending therefore the results obtained for the western European region to the whole World, under the same non-realistic assumption of no expansion of nuclear installed power, two main considerations can be brought.

Taking at first into account the consumption of natural Uranium resources, a fully-developed closed fuel cycle implementing ALFRs requires (from Table 14.3) a yearly input feed of some 303 t of Uranium (either natural or depleted) to provide the World's electric energy demand.

According to the most recent natural Uranium resources evaluations [8] (reported in Table 5.1), this consumption rate would allow for a reliable energy source (at the same World's nuclear electric energy annual production rate as in 2007) for more than 18000 years.

Even removing the optimistic assumption of no expansion of the nuclear installed power, thus supposing again that the World nuclear energy capacity will grow from 372 GWe in 2007 to between 509 GWe (+37%) and 663 GWe (+80%) by 2030 [8], the annual Uranium requirements are anticipated to rise to between 415 t and 540 t: assuming the expansion of the nuclear capacity will follow a linear trend, the availability of natural Uranium resources is expected to be accordingly worked out by between 1442 y and 1004 y.

Regarding the masses accumulated every year in the SF stocks, and considering a fully-developed ALFRs fleet for the whole World (under the assumption of constant installed nuclear electric energy capacity), some 300 t of spent UOX are accumulated yearly. Apart from FPs, only 4.5 t of Pu are produced every year, together with $\sim$ 0.2 t Am, 0.02 t Np and 0.04 t Cm.

It is to be noticed that an even better figure can be accomplished, since the ALFR recycling strategy allows for a homogeneous reprocessing of the spent fuel: only the fission products must be separated indeed from the matrix in order to produce the new fresh fuel. According to this, and because of the great difference between the masses of the Actinides and of the FPs, an increase of the separation efficiency can be easily supposed, with relatively simple technological solutions, that is, deployable in a short future.

Assuming for instance a separation efficiency of 10 pcm, the World annual production of TRUs would be 0.476 t in the whole. The dispersion of this small amount of long-lived radioisotopes among the FPs mass ($\sim$ 300 t) would result in the possibility of abandoning the geological repository solution, leaving the SF decay for few hundreds years within dedicated surface pool deposits, until the radiotoxicity of the waste is compatible with its controlled release into the environment.

In any case, deeper evaluations are needed to define the viability of such a rosy strategy, taking into detailed account the radiotoxicity of such a SF after the FPs have decayed.

Part IV

Towards the Sustainable Scenario: the ELSY/ALFR Demonstrator Reactor

CHAPTER 15

THE NEED FOR DEMONSTRATION IN ELSY/ALFR VALIDATION

L'art est une démonstration dont la nature est la preuve.

Amandine-Aurore-Lucile Dupin (George Sand) (1804-1876)

Abstract. The aim at developing a Generation IV nuclear system adopting the highly corrosive lead as coolant poses several key issues for the design of LFRs, mainly to what concerns lead technology and materials, potentially high mechanical loading, main safety functions, special operations and fuel and core design.
Despite some experience developed in Russia in the field of submarine propulsion, a massive Research and Development action is needed, focused on the basis of lead chemistry and material compatibility, aimed at developing mature technologies for safe and reliable operations in lead environment.
An European research laboratory on lead has been established during the 6^{th}, and will be continued also in the 7^{th} EURATOM Framework Programme, for addressing some of the main issues identified for LFRs. Nevertheless, a further intense R&D activity is still required to investigate the viability of LFRs in their whole.

Introduction

In 2004, the GIF organized PSSCs for every Generation-IV reactor candidate typology. In particular, the LFR-PSSC, whose first formal meeting was held in March 2005 in Monterrey, immediately begun the work to develop the LFR-SRP [44]. The committee selected two pool-type reactor concepts as candidates for international cooperation and joint development in the GIF framework: these are the SSTAR [45] and the ELSY [12].

In evaluating and planning research for these LFR concepts, the LFR-PSSC has followed the general aims of the Generation IV Roadmap [46]; thus, efforts have focused on design optimization with respect to sustainability, economics, safety and reliability, and proliferation resistance and physical protection.

Consideration of these factors has guided the identification of research necessary to bring these concepts to fruition. The needed research activities are identified and described in the SRP. It is expected that in the future, the required efforts could be organized into four major areas of collaboration and formalized as projects:

1. system integration and assessment;
2. lead technology and materials;
3. system and component design; and
4. fuel development.

In this chapter, past and ongoing research is summarized and the key technical issues and corresponding future R&D activities are discussed [47].

15.1 The ELSY/ALFR innovation

The design of LFRs poses several key issues for their deployment. They are mainly focused on the research activities and future R&D requirements for the ELSY/ALFR central station plant since the rapid current development of the latter system design. The SSTAR program is proceeding indeed at a slower pace, but shares many of the same research needs and objectives.

Table 15.1 provides a summary of the key issues, organized into main areas, highlighted by the design of the reference LFR systems (ELSY and SSTAR) according to the LFR-SRP.

15.1.1 Lead technology and materials

Lead is characterized by a high melting point and a very high boiling point (see Chapter 7). The high boiling point has a beneficial impact to the

Table 15.1: Summary of LFR key issues

General issue	Specific issue
Lead technology	Pre-purification
	Purification during operation
	Oxygen control
Materials resistant to corrosion in lead	Material corrosion at high temperatures
	Reactor vessel corrosion
	Fuel cladding
	Reactor internals
	Heat removal
	Pump impeller[1]
Potentially high mechanical loading	Earthquake
	SGTR accident
	CO_2 Tube rupture
Main safety functions	Diversified, reliable, redundant DHR
	Diversified, reliable, redundant reactor shut down system
Special operations	Refueling in lead
	ISI & Repair
Fuel and core design	Fuel selection
	Lead-fuel interaction
	Failed fuel detection
	Needs of appropriate computer codes
Demo	Technology demonstration reactor

safety of the system, whereas the high melting point requires new engineering strategies to prevent freezing of the coolant anywhere in the system, especially at reactor shut down and at refueling. Lead, especially at high temperatures, is also relatively corrosive towards structural materials with a consequent necessity of careful control of lead purity and accurate choice of the structural materials for different components [37].

Nuclear grade lead to be used as a coolant in fast reactors is required to be of higher quality than current high-purity industrial lead. It is essential indeed to control the concentrations of impurities, both because of the potential for activation and also because of the possible effect on corrosion, mass transfer and scale formation at heat transfer surfaces.

Corrosion of structural materials in lead is one of the main issues for the design of LFRs. Structural materials will be protected by the superficial oxide barrier generated by the controlled amount of dissolved oxygen in the melt, and the theoretical range of dissolved oxygen at which a LFR should be operated is known. However, simple and reliable oxygen control systems

have to be explored and tested in detail to guarantee an effective monitoring of structurals oxidation.

It is expected that assessments of fuel cladding and structural core materials, subjected to both high temperature in a lead environment and fast flux, are critical remaining issues.

15.1.2 Potentially high mechanical loading

Peculiar to a LFR design, besides the high density of the coolant, is the integration of the SG or IHX equipment inside the reactor vessel. This implies the risk of a large potential load in the case of an earthquake and of a new load brought about by the SGTR or IHX tube rupture accidents.

15.1.3 Main safety functions

Lead as the coolant requires specific solutions for the two main safety functions of DHR and reactor shutdown.

15.1.4 Special operations

Operations in lead are challenging because of the high temperature, high density and opacity. Similar issues to those of refueling exist also for In-Service Inspection (ISI).

15.1.5 Fuel and core design

In general, it is recognized that the LFR and the SFR have considerable overlap in terms of advanced fuels and associated research needs.

Peculiar issues requiring research within the LFR programme include the lead-fuel interaction, the detection of failed fuel, and the qualification of advanced fuels (e.g.: MA-bearing fuels, high-burnup and high-temperature fuels, etc.).

The lack of qualified thermal hydraulic and neutronic codes also requires an important R&D effort.

Several studies have shown that the standard models used in current computational fluid dynamic (CFD) codes are not sufficient to predict adequately heat transfer in heavy metal environment.

15.2 Research and Development strategies

During the 1970's and 80's, considerable experience was developed in Russia in the use of LBE for reactors dedicated to submarine propulsion. Russian researchers have continued to develop new reactor designs based on both LBE (*i.e.*, the SVBR reactor) and lead (*i.e.*, the BREST reactor) as primary coolants.

More recently an extensive R&D program was initiated in Europe and is still ongoing. These efforts, conducted under the IP-EUROTRANS [48], VELLA [15] and ELSY (see Chapter 7) projects of the EURATOM FP6, and the GETMAT project of the FP7, are addressing many of the main issues identified in Table 15.1.

In Japan, the Tokyo Institute of Technology is mainly focused on corrosion behavior of materials and the performance of oxygen sensors in high temperature liquid lead. In the USA, in the past considerable effort was devoted to investigations of lead corrosion and materials performance issues as well as system design of the SSTAR reactor, while more recently the focus has included the development of the desired characteristics and design of a Technology Pilot Plant (TPP) or demonstrator reactor [45].

Anyway, the main issues described in the previous section require a further intense R&D activity to investigate the viability of LFRs in their whole. The proposed strategy and R&D needed to address them are here presented and discussed.

15.2.1 Lead technology and materials

For the GIF LFR concepts, lead has been chosen as the coolant rather than LBE to drastically reduce the amount of alpha-emitting ^{210}Po isotope formed in the coolant relative to LBE, and to eliminate dependency upon bismuth which might be a limited or expensive resource.

Contamination of the lead coolant by metal oxide fines is inherent to reactor operations, but will be strictly controlled to minimize this phenomenon. Owing to the fact that reducible metal oxide fines dissolve in the melt with increasing temperature and are therefore desirable for maintaining the amount of dissolved oxygen (buffering effect) and hence the integrity of the oxide barrier against corrosion/erosion, a compromise between extensive purification and effective corrosion protection is being sought and confirmed by testing.

Different technologies for oxygen control, such as control via cover gas or via treatment of coolant by-pass streams, have been explored over the past several years. The available experience is mainly based on LBE-cooled loop type facilities. The application to pure lead and large pool-type reactors requires additional investigation particularly on determination of oxygen activity level for the chosen thermal cycle, the different technological solutions for oxygen control, the amount and location of the oxygen sensors and the different options for in-service purification.

At present, most of the R&D activities in the area of instrumentation development have been devoted to oxygen sensors; much of the remaining instrumentation is based on equipment that is in conventional use in the nuclear industry, but qualification in the lead environment is needed.

Concerning structurals corrosion, experimental campaigns intended to characterize the corrosion behavior of industrial steels (namely AISI 316 and

T91) have been completed [37]. A larger effort has been dedicated to short-/medium term corrosion experiments in stagnant and also in flowing LBE. These studies, which considered coolant flow velocities of $1 \div 2$ m s^{-1} and an exposure time of 2000 hours were completed at the CORRIDA loop at Forschungszentrum Karlsruhe (FZK), the CU2 loop at the Institute of Physics and Power Engineering (IPPE), the LECOR loop at ENEA, and the LINCE loop at Centro de Investigaciones Energética, Medioambientales y Tecnológicas (CIEMAT). In addition, a few experiments have been carried out in pure Pb (*i.e.*, CHEOPE III at ENEA). Knowledge is still missing on medium/long term corrosion behavior in flowing lead. Experiments confirm that corrosion of steels strongly depends on the operating temperature and dissolved oxygen. Indeed, at relatively low oxygen concentration, the corrosion mechanism changes from surface oxidation to dissolution of the structural steel. Moreover, a relationship between oxidation concentration, flow velocity, temperature and stress conditions of the structural material has been observed as well [49, 50].

Compatibility of Ferritic/martensitic and austenitic steels with lead has been extensively studied [37] and it has been demonstrated that generally, in the low temperature range, e.g.: below 450 °C, and with an adequate oxygen activity in the liquid metal, both types of steels build up an oxide layer which behaves as a corrosion barrier. However, in the higher temperature range, *i.e.*, above $\sim$ 500 °C, corrosion protection through the oxide barrier seems to fail [49]. Indeed, a mixed corrosion mechanism has been observed, where both metal oxide formation and dissolution of the steel elements occur.

An alternative corrosion protection barrier is worth to be envisaged. It has been demonstrated that, especially in the high temperature range, the corrosion resistance of structural materials can be enhanced by FeAl alloy coating. Corrosion tests performed on GESA treated samples in flowing HLM (heavy liquid metal) up to 600 °C have confirmed the effectiveness of this method [51], but the Al content in the coating needs to be controlled in order to assure a long-term corrosion protection capability.

As the next step, composition control, and the development of a qualification method for those surface layers, will be developed. Testing of T91 specimens representative of fuel cladding, FeCrAlY coated and GESA treated (at FZK) will start in 2009 in flowing lead in the CHEOPE loop at ENEA.

T91 and AISI 316 steels have also been tested both in lead and LBE to assess the phenomena of embrittlement and fatigue: the T91-LBE, and certainly the T91-lead combinations are subject to embrittlement, while it is still undetermined in the cases of 316L-lead and 316L-LBE. The eventual combined effect of including neutron irradiation has not been sufficiently investigated. A main objective therefore is to determine whether or not irradiation will promote embrittlement and corrosion attack by these heavy liquid metals.

Concerning irradiated structurals behavior in lead-LBE, it is expected that

the planned Post Irradiation Evaluation (PIE) of the MEGAPIE target will provide unique data regarding the combined effects of irradiation in a proton-neutron spallation environment, corrosion/erosion/embrittlement by flowing LBE and cyclic thermal/mechanical loading on the properties of T91 steel [52].

Specimens are also being irradiated in a neutron spectrum and in contact with static LBE in the BR2 (at SCK, Belgium) and HFR (at NRG, Netherlands) reactors for exposures up to 5 dpa at temperatures ranging from 300 to 500 °C. However, data at higher doses and in a fast neutron spectrum in pure lead are needed for the design of the LFR.

An irradiation campaign of different materials of interest (T91, T91 with treated surfaces and welds and SS316L) has been proposed in the BOR60 reactor (LEXUR II experiment of the GETMAT project) in liquid lead with a maximum exposure of 16 dpa.

According to this R&D summary, it is to be noticed that near-term deployment of the LFR is possible only by limiting the core outlet temperature to around 500 °C. The possibility of operating at higher temperature offered by the high boiling point of lead will be exploited only in the longer term after successful qualification of new materials such as ODS steels, ceramics and refractory metals. Reactor internals operate at lower temperature than fuel cladding and can be protected by relying on oxide layer formation and oxygen activity control in the melt. An even more favorable condition is seen for the reactor vessel which in normal operating condition can be maintained at a uniform temperature of about 400 °C.

With a primary coolant thermal cycle of 400-480 °C as proposed in ELSY, also the SG tubes operate within an acceptable temperature range, but use of aluminized steels could avoid lead pollution and heat transfer degradation brought about by a thick metal oxide layer.

Because of the relatively high speed between structural material and lead, pump impellers are subjected to severe corrosion-erosion conditions that cannot be sustained in the long term. A new material (Maxthal: Ti3SiC2) tested in stagnant conditions with dissolved oxygen and large temperature range has shown remarkably good behavior. Tests are planned in Europe on specimens exposed to flowing lead at speeds up to 20 m s^{-1}.

15.2.2 Potentially high mechanical loading

An ELSY mitigating feature to the effects of the earthquakes is the use of at least 2D seismic isolators which reduce the mechanical loads, but are relatively inefficient against lead sloshing. Qualification of mechanical codes with experimental data is necessary, but no activity has been initiated so far.

Installation of SGs inside the vessel in a way that enables operation under accident conditions while maintaining a short vessel dimension is a major

challenge of the ELSY LFR design. During reactor operations, the integration of SGs within the vessel requires:

- a sensitive and reliable leak detection system;
- a highly reliable depressurization and isolation system.

In ELSY the feed-water and steam manifolds are arranged above the reactor roof to eliminate the risk of a catastrophic failure inside the primary boundary. Three provisions have been conceived to mitigate the consequences of the SGTR accident:

1. the first provision is the installation on each tube of a check valve close to the steam header and of a Venturi nozzle close to the feed water header;
2. the second provision aims at ensuring that the flow of any feedwater-steam-primary coolant mixture be re-directed upwards, thereby preventing the risk of large pressure waves propagation across the reactor vessel;
3. the third provision prevents the pressurization of the vessel by discharging steam into an outer enclosure.

An extensive experimental activity will be carried out to obtain better understanding of each of these phenomena and especially to verify the new solution proposed in ELSY to prevent pressure wave propagation. Preliminary tests are planned in Europe aiming also at the qualification of the mechanical codes.

15.2.3 Main safety functions

For the large ELSY system an innovative dip cooler operating with pool water at ambient pressure has been conceived and a mock up will be shortly manufactured for testing in the ICE loop (Integral Circulation Experiment) of the CIRCE facility at ENEA.

The design of control rods operating inside a LFR core is at an initial stage and a remaining design effort as well as test qualification remains to be planned. The main issue of concern is control rod insertion time owing to buoyancy.

15.2.4 Special operations

Considering the obvious difficulty of handling fuel elements in lead, special provisions have been adopted for ELSY to overcome this issue. In detail, the fuel elements have been designed with an extended upper part that

extends above the lead coolant surface to allow the use of a handling machine operating in gas at ambient temperature.

Similar issues to those of refueling exist also for In-Service Inspection (ISI). The simplicity of the primary system is one of the keys to address the ISI&R issue. Thus, the present reference configuration of ELSY with extended fuel elements allows the elimination of the core support plate, one of the most difficult components for ISI. It should also be noted that in ELSY, all in-vessel components are removable for inspection or replacement. In any case, the capability to perform ISI in lead is an acknowledged issue, and an appropriate R&D program will be initiated.

15.2.5 Fuel and core design

To avoid duplication of effort and considering the worldwide limited capability for fuel irradiation, especially in representative fast neutron spectra, fuel development activities for the LFR are mainly devoted to the qualification of fuel cladding, whereas the development of the fuel itself is strongly dependent on the fuel development programme for the SFR. Peculiar issues requiring research within the LFR programme include the lead-fuel interaction, the detection of failed fuel, and the qualification of advanced fuels (e.g. MA-bearing fuels, high-burnup and high-temperature fuels).

Concerning the lack of qualified thermal hydraulic and neutronic codes, a large activity has been already performed to extend to lead the codes qualified for Na and water-cooled reactors. Lead physical data and correlations have been embodied in thermal hydraulic (e.g.: Relap, CFD) and neutronic (e.g. ERANOS, FLUKA, MCNP) codes. In particular the data resulting from the MEGAPIE irradiation test and post-test analyses is valuable for both thermal hydraulics and neutronics.

Qualification of neutronic codes is also planned in the GUINEVERE project: a lead-based, zero-power test facility is being assembled at SCK-CEN in close collaboration with several European Partners in IP-EUROTRANS. The GUINEVERE-project will provide a unique experiment with a continuous beam coupled to a fast-spectrum, sub-critical reactor allowing full investigation of the methodology of reactivity monitoring for subcritical cores, but also offering possibilities for zero-power critical experiments with a pure lead-cooled core.

To what concerns the thermal hydraulic behavior of complex components in a pool-type reactor, a thorough understanding will be gained by three different experiments, which have the aim at characterizing, respectively, a single fuel rod, a representative fuel bundle, and a cooling loop of a core sector.

- In the single rod experiment at the TALL facility (KTH, Sweden), a pin made of T91 has been tested with 3-21 kW input power range

and coolant flow speed from 0.3 m s^{-1} for natural convection up to 2.3 m s^{-1} for forced convection.

- A Mock up of a fuel rod bundle with 19 rods, 430 kW, is in assembly at FZK, redundantly equipped with instrumentation to measure local temperatures and flow rate distribution within the sub-channels.
- The mock up of a 800 kW, 37 rods fuel rod bundle is under procurement to be installed in the ICE loop of the CIRCE facility at ENEA. The ICE loop is representative of a typical pool configuration with a small riser and a large downcomer. Operation in forced and natural circulation can be simulated as well as the transient behavior from forced to natural circulation and the phenomenon of lead stratification in the downcomer.

CHAPTER 16

DEMO CHARACTERISTICS FOR ELSY/ALFR VALIDATION

Science is the systematic classification of experience.

George Henry Lewes (1817-1878)

Abstract. Despite the intense basic research in the field of lead properties and materials compatibility, an intense R&D activity is required to investigate the viability of LFRs in their whole. In particular, as recognized by the LFR Steering Committee to what concerns the development of the two Generation IV candidate systems ELSY and SSTAR, it is therefore required the development of a common Technology Pilot Plant to support the deployment of both types of systems.
According to this, the Italian government started in 2008 a preliminary investigative analysis for the design of a LFR Demonstrator reactor (DEMO) validating lead technology and overall system behavior.
Within this frame, a set of general objectives and requirements, as well as the design approach and base methodology, have to be defined, for addressing DEMO to cope with the aim at significantly supporting the ELSY, as well as the ALFR, development.

Introduction

As widely discussed in chapter 15, the development of LFRs innovative designs require fuels, materials, systems and components R&D. The LFR-SRP lays out a dual track approach to completing a cooperative research programme for the two recommended systems (SSTAR and ELSY) with convergence to the design of a single, combined Technology Pilot Plant (TPP) to support the eventual deployment of both types of systems.

Within this frame, a particular effort has been envisaged by the Italian government in 2008 in order to support the nuclear research, focusing, among other objectives, on the conception of a demonstration reactor (DEMO) validating lead technology and overall system behavior, therefore significantly supporting the ELSY, as well as the ALFR, development.

According to this, it is therefore necessary to establish an approach and bases for designing an ELSY/ALFR technology demonstrator that could initiate generally short-term construction, with an acceptable level of technical and programmatic risk, by identifying suitable design parameters.

A set of general objectives and requirements that must be met have to be first identified. These constrain the range of options to be evaluated and also help identifying the research and development that must be completed to control the risks associated with design, construction and operation of the facility.

16.1 Demonstration objectives uncoupling

A demonstration reactor is expected to prove the viability of technology for use in a future commercial power plant, construction and operation, with the purpose of attesting the general strategy to use, to the largest extent. This means that the demonstration may not be prototypical of the commercially viable design, but will contribute significantly to reducing uncertainties about construction and licensing, being a compromise between demonstration of developed technology and testing of emerging technology.

Anyway, the facility should be also capable of demonstrating the operational and safety performance required in a commercial plant design, and thus the reactor core and primary coolant path should be as much prototypical as possible.

A number of core design parameters are then identified on the basis of both objectives and technological constraints, assuming the guidelines addressing to DEMO will have to cover the whole project. This implies that R&D priorities focus on the major fields of investigation listed below:

- neutronics,
- thermal-hydraulics,

- mechanics,
- materials,
- systems and components,
- balance of plant,
- safety requirements,
- performance requirements,
- tools and methodology.

It is pointed out that DEMO has to give priority to those issues which can be examined only in a nuclear environment, *i.e.* under neutronic irradiation: it follows that other non-nuclear support facilities are required for investigating those aspects not closely related to neutrons, such as experimental heat transfer and pressure drops correlations, corrosion mechanism of steels, etc.

In addition, some of these non-neutronic analyses have necessarily to be performed before, in order to help designing DEMO itself and to make it operate always in safe conditions, *i.e.*, assuring all the safety requirements concerning technological limits are always respected.

Obviously, every experimental datum coming from DEMO will be used to get one more confirmation on the suitability of estimations. Otherwise, it would be necessary to keep some adequate margins of uncertainty into account while designing DEMO and, once it is operating, to investigate and fix those aspects not precisely defined *a priori*.

16.2 Criteria for DEMO parameters selection

The first step towards the conceptual design of a DEMO of ELSY/ALFR is to define clearly what demonstrative of ELSY/ALFR means, *i.e.* which issues of ELSY/ALFR are to be investigated/validated in DEMO, which objectives have to be reached, and which kind of analyses have to be performed in order to achieve them at best: this implies that DEMO has to be designed in order to answer as many questions as possible about ELSY/ALFR.

The hypothesis of a DEMO as an ELSY merely scaled down, while strongly keeping as far as possible the same parameters, would be misleading and has to be rejected.

An important second point is to realize as some tests/verifications can be fully performed in one or few devoted DEMO fuel elements, avoiding any odd conditioning of the whole core in designing it.

Finally a last important point is to classify the parameters in the following classes:

a. those that must be the same of the ELSY/ALFR ones (e.g.: materials..);

b. those that could be the same of ELSY/ALFR ones, but because safety and licensing reasons it is advisable having only in devoted fuel elements (e.g.: peak BU), instead on the whole core;

c. those that are, or are directly depending on, technological limits, generally the same of ELSY/ALFR (e.g.: max temperature of the clad, etc.) but not necessarily reached at their maximum in DEMO (e.g.: linear power rating, etc.);

d. those that could in principle be different but it is advisable to keep the same for a better and more persuasive coherence of the validation (e.g.: square wrapper-less fuel element, etc.);

e. those that do not need to be experimented or verified under irradiation, *i.e.*, in DEMO (e.g.: pin diameter and pitch for heat transfer correlation etc.); and

f. those that cannot be the same (e.g.: enrichment) and in case could be included in the class **b**.

After such a preliminary work, the criteria to assign a level of (relative) importance to each issue will have to be set up, in order to establish which the priorities of the analyses are and consequently, to determine the actual TPP design parameters.

It is important to make a clear distinction between ELSY/ALFR parameters and DEMO parameters: the latter have to be set up *ex-novo* or not, according to the above classification, on the basis of the objectives pursued.

Concerning tools and methodology, being ELSY a European project, tools and approach are those shared and agreed by all the European partners. It seems reasonable to keep them the same for DEMO; this will guarantee coherence in the analyses performed and allow code development and improvement (qualifying and validating methodology, tools and basic data) associated with design confirmation as well (**d.** class).

Therefore it is recommended to perform neutronic analyses by means of MCNP and ERANOS codes, JEFF3.1 library and thermal-hydraulic analysis and transients by means of RELAP and SIMMER codes. Of course, parallel calculations by different codes/libraries could increase the principal ones reliability and could be validated by DEMO when in operation.

Aiming at establishing the parameter approach and technological constraints for DEMO design, it is also to be pointed out that:

- it will be convenient to have a neutron flux as high as possible so that the kinetics of the processes can be speeded up, obtaining the wished

values of neutron fluence after a span of irradiation time as short as possible in order to optimize costs and efficiency;

- it would be interesting to be able to reproduce in a certain testing zone the same neutron spectrum as in ELSY/ALFR, in view of evaluating aspects related to burnup and MAs recycling performances.

Evaluating then the viable range for the parameters that could be applied to the demonstration facility, some criteria for the preliminary design of DEMO can be pointed out.

The power level does not generally impact the possibility of performing a technology demonstration but it will impact costs. Ideally there is a wide range of power levels that could be acceptable to the technology demonstration. A 250 MWth size plant is probably the minimum size that will meet the technology demonstration objectives, facilitating the incorporation of testing locations in the core as well.

Preliminary economical analyses [53] have proved that decreasing the power level under the mentioned minimum value will let plant costs unvaried without bringing any advantages. On the other hand, increasing the power level above the minimum will increase costs, but it is not expected to heighten programmatic risk or impact the possibility of construction and demonstration.

Therefore, 250 MWth has been chosen as reference size; however, whether a larger size core is needed to meet the above-mentioned performance requirements, it might be allowed to increase DEMO size.

DEMO core materials (namely fuel, clad and structure, coolant) should be the same of ELSY ones so that DEMO may be as much representative as possible.

Conventional MOX is considered as reference fuel thanks to its availability and state of qualification. It fits with DEMO short term deployment requirements, not introducing additional risk of delay for use. On the basis of ELSY calculations, 95% theoretical density (10.934 and 11.414 g cm^{-3} for U and Pu dioxides, respectively, at 20 °C) and 1.97 as stoichiometric ratio are suggested as reference values.

Concerning pellet design, the choice of testing peak burn-up only in devoted fuel elements ad hoc designed allows the use of solid pellets. A spare solution consists in taking hollowed pellets into account in the case a higher linear rate is required. The main fuel-associated technological constraint is indeed its centerline temperature, which is governed by the linear heat rating. Evaluations carried out on ELSY MOX demonstrated that a maximum value (peak linear heat rating) of 320 W cm^{-1} guarantees that the fuel maximum temperature has an adequate safety margin against the melting.

Demonstration of fuel clad adequacy represents the major challenge to an early LFR demonstration reactor. Assuring adequate resistance to coolant corrosion under the reactor temperature and radiation environment is the

major uncertainty that must be resolved. The cladding must also be demonstrated to be compatible with the fuel through operational and low probability transients, including those postulated to occur during severe accidents. Ferritic-martensitic steels appear to be candidates materials for fuel cladding and structures which are under high irradiation flux. In particular, the candidate material for DEMO cladding is the 9Cr-1Mo ferritic-martensitic, high-chromium alloy steel T91.

One of the key limiting factors in the development and deployment of lead-cooled reactor systems is the corrosion of cladding and structural materials. Russian experience has shown that operation at temperatures above 550 °C must be approached with caution. Dissolution must be prevented or minimized for the structural cladding and target materials. One measure that is widely being used for temperatures in the range up to 500 °C is dissolution of oxygen in lead until the oxygen content reaches a level that allows oxidation of the structural material but not oxidation of the coolant. Anyway, structural parts exposed to high thermal loads like cladding tubes, which reach temperatures above 500 °C, need additional protection measures. As a result of experiments mainly with GESA and pack cementation alloyed steels, it was shown that FeAl coating acts as an effective corrosion barrier at temperatures up to 600 °C in molten lead with controlled oxygen activity. Hence, both austenitic and martensitic steels are expected to fulfill the requirements concerning corrosion protection in the medium/long term.

Concerning an inferior limit on temperatures, experiments have shown that corrosion rate remains negligible up to 400 °C for both ferritic-martensitic steel and stainless steels. Even if a low-temperature primary cycle is selected, a large program of basic technology confirmation is necessary covering several aspects like materials specification and fabricability, materials characterization in lead, materials characterization under irradiation, advanced thermal-hydraulics, measurement techniques and system behavior confirmation by means of large-scale integral tests.

On the basis of the above considerations regarding clad maximum temperatures (600 °C and 500 °C whether a successful qualification of superficial treatments is achieved or not, respectively), a dual approach is considered in evaluating DEMO preliminary design proposal: for a short term deployment, it is advisable to rely on a maximum cladding temperature of 500 °C, while for a longer term deployment a maximum cladding temperature of 600 °C can be considered.

Austenitic steels, due to the large database available for such materials, especially those of low-carbon grade, are candidates for components operating at relatively low temperatures and low irradiation fluences, as is the case of the reactor vessel.

A coolant inlet temperature of 400 °C is required in order to avoid excessive embrittlement of structural materials subjected to fast neutron flux. In addition, a sufficient margin from the lead melting point (327 °C) is pro-

vided (such a risk is reduced by the choice of a pool-type system as well). A limit on the coolant velocity must be respected to protect the clad wall from erosion risks. Hence, the maximum bulk velocity allowed is assumed to be 2 m s^{-1}.

Table 16.1 shows a very preliminary proposal for DEMO core parameters, according to the discussed criteria.

Table 16.1: Initial and guessed DEMO core parameters

Parameter (class)	DEMO	ELSY
Reactor Thermal Power (f) [MW]	~ 250	1500
Fuel (a)	MOX	MOX+MA
Pellet smear density (a)	0.95	0.95
$UO_{1.97}$ theoretical density at 20 °C (a) [g cm^{-3}]	10.92	10.92
$PuO_{1.97}$ theoretical density at 20 °C (a) [g cm^{-3}]	11.35	11.35
Peak clad temperature (a) [°C]	550	550
Core inlet temperature (a) [°C]	400	400
Core outlet temperature (d) [°C]	480	480
Maximum linear power (a) [W cm^{-1}]	320	320
Pin diameter (e) [mm]	6.0	10.5
Clad thickness (e) [mm]	0.40	0.60
Gap thickness (e) [mm]	0.10	0.16
Pitch (e) [mm]	10.00	13.69
Peak linear power (c) [W cm^{-1}]	160	320
Coolant velocity (c) [m s^{-1}]	$2.0 \div 2.5$	~ 1.5
Active core height (f) [cm]	60	90
Active core diameter (f) [cm]	TBC	~ 490
Pressure drop (e) [bar]	~ 1.5	~ 1
Average core power density (f) [W cm^{-3}]	~ 150	108
Pellet power density (f) [W cm^{-3}]	~ 600	~ 300
Flux (f)	2 x Ref.	Ref.
Enrichment (f) [$^{v}/_{0}$]	TBC	~ 17
Breding ratio (f)	TBC	~ 1
Peak burnup (b) [MWd kg^{-1}]	~ 100	100

CHAPTER 17

NEUTRONIC DESIGN OF DEMO

We see only what we know.

Johann Wolfgang von Goethe (1749-1832)

Abstract. The overall development of DEMO has been carried out in the frame of the "New Nuclear Fission" call of the "Accordo di Programma" (a national R&D program supported by the Italian Minister of Economic Development). The efforts in the development of DEMO have been then supported also by a International Nuclear Energy Research Initiative signed between ENEA and the Argonne National Laboratory under the auspices of the EURATOM – US DOE agreement.
In this framework, the neutronic design of DEMO – developed in ENEA by a collaboration with the University of Bologna and the Polytechnic of Milan – is concerned. In particular, both the preliminary configuration of the DEMO core and its engineered layout are here presented. Aiming at proving the viability of the ELSY concept, the design of DEMO has been oriented at demonstrating the main neutronic features due to the fast spectrum of LFRs, targeting a maximization of the neutron flux as main design goal.
The matter of this work is also reported in the "Accordo di Programma" Deliverable 41 of the first annuity (for the preliminary core design investigation) and in a forthcoming Deliverable of the second annuity (for the design of the final core configuration).

Introduction

Moving from the initiative of the Italian government to support the design of an LFR demonstrator reactor, ENEA and the Argonne National Laboratory (ANL) signed an International Nuclear Energy Research Initiative (I-NERI) in order to define a first reference configuration of DEMO, under the auspices of EURATOM – US DOE Agreement.

Concerning the Italian participation, a series of specific agreements were signed between ENEA and the Italian nuclear universities to set up a cooperation tissue relaunching the research capabilities for a new nuclear age. In particular, the neutronic design of DEMO has been completely developed by ENEA, the University of Bologna and the Polytechnic of Milan.

17.1 Preliminary overall analysis

As a first step in the neutronic design of DEMO, a conceptual analysis has been carried out to retrieve, starting from the main neutronic properties of ELSY, a preliminary assessment of the DEMO core aiming at maximizing the neutron flux. Exploiting the rationales of the core design described in Chapter 11, a strategy has been chosen in order to increase the neutron flux: the reduction of the fuel pin diameter (a similar analysis has been also performed to optimize the configuration of the FAst Spectrum Transmutation Experimental Facility (FASTEF), as described in Appendix C).

A dual-track approach has been followed in this preliminary phase: a set of proposed core configurations are based on 600 °C as maximum clad temperature (medium/long term deployment); on the other hand, possible core configurations are proposed relying on 500 °C as maximum clad temperature (short term deployment).

Considering the possibility of relying on a maximum clad temperature of 600 °C, five DEMO core configurations have been explored on the basis of different performance needs.

Moving from ELSY core referring parameters as starting point, the basic approach consists in conveniently benefiting from the additional 50 °C available on the clad surface. As a further development, one of the presented configurations has been elaborated in order to move towards possibly higher values of the neutron flux; for such a more detailed elaboration, hollowed pellets have been taken into account and the core active height has been considered as a free variable. Clad and gap thicknesses have been evaluated as well.

As a first step, all the core parameters have been kept constant except for the coolant outlet temperature, which has been heightened by 50 °C. Coherently, the lead bulk velocity has been reduced to 0.99 m s^{-1}. This configuration enables the same FA characteristics as ELSY to be kept (with

the distinction of not providing DEMO FAs with any central channel devoted to finger absorbers). In the case of 21 x 21 lattice (with four corner pins and the central position replaced with structure), a thermal power of 250 MW, combined with an active core height of 90 cm, would require a core composed by around 27 FAs (in the case of 17 x 17 lattice, 42 FAs would be required to reach the aimed power size. The latter solution would permit more flexibility with respect to conceiving materials testing locations).

Given the enhanced radial buckling, a higher Pu enrichment is likely to be needed; consequently, a lower value for the breeding ratio is expected.

Table 17.1: DEMO-600 first option core parameters

Parameter	ELSY	DEMO-600 (I)
Thermal Power [MWt]	1500	250
Max Clad Temperature [°C]	550	600
Clad Outer Diameter [mm]	10.5	10.5
Fuel Column Height [mm]	900	900
Fuel Rod Pitch [mm]	13.9	13.9
Coolant Inlet Temperature [°C]	400	400
Coolant Outlet Temperature [°C]	480	530
Coolant Velocity [m s^{-1}]	1.61	0.99
Max Linear Power [W cm^{-1}]	320	320
Average Neutron Flux [cm^{-2} s^{-1}]	$2.1 \cdot 10^{15}$	$<$ ref
Av. Fuel Power Density [W cm^{-3}]	385	$=$ ref
Average Pu Enrichment [$^{w}/_{0}$]	17.59	$>$
Breeding Ratio	0.94	$<$
Peak Burn-up [MWd kg^{-1}]	100	$<$
N. Fuel Rods / FA	428	436/284
FA size [mm]	291.9	291.9/237
Total N. FAs	162	27/42
Active Core Diameter [cm]	464.9	175

The second solution envisions the possibility of moving towards higher values of neutron flux. To achieve this goal, the pin outer diameter has been reduced to 6 mm, requiring a coherent diminution of the linear rating in order to maintain the delta T between the coolant bulk and the clad surface constant. Keeping a same pin pitch, a further reduction of coolant velocity has been calculated. As a result, in this configuration the power density results 1.75 times ELSY one while the neutron flux will be increased by some extension. In the case of 21 x 21 lattice, a thermal power of 250 MW would require a core composed by about 48 FAs (in the case of 17 x 17 lattice, 73 FAs would be required to reach the aimed power size).

Even if the radial buckling is slightly decreased with respect to the previous

option, a really significant reduction of the fuel volume fraction results in a further criticality loss; hence, an even higher enrichment than option 1 and *a fortiori* than ELSY would be required.

Table 17.2: DEMO-600 second option core parameters

Parameter	ELSY	DEMO-600 (II)
Thermal Power [MWt]	1500	250
Max Clad Temperature [°C]	550	600
Clad Outer Diameter [mm]	10.5	6.0
Fuel Column Height [mm]	900	900
Fuel Rod Pitch [mm]	13.9	13.9
Coolant Inlet Temperature [°C]	400	400
Coolant Outlet Temperature [°C]	480	530
Coolant Velocity [m s^{-1}]	1.61	0.36
Max Linear Power [W cm^{-1}]	320	226
Average Neutron Flux [cm^{-2} s^{-1}]	$2.1 \cdot 10^{15}$	1 ref $< \varphi <$ 1.7 ref
Average Fuel Power Density [W cm^{-3}]	385	1.7 ref
Average Pu Enrichment [$^{w}/_{0}$]	17.59	»
Breeding Ratio	0.94	«
Peak Burn-up [MWd kg^{-1}]	100	<
N. Fuel Rods / FA	428	436/284
FA size [mm]	291.9	292/237
Total N. FAs	162	48/73
Active Core Diameter [cm]	464.9	233

The third option develops the previous one towards a more compact core configuration by exploiting the possibility of reinstating the reference average lead velocity (1.61 m s^{-1}). Consequently, the pin pitch has been coherently reduced; the fuel volume fraction results considerably enhanced with respect to the previous solution but still slightly minor than ELSY configuration. The power density results 1.7 times ELSY one. In the case of 21 x 21 lattice, a thermal power of 250 MW would require a core composed by about 48 FAs (in the case of 17 x 17 lattice, 73 FAs would be required to reach the aimed power size).

The radial buckling results enhanced, and due to the more compact configuration, a much less high Pu enrichment than the previous configuration (but still higher than ELSY one) would be likely to be needed.

A drawback affecting this solution concerns protection against accidental transients due to a significant reduction of the hydraulic diameter and therefore to a decreased free convection. Hence, safety conditions fulfillment must be carefully verified. In the event that safety requirements were not met, it would be possible to act on the core active height by reducing it.

Table 17.3: DEMO-600 third option core parameters

Parameter	ELSY	DEMO-600 (III)
Thermal Power [MWt]	1500	250
Max Clad Temperature [°C]	550	600
Clad Outer Diameter [mm]	10.5	6.0
Fuel Column Height [mm]	900	900
Fuel Rod Pitch [mm]	13.9	8.1
Coolant Inlet Temperature [°C]	400	400
Coolant Outlet Temperature [°C]	480	530
Coolant Velocity [m s^{-1}]	1.61	1.61
Max Linear Power [W cm^{-1}]	320	182
Average Neutron Flux [cm^{-2} s^{-1}]	$2.1 \cdot 10^{15}$	1 ref $< \varphi <$ 1.7 ref
Av. Fuel Power Density [W cm^{-3}]	385	1.7 ref
Average Pu Enrichment [$^{w}/_{0}$]	17.59	$>$
Breeding Ratio	0.94	$<$
Peak Burn-up [MWd kg^{-1}]	100	$<$
N. Fuel Rods / FA	428	436/284
FA size [mm]	291.9	170/138
Total N. FAs	162	48/73
Active Core Diameter [cm]	464.9	136

The fourth option envisions the possibility of benefiting from the additional 50 °C available by increasing the driving thermal drop between clad surface and coolant bulk. Therefore, the lead outlet temperature has been let unvaried (480 °C), as well as the pin pitch has been turned to ELSY value. The pin outer diameter has been first reduced by 50%, but because of pin fabricability evaluations, it has been considered advisable to fix an inferior limit on pin outer diameter at 6 mm. The lead velocity has been reduced to about 1 m s^{-1}. As a result, in this configuration the power density is tripled compared to ELSY one. In the case of 21 x 21 lattice, a thermal power of 250 MW would require a core composed by about 27 FAs (in the case of 17 x 17 lattice, 42 FAs would be required to reach the aimed power size).

Given the enhanced geometrical buckling and the really significant reduction of the fuel volume fraction resulting in a further criticality loss, a higher Pu enrichment is likely to be needed.

The last presented option develops the previous one towards a more compact core configuration by exploiting the possibility of reinstating the reference lead velocity (1.61 m s^{-1}). Consequently, the pin pitch has been coherently reduced; the fuel volume fraction results enhanced with respect to the previous solution but still much lower than ELSY one. In the case of 21 x 21 lattice, a thermal power of 250 MW would require a core composed

Table 17.4: DEMO-600 fourth option core parameters

Parameter	ELSY	DEMO-600 (IV)
Thermal Power [MWt]	1500	250
Max Clad Temperature [°C]	550	600
Clad Outer Diameter [mm]	10.5	6.0
Fuel Column Height [mm]	900	900
Fuel Rod Pitch [mm]	13.9	13.9
Coolant Inlet Temperature [°C]	400	400
Coolant Outlet Temperature [°C]	480	480
Coolant Velocity [m s^{-1}]	1.61	1.04
Max Linear Power [W cm^{-1}]	320	320
Average Neutron Flux [cm^{-2} s^{-1}]	$2.1 \cdot 10^{15}$	> ref
Av. Fuel Power Density [W cm^{-3}]	385	3 ref
Average Pu Enrichment [$^{w}/_{0}$]	17.59	»
Breeding Ratio	0.94	«
Peak Burn-up [MWd kg^{-1}]	100	<
N. Fuel Rods / FA	428	436/284
FA size [mm]	291.9	292/237
Total N. FAs	162	27/42
Active Core Diameter [cm]	464.9	174

by about 27 FAs (in the case of 17 x 17 lattice, 42 FAs would be required to reach the aimed power size).

Given the enhanced geometrical buckling and the really significant reduction of the fuel volume fraction resulting in a further criticality loss, a higher Pu enrichment is likely to be needed.

The third core option has been selected among the five alternatives presented as it is characterized by both the highest values of neutron flux and a fairly compact configuration. An attempt has been made in order to enhance the power density as far as possible by taking hollowed pins into account. Given the low value of the third configuration's linear power – compared with the limit of 320 W cm^{-1} – the possibility of enhancing the power density by enlarging the cladding outer diameter has been explored.

A constraint has been set on the maximum pellet hole diameter so that fabricability-related problems are prevented; gap and cladding thicknesses have been scaled in proportion to the pellet radius and the linear power has coherently determined. In order to maintain the total pin power constant, the fuel column height has been reduced; the pin pitch has been adjusted coherently (option III-a).

Due to the reduced fuel volume fraction, a further development of the latter configuration has been made by reinstating the pin-pitch to its previous

Table 17.5: DEMO-600 fifth option core parameters

Parameter	ELSY	DEMO-600 (V)
Thermal Power [MWt]	1500	250
Max Clad Temperature [°C]	550	600
Clad Outer Diameter [mm]	10.5	6.0
Fuel Column Height [mm]	900	900
Fuel Rod Pitch [mm]	13.9	11.6
Coolant Inlet Temperature [°C]	400	400
Coolant Outlet Temperature [°C]	480	480
Coolant Velocity [m s^{-1}]	1.61	1.61
Max Linear Power [W cm^{-1}]	320	320
Average Neutron Flux [cm^{-2} s^{-1}]	$2.1 \cdot 10^{15}$	» ref
Av. Fuel Power Density [W cm^{-3}]	385	3 ref
Average Pu Enrichment [$^{w}/_{0}$]	17.59	>
Breeding Ratio	0.94	<
Peak Burn-up [MWd kg^{-1}]	100	<
N. Fuel Rods / FA	428	436/284
FA size [mm]	291.9	244/198
Total N. FAs	162	27/42
Active Core Diameter [cm]	464.9	147

value. In order to maintain the same delta T between inlet and outlet, the active height has been further reduced (option III-b). Both solutions require accurate verification of safety conditions fulfillment concerning protection against accidental transients, due to the significant reduction of the hydraulic diameter.

In case that a short term schedule is referred to, a conservative design approach aimed at reducing technological risk is appropriate: it would be advisable to rely on a maximum cladding temperature of 500 °C, which guarantees protection against corrosion and dissolution under proper oxygen control (it is recalled that for exposure times up to 7000 h, austenitic steels can be employed in lead environment with the appropriate control of oxygen activity up to a temperature of 500 °C, while martensitic steels can be probably used in such an environment up to 550 °C, but for limited time because of the high oxidation rate; hence, a safety threshold has been set at 500 °C for the cladding too).

Four DEMO core configurations have been explored on the basis of different performance needs. Moving from ELSY referring parameters as starting point, the basic approach consists in redesign the core taking 50 °C less – available on the clad maximum temperature – into account.

As a first step, all the core parameters have been kept constant except for

Table 17.6: DEMO-600 sixth option core parameters

Parameter	DEMO-600 (III)	DEMO-600 (III-a)
Thermal Power [MWt]	250	250
Max Clad Temperature [°C]	600	600
Clad Outer Diameter [mm]	6.0	6.5
Clad Thickness [mm]	0.34	0.37
Gap Thickness [mm]	0.08	0.09
Pellet Outer Radius [mm]	2.57	2.79
Pellet Inner Radius [mm]	0.57	1.24
Fuel Column Height [mm]	900	827
Fuel Rod Pitch [mm]	8.1	8.4
Coolant Inlet Temperature [°C]	400	400
Coolant Outlet Temperature [°C]	530	530
Coolant Velocity [m s^{-1}]	1.61	1.61
Max Linear Power [W cm^{-1}]	182	199
Av. Pellet Power Density [W cm^{-3}]	1.7 ref	1.6 ref
Av. Pin Power Density [W cm^{-3}]	1.7 ref	1.9 ref
Average Pu Enrichment [$^{w}/_{0}$]	>	>
Average Neutron Flux [cm^{-2} s^{-1}]	1 ref $< \varphi <$1.7 ref	1 ref $< \varphi <$ 1.9 ref
Fuel Volume Fraction	0.30	0.28

the coolant outlet temperature, which has been reduced by 40 °C. Coherently, the pin pitch has been enlarged to 17.3 mm. In the case of 21 x 21 lattice, a thermal power of 250 MW, combined with an active core height of 90 cm, would require a core composed by 27 FAs (in the case of 17 x 17 lattice, about 42 FAs would be required to reach the aimed power size. The latter solution would permit more flexibility with respect to conceiving materials testing locations). The corresponding active core diameter has been estimated to be roughly 220 cm. Given both the enhanced geometrical buckling and the significantly lower fuel volume fraction, a higher Pu enrichment is likely to be needed; consequently, a lower value for the breeding ratio is expected.

The second solution envisions the possibility of moving towards higher values of neutron flux. To achieve this goal, the pin outer diameter has been reduced to 6 mm, requiring an equal diminution of the linear rating in order to maintain the delta T between the coolant bulk and the clad surface constant. The pin pitch has been coherently adjusted to 12.3 mm. As a result, in this configuration the power density results 1.7 times ELSY one. In the case of 21 x 21 lattice, a thermal power of 250 MWth would require a core composed by about 48 FAs (in the case of 17 x 17 lattice, 73 FAs would be

Table 17.7: DEMO-600 seventh option core parameters

Parameter	DEMO-600 (III)	DEMO-600 (III-b)
Thermal Power [MWt]	250	250
Max Clad Temperature [°C]	600	600
Clad Outer Diameter [mm]	6.0	6.5
Clad Thickness [mm]	0.34	0.37
Gap Thickness [mm]	0.08	0.09
Pellet Outer Radius [mm]	2.57	2.79
Pellet Inner Radius [mm]	0.57	1.24
Fuel Column Height [mm]	900	711
Fuel Rod Pitch [mm]	8.1	8.1
Coolant Inlet Temperature [°C]	400	400
Coolant Outlet Temperature [°C]	530	530
Coolant Velocity [m s^{-1}]	1.61	1.61
Max Linear Power [W cm^{-1}]	182	199
Av. Pellet Power Density [W cm^{-3}]	1.7 ref	1.6 ref
Av. Pin Power Density [W cm^{-3}]	1.7 ref	1.9 ref
Average Pu Enrichment [$^{w}/_{0}$]	>	>
Average Neutron Flux [cm^{-2} s^{-1}]	1 ref $< \varphi <$1.7 ref	1 ref $< \varphi <$ 1.9 ref
Fuel Volume Fraction	0.30	0.30

required to reach the aimed power size).

Given the slightly enhanced geometrical buckling associated with a further reduction of fuel volume fraction, a higher Pu enrichment than in the previous option is likely to be needed; consequently, a lower value for the breeding ratio is expected.

The third solution assesses the possibility of partitioning the availability loss of 50 °C on the clad maximum temperature between both a coolant outlet temperature reduction and a linear heat rating diminution. Therefore, a lead outlet temperature of 450 °C and a peak linear power of 237 W cm^{-1} have been set. Due to a pin pitch enlargement to 14.6 mm, this configuration fuel volume fraction results slightly reduced compared with ELSY one. In the case of 21 x 21 lattice, a thermal power of 250 MW would require a core composed by about 37 FAs (in the case of 17 x 17 lattice, 57 FAs would be required to reach the aimed power size).

Given the enhanced geometrical buckling, a higher Pu enrichment is likely to be needed; consequently, a lower value for the breeding ratio is expected.

The last solution envisions the possibility of achieving higher values of neutron flux starting from the previous configuration. To reach such a purpose, the pin outer diameter has been reduced to 6 mm, requiring a coherent

Table 17.8: DEMO-500 first option core parameters

Parameter	ELSY	DEMO-500 (I)
Thermal Power [MWt]	1500	250
Max Clad Temperature [°C]	550	500
Clad Outer Diameter [mm]	10.5	10.5
Fuel Column Height [mm]	900	900
Fuel Rod Pitch [mm]	13.9	17.3
Coolant Inlet Temperature [°C]	400	400
Coolant Outlet Temperature [°C]	480	440
Coolant Velocity [m s^{-1}]	1.61	1.61
Max Linear Power [W cm^{-1}]	320	320
Average Neutron Flux [cm^{-2} s^{-1}]	$2.1 \cdot 10^{15}$	$<$ ref
Av. Fuel Power Density [W cm^{-3}]	385	$=$
Average Pu Enrichment [$^{w}/_{0}$]	17.59	$>$
Breeding Ratio	0.94	$<$
Peak Burn-up [MWd kg^{-1}]	100	$<$
N. Fuel Rods / FA	428	436/284
FA size [mm]	291.9	364/295
Total N. FAs	162	27/42
Active Core Diameter [cm]	464.9	218

diminution of the linear rating in order to maintain the delta T between the coolant bulk and the clad surface constant. The pin pitch has been coherently adjusted to 10 mm. As a result, in this configuration the power density results 1.3 times ELSY one. In the case of 21 x 21 lattice, a thermal power of 250 MW would require a core composed by about 65 FAs (in the case of 17 x 17 lattice, 99 FAs would be required to reach the aimed power size).

Given the enhanced geometrical buckling and a reduction of the fuel volume fraction resulting in a further criticality loss, a higher Pu enrichment is likely to be needed.

17.2 DEMO computational model

All neutronics computations for the assessment of the final DEMO configuration have been performed only by deterministic methods. In this early design stage no rationale has been envisaged indeed in following the same approach than in ELSY (parallel evaluation also by Monte Carlo calculations). The use of stochastic methods is therefore intended to be introduced in phase of assessing the final design.

In detail, deterministic analysis has been performed by means of the ERANOS (European Reactor ANalysis Optimized System) formulary [7], the

Table 17.9: DEMO-500 second option core parameters

Parameter	ELSY	DEMO-500 (II)
Thermal Power [MWt]	1500	250
Max Clad Temperature [°C]	550	500
Clad Outer Diameter [mm]	10.5	6.0
Fuel Column Height [mm]	900	900
Fuel Rod Pitch [mm]	13.9	12.3
Coolant Inlet Temperature [°C]	400	400
Coolant Outlet Temperature [°C]	480	440
Coolant Velocity [m s^{-1}]	1.61	1.61
Max Linear Power [W cm^{-1}]	320	182
Average Neutron Flux [cm^{-2} s^{-1}]	$2.1 \cdot 10^{15}$	1 ref $< \varphi <$ 1.7 ref
Av. Fuel Power Density [W cm^{-3}]	385	1.7 ref
Average Pu Enrichment [$^{w}/_{0}$]	17.59	»
Breeding Ratio	0.94	«
Peak Burn-up [MWd kg^{-1}]	100	<
N. Fuel Rods / FA	428	436/284
FA size [mm]	291.9	257/210
Total N. FAs	162	48/73
Active Core Diameter [cm]	464.9	205

same reference tool used for the ELSY design.

17.2.1 ERANOS model

As for the ELSY design, the deterministic analysis has been carried out by means of the ERANOS v. 2.1 code [7], by a two-step process:

1. a transport calculation to evaluate the multi-group cross-sections (both microscopic and macroscopic) for every cell defined in the problem, and

2. a variational-coarse mesh nodal transport calculation to solve the multi-group Boltzmann equation in the whole reactor system.

The multigroup cross-sections set has been produced by means of ECCO [18], starting from rough nuclear data taken by the JEFF3.1 [30] data library, treating the main nuclides with a fine energy structure (1968 groups) and condensing the obtained cross-sections in a 33 groups scheme for reactor calculations. Very refined cell descriptions – according to ECCO capabilities – have been adopted for the main cells (*i.e.*,for the cells surrounding the active zone).

For the DEMO characterization, the simulation domain has been extended to account also for the structural regions surrounding the core, acting as a

Table 17.10: DEMO-500 third option core parameters

Parameter	ELSY	DEMO-500 (III)
Thermal Power [MWt]	1500	250
Max Clad Temperature [°C]	550	500
Clad Outer Diameter [mm]	10.5	10.5
Fuel Column Height [mm]	900	900
Fuel Rod Pitch [mm]	13.9	14.5
Coolant Inlet Temperature [°C]	400	400
Coolant Outlet Temperature [°C]	480	450
Coolant Velocity [m s^{-1}]	1.61	1.61
Max Linear Power [W cm^{-1}]	320	237
Average Neutron Flux [cm^{-2} s^{-1}]	$2.1 \cdot 10^{15}$	< ref
Av. Fuel Power Density [W cm^{-3}]	385	0.7 ref
Average Pu Enrichment [$^{w}/_{0}$]	17.59	»
Breeding Ratio	0.94	«
Peak Burn-up [MWd kg^{-1}]	100	<
N. Fuel Rods / FA	428	436/284
FA size [mm]	291.9	307/248
Total N. FAs	162	37/57
Active Core Diameter [cm]	464.9	245

neutron reflector. A cross-cut representation of a simplified cylindrical model of DEMO is depicted in Figure 17.1.

The final characterization of the system has to be performed therefore on refined simulation models, adopting a 3D Cartesian representation of the domain in order to discriminate each FA for evaluating the actual power/FA distribution.

17.3 Engineerization of DEMO and final optimization analysis

Starting from the results presented in section 17.1, a rearrangement of the core has been done according to the need of a staggered lattice of FAs for their easier insertion and removal in the core, as well as to the idea to move from traditional concept CRs to FARs systems.

The ERANOS model has been therefore modified in order to account for the introduction of the FARs. In particular, since the possibility of representing only cylindrical or homogeneous regions in the FA lattice, the inner positions (containing the structural box beam and – eventually – the FAR) have been specifically modeled in order to preserve – as far as possible – the

Table 17.11: DEMO-500 fourth option core parameters

Parameter	ELSY	DEMO-500 (IV)
Thermal Power [MWt]	1500	250
Max Clad Temperature [°C]	550	500
Clad Outer Diameter [mm]	10.5	6.0
Fuel Column Height [mm]	900	900
Fuel Rod Pitch [mm]	13.9	10.0
Coolant Inlet Temperature [°C]	400	400
Coolant Outlet Temperature [°C]	480	450
Coolant Velocity [m s^{-1}]	1.61	1.61
Max Linear Power [W cm^{-1}]	320	135
Average Neutron Flux [cm^{-2} s^{-1}]	$2.1 \cdot 10^{15}$	≈ ref
Av. Fuel Power Density [W cm^{-3}]	385	1.3 ref
Average Pu Enrichment [$^{w}/_{0}$]	17.59	»
Breeding Ratio	0.94	«
Peak Burn-up [MWd kg^{-1}]	100	<
N. Fuel Rods / FA	428	436/284
FA size [mm]	291.9	210/170
Total N. FAs	162	65/100
Active Core Diameter [cm]	464.9	210

heterogeneity of the cell.

As for the final ELSY design, two different arrangements of homogeneous regions have been envisaged to distinguish FAs provided of a FAR from the remaining ones:

- for the FA without a FAR (or with the FAR withdrawn), the central position(s) is only filled by cover gas (Argon), while the remaining boundary cells are represented by an homogeneous mixture of the remaining void, the steel the box beam is made of, the Lead flowing outside the box beam and the steel representing the three spacer grids placed along the active height (in order to preserve the total amount of steel in the active zone);
- an analogous description has been adopted also for the FAs with a FAR inserted, substituting the void with the materials the FAR is made of, that is, B_4C in the central position(s) and the remaining B_4C, the Helium in the absorber-clad gap and the clad steel in the surrounding positions.

A series of core configurations has been investigated (the s.c. "GPS" layouts) to point out the optimal core in order to obtain the highest flux as possible, with reactor power almost fixed to 265 MWth. All the investigated

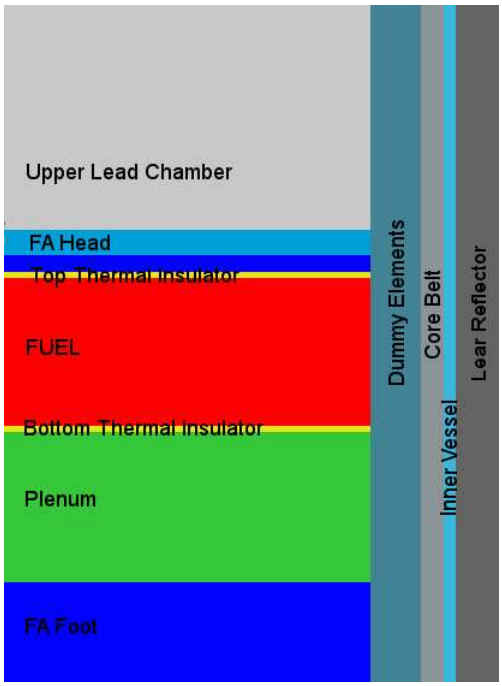

Figure 17.1: Simplified 2D cylindrical ERANOS computational domain for DEMO design.

configurations explicated around the same fuel pin design, with the only exception of the active height: as a result, the pitch has been set - for every core layout - according to the actual power generated by the average pin, considering the Lead velocity fixed at 2 m s^{-1}.

The former four configurations investigated (namely "GPS1" to "GPS4") provided useful information to what concerns the intrinsic criticality associated to the overall shape of the system, as well as the coolant reactivity worth in terms of volume fraction in the elementary cell. It is known indeed that the higher the active zone the fewer - at fixed power - the fuel pins (thus more critical the system in terms of geometrical buckling), but - on the other side - the larger the coolant flow channel (thus less critical the system in terms of coolant density worth): an evaluation of the two effects is therefore needed in order to point out a compromise between the height of the active zone and the pins pitch in the FA, to maximize the criticality of the system so to control the fuel enrichment, thus to maximize the neutron flux.

The core has been also segmented into enrichment zones to flatten the power/FA distribution, so to improve economics. The maximum value allowed for the maximum-to-average power/FA Distribution Factor (FADF) was fixed at 1.2.

The main core characteristics and performances for the first four configurations, as produced by ERANOS v.2.1 [7] with the JEFF 3.1 cross sections library [30], are shown in Tables 17.12 and 17.13.

Table 17.12: Resume of GPS1-2 core configurations main core characteristics and performances

Parameter	Unit	GPS1	GPS2
Thermal power	MW	265	280
Active height	cm	42.0	60.0
Lattice pitch	mm	8.71	9.81
Pins per FA	-	25x25-5x5-4	22x22-4x4-4
Inn/Int/Out FAs	-	7/12/18	10/14/16
Inn/Int/Out Pu enr.	$^{v}/_{0}$	29.5/33.9/34.7	26.0/30.8/33.0
k_{eff}	-	1.00150	0.99129
FADF	-	1.19	1.13
Max. linear power	W cm^{-1}		
Max. flux	cm^{-2} s^{-1}	$6.47 \cdot 10^{15}$	$6.17 \cdot 10^{15}$

Table 17.13: Resume of GPS3-4 core configurations main core characteristics and performances

Parameter	Unit	GPS3	GPS4
Thermal power	MW	265	232
Active height	cm	65.0	70.0
Lattice pitch	mm	8.80	8.80
Pins per FA	-	28x28-6x6-4	28x28-6x6-4
Inn/Out FAs	-	7/12	7/12
Inn/Out Pu enr.	$^{v}/_{0}$	30.0/34.0	33.0/35.0
k_{eff}	-	1.02586	1.04834
FADF	-	1.20	1.19
Max. linear power	W cm-1		
Max. flux	cm^{-2} s^{-1}	$8.75 \cdot 10^{15}$	$7.32 \cdot 10^{15}$

As shown by the results of Tables 17.12 and 17.13, it is preferable to move to short cores since the coolant density worth exceeds the criticality due to the geometrical buckling optimization.

All the information and worth pointed out by the preliminary calculations have been used to characterize a core with the best performances allowed by the staggered FAs scheme and the power of the system, considered fixed as a first step. To take advantage of the coolant worth in the elementary cell,

it was allowed to increase the Lead flow velocity from 2 to 3 m s^{-1} so to raise the core by a 50% without increasing the pins lattice pitch. Further four configurations have been analyzed to exploit the features of the overall system arrangement, now taking into account also the evolution of the fuel with BU rather than a simple static analysis at Beginning of Life (BoL). To limit the criticality swing an open multi-batches cycle strategy has been envisaged, analogously to the ELSY case [41]. The neutronic calculations have been performed in a single batch hypothesis with a suited time step, since it was proved [5] the equivalence between the two strategies in terms of criticality swing during irradiation. Assuming 2 y fuel residence time - by scaling the same ELSY parameter according to the fluxes ratio -, under a three-batches hypothesis (the length of the cycle thus being 0.67 y) the mean aging of the fuel at Beginning of Cycle (BoC) and End of Cycle (EoC) would be 0.67 and 1.33 y respectively, as shown in Table 17.14 (cells with two values refer to the aging of the batch just before/immediately after the refueling). The proper time step for a simulation in one-batch approximation (valid after a transitory start up of 1.33 y) results then 0.67 y.

Table 17.14: Scheme of a three-batches cycle hypothesis

Time [y]	Fuel aging		
	1^{st} batch	2^{nd} batch	3^{rd} batch
0	0.00	0.00	0.00
0.67	0.67/0.00	0.67	0.67
1.33	0.67	1.33/0.00	1.33
2.00	1.33	0.67	2.00/0.00
2.67	2.00/0.00	1.33	0.67

A successive refinement procedure allowed to determine the Pu enrichments for the two zones so to obtain an admissible FADF at EoC. As a matter of facts, because of the high enrichments needed for DEMO criticality, an insufficient breeding during irradiation is found, which in turn imply a monotonic decrease of the reactivity. Aiming therefore at a $k_{\text{eff}} = 1$ at EoC without any absorber inserted in the active zone, the distributed regulation system foreseen (made of FARs) can be therefore used also to further flatten the power/FA distribution, guaranteeing the respect of the fixed limit also at BoC.

Tables 17.15 and 17.16 resumes the main core characteristics, the cycle hypotheses considered and the corresponding core performances for the last preliminary configurations.

Table 17.15: Resume of GPS5-6 core configurations main core characteristics and performances

Parameter	Unit	GPS5	GPS6
Thermal power	MW	265	265
Active height	cm	65.0	65.0
Lattice pitch	mm	8.53	8.53
Pins per FA	-	28x28-6x6-4	28x28-6x6-4
Inn/Out FAs	-	10/14	10/14
Inn/Out Pu enr.	$^{v}/_{0}$	29.5/34.0	29.0/33.5
Fuel residence time	y	2	2
Number of batches	-	3	3
Cycle length	y	0.67	0.67
BoC/EoC k_{eff}	-	1.07209/1.01905	1.06203/1.00953
BoC/EoC FADF	-	1.19/1.17	1.19/1.17
Max. linear power	W cm^{-1}		
BoC/EoC max. flux	cm^{-2} s^{-1}	5.53/5.86 $\cdot 10^{15}$	5.60/5.93 $\cdot 10^{15}$

Table 17.16: Resume of GPS7-8 core configurations main core characteristics and performances

Parameter	Unit	GPS7	GPS8
Thermal power	MW	265	265
Active height	cm	65.0	65.0
Lattice pitch	mm	8.53	8.53
Pins per FA	-	28x28-6x6-4	28x28-6x6-4
Inn/Out FAs	-	10/14	10/14
Inn/Out Pu enr.	$^{v}/_{0}$	28.0/33.5	28.5/33.0
Fuel residence time	y	2	2
Number of batches	-	3	3
Cycle length	y	0.67	0.67
BoC/EoC k_{eff}	-	1.05062/0.99925	1.05190/0.99999
BoC/EoC FADF	-	1.16/1.15	1.19/1.17
Max. linear power	W cm^{-1}		
BoC/EoC max. flux	cm^{-2} s^{-1}	5.59/5.93 $\cdot 10^{15}$	5.67/6.00 $\cdot 10^{15}$

17.4 Results and final layout

The information collected by means of the preliminary analysis described in the previous subsection lead to the characterization of a core complying with all the technological constraints regarding criticality and power/FA distribu-

tion flattening. A further constraint has been then pointed out regarding the maximum admissible Pu enrichment of the fuel because of proliferation resistance. Despite in literature the classical limit on Pu enrichment is fixed at 35%, it was chosen to keep the maximum enrichment within 33%. This choice imposed to enlarge the core in order to add more FAs so to dilute the fissile. To not reduce the maximum flux (main design goal), the power has been consequently increased to 300 MWth, trying to maintain the same maximum linear power rate as the previous cases, about 374 W cm^{-1} (some discrepancies are expected because of the different BU coming from the higher flux, which in turn implies a re-adjustment of the Pu enrichments).

Some iterative refinements (explicated around the "GPS9" configuration) were needed to re-compute the two optimal enrichments for core criticality and power/FA distribution flattening. It was chosen to exploit the imposed limit for the FADF (1.2 at EoC) in order to maximize the neutron flux, and to move to a four-batches strategy for keeping the k_{eff} swing in.

17.4.1 Final layout

The final core scheme is shown in Figure 17.2: the 10 yellow elements represent the FAs in the inner enrichment zone, while the 14 red ones are in the outer enrichment zone. The positions occupied by blue circles represent the structural dummies positions, for both core compactness (in analogy with the ELSY core layout [41, 13]) and neutrons shielding. The outer circle delimits the inner surface of the core barrel. Detailed CAD drawings of the fuel pin, FA, spacers grids and dummy elements for the final configuration have been also produced according to the overall system design, and are collected in Appendix D.

For the system control and criticality regulation during operation, FARs have been introduced in the core exploiting the thimble guide (closed to Lead) represented by the structural box beam in the center of each FA, in analogy with the ELSY one [41, 32]. The FARs are made of an absorber cylinder 85 cm long and 42.6 mm diameter. Detailed CAD drawings of the FAR and of its positioning (both withdrawn and completely inserted) with respect to the DEMO FA are provided in Appendix D.

The absorbers system has been split into two sets: a first one for criticality swing compensation during the cycle and shutdown of the reactor, and a second one for the system control. The first set, made up of 20 motorized FARs equipped with B_4C enriched at 42 $^{a}/_{0}$ in ^{10}B, must provide - against partial insertion - the anti-reactivity needed for criticality swing compensation during the cycle. An excess of anti-reactivity has been also foreseen against the insertion of the remaining absorbing length in the active core by electro-magnetic release of the FARs: further 3000 pcm must be therefore provided by the same set, to represent a first reactor shut-down system. The second system, for reactor control, is made up of 4 passive FARs, equipped

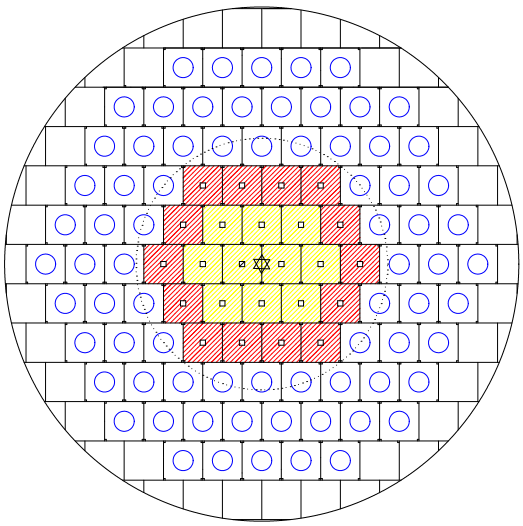

Figure 17.2: DEMO final ("GPS10") core configuration: inner (yellow) and outer (red) FAs arrangement.

with 90 $^{a}/_{0}$ ^{10}B enriched B_4C, to be let drop into the active zone in case of electro-magnetic blockage release. Also this set must provide the 3000 pcm anti-reactivity margin for safe shut-down of the reactor, in order to represent an independent, redundant safety system.

The two systems have been distributed among the FAs positions as shown in Figure 17.3.

17.4.2 Results

The results of ERANOS neutronic simulations showed an incredibly high neutron flux characterizing this configuration, about $7.4 \cdot 10^{15}$ cm^{-2} s^{-1} during the cycle, far above the initial aims (at least 2.5 times the reference ELSY one, about $2.5 \cdot 10^{15}$ cm^{-2} s^{-1}). Such a flux would also allow to further reduce the cycle length in order both to lower the huge reactivity swing due to BU, some 4000 pcm, and to contain the fuel swelling to avoid excessive stresses by PCMI.

The main characteristics and performances of the final optimized configuration ("GPS10") are resumed in Table 17.17.

The absorbers system has been split into two sets: a first one for criticality swing compensation during the cycle and shutdown of the reactor, and a second one for the system control. The first set, made up of 20 motorized FARs equipped with B_4C enriched at 42 $^{a}/_{0}$ in ^{10}B, must provide - against partial insertion - the 4000 pcm anti-reactivity needed for criticality swing compensation during the cycle. An excess of anti-reactivity has been also foreseen against the insertion of the remaining absorbing length in the active

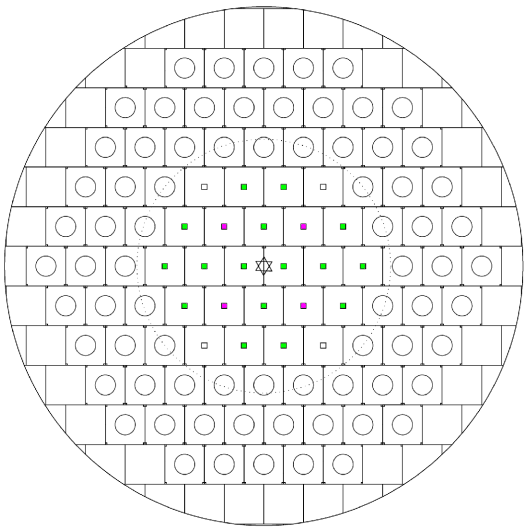

Figure 17.3: Control (magenta) and regulation (green) FARs positioning in the DEMO core (GPS10 configuration).

Table 17.17: GPS10 configuration main core characteristics and performances

Parameter	Unit	GPS10
Thermal power	MW	300
Active height	cm	65.0
Lattice pitch	mm	8.53
Pins per FA	-	28x28 - 6x6 - 4
Inn/Out FAs number	-	10 / 14
Inn/Out Pu enr.	$^{v}/_{0}$	29.3 / 32.2
Fuel residence time	y	2
Number of batches	-	4
Cycle length	month	5
BoC/EoC k_{eff}	-	1.04238 / 1.00093
BoC/EoC FADF	-	1.23 / 1.20
BoC/EoC max. linear power	W cm^{-1}	381 / 371
BoC/EoC max. neutron flux	cm^{-2} s^{-1}	$7.27 \cdot 10^{15}$ / $7.54 \cdot 10^{15}$

core by electro-magnetic release of the FARs: further 3000 pcm must be therefore provided by the same set, to represent a first reactor shut-down system. The second system, for reactor control, is made up of 4 passive FARs, equipped with B_4C enriched at 90 $^{a}/_{0}$ in ^{10}B, to be let drop into the active zone in case of electro-magnetic blockage release. Also this set

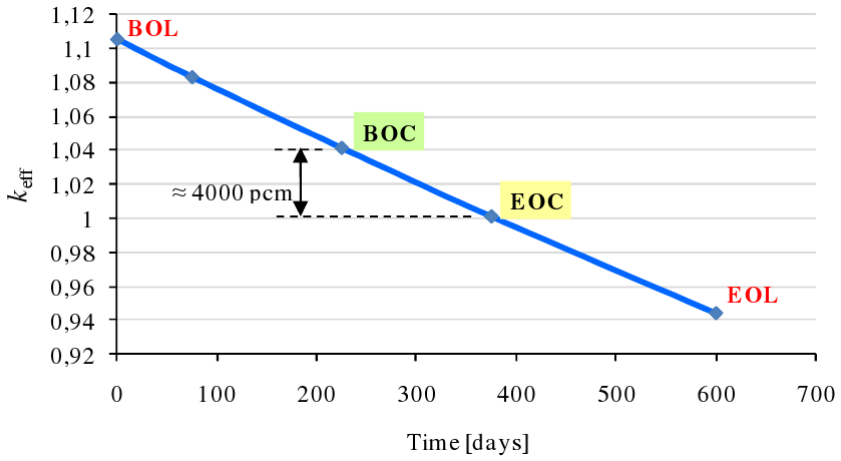

Figure 17.4: Criticality swing during irradiation for the final DEMO configuration.

must provide the 3000 pcm anti-reactivity margin for safe shut-down of the reactor, in order to represent an independent, redundant safety system.

As shown in Table 17.18, the two systems, distributed among the FAs positions according to Figure 17.3, are able to provide the design anti-reactivity.

Table 17.18: Control and regulation systems worth

System	Insertion	Anti-reactivity [pcm] Aimed	Actual
Regulation FARs at BoC	complete	7000	11312
Control FARs at BoC/EoC	complete	3000	4624/4856

Investigating the variation of the regulation FARS as a function of their progressive insertion in the core, the typical sigmoid represented in Figure 17.5 has been found. According to this, it can be seen that an average FARs insertion of some 32.5 cm introduces the required anti-reactivity to compensate the over-criticality at BoC.

The uniform insertion of the regulation FARs was found to satisfy also the requirement of power/FA distribution flattening, modifying the flux spatial distribution so as to reduce the FADF at BoC from 1.23 to 1.20, as desired. This uniform insertion can be adopted in order to exploit the peak flux in the central position to obtain over-irradiated fuel pins for testing. On the other hand, a differential FARs insertion strategy would allow to mitigate the FADF and therefore to increase the power without overcoming the design limits.

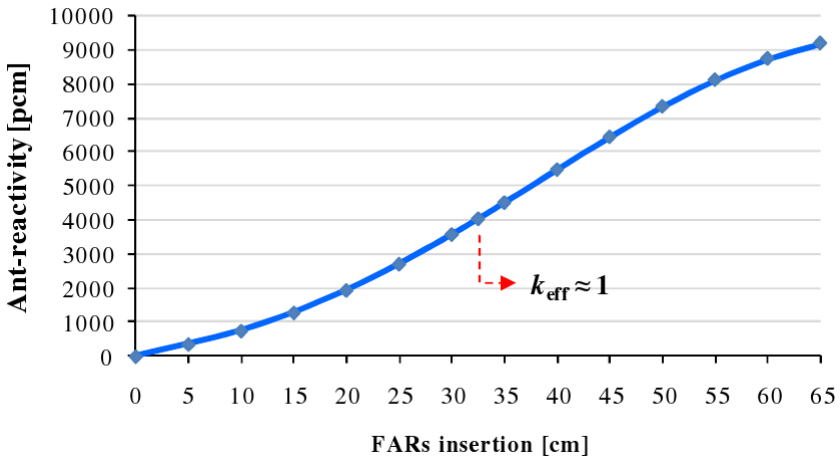

Figure 17.5: DEMO regulation FARs anti-reactivity vs insertion curve.

Part V

Concluding Remarks

CHAPTER 18

CONCLUSIONS

A science is any discipline in which the fool of this generation can go beyond the point reached by the genius of the last generation.

Max Gluckman (1911-1975)

Abstract. The present thesis described the work performed on the conceptual solution of the nuclear energy sustainability problem.
The research for an optimal reactor to be candidated for the forthcoming Generation of nuclear power plants has been inserted in the frame of scenario studies, so as to prove the effectiveness of the proposed solution.
A thorough reflexion concerning the sustainability issues related to nuclear energy production allowed to formalize the s.c. Adiabatic Reactor Theory – for the definition of a zero-impact reactor to what concerns both the optimal exploitation of Uranium resources and the minimization of the Long Lived Radioisotopes in the High Level Wastes produced by the related fuel cycle – and, consequently, a New Paradigm for Nuclear Power, aimed at designing the core of a nuclear reactor around its adiabaticity feature.
Finally, to face the innovations included in the proposed solution, a Lead-cooled demonstrator reactor has been conceived and designed for proving the technology to be implemented in the First-of-a-Kind industrial power plant, with the aim at attesting the general strategy to use, to the largest extent, thus making the aimed nuclear renaissance come true.

Concluding remarks and perspectives

Evolution is greedy for energy.

Besides this peremptory statement an undeniable truth is concealed: the as irrepressible as right aspiration to high wellness standard of a continuously growing population imposes an unceasing research for new energy sources. As a matter of fact, the history of human society passes through several energy revolutions which boosted its evolution up to the present condition.

But the last years of this unbridled growth brought up a crucial problem for humanity: to ensure the availability of certain energy sources for future generations. The wild usage of natural resources, together with the superficial care spent for wastes management and disposal, spoiled the certainties on the present energetic scenario.

Significant solutions must be conceived for overcoming this "surviving problem", by proposing new ways of approaching and solving the energy question. In this frame it is evident as nuclear energy, with its enormous energy concentration, can (or even must) play a major role, provided it is able to overcome the two main issues of present generation nuclear power plants, related to the availability of natural resources for a far future and the production of long-lived radioactive waste.

The environmental requirements embedded in the previous lines, which is what we call sustainability, represent therefore the necessary password for the public acceptance of nuclear energy as most charming and effective energy source for the future, thus making the forthcoming nuclear renaissance come true.

A new generation nuclear reactor is indeed desired by the actual industrialized world, exploiting an efficient use of Uranium natural resources also by recycling the valuable components of the spent fuel coming from existing reactors, and minimizing - at the same time - the TRUs abundance in the final waste. According to this, the footprint of such innovative systems would be greatly reduced, extending the availability of this "new-clear" energy source for a longer time horizon, with negligible environmental impact.

The present PhD thesis summarizes the three-years study about the neutronic investigation of a new concept Lead-cooled Fast Reactor, chosen among the Generation IV candidate typologies, since it is top rated in sustainability.

The European Lead-cooled SYstem (ELSY) has been at first investigated. The neutronic analysis of the ELSY core has been performed via deterministic analysis by means of the ERANOS code, in order to retrieve a stable configuration for the overall design of the reactor. Further analyses have been carried out by means of the Monte Carlo general purpose transport code MCNP, in order to check the former one and to define an exact model of the system.

An innovative system of absorbers has been conceptualized and designed for both the reactivity compensation and regulation of the core due to cycle

swing, as well as for safety in order to guarantee the cold shutdown of the system in case of accident.

Moving from the results regarding the ELSY fuel cycle, a thorough reflexion on the nuclear equilibrium allowed then to define the "extended" equilibrium state concept. According to this, the s.c. Adiabatic Reactor Theory has been formalized – for the definition of a zero-impact reactor to what concerns both the optimal exploitation of Uranium resources and the minimization of the Long Lived Radioisotopes in the High Level Wastes produced by the related fuel cycle –, together with a New Paradigm for Nuclear Power, aimed at designing the core of a nuclear reactor around its adiabaticity feature.

The New Paradigm has been applied then to the core design of an Adiabatic Lead Fast Reactor complying with the ELSY overall system layout. A complete core characterization has been done in order to asses criticality and power flattening; a preliminary evaluation of the safety parameters has been also done to verify the viability of the system.

Burn up calculations have been then performed in order to investigate the operating cycle for the Adiabatic Lead Fast Reactor; the fuel performances have been therefore extracted and inserted in a more general analysis for an European scenario. The present nuclear reactors fleet has been modeled and its evolution simulated in order to investigate the materials fluxes to be managed in the European region. Such a futuristic scenario has been compared then with the present one to prove the advantages introduced by the adoption of new concept reactors.

As expected from theory, the proposed scenario allows for a reduction of the natural Uranium resources, extending the availability of nuclear energy from 92 to more than 18000 years. At the same time, the TransUranics – representing the long lived component of the waste – in the spent fuel can be reduced by a factor ~ 20 (because of the unavoidable losses in the spent fuel reprocessing). An even more optimistic figure can be envisaged considering the possibility of relying on the homogeneous reprocessing of the waste.

According to this, a wider scenario can be envisaged, in which electricity represents the main energy source for practical use – for instance by replacing a large portion of the actual energy consumption for transport by electric energy and increasing the nuclear penetration in electric energy production to the detriment of fossil fuels. Such a scenario, besides the high reliability of energy production, would also allow for a sensible reduction of the total greenhouse gases, as aimed by the Kyoto protocol.

Finally, since both ELSY and the ALFR represent new concept systems based upon innovative solutions, the neutronic design of a demonstrator reactor has been carried out: such a system is intended to prove the viability of technology to be implemented in the First-of-a-Kind industrial power plant, with the aim at attesting the general strategy to use, to the largest extent. It was chosen then to base the DEMO design upon a compromise between demonstration of developed technology and testing of emerging technology

in order to significantly subserve the purpose of reducing uncertainties about construction and licensing, both validating ELSY/ALFR main features and performances, and to qualify numerical codes and tools.

Despite the deep analysis conducted with the present work, all the results are intended to be preliminary. Notwithstanding the design of the Adiabatic Lead-cooled Fast Reactor has been borrowed from the ELSY one, refined thermal-hydraulics, thermal-mechanics and safety analyses are needed to assess the final layout. Moreover, the lack of data on the compatibility of structures in a lead environment require the successful demonstration of the technological viability of a Lead-cooled Fast Reactor.

According to this, also the design of DEMO must be thoroughly refined in order to verify whether it meets the stringent safety constraints required for its licensing.

Appendices

APPENDIX A
SUMMARY OF MATERIALS PROPERTIES

A quote is always nice to have.

The Quotee (1492-1493)

Introduction

The simulation of nuclear systems by means of numerical codes, such as ERANOS [7] or MCNP[17], requires the compiling of proper input files, describing the geometric configuration and material composition of the reactors. The comparison of the results obtained with different codes (needed in order to design new systems, due to the different transport equation solution models implemented in such codes) may hold if and only if it is found to fulfill equivalence criteria which guarantee the mutual consistency of the simulations, in particular to what concerns material compositions.

A.1 Fuel

One of the most important parameters to be considered for the equivalence of the two different calculations is the mass of fissile in the fuel region. Referring to Mixed Oxide (MOX) fuel for fast reactors, the isotopic vectors used for Pu and U are shown in Table A.1. The isotopic composition is the one extracted from a UO_2 spent fuel of a typical PWR (4.5% ^{235}U initial enrichment), unloaded at 45 MWd kg^{-1} burn-up and cooled down for 15 years [54].

Table A.1: Isotopic composition of actinide vectors

Plutonium		Depleted U		Americium		Curium	
Isotope	[w/o]	Isotope	[w/o]	Isotope	[w/o]	Isotope	[w/o]
^{238}Pu	2.333	^{234}U	0.003	^{241}Am	82.118	^{243}Cm	1.533
^{239}Pu	56.873	^{235}U	0.404	^{242}Am	0.000	^{244}Cm	69.763
^{240}Pu	26.997	^{236}U	0.010	^{242}Am*	0.277	^{245}Cm	26.588
^{241}Pu	6.104	^{238}U	99.583	^{243}Am	17.605	^{246}Cm	2.074
^{242}Pu	7.693					^{247}Cm	0.039
						^{248}Cm	0.003

Concerning the MAs, while the Neptunium vector contains the ^{237}Np isotope only, the Americium and Curium vectors have been obtained by mixing the MAs coming from the same spent fuel. In particular:

- 90% of the MAs is obtained from a 15 years cooled spent fuel;
- the remaining 10% is retrieved from a fuel cooled and storaged for 30 years.

The mutual abundances of MAs derive from the spectrum of irradiation of LWRs and the cooling time. Under the assumptions presented above, the

relative atomic content of the generic MAs vector can be expressed as:

$$\mathrm{Np} : \mathrm{Am} : \mathrm{Cm} = 32.4 : 55.6 : 12.0\,.$$

Besides the isotopic characterization of the components vectors, also the mutual abundances of the latter must be unequivocally defined. According to the different syntaxes for compiling the input files of the main neutronic codes, it is needed to define a relation for the conversion of volume fractions (VFs) into either atomic or weight fractions (respectively AFs and WFs), and vice versa. Taking into account the AF at first, it can be noticed that the commonly used PuO_x VF, defined as

$$\mathrm{VF} = \frac{V_{\mathrm{PuO_{x1}}}}{V_{\mathrm{PuO_{x1}}} + V_{\mathrm{UO_{x2}}}}\,, \tag{A.1}$$

can be rewritten to highlight the dependence on the AF as

$$\mathrm{VF} = \frac{1}{1 + \frac{n_{\mathrm{UO_{x2}}}}{n_{\mathrm{PuO_{x1}}}} \frac{v_{\mathrm{UO_{x2}}}}{v_{\mathrm{PuO_{x1}}}}}\,, \tag{A.2}$$

where both the molecules number $n_{\mathrm{ActO_x}}$ and the molecular volumes $v_{\mathrm{ActO_x}}$ have been introduced.

Similarly the AF can be written as

$$\mathrm{AF} = \frac{n_{\mathrm{PuO_{x1}}}}{n_{\mathrm{PuO_{x1}}} + n_{\mathrm{UO_{x2}}}} = \frac{1}{1 + \frac{n_{\mathrm{UO_{x2}}}}{n_{\mathrm{PuO_{x1}}}}}\,. \tag{A.3}$$

By retrieving the molecules numbers ratio from (A.2) and substituting into (A.3) it can be found the desired relation:

$$\mathrm{AF} = \frac{1}{1 + \frac{v_{\mathrm{PuO_{x1}}}}{v_{\mathrm{UO_{x2}}}} \frac{1-\mathrm{VF}}{\mathrm{VF}}}\,. \tag{A.4}$$

The WF can also be obtained similarly, by introducing into the latter expression the molecular masses $m_{\mathrm{ActO_x}}$:

$$\mathrm{WF} = \frac{1}{1 + \frac{m_{\mathrm{UO_{x2}}}}{m_{\mathrm{PuO_{x1}}}} \frac{v_{\mathrm{PuO_{x1}}}}{v_{\mathrm{UO_{x2}}}} \frac{1-\mathrm{VF}}{\mathrm{VF}}}\,. \tag{A.5}$$

The key parameter for the conversion of VF into either AF or WF is the molecular volume $v_{\mathrm{ActO_x}}$. It can be retrieved by approximately considering the $ActO_x$ lattice as a regular structure of cubes (see Figure A.1) with both edge and pitch $a_{\mathrm{ActO_x}}$, the s.c. *lattice parameter*.

Several evaluations of actinides dioxides lattice parameters can be found both in literature and in nuclear databases. Referring to the most recent and exhaustive paper in literature [55], the main actinide dioxides lattice parameters are (at 298 K):

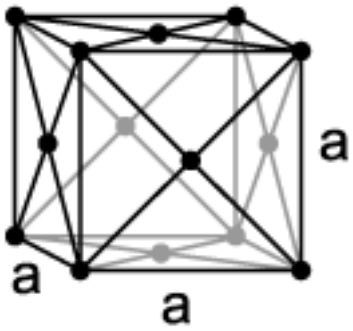

Figure A.1: Scheme of the cubic, face centered lattice of actinides dioxide.

Table A.2: Main actinide dioxides lattice parameters

Dioxide	a [Å]
UO_2	5.4704
PuO_2	5.3960

For nonstoichiometric molecules, the lattice parameter is found to be slightly modified from the reference values tabulated: in particular, different behaviors of the lattice parameter are found for different O contents (x).

For UO_x a decrease of the lattice parameter is observed for increasing x and vice versa. From experimental observations it could be possible to extrapolate the two relations [56]

$$a_0 = 5.4704 + 0.0175\,(2 - \mathrm{x}) \tag{A.6a}$$

$$a_0 = 5.4704 + 0.094\,(2 - \mathrm{x}) \tag{A.6b}$$

for $\mathrm{x} < 2$ and $\mathrm{x} > 2$ respectively. The lattice parameter is expressed in ångström [Å].

On the other side, PuO_x exibits an opposite trend, with increasing lattice parameter for increasing O content, according to the relations [57, 58] (lattice parameter expressed in ångström [Å])

$$a_0 = 6.1503 - 0.3789\,\mathrm{x} \tag{A.7a}$$

$$a_0 = 5.3643 + 0.01746\,\mathrm{x} + 0.004\,U\,(\mathrm{x} - 2.025) \tag{A.7b}$$

fitting experimental data respectively for $\mathrm{x} < 2$ and $\mathrm{x} > 2$. The function $U\,(t)$ appearing in (A.7b) is the unitary step function, defined as

$$U\,(t) = \begin{cases} 0 & t < 0 \\ 1 & t \geq 0 \end{cases}$$

The effect of the thermic dilatation on the lattice structure of actinide dioxides has been deeply investigated in literature in order to retrieve a linear expansion law for the lattice parameter as a function of temperature.
In particular, for the main actinide dioxides (UO_2 and PuO_2), the following expressions are here considered:

- UO_2 (Figure A.2):
  - Martin [59]

$$L(T) = \begin{cases} L(273)\left(9.9734\cdot10^{-01} + 9.802\cdot10^{-06}\,T - 2.705\cdot10^{-10}\,T^2 + \right. \\ \quad \left. +4.391\cdot10^{-13}\,T^3\right) & 273K \le T \le 923K\,, \\ L(273)\left(9.9672E-01 + 1.179E-05\,T - 2.429E-09\,T^2 + \right. \\ \quad \left. +1.219E-12\,T^3\right) & 923K \le T \le 3120K\,; \end{cases} \tag{A.8}$$

  - Yamashita *et al.* [55]

$$L(T) = 5.45567\cdot10^{-01} + 4.581\cdot10^{-06}\,T + 1.0355\cdot10^{-09}\,T^2 - 2.736\cdot10^{-13}\,T^3\,. \tag{A.9}$$

- PuO_2 (Figure A.3):
  - Yamashita *et al.* [55]

$$L(T) = 5.38147\cdot10^{-01} + 4.452\cdot10^{-06}\,T + 7.184\cdot10^{-10}\,T^2 - 1.995\cdot10^{-14}\,T^3\,. \tag{A.10}$$

Such relations, obtained for stoichiometric dioxides, have been found to satisfy the dilatation behavior of nonstoichiometric molecules too.
Finally, the actual fuel density must take into account the porosity resulting from the sintering process. The experience in MOX fabrication indicates that fuel pellets with $90 \div 97\%$ theoretical density can be produced.
In this work both a pure ("fresh") and a MA-doped MOX are considered. Different stoichiometric ratios have been accounted for in the present thesys. In particular, it is worth recalling the obtained UO_x and PuO_x practical densities at 20 °C, under the common hypothesis of 5% porosity, for the most common applications investigated:

x	density [g cm^{-3}]	
	UO_x	PuO_x
1.95	10.95	11.46
1.97	10.934	11.414

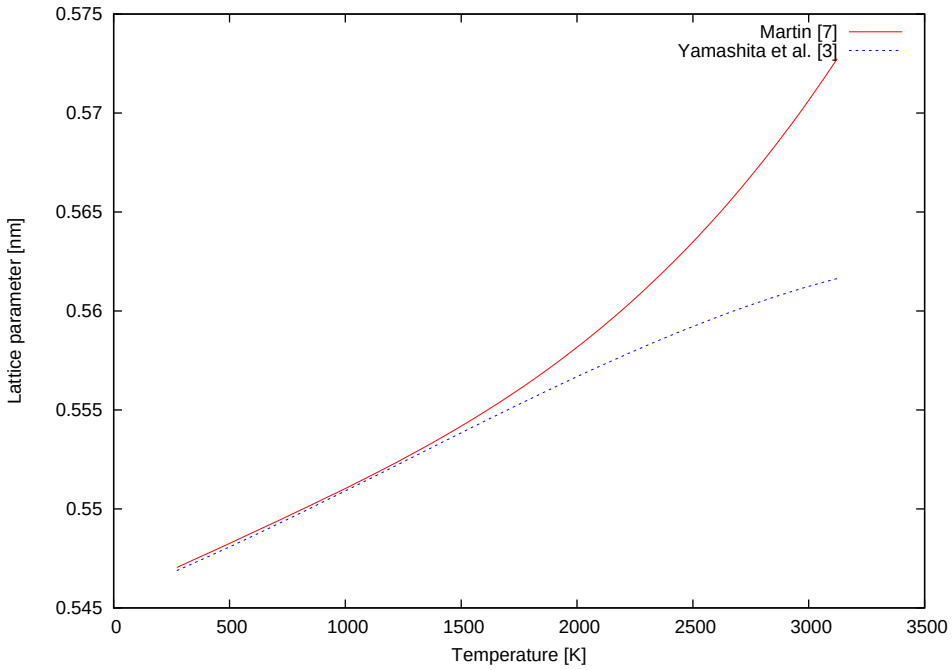

Figure A.2: Comparison of different thermal expansion laws for UO_2.

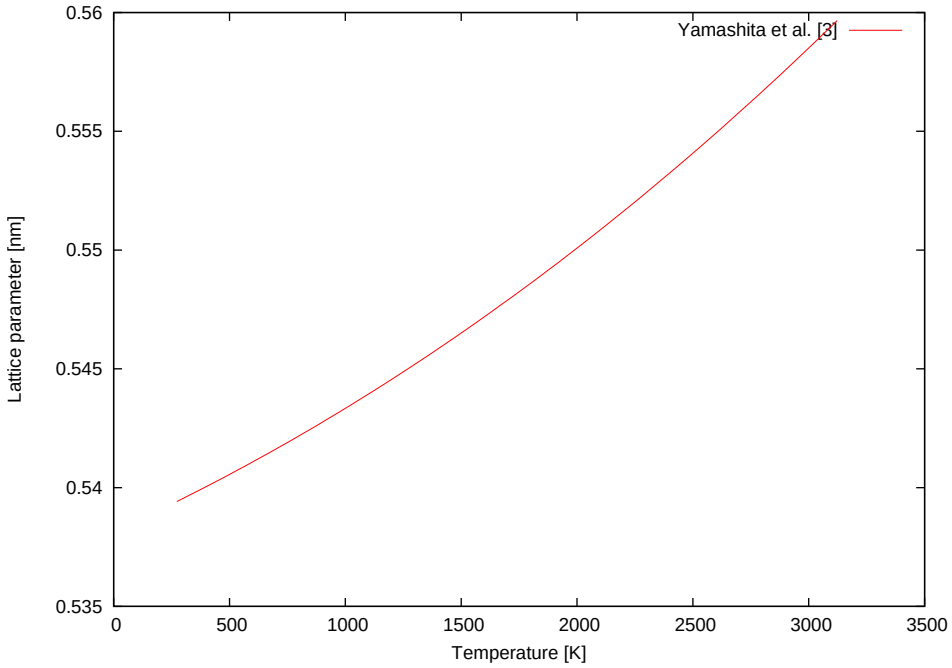

Figure A.3: Thermal expansion of PuO_2.

In general, for a MAs doped fuel, the theoretical density of the mixture can be retrieved by the following equation [16]:

$$\rho_{\text{fuel}} = 0.95 \cdot \cdot \frac{4 \cdot 10^6}{(547+30.1xN_U+(11x-3.6)N_{Np}+(11x-7.4)N_{Pu}+(11x-9.3)N_{Am}+(11x-11.2)N_{Cm})^3} \quad \text{(A.11)}$$

in which N_{Ac} is the concentration of actinide Ac in the fuel and $y = 2 - x$ is the hypostoichiometry of the mixed oxide $AcO_x = AcO_{2-y}$. The factor 4 at numerator refers to the number of molecules in the typical face-centered cubic lattice of Actinide dioxides.

A.2 Structural materials

ELSY (thus the ALFR) capitalizes on the strong synergy with other two EU projects: IP EUROTRANS [14] and VELLA (The integrated Infrastructure initiative devoted to the dissemination of knowledge in the field of Lead and Lead-alloys technology [15]). In both projects, the Ferritic-Martensitic Steel (FMS) T91 has been considered as first option for clad and near-core internals, because of its high irradiation resistance and promising ongoing R&D on technology of its protection against corrosion [16].

The remaining structural materials envisioned for ELSY are the 316LN Stainles Steel for the Reactor Vessel (RV) and the 316L SS for the remaining internals.

A.2.1 Ferritic-martensitic steel T91

The FMS T91 (whose elemental composition is reported in Table A.3) has been chosen as reference for the clad and near-core internals (that is: the inner vessel and all the structures within the latter) mainly because of its low embrittlement in a fast-neutron flux. Both ELSY and the ALFR take advantage from their relatively high minimum temperature (400 °C), since the embrittlement in fast flux is more critical at lower temperatures. At the same time, the corrosion by molten lead is minimized by the limitation of the core outlet temperature at 480 °C (so as to guarantee a maximum clad operating temperature below 550 °C to reduce the technological risk).

In the temperature range of interest the variation of the T91 FMS density with temperature is described by the linear relation [16]:

$$\rho(T) = a + bT + cT^2 = 7.799 - 0.201 \cdot 10^{-3}T - 1.102 \cdot 10^{-7}T^2 \quad \text{(A.12)}$$

This relation has been used to obtain the reference density of T91 FMS at 293.15 K: 7.731 g cm^{-3}. Indeed the FMS thermal expansion has been calculated by considering the general linear expansion law:

$$L(T) = L_0\beta = L_0(1 + \bar{\alpha}(T - T_0)) \quad \text{(A.13)}$$

Table A.3: Chemical composition of the T91 FMS

Element	Abundance [$^{w}/_{0}$]
Cr	9.0
Mo	1.0
Nb	0.1
Mn	0.6
Si	0.5
Ni	0.2
V	0.2
Fe	88.4

by integrating between the reference and working temperatures the instantaneous coefficient of linear thermal expansion described by [16]:

$$\alpha(T) = 7.3 \cdot 10^{-6} + 1.201 \cdot 10^{-8} T - 4.642 \cdot 10^{-12} T^2 \,. \tag{A.14}$$

As mentioned, the behavior of the FMS T91 is under extensive investigation in different FP6 R&D programs and further efforts are foreseen to be dedicated also in the FP7. As a matter of fact, in the temperature range of interest (*i.e.*, above 500 °C) typical corrosion protection through oxyde barrier seems to fail [60, 61, 49].

Particular attention is therefore devoted to the development of more efficient corrosion barriers. To improve the T91 resistance in a lead environment, two options are considered:

- a superficial aluminization (FeCrAlY coated);
- the GESA treatment [62].

Preliminary investigations have shown that the GESA treatment leads to a surface with a high corrosion resistance. The new developments of corrosion resistant steels and protective layers [63, 64] indicate that, in a HM environment with a bulk velocity of about 2 m s^{-1}, reaching operation periods longer than 5 years is possible. Therefore the limit imposed by the corrosion on the fuel residence time has been assumed 5 years (as a rather realistic option) and 10 years as a futuristic option.

A.2.2 316 stainless steels family

The more traditional 316 stainless steels can be envisaged for their use in ELSY internals farther from the core, since the lower neutron irradiation induced embrittlement. In particular, the two steels 316LN and 316L have been considered for the RV the remaining internals, respectively. Their chemical

composition ranges are presented in Table A.4 as provided by the ASME code: the mean values in the allowed range have been assumed as actual concentrations for the computations.

Table A.4: Chemical compositions of the 316L and 316LN SS

Element	Abundance [$^{w}/_{0}$]	
	SS316L	SS316LN
C	MAX 0.030	MAX 0.030
Mn	MAX 2.000	MAX 2.000
P	MAX 0.045	MAX 0.045
S	MAX 0.030	MAX 0.030
Si	MAX 0.750	MAX 0.750
Cr	16.0 - 18.0	16.0 - 18.0
Ni	10.0 - 14.0	10.0 - 14.0
Mo	2.0 - 3.0	2.0 - 3.0
N	MAX 0.100	0.100 - 0.160
Fe	*Complement*	

The density of both these steels are assumed equal to 8.0 g cm^{-3} at 20 °C.

A.3 Coolant

Even if reactor grade Lead coolant could contain various levels of impurity concentrations according to the degree of purification (e.g.: from 99.985% up to 99.9999% purity), in this analysis all the computations have been performed assuming pure Lead (without impurities). The isotopic composition assumed is therefore the natural one, shown in Table A.5.

Table A.5: Isotopic compositions of pure Lead

Isotope	Abundance [$^{a}/_{0}$]
^{204}Pb	1.42
^{206}Pb	24.1
^{207}Pb	22.1
^{208}Pb	52.38

In the temperature range of interest (600 to 1800 K) the molten Lead density (at normal pressure) is described by the linear relation [16]

$$\rho(T) = 11.367 - 1.1944 \cdot 10^{-3} T \tag{A.15}$$

which leads to a density of 11.017 g cm^{-3} at 20 °C.

APPENDIX B

THE "ADIABATIC CONCENTRATOR" CODE

A quote is always nice to have.

The Quotee (1492-1493)

Introduction

In order to solve the equilibrium composition of the fuel, given the neutron spectrum (that is: the effective one-group fission, capture, (n,2n) and inelastic microscopic cross-sections) and the average power density in the fuel (function of the maximum linear rating allowed for clad integrity, see Chapter 11), a small FORTRAN 90 code has been set up and benchmarked by means of the FISPACT irradiation code [65].

The code is able to compute the equilibrium fuel vector in case of either static or extended nuclear equilibrium, with user defined refueling and irradiation periods.

The "Adiabatic Concentrator" code is made of to a main program and several subroutines organized according to the main task they are devoted to. The whole structure of the code is presented and discussed in detail in the following sections.

B.1 "Adiabatic Concentrator" code lists

The FORTRAN main program organizes the logical flow path for the entire code, starting from the input of the main parameters for the execution by command line to the plot of the results in text (ASCII) files.

At first, the user is asked to provide three input files, containing respectively the one-group microscopic cross-sections (together with eventual branching ratios for different transmutation channels), the radioactive decay constants (together with the branching ratios for the different decay channels) and the isotopic fractions for the feed vector. Starting from this elementary data, the main global variables are initialized. Examples of the three input files are shown below.

Sample cross-section file.

	capture	fission	nxn	inelastic	branch
U234	5.4178E-01	2.9495E-01	0.0000E+00	0.0000E+00	1.0000E+00
U235	5.3728E-01	1.8791E+00	0.0000E+00	7.4512E-01	1.0000E+00
U235m	0.0000E+00	0.0000E+00	0.0000E+00	0.0000E+00	1.0000E+00
U236	4.0769E-01	8.6783E-02	5.3138E-04	0.0000E+00	1.0000E+00
U237	5.5533E-01	9.3454E-01	0.0000E+00	0.0000E+00	1.0000E+00
U238	2.8221E-01	3.4603E-02	1.0449E-03	0.0000E+00	1.0000E+00
U239	1.0000E-10	1.0000E-10	1.0000E-10	0.0000E+00	1.0000E+00
Np237	1.5374E+00	3.1409E-01	0.0000E+00	0.0000E+00	1.0000E+00
Np238	1.7130E-01	3.5127E+00	0.0000E+00	0.0000E+00	1.0000E+00
Np239	1.9159E+00	4.3768E-01	0.0000E+00	0.0000E+00	1.0000E+00
Pu238	5.2625E-01	1.2039E+00	0.0000E+00	0.0000E+00	1.0000E+00
Pu239	4.8672E-01	1.7525E+00	0.0000E+00	0.0000E+00	1.0000E+00
Pu240	4.7690E-01	3.5662E-01	0.0000E+00	0.0000E+00	1.0000E+00
Pu241	4.7463E-01	2.5050E+00	0.0000E+00	0.0000E+00	1.0000E+00

Pu242	4.9278E-01	2.4989E-01	0.0000E+00	0.0000E+00	1.0000E+00
Pu243	3.8094E-01	8.1821E-01	0.0000E+00	0.0000E+00	1.0000E+00
Am241	1.9449E+00	2.4218E-01	0.0000E+00	0.0000E+00	9.1624E-01
Am242	4.2031E-01	3.0885E+00	0.0000E+00	3.4061E-01	1.0000E+00
Am242m	4.8404E-01	3.0724E+00	0.0000E+00	4.9213E-01	1.0000E+00
Am243	1.4906E+00	1.7442E-01	0.0000E+00	0.0000E+00	6.5460E-02
Am244	8.1738E-01	3.1596E+00	0.0000E+00	0.0000E+00	1.0000E+00
Am244m	7.5291E-01	3.1593E+00	0.0000E+00	0.0000E+00	1.0000E+00
Cm242	4.6527E-01	6.0821E-01	0.0000E+00	0.0000E+00	1.0000E+00
Cm243	2.9007E-01	3.2338E+00	0.0000E+00	0.0000E+00	1.0000E+00
Cm244	8.4514E-01	3.9610E-01	0.0000E+00	0.0000E+00	1.0000E+00
Cm245	5.2332E-01	2.7026E+00	0.0000E+00	0.0000E+00	1.0000E+00
Cm246	5.0919E-01	2.5931E-01	0.0000E+00	0.0000E+00	1.0000E+00
Cm247	4.8008E-01	2.2579E+00	0.0000E+00	0.0000E+00	1.0000E+00
Cm248	2.7529E-01	2.6672E-01	0.0000E+00	0.0000E+00	1.0000E+00

Sample decay file.

	lambda	alg	alm	bm	bp	ga
U234	8.952975E-14	1.000E+0	0.000E+0	0.000000E+0	0.000E+0	0.000E+0
U235	3.122983E-17	1.000E+0	0.000E+0	0.000000E+0	0.000E+0	0.000E+0
U235m	4.620981E-04	0.000E+0	0.000E+0	0.000000E+0	0.000E+0	1.000E+0
U236	9.386954E-16	1.000E+0	0.000E+0	0.000000E+0	0.000E+0	0.000E+0
U237	1.188524E-06	0.000E+0	0.000E+0	1.000000E+0	0.000E+0	0.000E+0
U238	4.919327E-18	1.000E+0	0.000E+0	0.000000E+0	0.000E+0	0.000E+0
U239	4.926419E-04	0.000E+0	0.000E+0	1.000000E+0	0.000E+0	0.000E+0
Np237	1.024879E-14	1.000E+0	0.000E+0	0.000000E+0	0.000E+0	0.000E+0
Np238	3.789578E-06	0.000E+0	0.000E+0	1.000000E+0	0.000E+0	0.000E+0
Np239	3.404429E-06	0.000E+0	0.000E+0	1.000000E+0	0.000E+0	0.000E+0
Pu238	2.506220E-10	1.000E+0	0.000E+0	0.000000E+0	0.000E+0	0.000E+0
Pu239	9.116364E-13	6.000E-4	9.994E-1	0.000000E+0	0.000E+0	0.000E+0
Pu240	3.348500E-12	1.000E+0	0.000E+0	0.000000E+0	0.000E+0	0.000E+0
Pu241	1.541992E-09	2.450E-5	0.000E+0	9.999755E-1	0.000E+0	0.000E+0
Pu242	5.887906E-14	1.000E+0	0.000E+0	0.000000E+0	0.000E+0	0.000E+0
Pu243	3.885006E-05	0.000E+0	0.000E+0	1.000000E+0	0.000E+0	0.000E+0
Am241	5.085505E-11	1.000E+0	0.000E+0	0.000000E+0	0.000E+0	0.000E+0
Am242	1.201878E-05	0.000E+0	0.000E+0	8.270000E-1	1.730E-1	0.000E+0
Am242m	1.558834E-10	4.600E-3	0.000E+0	0.000000E+0	0.000E+0	9.954E-1
Am243	2.982300E-12	1.000E+0	0.000E+0	0.000000E+0	0.000E+0	0.000E+0
Am244	1.906345E-05	0.000E+0	0.000E+0	1.000000E+0	0.000E+0	0.000E+0
Am244m	4.443251E-04	0.000E+0	0.000E+0	9.995500E-1	4.500E-4	0.000E+0
Cm242	4.928151E-08	1.000E+0	0.000E+0	0.000000E+0	0.000E+0	0.000E+0
Cm243	7.553111E-10	9.976E-1	0.000E+0	0.000000E+0	2.400E-3	0.000E+0
Cm244	1.214340E-09	1.000E+0	0.000E+0	0.000000E+0	0.000E+0	0.000E+0
Cm245	2.585830E-12	1.000E+0	0.000E+0	0.000000E+0	0.000E+0	0.000E+0
Cm246	4.617553E-12	9.997E-1	0.000E+0	0.000000E+0	0.000E+0	0.000E+0
Cm247	1.408946E-15	1.000E+0	0.000E+0	0.000000E+0	0.000E+0	0.000E+0
Cm248	6.315963E-14	9.174E-1	0.000E+0	0.000000E+0	0.000E+0	0.000E+0

Sample feed file.

```
          abundance
U234        0.00003
U235        0.00404
U236        0.00010
U238        0.99583
```

The user is then asked to provide the name for the output file, together with the average power density `dPowerDensity` in the fuel (in MW cm^{-3}), the stoichiometric ratio `dStoichiometry` for the fuel oxides together with the porosity `dPorosity` of the pellet, and the total cycle length. According to the input value, the user is also allowed to choose between the static and the extended equilibrium solver: by setting a total cycle length equal to `0`, the static equilibrium will be solved; on the other hand, any other value will be set as irradiation time, and the user asked to provide also a total aging time and the simulation time step `dDeltat`.

The solver for the static equilibrium approaches the matrix problem formulated in subsection 10.3.1 iteratively [66]. The problem has been decomposed into two nested iteration loops: the outer iterations account for the convergence of the integral flux in the fuel, while the inner ones for the solution of the equilibrium vector.

Starting from a attempt flux `dFlux` and iterating until convergence has been reached, the equilibrium matrix problem is updated (according to the new flux estimate) and solved by a traditional Successive Over-Relaxation method [67]. Starting from the new concentrations vector `dConc` and the actinides abundances in the latter (`dU`, `dPu`, `dAm`, `dNp` and `dCm`), the actual density of the fuel is recomputed as described by equation (A.11), and the of the flux value updated for normalization of the fission rate density to the total thermal power density.

```
      dDensity=dPorosity*4.D0/(1.0D-6*((5.47D2-3.6D0*dNp-7.4D0*dPu-
     &  9.3D0*dAm-1.12D1*dCm-(dStoichiometry-2.D0)*(3.01D1*dU+
     &  1.1D1*(dAm+dCm+dNp+dPu)))**3))

      dFlux=dPowerDensity*SUM(dConc(:))/(SUM(tActinides(:)%xsec%
     &  fission*dConc(:))*dDensity*3.20435306D-17)
```

For the solution of the extended equilibrium vector, the irradiation and decay periods are preliminary segmented into `iTt` and `iTd` steps respectively. The time dependence of the matrix problem formulated in subsection 10.3.2 requires also the definition of the time integration parameter ϑ. In the present model it has been set `dTheta` $= 0.5$.

The decay matrix is created at first, and then converted into the corresponding decay operator $\underline{A}_D$ of equation 10.11. Since the decay phase is independent on the flux, it is possible to compute the recursive decay oper-

ator $\underline{A}_D^{t_D}$ describing the complete evolution during the ex-core aging before the iterative solution phase.

The irradiation evolution must be computed iteratively, since - as in the steady state problem - the irradiation matrix (thus the irradiation operator $\underline{A}_O$) depends on the flux, which is a function of the actual fissile concentration in the fuel. On the other hand, the analytic formulation of the matrix problem 10.13 allows to obtain the aimed equilibrium fuel vector by inversion of the compound matrix including both the decay and irradiation operators. A single order of iterations is therefore envisaged, to update the flux and recompute the irradiation operator for every equilibrium vector estimate.

B.1.1 The "Nuclear" module

The main variables for use in the "Adiabatic Concentrator" code are defined in the "Nuclear" module. In particular, exploiting the FORTRAN `TYPE` syntax, three new variable types have been defined:

- a "CROSSSECTION" type collecting, as `DOUBLE PRECISION` FORTRAN variables, all the one-group microscopic cross-sections for each nuclide;

```
TYPE CROSSECTION
  DOUBLE PRECISION :: fission    ! Fission X-Sections [barn]
  DOUBLE PRECISION :: capture    ! Capture X-Sections [barn]
  DOUBLE PRECISION :: elastic    ! Elastic X-Sections [barn]
  DOUBLE PRECISION :: inelastic  ! Inelastic X-Sections [barn]
  DOUBLE PRECISION :: nxn        ! (n,xn) X-Sections [barn]
  DOUBLE PRECISION :: total      ! Total X-Sections [barn]
END TYPE CROSSECTION
```

- a "RADDECAY" type including, as `DOUBLE PRECISION` FORTRAN variables, the decay constant and the vector of branches for every decay channel;

```
TYPE RADDECAY
  DOUBLE PRECISION :: lambda     ! Decay constant [s-1]
  DOUBLE PRECISION :: branch(7)  ! Fraction of Decays/Channel
END TYPE RADDECAY
```

- a "NUCLIDE" type, which defines all the properties for each isotope in the simulation, such as the chemical symbol, both atom and mass numbers, a flag discriminating a metastable state and its transmutation affinity (both collisional-induced and natural by decay) inheriting the previous types;

```
TYPE NUCLIDE
  CHARACTER(LEN=2) :: Nn         ! Symbol
  INTEGER          :: Z          ! Atom Number
  INTEGER          :: A          ! Mass Number
  LOGICAL          :: m          ! Metastable State
  TYPE(CROSSECTION):: xsec       ! Cross Sections Type
```

```
    DOUBLE PRECISION :: branch     ! Captures-to-Ground Fraction
    TYPE(RADDECAY)   :: decay      ! Radioactive Decay Type
  END TYPE NUCLIDE
```

The body of the module includes some elementary functions that allow the code to perform elementary operations on the "NUCLIDE" types, such as initialize, for each "NUCLIDE", the microscopic cross-sections in the corresponding "CROSSSECTION" field; or parse any string of the type `SyAAAm` in order to retrieve the corresponding isotope elementary information such as the chemical symbol, the mass number and the toggle metastable.

B.1.2 The "Chemical" module

The properties database for all the known nuclides is collected in the "Chemical" module. The database is organized through the definition of an "ISOTOPE" FORTRAN variable `TYPE`, which includes, besides the chemical symbol and both the corresponding atom and mass numbers, the main properties of each isotope, such as the molar mass, its natural abundance and decay time.

```
TYPE ISOTOPE
  CHARACTER(LEN=2):: cSymbol
  INTEGER:: iZ
  INTEGER:: iA
  DOUBLE PRECISION:: dMolarMass
  DOUBLE PRECISION:: dNaturalAbundance
  DOUBLE PRECISION:: dDecayTime
END TYPE ISOTOPE
```

An "ISOTOPE" type vector, `MChe_tIsotopesLibrary`, is then defined and initialized for the 1061 isotopes of the nuclide chart. This huge work has been done to let every FORTRAN code including the "Chemical" module to embed all the main isotopic information through a browsable and easy interface.

Some standardized "query" functions have been also added as member functions and subroutines of the "Chemical" module, providing a pre-defined interface to retrieve, as a function of the isotope "zaid"[1]:

- its decay constant;

```
!!!!!!!!!!!!!!!!!!!!!!!!!!!!!!!!!!!!!!!!!!!!!!!!!!!!!!!!!!!!!!!!!!!!!!!
! MChe_Zzaid2DecayTime                                                  !
!    This function extracts the half life (in seconds) of an isotope !
!    isotope from the database array of ISOTOPE types,                 !
```

[1] The term "zaid", borrowed from the MCNP language [68], is a number uniquely identifying an isotope. It is obtained by summing the atom number Z multiplied by 1000 to the mass number A of the isotope:

$$\texttt{zaid} = 1000 \cdot Z + A\,.$$

```
!    starting from the zaid number of the nuclide.          !
!!!!!!!!!!!!!!!!!!!!!!!!!!!!!!!!!!!!!!!!!!!!!!!!!!!!!!!!!!!!!!!!
  FUNCTION MChe_Zzaid2DecayTime(zzaid)
```

- its natural abundance;

```
!!!!!!!!!!!!!!!!!!!!!!!!!!!!!!!!!!!!!!!!!!!!!!!!!!!!!!!!!!!!!!!!
! MChe_Zzaid2Abundance                                          !
!    This function extracts the natural abundance of an       !
!    isotope in the respective element composition from the   !
!    database array of ISOTOPE types, starting from the zaid  !
!    number of the nuclide.                                   !
!!!!!!!!!!!!!!!!!!!!!!!!!!!!!!!!!!!!!!!!!!!!!!!!!!!!!!!!!!!!!!!!
  FUNCTION MChe_Zzaid2Abundance(zzaid)
```

- its mass;

```
!!!!!!!!!!!!!!!!!!!!!!!!!!!!!!!!!!!!!!!!!!!!!!!!!!!!!!!!!!!!!!!!
! MChe_Zzaid2Mass                                               !
!    This function extracts the mass (in amu) of an isotope   !
!    from the database array of ISOTOPE types, starting from  !
!    the zaid number of the nuclide.                          !
!!!!!!!!!!!!!!!!!!!!!!!!!!!!!!!!!!!!!!!!!!!!!!!!!!!!!!!!!!!!!!!!
  FUNCTION MChe_Zzaid2Mass(zzaid)
```

APPENDIX C

NEUTRON FLUX ENHANCEMENT STRATEGIES

The concrete is a combination of abstractions.

Leon Trotsky (1879-1940)

Introduction

The deep analysis on the dependencies occurring among core parameters, presented in Chapter 11, can be used also to redefine a core configuration in order to improve some objectives towards target values. As an example, the FAst Spectrum Transmutation Experimental Facility (FASTEF) [69] core has been taken into account: this experimental facility aims at representing the European facility for neutron irradiation in the hard spectrum of LFRs (see section 7.1.1), being also candidated as design concept for the XT-ADS (the short-term demonstrator of transmutation and ADS behaviour in the EURATOM FP6 [14]). In this case, an optimization process for the core is needed in order to obtain a high neutron flux, so to optimize the time for irradiation by reducing the in-pile residence time of specimens to get the desired fluence.

The results of this work, presented to the Central Design Team (CDT) [70] in charge of the development of FASTEF, have been assumed as starting point for the design of the final FASTEF core configuration [71].

C.1 Flux heighten strategies

Conceptually, an increase of the flux in an optimized configuration, with respect to a reference case, can be pursued either by increasing the power density in the fuel with fixed enrichment, or by reducing the fuel enrichment at fixed power density.

In order to develop an effective strategy to heighten the flux, all the actual technological constraints must be well defined to exploit every margin for maximizing the flux increase.

At least three elementary strategies can be identified in approaching the flux heighten task. They will be presented and discussed in the following subsections.

C.1.1 Via linear power increase

The first and easier approach is based on a direct action on the flux so as to increase the linear power in the fuel pin. This so rough as effective approach implies directly, on the other hand, the need to modify the cooling of the pins in order to keep the maximum temperature on the clad in the hot pin. A new enthalpy balance in the channel must be therefore coped with, taking also into account the need to compensate for the higher temperature required by the clad to evacuate the higher linear power from the pin.

Two possible counteractions can be pursued, each one introducing some drawbacks to the method:

1. an increase of the coolant velocity, but to the detriment of the pressure

drop through the core and the erosion resistance of the structures;

2. an increase of the flow area, which implies a higher coolant volumetric fraction in the cell, resulting both in a reactivity loss (which in turn can be compensated by increasing the fuel enrichment, partially reducing the benefits on the flux) and a reduction of the fast fraction of the spectrum (because of the higher moderation in the cell).

Whether it is possible to increase the power, it could worth compensating the reactivity loss due to fuel dilution in the elementary cell, by increasing the number of fuel pins in the system not to loose the gain on the flux.

C.1.2 Via fuel pin diameter reduction

Another possible strategy can be pursued by reducing the pin (pellet) diameter, proportionally reducing also the linear rating to preserve the thermal condition on the cladding. This "counterintuitive" approach relies on the fact that a reduction of the pin diameter by some $x\%$ implies a reduction of the fuel cross-section by $\sim 2x\%$ (or even more in case of hollowed pellets). According to this, the power density in the fuel is increased (at least) by some $x\%$ despite the reduction of the linear rating: hence the flux level must be increased (as desired) in the whole system to achieve the higher power density in the smaller pin.

The immediate drawback resulting from this approach is related to the loss of reactivity due to the smaller amount of fuel in the core. This requires either

- an increase of the fuel enrichment (which in turn depresses the flux), or
- a larger core (balancing the reduction of the total core power due to the lower linear rating in the pins).

C.1.3 Via active height reduction

The last possible approach for flux increase can be pursued by reducing the active height. As a matter of facts, this allows an equivalent reduction of the coolant flow area to keep the same thermal condition of the cladding while increasing the power density in the cell (but not in the fuel!).

In order to preserve criticality as well as the overall core power, the missing fuel must be rearranged by radially enlarging the core. On one hand the reactivity of the system is (in general) reduced because of the flat shape of FRs cores; on the other hand the more compact elementary cell (because of the reduction of its cross-section) gains reactivity (since the fuel volumetric fraction is increased): the combination of these effects results in a more reactive core, allowing an overall enrichment reduction, which in turn requires an increase of the flux to preserve the power.

C.2 The FAst Spectrum Transmutation Experimental Facility case study

In order to increase the neutron flux in the FASTEF core, starting from the preliminary XT-ADS [14] configuration [72], a huge amount of parametric calculations has been done by SCK-CEN [71] varying many core parameters (e.g.: p/d: $1.3 \div 1.5$; size: $56 \div 72$ FAs; power: $57 \div 80$ MWth; h: $40 \div 80$ cm, etc.) in different combinations of the latter.

The results of this enormous investigative analysis led to the conclusion that the most suitable core would have been the reference one, with power (thus the flux) re-normalized so that the fast component of the flux ends up to $1 \cdot 10^{15}$ cm^{-2} s^{-1} (s.c. "XT-ADS-HF" configuration). The power increase has been consequently compensated - in order to keep the cladding temperature below the technological limit - by reducing the inlet coolant temperature, thus allowing the higher power to be evacuated preserving the maximum temperatures in the channel.

Basically the HF variant, even if assuming the same geometry (pin, pitch, FA, core) of the reference XT-ADS configuration, differs from the latter because the power has been increased from 57 to 85 MWth (linear rating and power densities follow proportionally) and, because of the enthalpy balance in the channel:

- $\Delta T_{\text{out}-\text{in}}$ has been changed from 100 °C to 120 °C;
- T_{outlet} from 400 °C to 390 °C (because of T_{clad});
- T_{inlet} from 300 °C to 270 °C (accordingly);
- v_{coolant} from 1.39 to 1.72 m s^{-1} (2.50 m s^{-1} around spacers), and
- Δp_{core} from 707 to 1066 mbar.

Aiming at applying the presented flux heighten strategies to FASTEF, as starting point, Table C.1 resumes the main technological constraints assumed for the project in general, together with the present values (in the XT-ADS-HF configuration) for comparison, in order to point out the margins left for core optimization.

The following subsections resume few configurations modified according to the three flux heighten strategies proposed above: for each configuration, the conceptualization process will be justified step by step and the main evaluations briefly discussed. It must be noticed that the changes applied to the core parameters have been chosen to stress the effectiveness of the proposed strategies: the proposed configurations must be therefore considered as academic exercises rather than actually optimized solutions. In the same way, the new values for the core parameters have been evaluated by "paper and pencil", thus must not be considered as final but as some rough (even if reliable) estimate.

Table C.1: Technological constraints for FASTEF and present values for the XT-ADS-HF configuration

Parameter	Limit	Present value (XT-ADS-HF)
Power	100 MW	85 MW
Enrichment (Pu)	35%	33.5%
Linear power rating	400 W cm^{-1}	372 W cm^{-1}
T_{clad}	500 °C	496 °C
T_{inlet}	270 °C	270 °C
T_{outlet}	400 °C	390 °C
Velocity (bulk)	2 m s^{-1}	1.72 m s^{-1}
Velocity (spacer)	2.5 m s^{-1}	2.5 m s^{-1}
Core pressure drop	0.1 Mpa[1]	0.11 Mpa

C.2.1 Increased linear power configurations

Four configurations characterized by a higher linear power (thus defined the "HFC-P" series) are here presented.

As a first attempt, a modified configuration has been envisaged by increasing the core power by some 17% (from 85 to 100 MWth). In this case, it was chosen to compensate for the higher linear rating only by dilating the coolant channel, the coolant flow velocity being the same as reference.

The reactivity reduction due to the fuel dilution in the elementary cell (because of the larger coolant volume fraction) has been compensated by a proper increase of the fuel enrichment, to a partial detriment of the flux gain.

Table C.2: HFC-P1 main core parameters

Parameter	XT-ADS-HF	HFC-P1
P_{th} [MW]	85	100
Enrichment [%]	33.3	35
r_{fuel} [mm]	2.70	same
r_{hollow} [mm]	0.80	same
r_{clad} [mm]	3.275	same
p [mm]	9.17	9.83
p/d	1.40	1.50
h_{fuel} [mm]	600	same
R_{core} [mm]	875	935
$\phi > 0.75$ MeV [cm^{-2} s -1]	$1.0 \cdot 10^{15}$	$1.12 \cdot 10^{15}$
T_{outlet} - T_{inlet} [°C]	120	107
v_{coolant} (rod) [m s^{-1}]	1.72	same
v_{coolant} (spacers) [m s^{-1}]	2.50	< 2.50
T_{clad} [°C]	496	500
max$\{q'\}$ [W cm^{-1}]	372	440
Δp [mbar] / natural circulation	1066 / ref	750 / better

A possible variant of the HFC-P1 configuration can be attained by letting a moderate increase of the coolant volume fraction by means of an increase of the coolant flow velocity. According to this, the drawback related to the cell reactivity reduction, envisaged in the previous configuration, can be partially mitigated, taking advantage for the flux of the lower enrichment needed for criticality.

It is clear that the pressure drop in this configuration results increased (because of the velocity); on the other hand, the natural circulation ought be enough (as reference) in accidental condition since the still larger coolant flow area.

Two configurations have been further examined, following the same logical approach of the previous ones, but assuming a partial increase of the power (from reference 85 to 93 MWth). It is clear that the same pros and cons are found, but both reduced because of the lower peak linear power.

C.2.2 Reduced pin diameter configurations

According to the fuel pin diameter reduction strategy, three configurations (thus belonging to the "HFC-D" series) have been considered.

In the first configuration, the pin pitch has been reduced according to the reduction of the power. Despite the corresponding reduction of the coolant channel, according to this approach the subchannel looses reactivity (because of the reduction of the fuel volume fraction), which has been compensated only by an increased enrichment, to the detriment of the flux.

Table C.3: HFC-P2 main core parameters

Parameter	XT-ADS-HF	HFC-P2
P_{th} [MW]	85	100
Enrichment [%]	33.3	34
r_{fuel} [mm]	2.70	same
r_{hollow} [mm]	0.80	same
r_{clad} [mm]	3.275	same
p [mm]	9.17	9.50
p/d	1.40	1.45
h_{fuel} [mm]	600	same
R_{core} [mm]	875	900
$\phi > 0.75$ MeV [cm^{-2} s -1]	$1.0 \cdot 10^{15}$	$1.15 \cdot 10^{15}$
T_{outlet} - T_{inlet} [°C]	120	107
v_{coolant} (rod) [m s^{-1}]	1.72	2.00
v_{coolant} (spacer) [m s^{-1}]	2.50	$\sim$ 2.60
T_{clad} [°C]	496	500
max$\{q'\}$ [W cm^{-1}]	372	440
Δp [mbar] / natural circulation	1066 / ref	1200 / ok

Table C.4: HFC-P3 and HFC-P4 main core parameters

Parameter	XT-ADS-HF	HFC-P3	HFC-P4
P_{th} [MW]	85	93	93
Enrichment [%]	33.3	35	34
r_{fuel} [mm]	2.70	same	same
r_{hollow} [mm]	0.80	same	same
r_{clad} [mm]	3.275	same	same
p [mm]	9.17	9.56	9.37
p/d	1.40	1.46	1.43
h_{fuel} [mm]	600	same	same
R_{core} [mm]	875	910	900
$\phi > 0.75$ MeV [cm^{-2} s -1]	$1.0 \cdot 10^{15}$	$1.04 \cdot 10^{15}$	$1.08 \cdot 10^{15}$
T_{outlet} - T_{inlet} [°C]	120	112	112
v_{coolant} (rod) [m s^{-1}]	1.72	same	1.80
v_{coolant} (spacers) [m s^{-1}]	2.50	$<$2.50	$\sim$ 2.50
T_{clad} [°C]	496	500	500
max$\{q'\}$ [W cm^{-1}]	372	410	410
Δp [mbar] / natural circulation	1066 / ref	900 / better	1090 / ok

The second configuration implements a different compensation approach for the reactivity, by a new dimension of the core: more fissile is arranged indeed around the core to re-establish criticality.

The last configuration has been obtained by placing the T_{outlet} at 397 °C by reducing the pin lattice pitch (the higher T_{outlet} being permitted by the

Table C.5: HFC-D1 main core parameters

Parameter	XT-ADS-HF	HFC-D1
P_{th} [MW]	85	90
Enrichment [%]	33.3	35.4
r_{fuel} [mm]	2.70	2.43
r_{hollow} [mm]	0.80	same
r_{clad} [mm]	3.275	2.95
p [mm]	9.17	8.53
p/d	1.40	1.45
h_{fuel} [mm]	600	same
R_{core} [mm]	875	875
$\phi > 0.75$ MeV [cm^{-2} s -1]	$1.0 \cdot 10^{15}$	$1.10 \cdot 10^{15}$
T_{outlet} - T_{inlet} [°C]	120	same
v_{coolant} (rod) [m s^{-1}]	1.72	same
v_{coolant} (spacers) [m s^{-1}]	2.50	> 2.50
T_{clad} [°C]	496	488
max$\{q'\}$ [W cm^{-1}]	372	335
Δp [mbar] / natural circulation	1066 / ref	same / worse

Table C.6: HFC-D2 main core parameters

Parameter	XT-ADS-HF	HFC-D2
P_{th} [MW]	85	95
Enrichment [%]	33.3	same
r_{fuel} [mm]	2.70	2.43
r_{hollow} [mm]	0.80	same
r_{clad} [mm]	3.275	2.95
p [mm]	9.17	8.53
p/d	1.40	1.45
h_{fuel} [mm]	600	same
R_{core} [mm]	875	960
$\phi > 0.75$ MeV [cm^{-2} s -1]	$1.0 \cdot 10^{15}$	$1.16 \cdot 10^{15}$
T_{outlet} - T_{inlet} [°C]	120	same
v_{coolant} (rod) [m s^{-1}]	1.72	same
v_{coolant} (spacers) [m s^{-1}]	2.50	> 2.50
T_{clad} [°C]	496	488
max$\{q'\}$ [W cm^{-1}]	372	335
Δp [mbar] / natural circulation	1066 / ref	same / better

reduction of the linear rating).

The reduction of the pitch implies a higher pressure drop through the core, as well as worse conditions for natural circulation to set up.

Table C.7: HFC-D3 main core parameters

Parameter	XT-ADS-HF	HFC-D3
P_{th} [MW]	85	92
Enrichment [%]	33.3	same
r_{fuel} [mm]	2.70	2.43
r_{hollow} [mm]	0.80	same
r_{clad} [mm]	3.275	2.95
p [mm]	9.17	8.34
p/d	1.40	1.41
h_{fuel} [mm]	600	same
R_{core} [mm]	875	980
$\phi > 0.75$ MeV [cm^{-2} s -1]	$1.0 \cdot 10^{15}$	$1.16 \cdot 10^{15}$
T_{outlet} - T_{inlet} [°C]	120	127
v_{coolant} (rod) [m s^{-1}]	1.72	same
v_{coolant} (spacers) [m s^{-1}]	2.50	> 2.50
T_{clad} [°C]	496	500
max$\{q'\}$ [W cm^{-1}]	372	335
Δp [mbar] / natural circulation	1066 / ref	1130 / worse

C.2.3 Reduced active height configuration

Only one configuration has been considered according to the reduced active height strategy.

The pin pitch has been reduced according to the reduction of the active height: in this way the subchannel gains more reactivity (because the fuel volume fraction is increased) with respect to the geometrical reactivity loss (because the leakage is increased).

The net reactivity gain allowed for a decrease of the fuel enrichment, further increasing the neutron flux.

C.2.4 Combined strategies configurations

None of the elementary configurations proposed in the previous subsections showed dramatic benefit on the flux, even if not negligible (16%). Moreover, many scenarios respect the constraints and boundaries conditions, while some other slightly overcome them.

Summarizing, every approach exploits a subset of parameters, enhancing the neutronics performances to the detriment of some other (mainly thermal-hydraulic) parameter. Table C.9 resumes the main pros and cons of the proposed approaches.

From the summary table it can be seen that the adjustments applied to every configuration (to compensate the changes aimed at increasing the flux) often act in opposite directions on some parameters.

It can be therefore supposed to simultaneously apply the different ap-

Table C.8: HFG-H1 main core parameters

Parameter	XT-ADS-HF	HFG-H1
P_{th} [MW]	85	same
Enrichment [%]	33.3	31.7
r_{fuel} [mm]	2.70	same
r_{hollow} [mm]	0.80	same
r_{clad} [mm]	3.275	same
p [mm]	9.17	8.75
p/d	1.40	1.34
h_{fuel} [mm]	600	500
R_{core} [mm]	875	918
$\phi > 0.75$ MeV [cm^{-2} s -1]	$1.0 \cdot 10^{15}$	$1.07 \cdot 10^{15}$
T_{outlet} - T_{inlet} [°C]	120	same
v_{coolant} (rod) [m s^{-1}]	1.72	same
v_{coolant} (spacers) [m s^{-1}]	2.50	> 2.50
T_{clad} [°C]	496	same
max$\{q'\}$ [W cm^{-1}]	372	same
Δp [mbar] / natural circulation	1066 / ref	same / $\sim$ same

Table C.9: Pros and cons of the proposed flux heighten strategies

	HFC-P	HFC-D	HFG-H
PROS	Natural circulation	High φ	Low enrichment
CONS	v_{coolant}	High enrichment or large core or natural circulation	Natural circulation

proaches to combine the improvements and, at the same time, to compensate the drawbacks.

As first attempt, the most promising HFC-P configuration has been combined with the most effective HFC-D one. Only a partial increase of the core diameter has been applied because of the constraint on the core power.

According then to the summary pros/cons table:

- the pressure drop results increased (because of the velocity);
- while the natural circulation ought be enough (as reference);
- the enrichment is just partially increased (remaining on diameter).

In the second attempt, the HFC-D and HFG-H configurations have been taken into account. The dilution of the fuel in the cell because of pin reduction is compensated with a further reduction of the coolant channel, possible because of the reduced active height.

Table C.10: HFG-P4D2 main core parameters

Parameter	XT-ADS-HF	HFG-P4D2
P_{th} [MW]	85	104
Enrichment [%]	33.3	35
r_{fuel} [mm]	2.70	2.48
r_{hollow} [mm]	0.80	same
r_{clad} [mm]	3.275	3.00
p [mm]	9.17	8.83
p/d	1.40	1.47
h_{fuel} [mm]	600	same
R_{core} [mm]	875	1008
$\phi > 0.75$ MeV [cm^{-2} s -1]	$1.0 \cdot 10^{15}$	$1.17 \cdot 10^{15}$
T_{outlet} - T_{inlet} [°C]	120	114
v_{coolant} (rod) [m s^{-1}]	1.72	1.82
v_{coolant} (spacers) [m s^{-1}]	2.50	2.50 $\div$ 2.60
T_{clad} [°C]	496	495
max$\{q'\}$ [W cm^{-1}]	372	375
Δp [mbar] / natural circulation	1066 / ref	1100 / ok

According then to the summary pros/cons table:

- the natural circulation is slightly worsened (because of spacers).

Table C.11: HFG-D2H1 main core parameters

Parameter	XT-ADS-HF	HFG-D2H1
P_{th} [MW]	85	101
Enrichment [%]	33.3	32.2
r_{fuel} [mm]	2.70	2.48
r_{hollow} [mm]	0.80	same
r_{clad} [mm]	3.275	3.00
p [mm]	9.17	8.19
p/d	1.40	1.37
h_{fuel} [mm]	600	500
R_{core} [mm]	875	974
$\phi > 0.75$ MeV [cm^{-2} s -1]	$1.0 \cdot 10^{15}$	$1.15 \cdot 10^{15}$
T_{outlet} - T_{inlet} [°C]	120	same
v_{coolant} (rod) [m s^{-1}]	1.72	same
v_{coolant} (spacers) [m s^{-1}]	2.50	> 2.50
T_{clad} [°C]	496	same
max$\{q'\}$ [W cm^{-1}]	372	341
Δp [mbar] / natural circulation	1066 / ref	> 1066 / bit worse

As final attempt, the most promising HFC-P and HFC-D configurations have been combined with the HFC-H one. The resulting configuration re-

proposes the same reduction of core height and pin diameter, exploiting the concentration of the fuel in the cell to increase the flow area, and in turn the power.

According then to the summary pros/cons table:

- the pressure drop is decreased (because of flow area), and
- the natural circulation ought be enough (as reference).

Table C.12: HFG-P4D2H1 main core parameters

Parameter	XT-ADS-HF	HFG-P4D2H1
P_{th} [MW]	85	107
Enrichment [%]	33.3	same
r_{fuel} [mm]	2.70	2.48
r_{hollow} [mm]	0.80	same
r_{clad} [mm]	3.275	3.00
p [mm]	9.17	8.32
p/d	1.40	1.39
h_{fuel} [mm]	600	500
R_{core} [mm]	875	990
$\phi > 0.75$ MeV [cm^{-2} s -1]	$1.0 \cdot 10^{15}$	$1.18 \cdot 10^{15}$
T_{outlet} - T_{inlet} [°C]	120	same
v_{coolant} (rod) [m s^{-1}]	1.72	same
v_{coolant} (spacers) [m s^{-1}]	2.50	same
T_{clad} [°C]	496	500
max$\{q'\}$ [W cm^{-1}]	372	362
Δp [mbar] / natural circulation	1066 / ref	1000 / ok

APPENDIX D

DEMO FUEL PIN AND ASSEMBLY, ABSORBERS AND DUMMY ELEMENTS DESIGN

A quote is always nice to have.

The Quotee (1492-1493)

Introduction

To guide the neutronics and thermo-hydraulics analysis, detailed geometry information are needed for a correct modeling of the system. The main simulation tools are indeed almost capable to reproduce very precise geometries, hence retrieving punctual information on the system properties. Besides the main geometric information pointed out in the conceptual core design 17.1, such as the fuel pin diameter and active height, the lattice pitch, and so on, also the remaining regions surrounding the core have to be described, finalizing – for instance – the description of the coolant channel (for thermal/hydraulics simulations to correctly evaluate the pressure drops through the core) or of the reflectors and absorbers (for neutronics evaluations to retrieve precise evaluations of the fuel enrichment and of the control systems worth).

Some preliminary mechanical drawings have been therefore produced for the main components of the DEMO core. A high level of detail has been chosen, borrowing the plant layout of ELSY (see section 9.1): the same scheme for the fuel pin, the fuel assembly frame, the finger absorber rod and the spacer grid has been kept, with all dimensions and positioning corrected for the DEMO layout.

D.1 Detailed CAD drawings

Aiming DEMO at validating Lead technology for use in a future industrial LFR (see Chapter 15), it has been conceived to implement all the main technological solutions of ELSY, representing the latter the reference solution for a large-size Generation-IV LFR (as discussed in Chapter 7).

The need for detailed system information, together with the general constraint of an overall layout representative of ELSY [53], led the Author develop a complete set of preliminary mechanical drawings for the core.

In the following pages will be presented, in order:

1. a CAD drawing of the whole core layout;
2. a CAD drawing of the fuel pin;
3. a CAD drawing of the Finger Absorber Rod;
4. a CAD drawing of the Fuel Assembly frame;
5. a CAD drawing of the mutual positioning of a FAR with respect to the FA in both withdrawn and inserted positions;
6. a CAD drawing with details of the spacer grid in the pins lattice;
7. a CAD drawing of the dummy element.

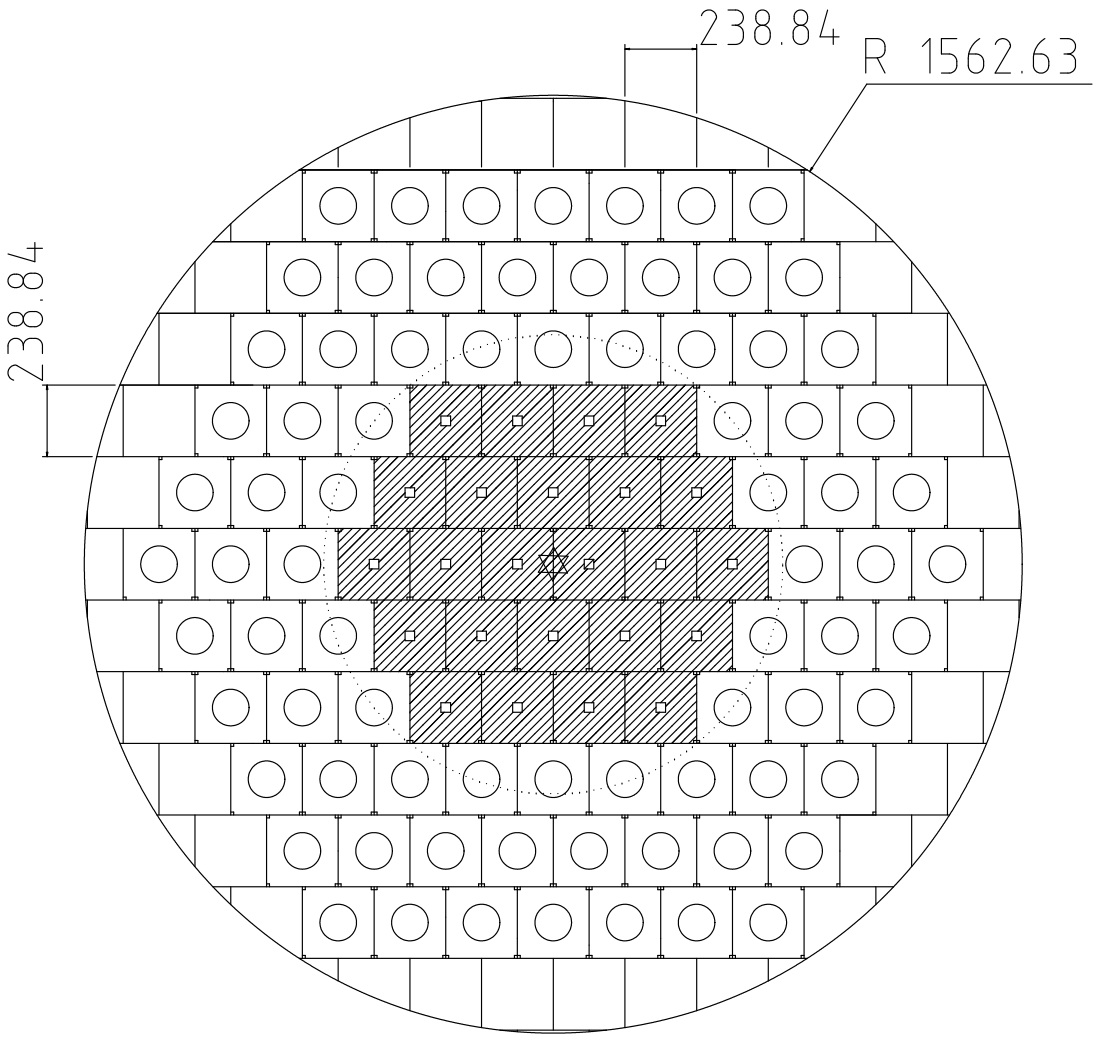

00	24-07-09	PRELIMINARY			G. GRASSO				
Rev. rev.	Data date	Descrizione description			Stato valid.	Eseguito made by	Controllo/ Approvazione checked by/ approved by	Autorizzazione emissione issue authorization	

Progetto project: DEMO	Comm.-R.comm. job no.: SC3020	Emittente issued by: FPN-FISNUC	G.A./Cent. S.A. site: A	ITER	Fornitore supplier	
Cliente customer: MSE	Cl. rin. cl. rin.	Tipo doc. doc. type	Form. size: A1	Scala scale: 1:5	Derivato da derived from	
Ragione soc. fornitore supplier	Sigl. code	Ident. fornitore/Rev. supplier ident./rev.			Sostituisce substitutes	
Ordine attivo/Contratto order: P9LU	Sistema system	Sog. disc. sog. titol	Impianto/Filiera plant		Identificativo componente equipment identif. code	

ENEA

Titolo title:

DEMO
GENERAL OUTLINE
OUTLINE

Disegno prodotto con sistema CAD – Gli originali firmati delle revisioni precedenti sono conservati in archivio.
drawing produced with CAD system – the signed originals of preceding revisions are stored in archive.

Programma utilizzato software used: QCad	Nome file file name: DEMO-GPS10-j01-REV-00.dxf

IDR/CED

Identificativo document no.: DEMO j01

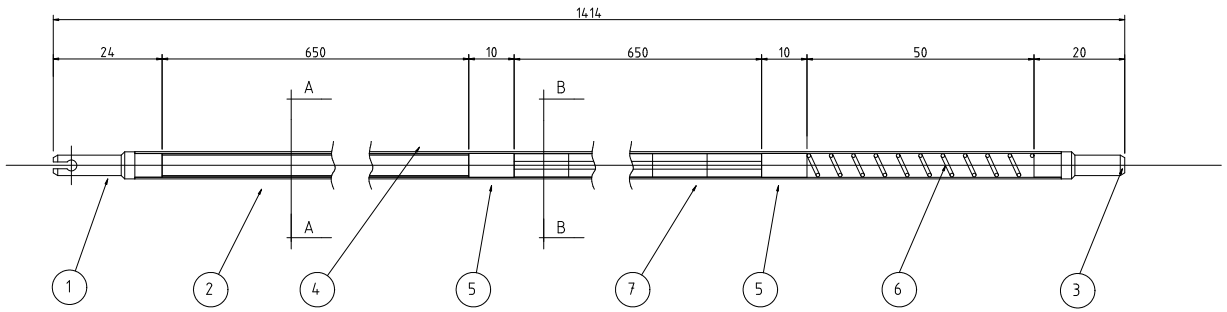

SECT. A-A

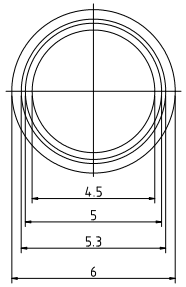

SECT. B-B

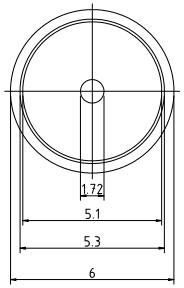

1

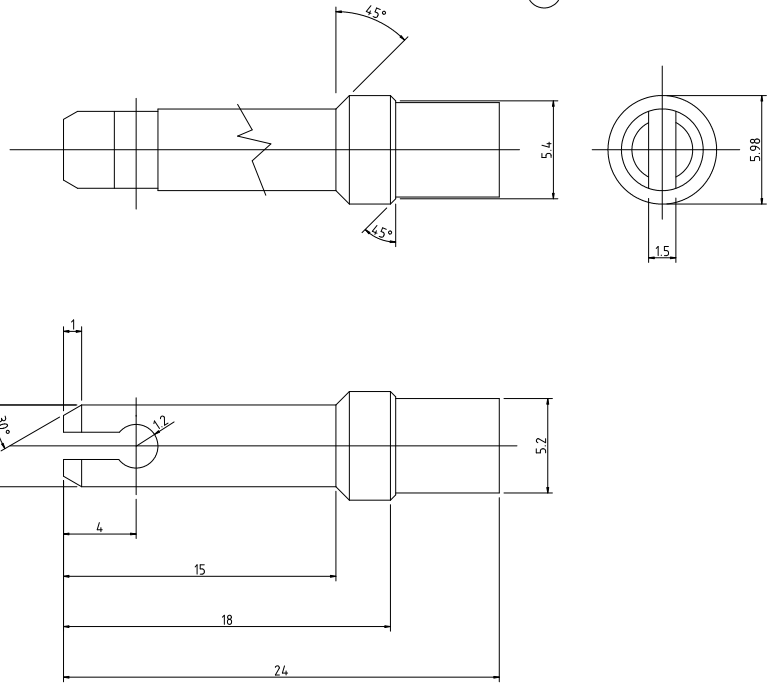

3

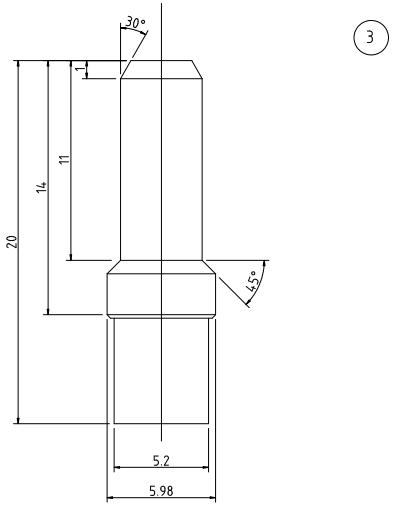

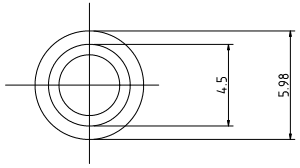

POS	DESCRIPTION	MATERIAL	QUANTITY
7	FUEL PELLET	T.B.D.	T.B.D.
6	SPRING	T.B.D.	1
5	INSULATOR	T.B.D.	2
4	PLENUM TUBE	SA 213 T91	1
3	TOP PLUG	SA 182 F91	1
2	CLADDING	SA 213 T91	1
1	BOTTOM PLUG	SA 182 F91	1

Rev.	Data	Descrizione	Stato valid.	Eseguito	Controllo/ Approvazione	Autorizzazione emissione
00	25-07-05	FIRST ISSUE		G. GRASSO		

Progetto: DEMO	Comm.-S.comm. job no.: SC3020	Emittente: FPN-FISNUC	Q.A.	Cont. s.n.	ITER	Fornitore
Cliente: MSE	Cl. rin. cl. rin.	Tipo doc. doc. type	Form. size: A1	Scala: 2:1	Derivato da: ELSY-21-DMMX-005-002-REV-00	
Ragione soc. fornitore	Rigi code	Ident. fornitore/Rev. supplier ident./rev.			Sostituisce substitutes	
Ordine attivo/Contratto: P9LU	Sistema system	Reg. disc. reg. filed	Impianto/Filiera plant		Identificativo componente equipment identif. code	

ENEA

Informazioni strettamente riservate di proprieta' ENEA - Da non utilizzare per scopi diversi da quelli per cui sono state fornite.
confidential information, property of ENEA. Not to be used for any purpose other than that for which it is supplied.

Titolo: DEMO
SQUARE FUEL ASSEMBLY
FUEL PIN

IDR/CED | Identificativo documento no.: DEMO_j02

Disegno prodotto con sistema CAD - Gli originali firmati delle revisioni precedenti sono conservati in archivio.
drawing produced with CAD system - the signed originals of preceding revisions are stored in archive.

Programma utilizzato software used: QCad | Name file file name: DEMO-GPS10-j02-REV-00.dxf

LONGITUDINAL SECTION

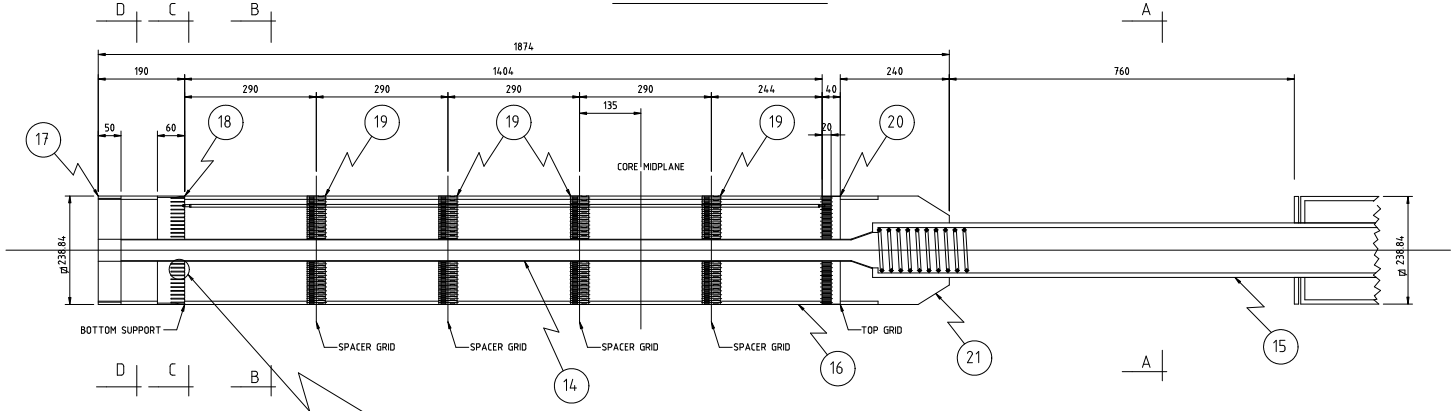

SECTION A-A

(Scale 2:1)

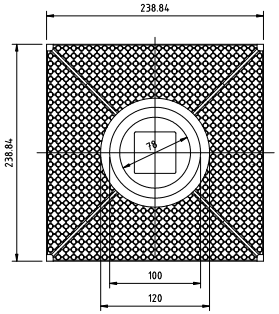

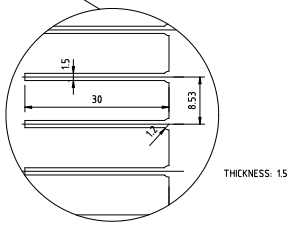

BOTTOM SUPPORT LATERAL GROOVE

TYPICAL

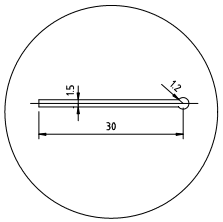

BOTTOM SUPPORT SECTION

TYPICAL

POS	DESCRIPTION	MATERIAL	QUANTITY
21	UPPER PLATE	SA 382 T91	4
20	TOP GRID	SA 382 T91	1
19	SPACER GRID	SA 382 T91	4
18	BOTTOM SUPPORT	SA 382 T91	1
17	LOWER STRUCTURE	SA 382 T91	1
16	LATERAL COLUMN	SA 382 T91	4
15	UPPER PIPE	SA 335 T91	1
14	LOWER PIPE	SA 335 T91	1

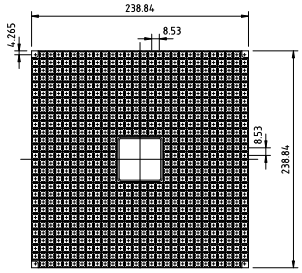

SECTION B-B

SPACER GRID (Scale 2:1)

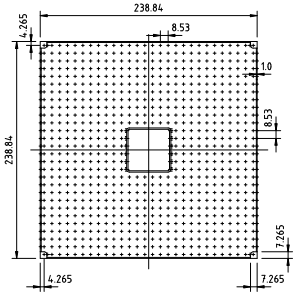

SECTION C-C

(Scale 2:1)

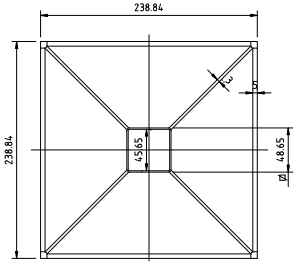

SECTION D-D

(Scale 2:1)

00	26-07-09	FIRST ISSUE	G. GRASSO

Rev. rev. | Data date | Descrizione description | Data valid. ignor. status | Realizzato made by | Controllato/ Approvato checked by/ approved by | Autorizzazione emissione ignor. authorization

Progetto project: DEMO	Comm.-S.comm. job no.: SC3020	Emittente issued by: FPN-FISNUC	Q.A. cert. n.a. atto: A	ITER	Fornitore supplier	
Cliente customer: MSE	Cl. rin. cl. rin.	Tipo doc. doc. type	Form. size: A1	Scala scale: 1:5	Derivato da derived from: ELSY-21-DMMX-005-001-REV-00	
Ragione soc. fornitore supplier	Rigi code	Ident. fornitore/Rev. supplier ident./rev.			Sostituisce substitutes	
Ordine attivo/Contratto order: P9LU	Sistema system	Reg. disc. reg. filed	Impianto/Piliera plant		Identificativo componente equipment identif. code	

ENEA

Titolo title: DEMO FRAME

Informazioni strettamente riservate di proprieta' ENEA - Da non utilizzare per scopi diversi da quelli per cui sono state fornite.

confidential information, property of ENEA. Not to be used for any purpose other than that for which it is supplied.

Disegno prodotto con sistema CAD - Gli originali firmati delle revisioni precedenti sono conservati in archivio. drawing produced with CAD system - the signed originals of preceding revisions are stored in archive.

Programma utilizzato software used: QCad | Nome File file name: DEMO-GPS10-J04-REV-00.dxf

IDR/CED | Identificativo document no.

DEMO j04

TYPICAL SPACER GRIDS

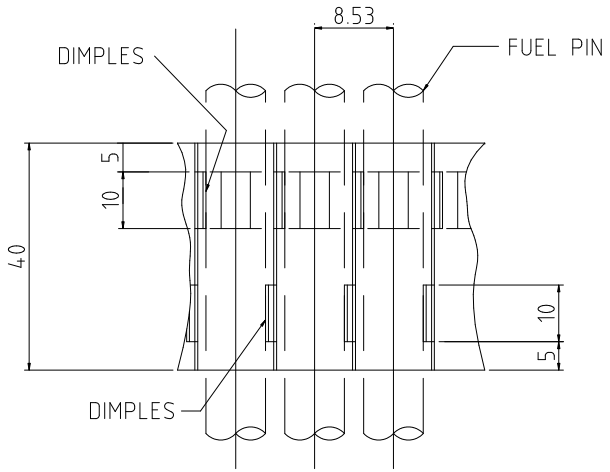

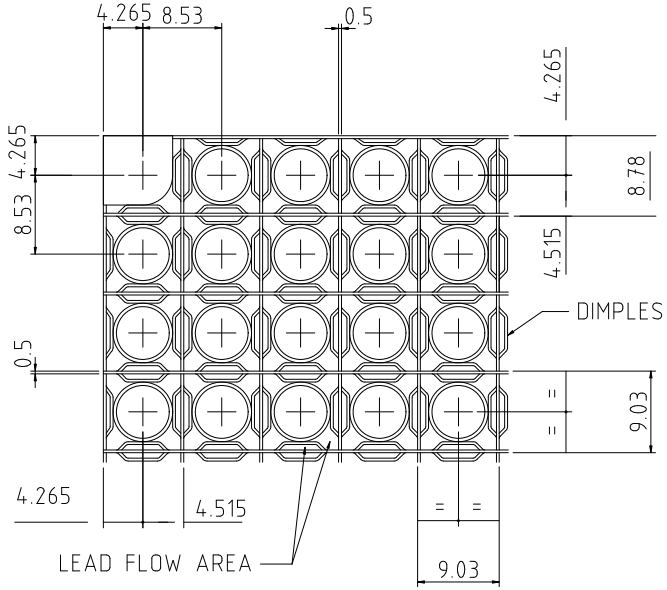

TYPICAL TOP GRID

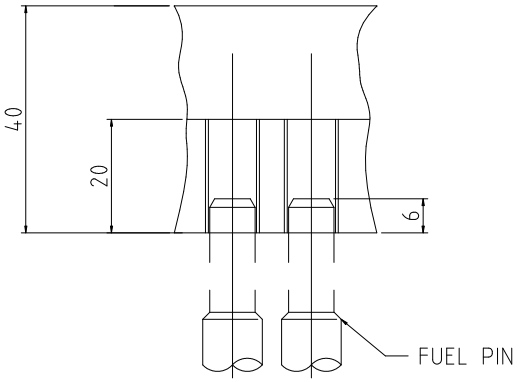

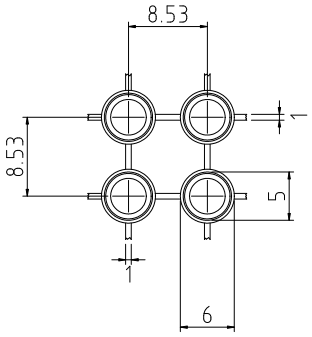

00	26-07-05	FIRST ISSUE			G. GRASSO		
Rev. rev.	Data date	Descrizione description			Data valid. inizio validità	Realizzato made by	Controllo/ Approvazione checked by/ approved by

Progetto project	DEMO	Comm.-S.comm. job no.	SC3020	Emittente issued by	FPN-FISNUC	D.C.Ident. ed. alle	A
Cliente customer	MSE	Cl. rin. cl. rin.	Tipo doc. doc. type	Form. size	A1	Scala scale	1:5
Regione soc. fornitore supplier		Sigl code	Ident. fornitore/Rev. supplier ident./rev.			Sostituisce substitutes	
Ordine attivo/Contratto order	P9LU	Sistema system	Reg. disc. reg. filed	Impianto/Filiera plant		Identificativo componente equipment identif. code	

ENEA

Titolo title: DEMO
GRID AND SPACERS

Disegno prodotto con sistema CAD - Gli originali firmati delle revisioni precedenti sono conservati in archivio.
drawing produced with CAD system - the signed originals of preceding revisions are stored in archive.

Programma utilizzato software used	QCad
Nome file file name	DEMO-GPS10-J06-REV-00.dwg

IDR/CED	Identificativo document no.

DEMO j06

LONGITUDINAL SECTION

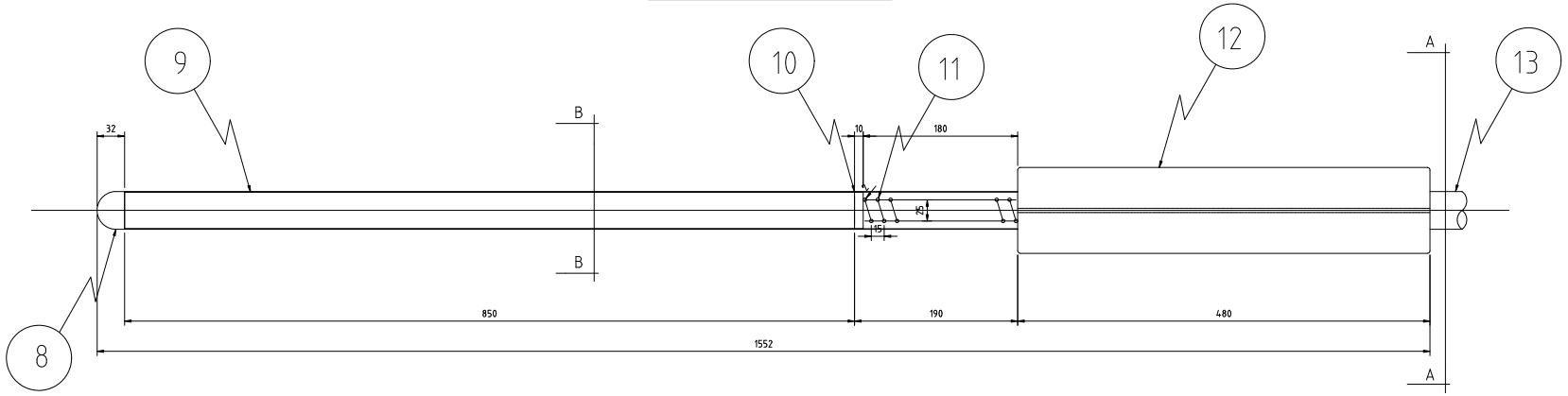

POS	DESCRIPTION	MATERIAL	QUANTITY
13	HOLDING COLUMN	SA 382 T91	1
12	DUMPER GUIDE	SA 382 T91	1
11	SPRING	T.B.D.	1
10	THERMAL INSULATOR	T.B.D.	1
9	ABSORBER PELLET	B_4C *	T.B.D.
8	LOWER PLUG	SA 182 T91	1

* 90% B^{10} ENRICHED FOR SHUT DOWN RODS

42% B^{10} ENRICHED FOR CONTROL RODS

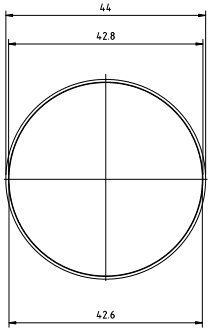

SECTION B-B

scale 1:5

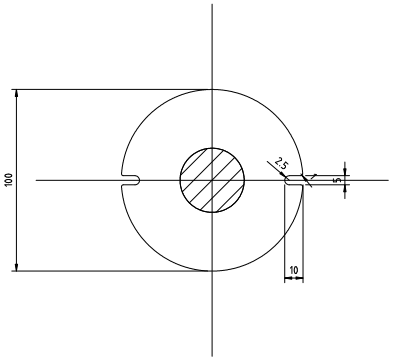

SECTION A-A

scale 1:2

Rev. rev.	Data date	Descrizione description	Data valid. issue status	Realizzato made by	Controllo/ Approvazione checked by/ approved by	Interferenze correlazione issue authorization
00	26-07-05	FIRST ISSUE		G. GRASSO		

Progetto project: DEMO	Comm.-Ecomm. job no.: SC3020	Emittente issued by: FPN-FISNUC	D.A./Ant. Mo. site: A	ITER	Fornitore supplier	
Cliente customer: MSE	Cl. rin. cl. rin.	Tipo doc. doc. type	Form. size: A1	Scala scale: 1:2.5	Derivato da derived from	
Regione soc. fornitore supplier	Sigl code	Ident. fornitore/Rev. supplier ident./rev.			Sostituisce substitutes	
Ordine attivo/Contratto order: P9LU	Sistema system	Reg. disc. reg. filed	Impianto/Filiera plant		Identificativo componente equipment identif. code	

ENEA

Informazioni strettamente riservate di proprieta' ENEA - Da non utilizzare per scopi diversi da quelli per cui sono state fornite.

confidential information, property of ENEA Not to be used for any purpose other than that for which it is supplied.

Title: DEMO
CONTROL ROD
AND SHOUT DOWN ROD

Disegno prodotto con sistema CAD - Gli originali firmati delle revisioni precedenti sono conservati in archivio.
drawing produced with CAD system - the signed originals of preceding revisions are stored in archive.

Programma utilizzato software used	QCad	Nome file file name	DEMO-GPS10-j03-REV-00.dxf

IDR/CED

Identificativo document no.: DEMO j03

LONGITUDINAL SECTION

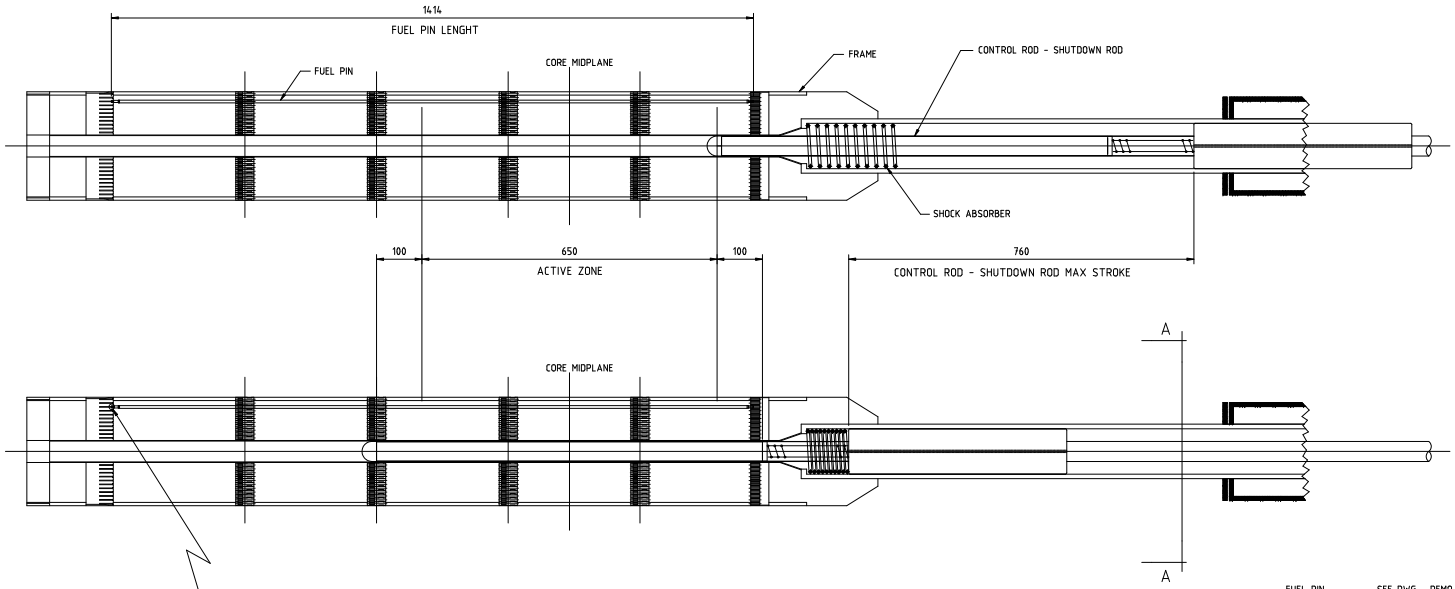

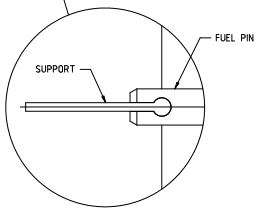

TYPICAL BOTTOM ANCHORAGE

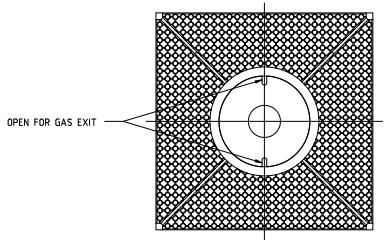

SECTION A-A

FUEL PIN	SEE DWG. : DEMO GPS10 j02
CONTROL ROD AND SHUTDOWN ROD	SEE DWG. : DEMO GPS10 j03
FRAME	SEE DWG. : DEMO GPS10 j04

Rev. rev.	Data date	Descrizione description	Stato valid. issue status	Realizzato made by	Controllo/ Approvazione checked by/ approved by	Interfacciamento omologazione issue authorization
00	26-07-05	PRELIMINARY		G. GRASSO		

Progetto project: ELSY	Comm.-R.comm. job no.: SC3020	Emittente issued by: FPN-FISNUC	D.Q.Sost. Qu. sta. A	ITER	Fornitore supplier	
Cliente customer: MSE	Cl. prin. el. cla.	Tipo doc. doc. type	Form. size A1	Scala scale 1:5	Derivato da derived from: ELSY 21 DMMX 005 001 REV 01	
Regione soc. fornitore supplier	Rigi code	Ident. fornitore/Rev. supplier ident./rev.			Sostituisce substitutes	
Ordine attivo/Contratto order: P9LU	Sistema system	Reg. disc. reg. filed	Impianto/Filiera plant		Identificativo componente equipment identif. code	

ENEA

Informazioni strettamente riservate di proprieta' ENEA - Da non utilizzare per scopi diversi da quelli per cui sono state fornite.

confidential information, property of ENEA Not to be used for any purpose other than that for which it is supplied.

Titolo title: DEMO GENERAL ASSEMBLY OUTLINE

Disegno prodotto con sistema CAD - Gli originali firmati delle revisioni precedenti sono conservati in archivio.
drawing produced with CAD system - the signed originals of preceding revisions are stored in archive.

Programma utilizzato software used: DCad	Nome file file name: DEMO GPS10 j05 REV 00.dxf

IDR/CED | Identificativo document no.: DEMO j05

LONGITUDINAL SECTION

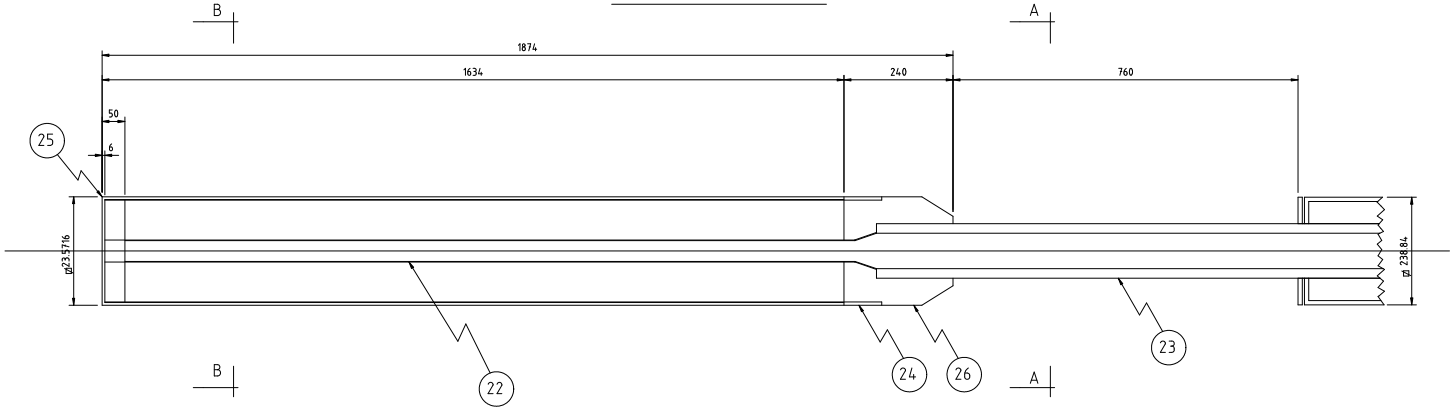

POS	DESCRIPTION	MATERIAL	QUANTITY
26	UPPER PLATE	SA 382 T91	4
25	LOWER STRUCTURE	SA 382 T91	1
24	LATERAL COLUMN	SA 382 T91	4
23	UPPER PIPE	SA 335 T91	1
22	LOWER PIPE	SA 335 T91	1

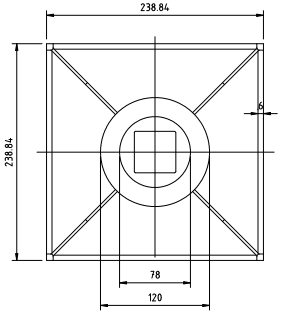

SECTION A-A

(Scale 2:1)

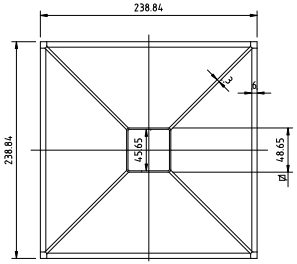

SECTION B-B

(Scale 2:1)

00	28-07-09	FIRST ISSUE		G. GRASSO			
Rev. rev.	Data date	Descrizione description	Visto valid.	Eseguito made by	Controllo/ Approvazione checked by/ approved by	Autorizzazione emissione issue authorization	

Progetto project: DEMO	Comm.-Ecomm. job no.: SC3020	Emittente issued by: FPN-FISNUC	Q.A./ Cat. S.A.	ITER	Fornitore supplier	
Cliente customer: MSE	Cl. rin. cl. rin.	Tipo doc. doc. type	Form. size: A1	Scala scale: 1:5	Derivato da derived from	
Ragione soc. fornitore supplier	Rigi code	Ident. fornitore/Rev. supplier ident./rev.			Sostituisce substitutes	
Ordine attivo/Contratto order: P9LU	Sistema system	Reg. disc. eng. filed	Impianto/Filiera plant		Identificativo componente equipment identif. code	

ENEA

Titolo title: DEMO
DUMMY ELEMENT

Disegno prodotto con sistema CAD - Gli originali firmati delle revisioni precedenti sono conservati in archivio.
drawing produced with CAD system - the signed originals of preceding revisions are stored in archive.

Programma utilizzato software used	QCad	Nome file file name	DEMO-GPS10-J07-REV-00.dxf

IDR/CED | Identificativo document no.: DEMO j07

APPENDIX E
ACRONYMS

4S Super Safe, Small and Simple reactor

A-DHR external Air Decay Heat Removal

ADS Accelerator Driven Subcritical system

ARE Above-Reactor Enclosure

BoC Beginning of Cycle

BORIS Battery Optimized Reactor Integral System

BR Breeding Ratio

BREST Russian acronym for Lead-cooled Fast Reactor

BU Burn Up

BWR Boiling Water Reactor

CANDLE Constant Axial Neutron During the Life of Energy reactor

CDT FP7 Central Design Team

CEA Commissariat à l'Énergie Atomique (Atomic Energy Commissariat)

CIEMAT Centro de Investigaciones Energética, Medioambientales y Tecnológicas (Research Center for Energy, Environment and Technology)

CR Control Rod

CRIEPI Central Research Institute of the Electric Power Industry of Japan

CTE Coefficient of Thermal Expansion

DHR Decay Heat Removal

DIENCA Dipartimento di Ingegneria Energetica, Nucleare e del Controllo Ambientale (Department of Energy and Nuclear Engineering and of Environmental Control)

DOE US Department Of Energy

DpA Displacements per Atom

DRC Direct Reactor Cooling

DU Depleted Uranium

EAC Environment-Assisted Cracking

EFIT European Facility for Industrial Transmutation

EFPD Equivalent Full-Power Day

ELSY European Lead-cooled SYstem

ENEA Agenzia Nazionale per le Nuove Tecnologie, l'Energia e lo Sviluppo Economico Sostenibile (Italian National Agency for the New Technologies, Energy and Sustainable Economic Development)

EoC End of Cycle

EOS Equation Of State

FA(s) Fuel Assembly(ies)

FADF power/FA Distribution Factor

FASTEF FAst Spectrum Transmutation Experimental Facility

FCTS Fuel Cycle Transition Scenarios

FMS Ferritic Martensitic Steel

FP(s) Fission Product(s)

FP5(6,7) 5^{th}(6^{th},7^{th}) EURATOM Framework Programme

FZK Forschungszentrum Karlsruhe (Karlsruhe Research Center)

GFP(s) Gaseous Fission Product(s)

GIF Generation IV International Forum

HLM Heavy Liquid Metals

HLRW High Level Radioactive Waste

HM(s) Heavy Metal(s)

HYPER HYbrid Power Extraction Reactor

IAEA International Atomic Energy Agency

ICE Indium-Cadmium Eutectic

IP Integrated Project

IPPE Institute of Physics and Power Engineering of Obninsk

ISI&R In-Service Inspection and Repair

JAEA Japan Atomic Energy Agency

JAERI Japan Atomic Energy Research Institute

KAERI Korea Atomic Energy Research Institute

KIT Karlsruhe Institute of Technology (formerly FZK)

LBE Lead-Bismuth Eutectic

LCF Low Cycle Fatigue

LEU Low-Enrichment Uranium

LFR Lead-cooled Fast Reactor

LIN Laboratorio di Ingegneria Nucleare (Nuclear Engineering Laboratory) of Montecuccolino

LLFP(s) Long-Lived Fission Product(s)

LLRW Low Level Radioactive Waste

LLW Long-Lived Waste

LMAC Liquid Metal Accelerated Creep

LME Liquid Metal Embrittlement

LOCA Loss Of Coolant Accident

MA(s) Minor Actinide(s)

MCNP Monte Carlo N-Particle transport code

MCP Main Coolant Pump

MOX Mixed OXide

MYRRHA Multy-purpose hYbrid Research Reactor for High-tech Applications

NEA Nuclear Energy Agency

NITI A. P. Aleksandrov Scientific Technical Research Institute of Sosnovy Bor

NRG Nuclear Research and Cons. Group

OECD Organisation for Economic Co-operation and Development

OKB Experimental Design Bureau

OKBM Design Bureau of Machine Building

PBWFR Pb-Bi cooled direct contact boiling Water Fast Reactor

PCMI Pellet-Clad Mechanical Interaction

PEACER Proliferation-resistant Environment-friendly Accident-tolerant Continuable-energy Economical Reactor

PFP(s) Pseudo-Fission Product(s)

PIE Post Irradiation Evaluation

PP Physical Protection

PR Proliferation Resistance

PRACS Primary Reactor Auxiliary Cooling System

PR&PP Proliferation Resistance and Physical Protection

PSSC GIF LFR Provisional System Steering Committee

PWR Pressurized Water Reactor

RCCS Reactor Concrete Cooling System

RVACS Reactor Vessel Air Cooling System

R&D Research and Development

SFR Sodium-cooled Fast Reactor

SG Steam Generator

SGTR Steam Generator Tube Rupture

SGU(s) Steam Generator Unit(s)

SLPLFR Steam Lift Pump type LFR

SNU Seoul National University

SRP System Research Plan

SSTAR Small Secure Transportable Autonomous Reactor

SVBR Russian acronym for Lead-Bismuth Fast Reactor

TOP Transient Of Power

TPP Technology Pilot Plant

ULOF Unprotected Loss Of Flow

VF Volume Fraction

W-DHR stored Water Decay Heat Removal

WPFC Working Party on Fuel Cycle

BIBLIOGRAPHY

[1] International Energy Agency. Key world energy statistics 2009. Technical report, IEA, 2009. 4

[2] European Technical Working Group on ADS, editor. *A European Roadmap for Developing Accelerator Driven Systems (ADS) for Nuclear Waste Incineration*. ENEA, 2001. 12

[3] World Energy Council. The role of nuclear power in europe. 2007. 12

[4] J.P. Grouiller *et al.* COSI, A Simulation Software for a Pool of Reactors and Fuel Cycle Plants: Application to the Study of the Deployment of Fast Breeder Reactors. In *Proceedings of Fast Reactors and Related Fuel Cycles*, KYOTO/Japan, October 1991. 19, 153, 167, 168, 169

[5] M. Samson *et al.* CESAR: A simplified evolution code for reprocessing applications. In *5th international nuclear conference on Recycling, Conditioning and Disposal (RECOD 98)*, Nice Acropolis, France, October 25-28 1998. 19, 167, 169

[6] H. Bateman. Solution of a system of differential equations occurring in the theory of radioactive transformations. *Proc. Cambridge Philos. Soc.*, 15:423–7, 1910. 19, 122

[7] G. Rimpault *et al.* The ERANOS code and data system for Fast Reactor neutronic analyses. In *International Conference on the PHYSics Of Reactors 2002 (PHYSOR2002)*, Seoul, Korea, 2002. 19, 90, 105, 106, 153, 219, 220, 224, 244

[8] OECD Nuclear Energy Agency and International Atomic Energy Agency. Uranium 2007: Resources, Production and Demand. Technical report, OECD, 2008. 47, 185

[9] H. Oigawa *et al.* Concept of waste management and geological disposal incorporating partitioning and transmutation technology. In *Tenth Information Exchange Meeting on Actinide and Fission Product Partitioning and Transmutation (IEMPT10)*, Mito, Japan, October 6-10 2008. 49

[10] L. Cinotti *et al.* Lead-cooled Fast Reactor. In *Conference on Euratom Research and Training in Reactor Systems (FISA 2006)*, Luxembourg, May 13-16 2006. 76

[11] L. Cinotti *et al.* The potential of the LFR and the ELSY Project. In *2007 International Congress on Advances in Nuclear Power Plants (ICAPP '07)*, Nice Acropolis, France, May 13-18 2007. 79

[12] L. Cinotti *et al.* The ELSY Project. In *International Conference on the Physics of Reactors 2008 (PHYSOR 2008)*, Interlaken, Switzerland, September 14-19 2008. 79, 191

[13] L. Cinotti. Reactor assembly preliminary configuration. Technical Report ELSY DOC 08 049, Del Fungo Giera Energia, June 2008. 81, 101, 227

[14] G. Rimpault. Definition of the detailed missions of both the Pb-Bi cooled XT-ADS and Pb cooled EFIT and its gas back-up option. Technical Report D1.1 Deliverable, EURATOM, 2006. 86, 249, 262, 264

[15] G. Benamati *et al.* VELLA Project: an initiative to create a common European research area on lead technologies for nuclear applications. In *European Nuclear Conference 2007 (ENC2007)*, Brussels, Belgium, September 16-20 2007. 86, 194, 249

[16] R. Thetford and V. Sobolev. Recommended properties of fuel, cladding and coolant for EFIT predesign. Technical Report D3.4 Deliverable, IP EUROTRANS DM3 AFTRA, November 2005. 87, 249, 250, 251

[17] F. B. Brown *et al.* MCNP Version 5. *Trans. Am. Nucl. Soc.*, 87:273, 2002. 90, 105, 153, 244

[18] G. Rimpault. Physics documentation of ERANOS: the ECCO cell code. Technical Report RT-SPRC-LEPh-97-001, CEA, October 1997. 90, 106, 153, 220

[19] Joint Evaluated File (JEF) project. The JEF-2.2 Nuclear Data Library. Technical Report JEFF Report 17, OECD/NEA, April 2000. 90, 91

[20] G. Rimpault *et al.* The ECCO/JEFF2 Library. Technical Report NT-SPRC-LEPh-92/231, CEA, 1992. 90, 106

[21] C. J. Gho and G. Palmiott. BISTRO: BIdimensionnel S_n TRansport Optimise - Un programme bidimensionnel de transport S_n aux differences finies. Technical Report NT-SPRC-LEPh-84-270, CEA, November 1984. 90

[22] J. M. Ruggeri *et al.* TGV: A coarse mesh 3 dimensional diffusion-transport module for the CCRR/ERANOS code system. Technical Report DRNR-SPCI-LEPh-93-209, CEA, February 1993. 90, 107, 153

[23] MUSE-4 Benchmark. Benchmark on computer simulation of MASURCA critical and subcritical experiments – final report. Technical report, OECD, 2005. 90

[24] R. E. MacFarlane and D. W. Muir. The NJOY Nuclear Data Processing System Version 91. Technical Report LA-12740-M, Los Alamos National Laboratories, October 1994. 91

[25] G. Grasso. MAT numbers table for isotope processing with NJoy. Technical Report LIN-M01.2007, LIN, 2007. 91

[26] G. Grasso. NJoyInputMaker: a tool for automatically processing cross section libraries with NJoy. Technical Report LIN-R06.2007, LIN, 2007. 91

[27] C. D. Fletcher and R. R. Schultz. *Relap5/Mod3 Code Manual Volume 5 - User's Guidelines*. Idaho National Engineering Laboratory, January 1992. 92

[28] A.V. Zhukov *et al.* Heat transfer in lead-cooled fast reactor (LCFR). In *International Topical Meeting on Advanced Reactors Safety (ARS'94)*, Pittsburgh, Pennsylvania, USA, April 17-21 1994. 92, 110

[29] M. Sarotto *et al.* Open Square Fuel Assembly design and drawings. Technical Report D6 Deliverable, EURATOM, May 2008. 93, 101, 104, 108

[30] Joint Evaluated File (JEF) project. The JEFF-3.1 Nuclear Data Library. Technical Report JEFF Report 21, OECD/NEA, 2006. 106, 108, 154, 155, 220, 224

[31] J. Krepel *et al.* Eql3d: Eranos based equilibrium fuel cycle procedure for fast reactors. *Ann. of Nucl. En.*, 36(5):550–561, 2009. 110, 156, 162

[32] C. Artioli *et al.* ELSY neutronic analysis by deterministic and Monte Carlo methods: an innovative concept for the control rod systems. In *International Congress on Advances in Nuclear Power Plants 2009 (ICAPP09)*, Tokio, Japan, May 10-14 2009. 110, 140, 156, 227

[33] P. Peerani. Elementi di neutronica per il codice di cella ECCO. Technical Report FT.WCD.00003, ENEA, May 1989. 116

[34] A. Mizutani and H. Sekimoto. Calculational Method of One-Group Nuclear Constants in Nuclear Equilibrium State. *J. Nucl. Sci. and Tech.*, 34(6):596–602, 1997. 123

[35] M. Salvatores *et al.* The physics of TRU transmutation - a systematic approach to the intercomparison of systems. In *International Conference on the Physics of Reactors (PHYSOR 2004)*, Chicago, USA, April 25-29 2004. 123

[36] L. Monti *et al.* Multi-recycling in the ENHS and the equilibrium core. *Prog. in Nucl. En.*, 50:262–8, 2008. 123

[37] Vv. Aa. Handbook on Lead-Bismuth Eutectic Alloy and Lead Properties, Materials Compatibility, Thermalhydraulics and Technologies. Technical report, OECD-NEA, 2007. 137, 138, 192, 195

[38] C. Artioli *et al.* Minor actinide transmutation in ADS: the EFIT core design. In *International Conference on the Physics of Reactors (PHYSOR 2008)*, Interlaken, Switzerland, September 14-19 2008. 142

[39] C. Artioli. A-BAQUS; a multi-entry graph assisting the neutronic design of an ADS. Case study: EFIT. In *Fifth International Workshop on the Utilisation and Reliability of High Power Proton Accelerator (HPPA 5)*, Mol, Belgium, May 6-9 2007. 142

[40] L. Cinotti *et al.* *Nuclear Engineering Handbook*, volume 2, chapter Lead-cooled Fast Reactor (LFR) design: safety, neutronics, thermal-hydraulics, structural mechanics, fuel, core and plant design. Springer, 2010. (IN PRESS). 153

[41] M. Sarotto *et al.* ELSY core design static, dynamic and safety parameters with the open square FA. Technical Report D8 Deliverable, EURATOM, April 2009. 164, 225, 227

[42] R. Sanchez *et al.* APOLLO 2: a user-oriented, portable modular code for multigroup transport assembly calculations. In *International conference on development of reactor physics and calculation methods*, Paris, France, April 27-30 1987. 170

[43] J. Vidal. Manuel d'utilisation du logiciel APOGENE_BBL (version 3.6). Technical Report NT-SPRC-LECy-06-349s, CEA, 2006. 170

[44] LFR Provisional System Steering Committee. System Research Plan for the Lead-cooled Fast Reactor (LFR). Technical report, Generation IV International Forum, 2008. 191

[45] C. Smith *et al.* SSTAR: the US Lead-cooled Fast Reactor (LFR). *J. Nucl. Mat.*, 376(3):255–9, 2008. 191, 194

[46] A Technology Roadmap for Generation IV Nuclear Energy Systems. Technical Report GIF-002-00, U.S. DOE Nuclear Energy Research Advisory Committee and the Generation IV International Forum, December 2002. 191

[47] C. F. Smith *et al.* Lead-cooled Fast Reactor (LFR) ongoing R&D and key issues. In *GIF Symposium*, Paris, France, September 9-10 2009. 191

[48] J. U. Knebel *et al.* IP EUROTRANS: A EUROpean Research Programme for the TRANSmutation of High Level Nuclear Waste in an Accelerator Driven System. In *8$^{\text{th}}$ Information Exchange Meeting on Actinide and Fission Product Partitioning & Transmutation (IEMPT8)*, Las Vegas, USA, November 9-11 2004. 194

[49] C. Fazio *et al.* Assessment of reference structural materials, heavy liquid metal technology and thermal-hydraulics for European waste transmutation ADS. In *International Conference on Nuclear Energy Systems for Future Generation and Global Sustainability (GLOBAL 2005)*, Tsukuba, Japan, October 9-13 2005. 195, 250

[50] C. Fazio *et al.* European research on heavy liquid metal technology for advanced reactor systems. In *15th Pacific Basin Nuclear Conference (15PBNC)*, Sydney, Australia, October 15-20 2006. 195

[51] C. Fazio *et al.* Structural materials, thermal-hydraulics studies and development of heavy liquid metal technologies for Accelerator Driven sub-critical transmutation Systems. In *Jahrestagung Kerntechnik 2008*, Hamburg, Germany, May 27-29 2008. 195

[52] C. Fazio *et al.* European cross-cutting research on structural materials for Generation IV and transmutation systems. *J. Nucl. Mat.*, 392(2):316–23, 2009. 196

[53] L. Cinotti. Private communication, May 2009. 206, 274

[54] V. Sobolev *et al.* Preliminary Fuel Pin and Hexagonal Assembly design (and drawings). Technical Report D5 Deliverable, EURATOM, May 2007. 244

[55] T. Yamashita *et al.* Thermal expansions of NpO_2 and some other actinide dioxides. *J. Nucl. Mat.*, 245:72–8, 1997. 245, 247

[56] N. A. Javed. Thermodynamic study of hypostoichiometric Urania. *J. Nucl. Mat.*, 43:219–24, 1972. 246

[57] L. A. Morales *et al.* Kinetics of reaction between Plutonium dioxide and water at 25 ţo 350 ¸ formation and properties of the PuO_{2+x} phase. Technical Report LA-13597-MS, Los Alamos National Laboratories, 1999. 246

[58] J. M. Haschke and T. H. Allen. Equilibrium and thermodynamic properties of the PuO_{2+x} solid solution. *J. Alloys Comp.*, 336:124–31, 2002. 246

[59] D. G. Martin. The thermal expansion of solid UO_2 and (U,Pu) mixed oxides - A review and recommendations. *J. Nucl. Mat.*, 152:94–101, 1988. 247

[60] F. Gnecco *et al.* Corrosion behaviour of steels in lead-bismuth at 823 k. *J. Nucl. Mat.*, 335:185–8, 2004. 250

[61] A. Aiello *et al.* Corrosion behaviour of steels in flowing LBE at low and high oxygen concentration. *J. Nucl. Mat.*, 335:169–73, 2004. 250

[62] A. Weisenburger *et al.* T91 cladding tubes with and without modified fecral coatings exposed in lbe at different flow, stress and temperature conditions. In *IV International Workshop on Materials for HLM Cooled Reactors and Related Technologies*, Rome, Italy, May 21-23 2007. 250

[63] G. Müller *et al.* Results of steel corrosion tests in flowing liquid Pb/Bi at 420-600 °C after 2000 h. *J. Nucl. Mat*, 301(1):40–6, 2002. 250

[64] F. Niu *et al.* Effect of oxygen on fouling behaviour in lead-bismuth coolant systems. *J. Nucl. Mat.*, 366(1–2):216–222, 2007. 250

[65] R. A. Forrest. *FISPACT-2007: user manual.* EURATOM/UKAEA Fusion Association, ukaea fus 534 edition, March 2007. 254

[66] R. Varga. *Matrix Iterative Analysis.* Prentice-Hall, Englewood Cliffs, NJ, 1962. 256

[67] D. Young. *Iterative Solutions of Large Linear Systems.* Academic Press, New York, 1971. 256

[68] X-5 Monte Carlo Team. *MCNP – A General Monte Carlo N-Particle Transport Code, Version 5 – Volume I: Overview and Theory.* Los Alamos National Laboratories, 2003. 258

[69] "Description of Work" to Euratom Collaborative Project. Central Design Team (CDT) for a FASt-spectrum Transmutation Experimental Facility. Grant agreement no. FP7-232527. 262

[70] P. Baeten *et al.* The next step for MYRRHA: the Central Design Team FP7 project. In *AccApp'09 Satellite meeting*, Vienna, Austria, May 06 2009. 262

[71] D. Maes *et al.* MYRRHA flux update. Technical report, SCK-CEN, 2009. 262, 264

[72] G. Van den Eynde *et al.* XT-ADS core neutronics & cycle analysis. Technical report, EURATOM, 2009. 264